To the Graduate Council:

I am submitting herewith a thesis written by Lokanath Patel entitled "The Effect of Carbon on the Formation of Sigma Phase in Formation of Sigma Phase in Austenitic Stainless Steel." I have examined the final copy of this thesis for form and content and recommend that it be accepted in partial fulfillment of the requirements for the degree of Master of Science, with a major in Metallurgical Engineering.

J. E. Spruiell

Joseph E. Spruiell, Major Professor

We have read this thesis
and recommend its acceptance:

Dan L. Olson

W. T. Becker

Accepted for the Council:

L. Evans Reed

Vice Chancellor
Graduate Studies and Research

THE EFFECT OF CARBON ON THE FORMATION OF SIGMA PHASE IN FORMATION OF SIGMA PHASE IN AUSTENITIC STAINLESS STEEL

A Thesis

Presented for the

Master of Science

Degree

The University of Tennessee, Knoxville

Lokanath Patel

December 1981

3055547

DEDICATION

This thesis is dedicated

to

Dr. Joseph E. Spruiell, Professor,
Department of Chemical, Metallurgical, and Polymer Engineering,
The University of Tennessee, Knoxville,

and to

my wife, Mrs. Basanti Patel
whose advice was instrumental in inspiring
the writing and finishing of this thesis.

Confused, worried, tired, restless, and nervous under the influence of physical and mental stress, the disciple, Aryuna, said to Lord Krishna, "Oh, Lord, I have become a slave of my desires; what shall I do? I am totally lost." And the Lord said, "Do not worry, my friend. Just follow me and work, because life without work will be sinful. Just do not expect reward or fruit from it, because nobody, including myself, has a right to results."

Translated from the ancient
Hindu book The Bhagabata Geeta

ACKNOWLEDGEMENTS

The author would like to express his sincere thanks to Dr. Joseph E. Spruiell, his major professor, for his continued guidance, advice, understanding, encouragement, and cooperation throughout the course of this research.

Thanks are extended to Dr. Ben F. Oliver and Dr. William T. Becker for their willingness to serve on the thesis committee. Dr. Oliver's valuable and timely advice on alloy preparation in his induction melting facilities is gratefully acknowledged. Thanks are also extended to Dr. Charlie R. Brooks for permitting some of his manuscript materials to be used in the thesis, and to Dr. Carl D. Lundin for his advice on selecting etching reagents for stainless steels.

The author is grateful to Mr. Tom Andress, a former University of Tennessee graduate student and now with the American Electric Power Corporation of Canton, Ohio, for his assistance on some electrolytic extraction and transmission electron microscopy. The author is also pleased to acknowledge the help of Mr. Bob McGill of the Electronics Shop for scanning electron microscopy and Mr. H. B. Thompson of the Machine Shop for his numerous efforts during the course of this investigation.

It is a pleasure to acknowledge Ms. Ann Lacava of The Manuscript Shop, Knoxville, Tennessee for her charming personality and professional advice on thesis preparation and binding and Ms. Julie Greenwood for doing a superb job on typing the manuscript.

Mr. Edwin Atkinson did a very professional job on the drafting.

The author acknowledges the generosity of Mr. Thomas Mauger, Manager of Materials Engineering, John Deere, Plow and Planter Works, for allowing him to take his extended vacation to finish his research.

To his parents, Mr. and Mrs. Kamal Lochan Patel, the author is most grateful for their financial and moral support. Finally, the author wishes to thank his wife, Basanti, his daughter, Veena, and his son, Suman, for standing by him in his good days, as well as bad days.

ABSTRACT

An investigation was undertaken to study the effects of carbon content (and chromium content) on the amount and rate of sigma phase formation in experimentally prepared iron-chromium-nickel-carbon alloys. Nine alloys were melted in a laboratory under vacuum or controlled atmosphere using high-purity raw materials as ingredients. The compositions were typically in the range for austenitic stainless steels, with a systematic variation of chromium and carbon content. The composition ranges for each alloying element varied as follows: carbon 0-0.40 wt.%, chromium 18-26 wt.%, nickel 14-17 wt.%, and balance iron.

Prior to aging, the alloys were grouped into three types based upon the pretreatments they received--namely, as-cast, cold-worked, and solution-treated conditions. The aging temperatures varied from 650-850°C (1200-1560°F), and the aging time ranged from 1-1000 hours.

Techniques such as x-ray diffraction, transmission electron microscopy, scanning electron microscopy, metallographic staining, and Magne Gage measurements (for ferrite content) were used to identify and characterize the phases present in the samples. The weight fraction of sigma phase was determined by quantitative metallographic techniques.

The sigma formation tendencies of the alloys were compared to and analyzed in terms of two semi-empirical theories: 1) the equivalent chromium content theory of Hull[14] and 2) the electron vacancy theory developed by Woodyatt et al.[117]

The major findings of this investigation include:

1. An increase of carbon content of the austenitic stainless steel alloys in the range of 0-0.40 wt.% retards sigma formation at a given equivalent chromium content.
2. The major source of the effect of carbon was the removal of the carbide (and sigma-forming) elements from solution by precipitation of carbides.
3. The most successful and quantitative analysis etchant was KOH-H_2O solution with controlled current density and etching time. This solution stains sigma phase to a reddish brown color, whereas other popular etchants, such as oxalic acid, HCl-HNO_3-H_2O solution, etc., do not.
4. Optical metallography was more suitable to estimate the percent sigma in the matrix than the bulk electrolytic extraction method because of suspected dissolution of sigma in the 10% HCl-90% CH_3OH solution as found by our studies, as well as numerous others reported in the literature.
5. Both the equivalent chromium content (ECC) and the electron vacancy number ($\bar{N}v$) theories are useful for predicting the formation of sigma phase in the austenitic stainless steels. Alloys with overall ECC > 17 $\pm$ 0.05 or $\bar{N}v$ of 2.85 $\pm$ 0.05 form sigma in the austenitic stainless steels. This value agrees well with a minimum $\bar{N}v$ of 2.95-3.05 for sigma formation in Fe-Cr-Co-Ni-Mo alloys reported by de Barbadillo in the 1977 Handbook of Stainless Steels.

6. The as-cast or cold-worked structures form sigma at a greater rate than the solution-treated alloys.
7. Ferrite in the austenitic stainless steel promotes sigma formation by the nucleation of sigma within the ferrite or at the austenite-ferrite interface.
8. The rate of sigma formation was greater at 750°C (1380°F) than at either 650°C (1200°F) or 850°C (1560°F).
9. The morphology of sigma phase varied. It was semi-continuous with massive dog-bone shape in the as-cast alloys to needle-like or massive globular (shaped) in the cold-worked or solution-treated alloys.

TABLE OF CONTENTS

CHAPTER		PAGE
I.	INTRODUCTION	1
	1. General Background of the Problem	1
	2. Scope of the Present Research	7
II.	LITERATURE REVIEW	9
	1. General Characteristics of Sigma Phase	9
	2. Effect of Sigma Phase on Properties of Stainless Steel	35
	3. Semi-Quantitative Prediction of Sigma Phase Formation in Austenitic Stainless Steel Alloys	44
	4. Kinetics of Sigma Phase Formation--The Effects of Variables on Sigma Phase Formation	58
III.	EXPERIMENTAL PROCEDURE	68
	1. Materials, Alloy Preparation, and Characterization	68
	2. Sample Preparation	71
	3. Heat Treatment	76
	4. Sample Nomenclature	77
	5. Optical Metallography	78
	6. Scanning Electron Microscopy (SEM)	82
	7. Transmission Electron Microscopy (TEM)	83
	8. Microhardness Measurements	84
	9. Bulk Extraction of Precipitates--Qualitative and Quantitative Analysis	85
	10. X-Ray Diffraction for Phase Identification	87
	11. Quantitative Microscopy	88
IV.	CHARACTERIZATION OF UNAGED MATERIALS	89
	1. Chemical Composition	89
	2. Ferrite Measurements	93
	3. Microstructures of As-Cast, Cold-Worked, and Solution-Treated Alloys	95
V.	CHARACTERIZATION OF THE AGED MATERIALS	110
	1. Optical Metallography and Microhardness Measurements	111
	2. Ferrite Measurements	156
	3. Bulk Extraction and X-Ray Diffraction--Quantitative Results	158
	4. Electron Microscopy	169
	5. Analysis of Aging Behavior	177

CHAPTER		PAGE
VI.	CONCLUSIONS AND RECOMMENDATIONS	200
	1. Conclusions	200
	2. Recommendations	204
LIST OF REFERENCES		206
APPENDICES		215
	A. Identification of Sigma Phase By Electron Diffraction	216
	B. Computer Program to Calculate At.% Cr, Fe, Ni, Etc. and the Average EVN, $\bar{N}v$, for Fe-Cr-Ni Alloys	236
	C. Solubility of Carbon With Temperature in Fe-Cr-Ni Alloys	240
	D. Variation of Stoichiometry Variations of $M_{23}C_6$ Carbide With Aging Temperature and Calculation of Electron Vacancy Number, $\bar{N}v$	245
	E. Temperature Profiles for Tubular Furnaces	256
	F. Intensity Vs. Energy Plots for Sigma, Austenite, and Carbide Phases	261
	G. Periodic Table of the Elements	265
	H. List of Symbols Used in the Text	270
VITA		275

LIST OF TABLES

TABLE		PAGE
I-1.	Composition of Standard Grades of Wrought Stainless and Heat-Resisting Steels	3
I-2.	Nominal Compositions of Nonstandard Grades of Wrought Stainless Steel	5
II-1.	Chemical Composition of Sigma Phase in Five Binary Systems	16
II-2.	Composition Ranges of Sigma Phases in Several Binary Systems	18
II-3.	E/A Ratio for Sigma Phase in Many Binary Alloy Systems	22
II-4.	Exchange Factor of Some Alloy Systems	33
II-5.	Room Temperature Tensile and Yield Strength Properties of Type 310 Alloy Aged at Various Times and Temperatures	39
II-6.	Effect of Sigma on Toughness at Elevated Temperatures for an Fe-25Cr-20Ni Alloy Steel	43
II-7.	Estimates of Coefficients, Standard Errors, F-Ratios, and Chromium Equivalents in Models Relating in Θ to Composition for Cast Stainless Steels Aged at 1500°F (816°C)	50
II-8.	Electron Vacancy Numbers ($\bar{N}v$) for the Elements Commonly Found in Austenitic Stainless Steel Alloy Matrices	57
II-9.	Alloy Compositions Used By Grot and Spruiell and Weiss and Stickler	61
III-1.	Chemical Compositions of the Special Austenitic Stainless Steel Alloys Prepared for This Study	70
III-2.	Amount of Cold Work Given to Each Alloy	73
III-3.	Final ASTM Grain Sizes of the Nine Special Alloys After Homogenization and Solution Treatment	75

TABLE		PAGE
III-4.	Sample Nomenclature for the Aging Time and Temperature	79
III-5.	Recommended Chemical and Electrolytic Etchants for Optical Metallography of Stainless Steel Alloys	81
IV-1.	Equivalent Chromium Content (ECC) and the Average Electron Vacancy Number (EVN or Nv) of the Laboratory-Prepared Alloys	90
IV-2.	Classification of the Nine Experimental Alloys Based Upon Their Overall Chemical Compositions	92
IV-3.	Ferrite Numbers (FN) of As-Cast, Cold-Worked (c.w.), and Solution-Treated Alloys Prior to Aging	94
V-1.	Percent Sigma Vs. % Carbon and % Cr for the Solution-Treated Alloys After Aging for 1000 Hours at 750°C	144
V-2.	Hardness of Various Phases in Austenitic Stainless Steel	155
V-3.	Ferrite Measurements of the Aged Solution-Treated Alloys	157
V-4.	Bulk Electrolytic Extraction Results Using 10% HCl-90% CH_3OH Solution	159
V-5.	Bulk Electrolytic Extraction Results Using 150 gm Citric Acid-100 gm KI-20 ml HCl-150 ml H_2O Solution	161
V-6.	d-Spacings of the Residue Obtained from Composition 9 (Sample 9-0-4) After Aging for 1000 Hours at 650°C	163
V-7.	Direct X-Ray Diffraction Results on Bulk Composition 9 (Sample 9-1-4) After Aging for 1000 Hours at 650°C	164
V-8.	Lattice Parameters from X-Ray Diffraction Data--c_o, a_o, and c_o/a_o Ratio for Sigma Phase	166
V-9.	Results By X-Ray Diffractometer on Powder Residue from Composition 8 (Sample 8-2-4) Aged for 1000 Hours at 650°C	167
V-10.	Identification of $M_{23}C_6$ Carbide By Debye-Scherrer Method	168
V-11.	Lattice Parameters of Sigma Phase from TEM Diffraction Data	176

TABLE		PAGE
V-12.	Wt.% Sigma Vs. Compositions for Group I, II, and III Experimental Alloys After Aging for 1000 Hours at 750°C (1380°F)	184
V-13.	Comparison of Experimental Observations of Sigma Formation With Predictions Based on ECC and EVN Semi-Empirical Theories for Commercial-Grade Stainless Steels and Weld Metals	185
A-A-1.	Interplanar Spacings of Austenite	228
A-A-2.	Ratios of d-Spacings in Face-Centered Cubic Systems .	229
A-C-1.	Effect of Temperature on Solubility of Carbon in Fe-Cr-Ni-C Alloys	242
A-C-2.	Available Carbon (for Carbide Formation) for Alloys at 650°C, 750°C, and 850°C	243
A-D-1.	Effect of Temperature on Stoichiometry (Chemical Formula) of $M_{23}C_6$ $(Cr_x\ Fe_y)_6$	247
A-D-2.	Amount of $M_{23}C_6$ Formation Based Upon $(Cr_x\ Fe_y)_6$ Formula for Alloys at Various Temperatures	248
A-D-3.	Elements in Solid Solution With the Matrix at 650°C, 750°C, and 850°C After Carbide Formation	249
A-D-4.	Electron Vacancy Number ($N\bar{v}$) at Room Temperature (RT), 650°C, 750°C, and 850°C	252

LIST OF FIGURES

FIGURE		PAGE
II-1.	Composition Ranges of Sigma Phases in Terms of Average Group Number	12
II-2.	Fe-Cr Binary Constitution Diagram	14
II-3.	Binary Sigma Phases	19
II-4.	Occurrence and Ranges of Stability of Binary Sigma Phases	20
II-5.	Ternary Phase Fields	24
II-6.	Fe-Cr-Ni Isotherm at 650°C and the Binaries Fe-Cr, Fe-Ni, and Ni-Cr	26
II-7.	Constitution Diagrams of Fe-C, Fe-Cr, and 70% Fe-Ni-Cr	27
II-8.	Isothermal Sections from the Fe-Cr-Ni System	29
II-9.	Effect of Carbon on Solubility of Carbides in 18Cr-8Ni Steels	30
II-10.	Relationship Between the Impact Energy at 20°C and Sigma Formation in Austenitic Stainless Steels	37
II-11.	Effect of Time and Temperature on Room Temperature Impact Values of 25Cr-20Ni Alloy	40
II-12.	Effect of Time and Temperature on the Ductility of 25Cr-20Ni Alloy Steel	41
II-13.	Corrosion Rates of a 0.12% C, 19.1% Cr, and 9.0% Stainless Casting in Nitric Acid After Sensitization at 800-1600°F (425-870°C) for One to Three Minutes	45
II-14.	Bend Angles Vs. Equivalent Cr Content of Kromarc Alloys After Aging for 1000 Hours at 816°C (1500°F)	49
II-15.	Simple Impact Test to Evaluate the Embrittlement of Cast Stainless Steel Pins on Aging	51
II-16.	Bend Angles Vs. Compositions of the Kromarc Alloys (1/4-Inch-Diameter) Upon Aging for 1000 Hrs. at 816°C (1500°F)	52

FIGURE		PAGE
II-17.	Time-Temperature-Precipitation Diagram of 316 Stainless Steel Solution-Treated at 1260°C for 1.5 Hour and Water-Quenched	60
II-18.	Time and Temperature Conditions Conducive to Sigma Phase Formation in 25Cr-20Ni Steel (Fe Base)	62
II-19.	Occurrence of Sigma in Fine-Grained, Unstressed IN-100	65
IV-1.	As-Cast Structure for Steel Composition Number 9	96
IV-2.	As-Cast Structure for Alloy Composition Number 10	97
IV-3.	As-Cast Structure for Composition Number 19	98
IV-4.	Optical Photomicrograph for Alloy Number 9 Given 50.3% Cold Work By Rolling	102
IV-5.	Optical Micrograph for Alloy Composition Number 8 After Cold Working (~50%)	103
IV-6.	Optical Photomicrograph for a Low-Carbon Solution-Treated Alloy	105
IV-7.	Optical Photomicrograph of a Medium-Carbon Solution-Treated Alloy	106
IV-8.	Optical Photomicrograph of a Medium-High Carbon Solution-Treated Alloy	107
V-1.	Effect of Chromium on Sigma Formation	112
V-2.	Effect of Carbon on Sigma Formation	114
V-3.	Effect of Aging Temperature on the Rate of Sigma Formation On a High-Carbon (0.4% C) Alloy	116
V-4.	Effect of Aging Temperature On a Low-Carbon (0.014% C) Alloy	119
V-5.	Effect of Aging Temperature On Sigma Formation for a Medium-Carbon (0.18% C) Alloy	122
V-6.	Effect of Aging Temperature for 1000 Hours in the Range of 650-850°C (1200-1560°F) On the Rate of Sigma Formation in Three Solution-Treated Alloys	125
V-7.	Effects of Initial Pre-Aging Treatments on Sigma Formation After Aging for 1000 Hours at 650°C	126

FIGURE PAGE

V-8. Optical Photomicrographs Showing the Effect of Aging Time (at 650°C) on Sigma Phase Transformation on a Low-Carbon (0.014% C) As-Cast Alloy 129

V-9. Effect of Aging Time (at 650°C) on Sigma Phase Transformation for Alloy 9, Which Was Cold-Worked Prior to Aging 133

V-10. Photomicrographs Illustrating the Effect of Aging Time (at 650°C) on Sigma Transformation for a Low-Carbon (0.014% C) Alloy Which Was Solution-Treated Prior to Aging 135

V-11. Photomicrographs Showing the Effect of Time and Cold Work on Sigma Phase Transformation 139

V-12. Diamond Pyramid Hardness Numbers (Microhardness) for Sigma and Austenite 154

V-13. SEM of the Solution-Treated Alloy Composition (9) After Aging for 1000 Hours at 650°C 171

V-14. X-Ray Fluorescence Spectra (Intensity Vs. Energy in KeV) from Sigma Phase (A) and the Austenitic Matrix (B) 172

V-15. X-Ray Fluorescence Spectra (Intensity Vs. Energy in KeV) from the Carbide (C) and the Austenitic Matrix (B) 173

V-16. Sigma Phase in Composition 9 as Revealed by Transmission Electron Microscope 174

V-17. Electron Diffraction Pattern from the Sigma Phase . . 175

V-18. Wt.% Sigma (Optical Metallographic Method) Vs. Overall ECC of the Nine Experimental Alloys Aged 1000 Hours at 750°C 187

V-19. Wt.% Sigma (Optical Metallographic Method) Vs. % Carbon of the Nine Experimental Alloys, Solution-Treated After Aging 1000 Hours at 750°C 188

V-20. Wt.% Sigma (Optical Metallographic Method) Vs. ECC of the Nine Experimental Alloys After Correcting for Carbide Precipitation and When Aged 1000 Hours at 750°C 190

FIGURE		PAGE
V-21.	Wt.% Sigma (Bulk Extraction Method) Vs. Overall ECC for Commercial-Grade Stainless Steel Alloys and Weld Metals Aged 1000 Hours at 750°C	191
V-22.	Wt.% Sigma (Bulk Extraction Method) Vs. ECC for Commercial-Grade Stainless Steel Alloys After Correcting for Carbide Precipitation at 750°C	192
V-23.	Wt.% Sigma (Optical Metallographic Method) Vs. EVN for the Pure Nine Laboratory Alloys After Correcting for Precipitation of $M_{23}C_6$ Carbide and Aging 1000 Hours at 750°C	194
V-24.	Wt.% Sigma (Bulk Extraction Method) Vs. EVN for Commercial Alloys After Correcting for Carbide Precipitation at 750°C	196
A-A-1.	A Simple Electron Diffraction Camera	218
A-A-2.	Austenite (γ) Phase Showing Typical Annealing Twins .	221
A-A-3.	Diffraction Pattern from the Austenite Phase as Shown in Figure A-A-2	222
A-A-4.	Vector Diagram Showing (hkl) Planes in FCC Systems .	223
A-A-5.	Vector Diagram for Sigma Identification	224
A-A-6.	Vector Diagram to Calculate the Angles Between Planes of Sigma Phase	225
A-A-7.	Vector Diagram to Compute Angles Between Planes for Sigma Phase	226
A-B-1.	FORTRAN IV Program to Calculate Average Electron Vacancy Number, $\bar{N}v$	238
A-B-2.	Computer Printout for Electron Vacancy Concentration for Composition 9 (Solution-Treated Alloy)	239
A-E-1.	Temperature Profile for Furnace No. 15 (650°C) . . .	258
A-E-2.	Temperature Profile for Furnace No. 16 (750°C) . . .	259
A-E-3.	Temperature Profile for Furnace No. 17 (850°C) . . .	260
A-F-1.	SEM Energy Dispersive Analyses for Austenite Matrix (Left) and Sigma Phase (Right)	263

FIGURE		PAGE
A-F-2.	SEM Energy Dispersive Analyses for Austenite Matrix (Left) and $M_{23}C_6$ Carbide (Right)	264
A-G-1.	Periodic Table of the Elements Showing Their Crystal Structure	267
A-G-2.	Periodic System of Elements Showing Transition Metals	268
A-G-3.	Periodic System of the Elements for Ferrous Metallurgists	269

CHAPTER I

INTRODUCTION

1. GENERAL BACKGROUND OF THE PROBLEM

The principal reason for the existence of stainless steel is its outstanding resistance to corrosion.[1,72] Besides their excellent corrosion resistance, stainless steels also exhibit a wide variety of excellent mechanical properties at room and cryogenic temperatures and possess superior creep rupture properties at elevated temperatures.[73] For example, type 304 and 304L stainless steels possess tensile strength greater than 300,000 pounds per square inch (psi) in a liquid hydrogen environment.[66] Because of their excellent material properties under very adverse conditions, stainless steels are prime materials selected by engineers for structural components for many chemical and nuclear reactor applications. In nuclear reactors, stainless steels are sometimes subjected to neutron irradiation dosage as high as 10^{22}-10^{23} neutron/cm^2 (Energy, E > 0.1 Mega electron Volt, MeV).[3] Such radiation environment causes the austenitic stainless steels to harden by the creation of dislocation loops[69] and minute voids in the metal, and, as a result, a considerable amount of ductility is lost. Despite this phenomenon, a recent survey[4] showed that stainless steels have been found to be reliable and successful in many operating nuclear environments.

Chemical compositions of standard grades of wrought and heat-resisting stainless steels are shown in Table I-1 based upon information given in the Metals Handbook (8th Edition), Volume 1. Stainless steels are generally grouped into three classes, which can be briefly described as follows:

1. Martensitic--Alloys of iron and chromium hardenable by heat treatment. They consist largely of the body-centered tetragonal (BCT) martensite phase. These alloys contain sufficient carbon relative to their chromium content to be austenitic at high temperatures. The carbon content ranges from 0.15 to 1.2% (by weight) and is sufficient to produce substantial hardening of the martensite phase.
2. Ferritic--Largely ferritic (BCC) iron-chromium alloys not hardenable by heat treatment. The chromium content relative to the carbon content is sufficiently high to avoid forming austenite at high temperatures.
3. Austenitic--Iron-chromium-nickel alloys predominantly austenitic in commercially heat-treated condition and non-hardenable by heat treatment. The element "nickel" is not mandatory in this class of steels and may be replaced by other austenite stabilizers, such as manganese or nitrogen.

It is worth mentioning that type 18-8 (18 wt.% Cr, 8 wt.% Ni, balance--Fe) is one of the most widely used austenitic stainless steel alloys.

TABLE I-1

COMPOSITION OF STANDARD GRADES OF WROUGHT STAINLESS AND HEAT-RESISTING STEELS

(AISI, 1959)

AISI type	Nominal composition, % C	Mn, max	Si, max	Cr	Ni	Other(a)
Austenitic Steels						
201	0.15 max	7.50(b)	1.00	16.00 to 18.00	3.50 to 5.50	0.25 max N
202	0.15 max	10.00(c)	1.00	17.00 to 19.00	4.00 to 6.00	0.25 max N
301	0.15 max	2.00	1.00	16.00 to 18.00	6.00 to 8.00	....
302	0.15 max	2.00	1.00	17.00 to 19.00	8.00 to 10.00	....
302B	0.15 max	2.00	3.00(d)	17.00 to 19.00	8.00 to 10.00	....
303	0.15 max	2.00	1.00	17.00 to 19.00	8.00 to 10.00	0.15 min S
303(Se)	0.15 max	2.00	1.00	17.00 to 19.00	8.00 to 10.00	0.15 min Se
304	0.08 max	2.00	1.00	18.00 to 20.00	8.00 to 12.00	....
304L	0.03 max	2.00	1.00	18.00 to 20.00	8.00 to 12.00	....
305	0.12 max	2.00	1.00	17.00 to 19.00	10.00 to 13.00	....
308	0.08 max	2.00	1.00	19.00 to 21.00	10.00 to 12.00	....
309	0.20 max	2.00	1.00	22.00 to 24.00	12.00 to 15.00	....
309S	0.08 max	2.00	1.00	22.00 to 24.00	12.00 to 15.00	....
310	0.25 max	2.00	1.50	24.00 to 26.00	19.00 to 22.00	....
310S	0.08 max	2.00	1.50	24.00 to 26.00	19.00 to 22.00	....
314	0.25 max	2.00	3.00(e)	23.00 to 26.00	19.00 to 22.00	....
316	0.08 max	2.00	1.00	16.00 to 18.00	10.00 to 14.00	2.00 to 3.00 Mo
316L	0.03 max	2.00	1.00	16.00 to 18.00	10.00 to 14.00	2.00 to 3.00 Mo
317	0.08 max	2.00	1.00	18.00 to 20.00	11.00 to 15.00	3.00 to 4.00 Mo
321	0.08 max	2.00	1.00	17.00 to 19.00	9.00 to 12.00	5 × C min Ti
347	0.08 max	2.00	1.00	17.00 to 19.00	9.00 to 13.00	10 × C min Cb-Ta
348	0.08 max	2.00	1.00	17.00 to 19.00	9.00 to 13.00	10 × C min Cb-Ta 0.10 max Ta
Martensitic Steels						
403	0.15 max	1.00	0.50	11.50 to 13.00	....	....
410	0.15 max	1.00	1.00	11.50 to 13.50	....	....
414	0.15 max	1.00	1.00	11.50 to 13.50	1.25 to 2.50	....
416	0.15 max	1.25	1.00	12.00 to 14.00	....	0.15 min S
416(Se)	0.15 max	1.25	1.00	12.00 to 14.00	....	0.15 min Se
420	0.15 min	1.00	1.00	12.00 to 14.00	....	....
431	0.20 max	1.00	1.00	15.00 to 17.00	1.25 to 2.50	....
440A	0.60 to 0.75	1.00	1.00	16.00 to 18.00	....	0.75 max Mo
440B	0.75 to 0.95	1.00	1.00	16.00 to 18.00	....	0.75 max Mo
440C	0.95 to 1.20	1.00	1.00	16.00 to 18.00	....	0.75 max Mo
501	0.10 min	1.00	1.00	4.00 to 6.00	....	0.40 to 0.65 Mo
502	0.10 max	1.00	1.00	4.00 to 6.00	....	0.40 to 0.65 Mo
Ferritic Steels						
405	0.08 max	1.00	1.00	11.50 to 14.50	....	0.10 to 0.30 Al
430	0.12 max	1.00	1.00	14.00 to 18.00	....	....
430F	0.12 max	1.25	1.00	14.00 to 18.00	....	0.15 min S
430F(Se)	0.12 max	1.25	1.00	14.00 to 18.00	....	0.15 min Se
446	0.20 max	1.50	1.00	23.00 to 27.00	....	0.25 max N

(a) Other elements in addition to those shown below are as follows: Phosphorus is 0.06% max in types 201, 202, 416, 416(Se), 430F, 430F(Se); 0.045% max in types 301, 302, 302B, 304, 304L, 305, 308, 309, 309S, 310, 310S, 314, 316, 316L, 317, 321, 347, 348; 0.20% max in types 303 and 303(Se). Sulfur is 0.030% max in types 201, 202, 301, 302, 302B, 304, 304L, 305, 308, 309, 309S, 310, 310S, 314, 316, 316L, 317, 321, 347, 348, 403, 405, 410, 414, 420, 430, 431, 440A, 440B, 440C, 446, 501 and 502; 0.15% min in types 303, 416 and 430F. (b) Mn range, 5.50 to 7.50. (c) Mn range, 7.50 to 10.00 (d) Si range, 2.00 to 3.00. (e) Si range, 1.50 to 3.00.

Source: Metals Handbook (8th Edition), Volume 1, Properties and Selection of Metals, American Society for Metals, Metals Park, Ohio, p. 409 (1961).

There is a minor variation to the above classification, in the sense that another group of stainless steels, "precipitation-hardenable (PPH) stainless steels," exists. This class of steel contains about 17 wt.% Cr, 4-7 wt.% Ni, plus some amount of P, Cu, Al, and Nb as aging additions. Chemical compositions of some precipitation-hardening grades are shown in Table I-2. This class of steels can be heat treated to relatively high strength and hardness at room temperature[66] as a result of precipitation of metal carbide(s) such as $M_{23}C_6$ which induces lattice strain. Aging temperatures can vary from 450°C to 680°C depending upon the grade, chemical composition, and desired mechanical properties.

With so many types of steels, a wide variety of physical, mechanical, and chemical properties can be obtained. However, each class of stainless steel is different. For example, martensitic grades possess high ultimate tensile strength but very limited ductility. Ferritic grades exhibit better resistance to corrosion than martensitic grades but are generally not as strong. Ferritic grades can also be polished to high lustres. Austenitic grades, on the other hand, are relatively soft, can be mechanically fabricated with ease because of their good ductility, and generally possess high impact energy even at cryogenic temperatures. All classes of stainless steels are required to have a minimum of 12 wt.% chromium to assure resistance to oxidation, but many stainless steel grades contain more chromium than this minimum required value.

For high-temperature applications, there are many properties that must be considered. Among these properties are mechanical strength,

TABLE I-2

NOMINAL COMPOSITIONS OF NONSTANDARD GRADES
OF WROUGHT STAINLESS STEEL

Tentative designation	Nominal composition, %						
	C	Mn	Si	Cr	Ni	Mo	Other
308L	0.025	1.75	0.40	21.00	10.00	....	....
316F	0.06	1.50	0.50	18.00	13.00	2.25	0.13 P, 0.15 S
317L	0.025	1.75	0.50	18.50	13.50	3.25	....
329	0.07	0.60	0.50	27.50	4.50	2.25	....
347F(Se)	0.05	1.25	0.50	17.50	9.50	....	0.13 P, 0.30 Se, 0.60 Cb
418	0.17	0.40	0.30	12.75	2.00	....	3.00 W
420F	0.38	0.45	0.35	13.50	....	....	0.21 Se or 0.18 S
422	0.20	0.65	0.50	12.00	0.75	1.00	1.00 W, 0.30 V
440F	1.00	0.40	0.40	17.00	....	....	0.18 Se or 0.08 S
442	0.06	0.50	0.50	21.00	....	....	....
443	0.06	0.50	0.50	21.00	....	....	1.00 Cu
Stainless W	0.07	0.50	0.50	16.75	6.75	....	0.80 Ti, 0.20 Al
17-4 PH	0.04	0.40	0.50	16.50	4.25	....	0.25 Cb, 3.60 Cu
17-7 PH	0.07	0.70	0.40	17.00	7.00	....	1.15 Al
PH 15-7 Mo	0.07	0.70	0.40	15.00	7.00	2.25	1.15 Al
AM-350	0.10	0.75	0.35	16.50	4.25	2.75	0.10 N
AM-355	0.13	0.85	0.35	15.50	4.25	2.75	0.12 N
16-18	0.05	0.50	0.40	16.00	19.00	....	....
20-29 Cu-Mo	0.05	0.75	1.00	20.00	29.00	2.20	3.20 Cu
17-10 P	0.12	0.75	0.50	17.00	10.50	....	0.28 P
HNM	0.30	3.50	0.50	18.50	9.50	....	0.25 P
Tenelon	0.08	14.50	0.50	17.00	....	....	0.40 N

Source: Metals Handbook (8th Edition), Volume 1, Properties and Selection of Metals, American Society for Metals, Metals Park, Ohio, p. 409 (1961).

ductility, notch sensitivity, corrosion and oxidation resistance, thermal expansion, thermal conductivity, thermal and mechanical shock resistance, microstructural stability, and behavior under cyclic (fatigue) conditions. The austenitic stainless steels (types 304, 316, 321, and 347) are, as a group, the preferred grades for high-temperature service. They are recommended for elevated temperature applications where temperatures may exceed 500°C (~950°F). At such temperatures, their creep strengths generally exceed those of the ferritic grades.[73]

Despite their excellent mechanical properties and corrosion resistance, austenitic stainless steels in service at elevated temperatures undergo certain microstructural changes which alter their mechanical and chemical behavior.[14,15,16] This is because of the fact that at such service temperatures, austenitic stainless steel is in a metastable state.[61] The well known "sensitization" to corrosion caused by the precipitation of carbides is one example. With respect to long-term high-temperature applications, one of the most troublesome instabilities is the precipitation of the sigma (σ) phase--a hard, brittle, nonmagnetic intermetallic compound of complex crystal structure with a BCT lattice. This sigma phase is similar to the compound FeCr and forms during aging of stainless steel alloys in the temperature range 500-950°C (~950-1700°F) depending upon chemical composition.

The equilibrium relationship, thermodynamically speaking, between the sigma phase and temperature is rarely ever realized because of the time dependence of the transformation from austenite to sigma phase. In the absence of high-temperature ferrite (BCC), precipitation of sigma phase is quite sluggish, being encountered only on prolonged exposure at

elevated temperature. However, in alloys that are predominantly austenitic, although containing some ferrite, sigma phase may form during ordinary commercial heat treatments.[8,9] Sigma precipitation causes a well documented reduction in low-temperature ductility and impact energy (toughness) but probably also reduces the creep ductility.[36]

To give an example on the devastating effect of sigma phase, Talbott and Furman[67] conducted impact tests and found that when sigma phase in Fe-Cr-Ni alloys was present in amounts exceeding 25 wt.%, the room temperature (20°C or 68°F) impact energy dropped down to 0 ft-lb from 40 ft-lb for an alloy which contains no sigma. Because of the adverse effect of sigma on mechanical properties, particularly on toughness, this problem has received a great deal of attention in the literature by previous researchers. In spite of this effort, there are many aspects of the problem of sigma phase formation in commercial steels which are not yet understood.

2. SCOPE OF THE PRESENT RESEARCH

Carbon is an important nonmetallic alloying element that invariably occurs in stainless steels when subjected to aging conditions. However, the effect of carbon on sigma formation in stainless steel alloys is not well documented in the literature at present. No experimental research, whether qualitative or quantitative, has been reported which deals specifically with this subject. Hull,[14] for example, studied the effect of Mn, Mo, W, V, Si, Ti, Nb, Ta, Ni, and Co on the embrittlement of austenitic stainless steels but failed to study the effect of carbon. Likewise, Gow and Harder[38] in 1950 mentioned that

lowering carbon content in austenitic stainless steels tends to increase the susceptibility to sigma formation. However, no quantitative data are available. The study on the effect of carbon on sigma formation will lead to a better understanding of the role played by carbon in controlling sigma formation in commercial alloys. This is the major objective of the present research. A secondary objective is to establish some predictive capability which could subsequently be used for alloy development in the future.

CHAPTER II

LITERATURE REVIEW

In this chapter, a summary of the significant results of published documents related to the problem of the present experimental research is described.

1. GENERAL CHARACTERISTICS OF SIGMA PHASE

Discovery and Importance of Studying Sigma Phases--A Broader Outlook

The presence of sigma* (σ) phase in the iron-chromium (Fe-Cr) system was suggested by Treischke and Tamman[78] in the year 1907, but it was not until 1927 that Bain and Griffiths[59] actually established the existence of this phase, which they found to be hard, brittle, and nonmagnetic. Bain and Griffiths also conducted a limited number of experiments on the iron-chromium-nickel (Fe-Cr-Ni) alloys and discovered that sigma phase also occurred in this ternary system. They concluded that sigma phase is nonexistent above a temperature zone, varying with composition (chromium ~20-50%, nickel ~8-18%) from 800-900°C (1470-1740°F) and that heating above this critical temperature develops ferrite phase which persists after moderate cooling rate. A few hours just below this critical temperature will develop the complicated brittle sigma phase. Further progress in establishing equilibrium diagrams showing the presence

---

*The name "sigma" (σ) was given to the hard phase by Jeffe and Foote[36] in 1936.

of sigma in iron-chromium alloys and in the iron-chromium-nickel was slow,[82] but certain compositions of iron-chromium-nickel systems were investigated.

In 1950, a comprehensive text[36] by the American Society for Testing and Materials (ASTM) was published on the Nature, Occurrence and Effects of Sigma Phase in many systems such as iron-chromium-molybdenum (Fe-Cr-Mo), iron-vanadium (Fe-V), chromium-cobalt (Cr-Co), and nickel-vanadium (Ni-V). It was concluded and later supported by many intensive investigations[39] that sigma phase is a topologically close-packed structure[39] which is body-centered tetragonal (BCT) with crystal lattice dimensions[14,16,36,80] that vary with the system composition but generally are in the range

$$c \text{ (unique axis)} = 4.5\text{-}4.8 \text{ Å}$$

$$a = 8.8\text{-}9.2 \text{ Å}$$

$$c/a \text{ Ratio} \simeq 0.52$$

$$(1 \text{ Å unit} = 10^{-8} \text{ cm}).$$

Sigma contains 30 atoms per unit cell.[7]

Hume-Rothery[75] has described an interesting relationship between sigma phase formation and "average group number" (AGN) in the periodic table of the elements. Because many valencies in group VA, VIIIB, or VIIIC (the elements where sigma forming tendencies exist) are in dispute, the relationship between valency and sigma forming tendency is difficult to describe. For example, for equi-atomic alloys in a Mo-Pd system, the average group number is (6+10)/2 = 8.

Figure II-1 shows that the sigma forming tendency exists predominantly in the range AGN = 6.4-6.8--a very striking phenomenon.

The sigma crystal structure has a strong resemblance to a hexagonal, close-packed (h.c.p.) structure since in sigma, atoms are arranged in layers. The crystal structure resemblance between sigma and the carbide with chemical formula $M_{23}C_6$ is interesting. The $M_{23}C_6$ carbide structure strongly resembles sigma when all the carbon atoms are removed by a process such as decarburization and when a slight shift in atom relationship is performed.[39]

Excellent review articles by Hattersley and Hume-Rothery,[81] Hall and Algie,[80] and Wernick[74] have been published. X-ray diffraction work[16] and electron diffraction work on sigma phase by Duhaj[12] is available. The most recent review article on sigma phase published by Marshall and Hooper[34] dealt only with its formation in austenitic stainless steels of commercial grade quality. Details of sigma phase formation such as rate of formation, morphology, and its distribution are much different in high-purity alloys, as shall be seen later.

Sigma Phase Formation--Iron-Chromium System

The initial understanding of sigma phase was based upon sigma phase discovered in iron-chromium systems. Therefore, this system is described in greater depth.

The sigma phase is generally found in systems involving transition elements[74] of the "Periodic Table of the Elements" (see Appendix G). Both iron and chromium are transition elements, and sigma phase occurs in this Fe-Cr system. Such systems are described by Hansen[44] and in

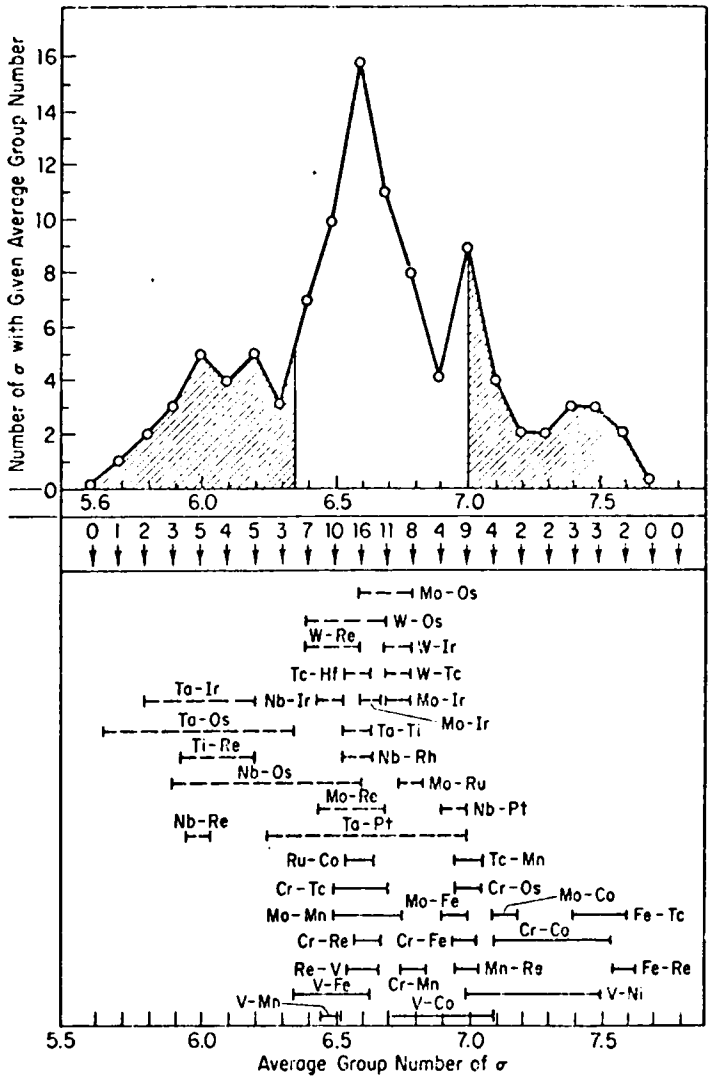


Figure II-1. Composition Ranges of Sigma Phases in Terms of Average Group Number.

Source: W. Hume-Rothery, Phase Stability in Metals and Alloys (P. S. Rudman, J. Stinger, and R. I. Jaffee, Editors). McGraw-Hill Book Co., New York, pp. 14-23 (1967).

the American Society for Metals (ASM) Metals Handbook (8th Edition), Volume 8.[71] The latest equilibrium diagram shown in the handbook is reproduced in Figure II-2. Upon examination, it is found that the sigma phase occurs in the equiatomic region (50 atomic percent (At.%) Cr, 50 At.% Fe) as an intermetallic compound. The extremely low rate of formation of this phase in very pure and undeformed iron-chromium alloys accounts for the fact that it is often difficult to detect its presence. The upper temperature at which sigma phase can be formed in the iron-chromium system is limited to 820°C, 46% chromium by weight. Below this temperature, sigma phase can form with composition varying from 40-49 weight percent (wt.%) chromium. The lower the transformation temperature, the slower sigma precipitates from alpha ferrite (α). There are some indications that alpha to sigma transformation may involve a transition state as explained by Hansen.[44] It is interesting to note that the alpha (α) and alpha plus sigma ($\alpha+\sigma$) boundaries have not been well established below 650°C. Above 600°C, studies[44] have shown that extremely long annealing cycles (greater than 100 days) at 600°C would shift the alpha and alpha plus sigma boundary line even below 26% chromium. As one can see, sigma can occur over a wide composition range.

Before single crystals were available, many tentative unit cell symmetries such as tetrogonal, cubic, or orthorhombic were proposed for the sigma phase. However, at present, sigma phase has been established to be BCT with c = 4.552 Å, a = 8.794 Å, with c/a ratio 0.518[14,36] in the Fe-Cr binary system.

The sigma phase unit cell is known to have 30 atoms per unit cell.[14,36,98] Chemical composition and purity of the alloy may

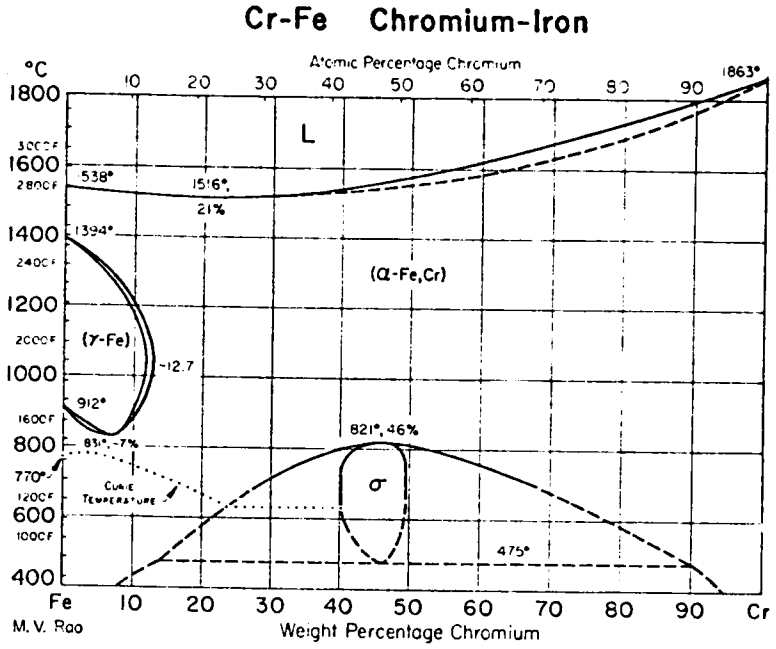


Figure II-2. Fe-Cr Binary Constitution Diagram.

Source: Metals Handbook (8th Edition), Volume 8, Metallography, Structures and Phase Diagrams, American Society for Metals, Metals Park, Ohio, p. 291 (1973).

influence the lattice parameters and c/a ratio to some extent.[16] Detailed x-ray studies have revealed that the majority of the atoms of sigma phase are arranged in two alternating quasi-hexagonal layers, but certain atoms are displaced to positions intermediate between the layers thus producing increased atomic packing.[98] There are five kinds of crystallographically equivalent positions for the 30 available atoms in the unit cell. Evidence obtained with the help of neutron diffraction[86] suggests that the sigma phases are somewhat ordered and that various atoms have a preference for one of the five positions.

Sigma Phase in Other Systems

Binary alloys. There are many binary systems where sigma phase is known to form. There are five well known systems where sigma forms, according to the work of Duwez and Baen[36] who have published their work in the ASTM Special Technical Publication (1950), Number 110, p. 48. The five published systems are Fe-Cr, Fe-V, Cr-Co, Cr-V, and Ni-V. In these systems, a definite relationship exists between composition and sigma phase. This is shown in Table II-1. It is clear from the table that sigma phase, whose presence was confirmed by many x-ray diffraction studies,[18,32] can deviate from the 50:50 (At.%) composition observed in the pure Fe-Cr system.

Sigma phase is an intermetallic compound, and its composition range is expected to be narrow. However, Wernick,[74] who studied some 39 well known and not so well known systems, found that sigma phase can

TABLE II-1

CHEMICAL COMPOSITION OF SIGMA PHASE
IN FIVE BINARY SYSTEMS

Alloy System	Composition (At.%)
Fe-Cr	50-50
Fe-V	48-52
Fe-V	58-42
Cr-Co	60-40
Co-V	50-50
Ni-V	50-50

Source: P. Duwez and S. R. Baen, "X-Ray Study of the Sigma Phase in Various Alloy Systems," published in ASTM Special Technical Publication, No. 110, Symposium on the Nature, Occurrence, and Effects of Sigma Phase, American Society for Testing and Materials, Philadelphia, Pennsylvania, p. 48 (1950).

have a broad chemical composition range (and temperature range of stability). This is shown in Table II-2.

Hall and Algie[80] have examined a larger number of sigma phases (than Wernick) occurring in many binary systems. The sigma phases, once again, were identified by x-ray diffraction. Hall and Algie found that the sigma phases had remarkably high hardness levels of up to Rockwell "C" 68. This hardness value is higher than the highest hardness for ferrons martensite that once can expect in the iron-carbon (Fe-C) system. With 100% martensitic structure, the highest hardness that can be obtained in an Fe-0.6% C steel typically is Rockwell "C" 66.[79]

Hall and Algie[80] showed that certain combinations of elements A and B tend to form sigma phase. One element from group V_A or VI_A of the periodic table* is called Type-A element, and the other, from the first, second, and third long period is called Type-B element. Such combinations where sigma phase may form are graphically shown in Figure II-3, after Hall and Algie[80] and in Figure II-4 after Nevitt and Beck.

It must be mentioned that the exchange factor--the fractional difference in the atomic radii $(r_A-r_B)/r_A$, expressed as percentage--partly governs the sigma phase formation in the binary systems where r_A = atomic radius for element A and r_B = atomic radius for element B. The exchange factors, as numbers, are listed in the upper right-hand corner of Figure II-3.

---

*See the latest "Periodic Table of the Elements," published by the Joint Committee on Powder Diffraction Standards, 1601 Park Lane, Swarthmore, Pennsylvania 19081. One such periodic table is reproduced in Appendix G.

TABLE II-2

COMPOSITION RANGES OF SIGMA PHASES
IN SEVERAL BINARY SYSTEMS*

System	Composition Range	System	Composition Range
VMn	13.4-24.5% V	CrCo	58-63% Cr
VFe	33.5-56% V	CrRu	63.5-66% Cr
VCo	43.5-68.0% V	CrRe	37.5-36.8% Cr
VNi	54.5-71%	CrOs	66% Cr
Nb_2Al		MoMn	40% Mo
NbNi		MoFe	50% Mo
NbRh	60% Nb	MoCo	60.5% Mo
NbPd	60% Nb	MoRu	60% Mo
NbRe	60% Nb	MoRe	33-52% Mo
NbOs	60% Nb	MoOs	65% Mo
NbIr	65% Nb	MoIr	70% Mo
NbPt	62.5% Nb	MoTc	25-30% Mo
Ta_2Al		WFe	60% W
TaRh	60% Ta	WCo	50% W
TaRe	50% Re	WRu	60% W
TaOs	50-75% Ta	WRe	37-58% W
TaIr	65-85% Ta	WOs	50-75% W
TaPt	68-82% Ta	WIr	70% W
CrMn	16-24% Cr	Cr_8Ni_5W	
CrFe	43-49% Cr		

*The percentages are atomic and only approximate.

Source: J. H. Wernick, "Topologically Closed-Packed Structures," published in Intermetallic Compounds (J. H. Westbrook, Editor), John Wiley and Sons, New York, p. 204 (1967).

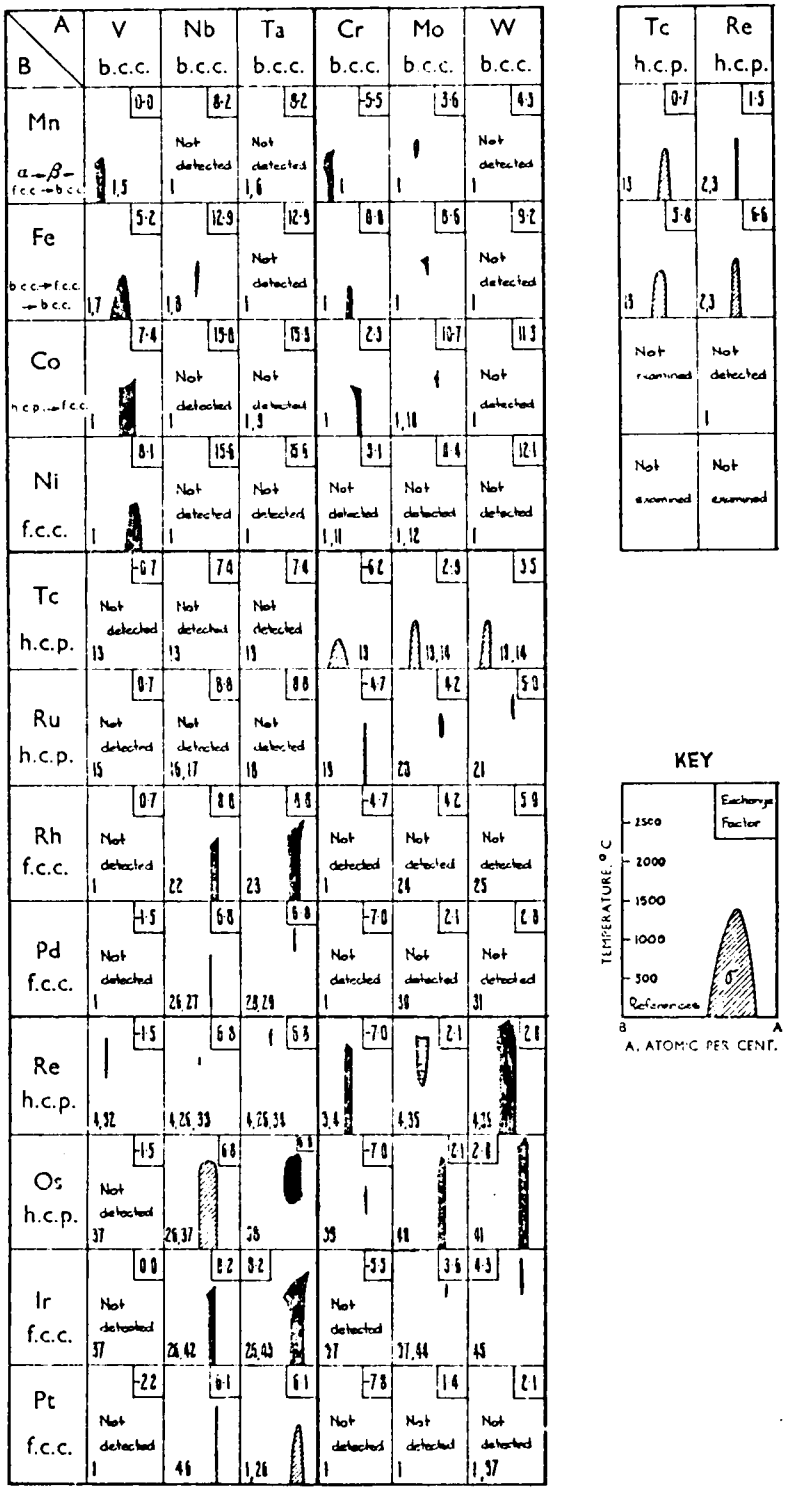


Figure II-3. Binary Sigma Phases.

Source: E. O. Hall and S. H. Algie, "The Sigma Phase," Review No. 104, J. Inst. Metals, Vol. 94, p. 61 (1966).

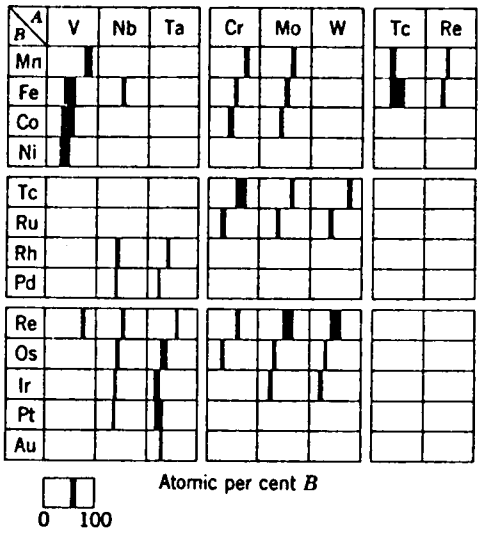


Figure II-4. Occurrence and Ranges of Stability of Binary Sigma Phases.

Source: After M. V. Nevitt in P. A. Beck (Editor), Electronic Structure and Alloy Chemistry of the Transition Elements, Wiley (Interscience), New York (1963).

Forty-two examples are shown in Figure II-3, but the systems Re-Fe, Te-Fe, Re-Mn, and Te-Mn do not fall under the definitions of Type-A and Type-B elements for sigma formation. These are anomalous examples. In addition, there are two instances of binary sigma phases containing aluminum, namely Nb-Al and Ta-Al, as well as another, Au-Ta. Eight other examples of sigma were reported in 1966 but have not been confirmed.(80)

Careful examination of both Figures II-2 and II-3 reveals that the ranges of composition of sigma phases are variable from system to system. In Figure II-4, it may be seen that ranges extending over several percent are possible. This type of behavior is characteristic of sigma phase (and many other intermetallic phases) and make it similar to the electron phases of noble metals.(98)

Since sigma phases are electron compounds, they appear at approximately constant values of electron/atom (e/a) ratios, as shown in Table II-3. Note that the e/a ratio is not a fixed constant.

The sigma unit cell in all binary cases studied is characteristically BCT in crystal structures with c/a ratio of $\simeq 0.52$.

Ternary and multicomponent alloys. Sigma phase also forms in many ternary systems just as they form in binary alloy systems. One immediate and important ternary system is Fe-Cr-Ni, where sigma phase is known to form in alloys containing about 18-30% Cr, 8-20% Ni, balance Fe, when aged below 900°C (<1650°F) for a long time. Other ternary systems where sigma is known to form are Fe-Cr-Mo, Fe-Mn-V, Fe-Cr-Co, Fe-Cr-W, Fe-V-Ni, and so on. Several ternary systems where sigma forms and their appropriate

TABLE II-3

E/A RATIO FOR SIGMA PHASE IN MANY BINARY ALLOY SYSTEMS

Binary System	e/a Ratio
Fe-Cr	7.00-7.12
Mn-Cr	6.76-6.84
Co-Cr	7.17-7.32
Mn-Mo	6.64
Fe-Mo	7.00-7.12
Co-Mo	7.20
Mn-V	6.52-6.66
Fe-V	6.20-6.92
Co-V	6.36-7.20
Ni-V	6.38-7.25
Fe-Nb	6.53-6.65

Source: E. O. Hall and S. H. Algie, "The Sigma Phase," Review No. 104, J. Inst. Metals, Vol. 94, pp. 61-88 (1966).

composition ranges are shown in Figure II-5, which is reproduced from the work of Hall and Algie.[80] The sigma which forms in the ternary systems, although crystallographically similar to that in the binary systems, is much different in chemical composition, as shall be seen later. Figure II-5 will also be explained in detail at a later stage because it describes many ternary systems of commercial applications.

When a third transition element is added to a binary alloy, as discussed before, the field of homogeneity is enlarged and often extends deep into the ternary section.[71,77] The extent and stability of sigma phase fields in ternary systems have been thoroughly discussed by Hall and Algie.[80] Certain results are shown in Figure II-5. Hattersley and Hume-Rothery[81] have shown that the phase stability in a ternary alloy A-B-C is controlled by the behavior of the binaries AB, BC, and CA, which means that not all elements can qualify as an additive to a binary system and be expected to extend the sigma range.

Most of the studies in ternary sigma phases are on alloys containing transition elements of the first long period of the "Periodic Table of the Elements" (see Appendix G). However, ternary sigma phases can have a nontransition element,[98] such as Al or Si, as not intentionally added material. The sigma phases on which extensive work has been done are Fe-Cr-Co, Ni-Fe-Cr, Ni-Cr-Co, Fe-Mn-Mo, Cr-Mn-Mo, Cr-Fe-Mo, Mo-Cr-Co, Fe-Mn-V, Co-Mn-V, Ni-Mn-V, Fe-Co-V, Fe-Ni-V, and Co-Ni-V. Referring to Figure II-5, it is clear that all areas arise as extensions of the known binary phase fields, with the exceptions of (Ni-Cr-Mo)σ, (Ni-Cr-W)σ, and (Ni-Cr-P)σ. The composition of the sigma is of the form

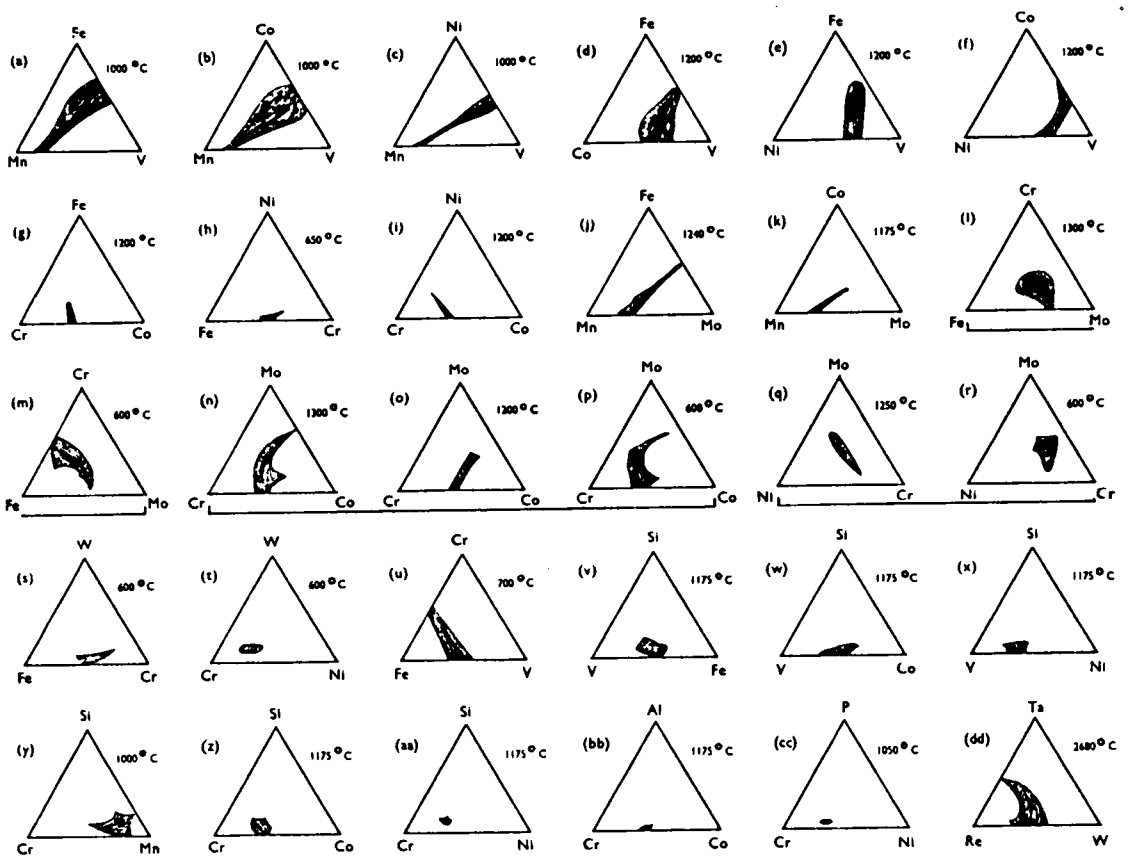


Figure II-5. Ternary Phase Fields.

Source: E. O. Hall and S. H. Algie, "The Sigma Phase," Review No. 104, J. Inst. Metals, Vol. 94, p. 61 (1966).

(CrMo)x (NiFe)y for a system having Cr, Mo, Ni, and Fe as components and x and y ≃ 1.[16]

The addition of certain elements, such as Si and P (electro-ve), have a stabilizing effect on sigma, whereas when other elements like aluminum (Al) are added in a concentration greater than 25 At.% to an Fe-Cr system, no sigma could be detected.[36] The elements carbon and nitrogen have a negative (retarding) effect on sigma formation in the Fe-Cr-Ni system[34] because of the depletion of matrix chromium by the formation of carbides or nitrides, respectively.

Alloys of chromium, nickel, and iron form the basis of many corrosion- and scale-resistant alloys.[89] They are also the principal ingredients or components of stainless steel alloys. Therefore, the phase equilibria of these alloys will be discussed.

The diffusion coefficient of nickel and chromium in iron is very, very slow and sluggish,[34] and, consequently, thermodynamic equilibrium in these alloys is hardly ever achieved. However, constitution diagrams developed by many researchers[18,34,71] over the years are available. One such diagram is reproduced in Figure II-6, which shows the Fe-Cr-Ni ternary isothermal section at 650°C, together with the three binary systems as a function of temperature. The relationship between the ternary section and the binaries Fe-Cr, Cr-Ni, and Ni-Fe systems is clearly observed.

In Figure II-7, Fe-C, Fe-Cr, and an isopleth for 70% Fe-Ni-Cr are shown for comparison purposes. In Figure II-6, it can be easily seen that as the Cr content is increased and Ni content decreased (keeping Fe content constant at 70%), one enters the phase field sigma in the

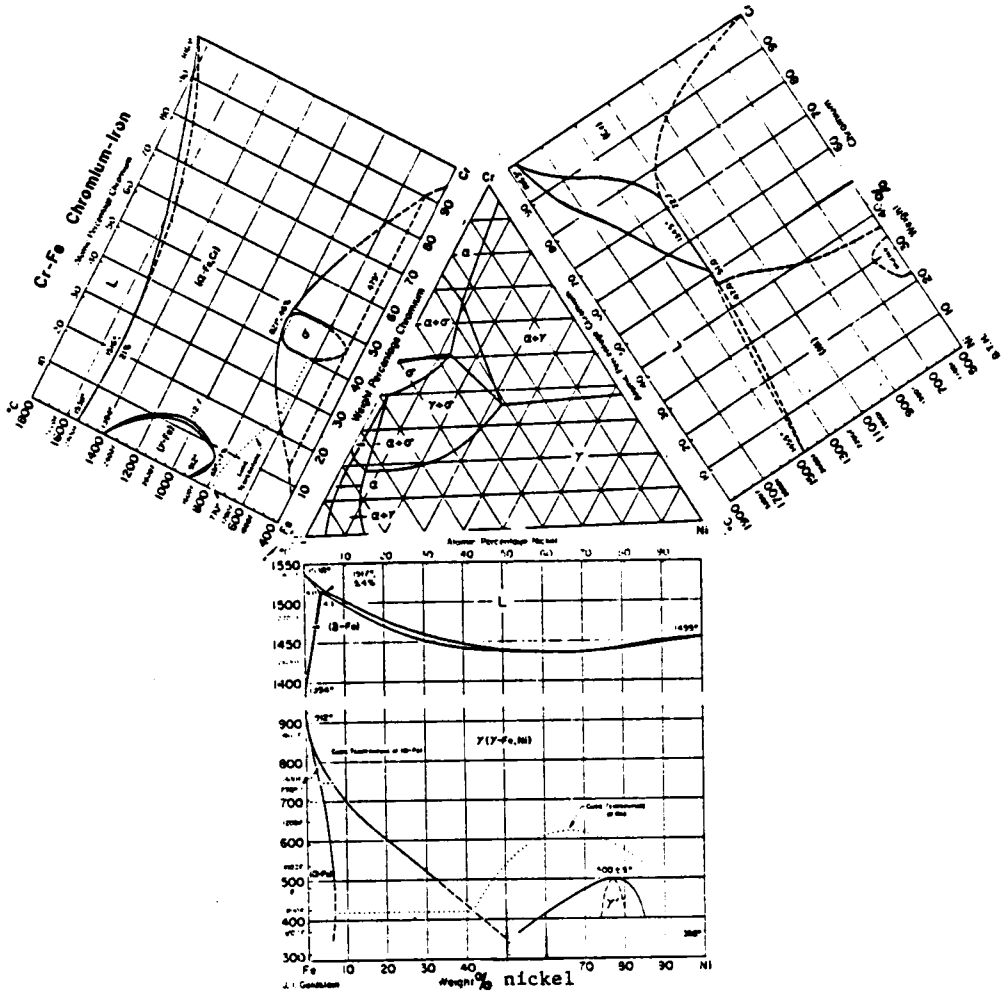


Figure II-6. Fe-Cr-Ni Isotherm at 650°C and the Binaries Fe-Cr, Fe-Ni, and Ni-Cr.

Source: Metals Handbook (8th Edition), Volume 8, American Society for Metals, Metals Park, Ohio (1973).

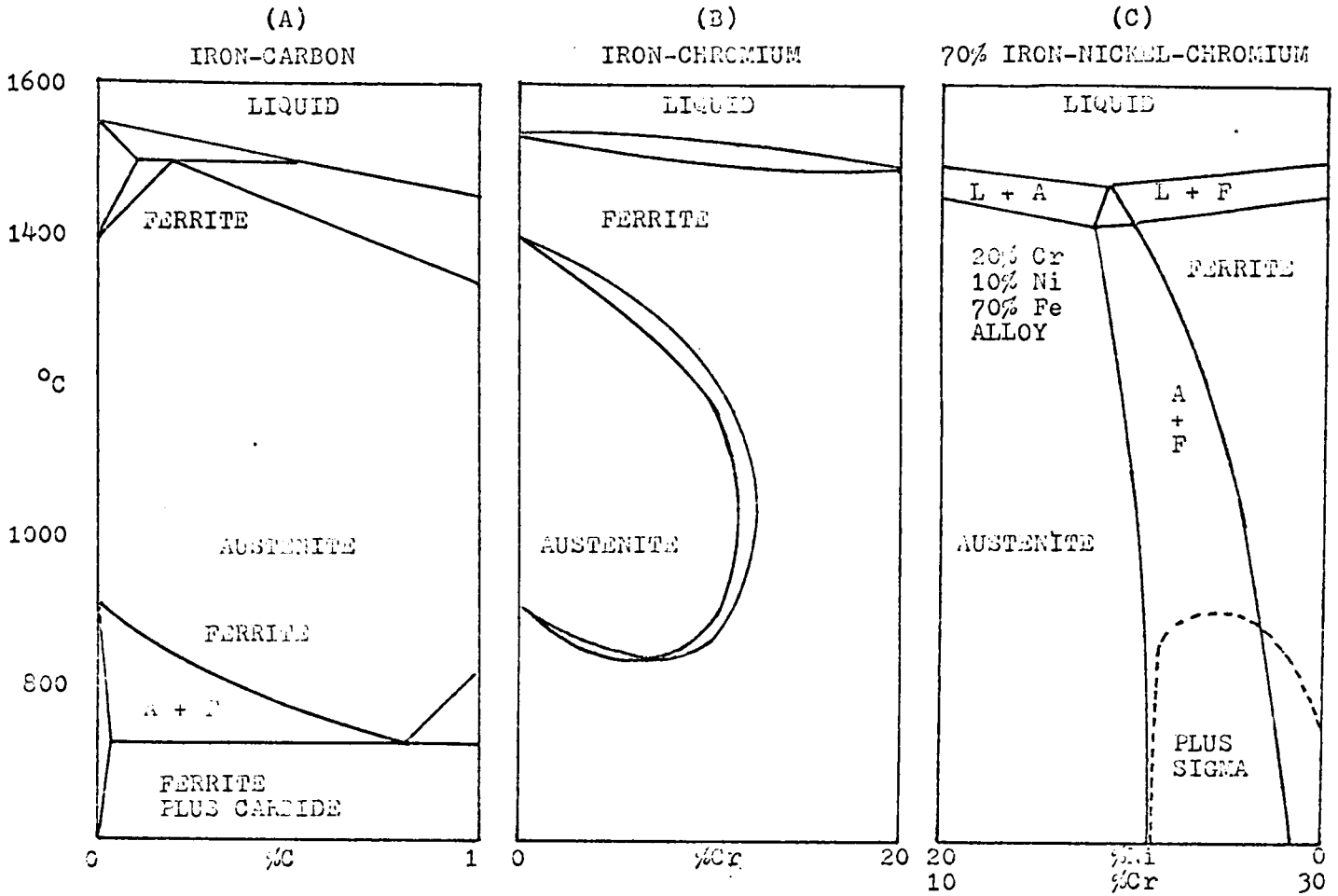


Figure II-7. Constitution Diagrams of Fe-C, Fe-Cr, and 70% Fe-Ni-Cr.

Source: Chang-Pin D. Chou, "The Effect of Ferrite Level on the Corrosion Resistance of Austenitic Stainless Steel Weld Metal," M.S. Thesis, The University of Tennessee, Knoxville, Tennessee, p. 5 (1977).

solid state below 900°C. As the temperature is increased, the sigma phase field narrows down significantly and ultimately disappears at 950-1100°C (1750-2000°F). This is shown in Figure II-8, published by Brooks[110] in his book Heat Treatment of Ferrous Alloys. In Figure II-7, the composition corresponding to a typical 18Cr-8Ni type austenitic stainless steel alloy is shown by a small circle.

Many stainless steel alloys involve more than three components. Consider a fourth element, such as carbon (C), to obtain a quaternary system consisting of Fe, Cr, Ni, and C as components. For such a system, the equilibrium relationships cannot be shown in two dimensions. This type of problem is often handled by keeping the three elements (Fe, Cr, Ni) constant and then varying the fourth element. Such a relationship is presented in Figure II-9 for an austenitic stainless steel of type 18-8. This diagram shows that for an alloy with 0.2% C in the 18-8 austenitic stainless steel, austenite is stable at ~1100°C (2000°F) or higher. This temperature increases with composition up to 0.6% C (approximately).

Morphology and Mechanism of Sigma Phase Formation

The development of morphology in metals and alloys is quite complex* and is not fully understood to date. However, it is known that it strongly depends on the nucleation and growth conditions of the growing phase in the parent matrix. Leitnaker and Bentley,[113] for example, noticed several distinct sigma phase morphologies in type 321 stainless steel.

---

*D. Turnbull and K. N. Tu, Phase Transformations, American Society for Metals, Metals Park, Ohio, p. 488 (1970).

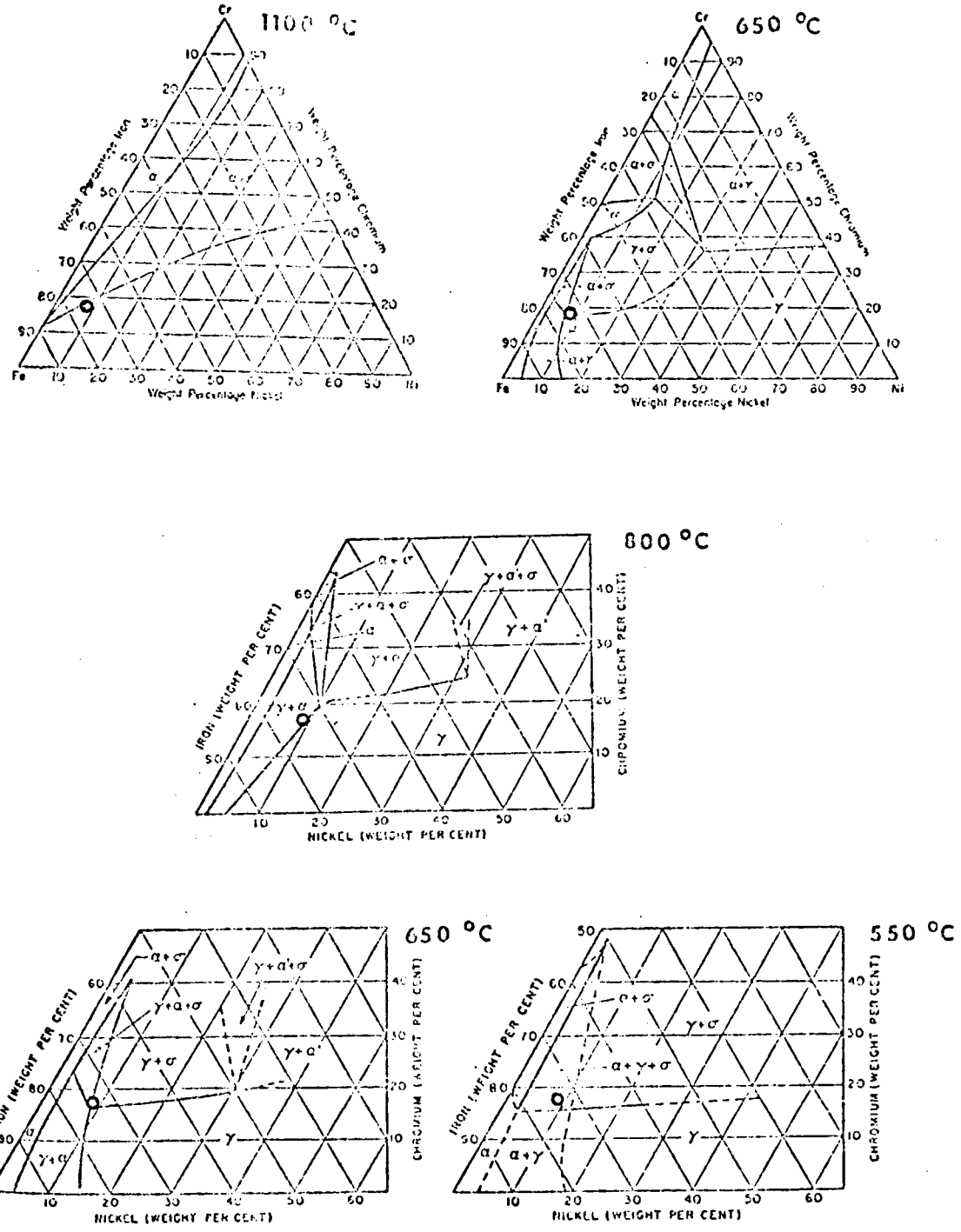


Figure II-8. Isothermal Sections from the Fe-Cr-Ni System. (The small circle locates the composition 18% Cr-8% Ni.)

Source: Upper two diagrams--Metals Handbook (8th Edition), Volume 8, American Society for Metals, Metals Park, Ohio (1973). Lower three figures--W. P. Rees, B. D. Burns, and A. J. Cook, "Constitution of Iron-Nickel-Chromium Alloys at 650-800°C," Journal of the Iron and Steel Institute, Volume 162, p. 325 (1949).

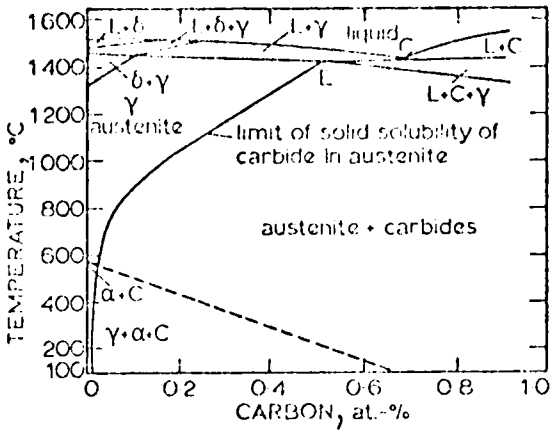


Figure II-9. Effect of Carbon on Solubility of Carbides in 18Cr-8Ni Steels.

Source: F. B. Pickering, "Physical Metallurgy of Stainless Steel Developments," Review 211, International Metals Reviews, pp. 227-268 (December 1976). (From F. H. Keating, Chromium-Nickel Austenitic Steels, Butterworths, London, by permission of the publishers.)

He found several crystallographic relationships between the sigma phase and the austenite matrix. His findings are as follows:

$[110]\gamma \quad || \quad [110]\sigma$

$[1\bar{1}2]\gamma \quad || \quad [112]\sigma \qquad \sigma$ = sigma phase

$(111)\gamma \quad || \quad (1\bar{1}1)\sigma \qquad \gamma$ = gamma (austenite matrix)

$(110)\sigma \quad || \quad (220)\gamma$

$[1\bar{1}1]\sigma \quad || \quad [\bar{1}12]\gamma$, and so on.

In their TEM investigations, Leitnaker and Bentley also found that the sigma phase varied in morphologies in its own appearance as well--from needle-like to massive globular in shape in the same alloy. Weiss and Stickler[16] have similarly noticed a variety of sigma morphologies in 316 aged stainless steels.

The sigma morphology has a strong influence on the mechanical properties* of steel. The amount, size, shape, and distribution all come under morphology. Marshall and Hooper[34] have mentioned that intragranular (within grains) sigma phase has less influence on mechanical properties than intergranular (along grain boundary) sigma particles, especially when associated with large grain size. In wrought-annealed steel (such as type 316), sigma phase occurs as globular particles at the austenite grain boundaries and triple grain junctions. However, in a duplex ferrite-austenite, as-cast steel, the sigma phase which may grow within the ferrite is generally a semi-continuous network structure.[22] This type of sigma is considered more detrimental on mechanical

---

*Frequently referred to at room temperature (25°C or 77°F). The effect is not as severe at elevated temperatures.

properties of steel than the sigma with globular to massive morphologies. When sigma is present in very fine dispersions throughout the matrix, it is considered not very harmful.[80]

The latest work by Leitnaker and Bentley[113] summarizes that there is no fixed orientation relationship between the sigma phase and the austenite matrix. They conclude that there is little difference in free energy among a number of sigma-matrix orientations.

Sigma phase has been found to precipitate at locations of high free energies which provide a driving force for the precipitation reaction. Such locations are usually dislocations, twin boundaries, triple grain junctions, stacking faults, grain boundaries, and foreign objects such as oxide or carbide inclusions.[34,80]

Various factors affecting sigma formation which have been proposed in the literature are discussed below:

1. Formation of sigma phase needs a favorable (small) exchange factor $[(r_A-r_B)/r_A] \times 100$, as shown in Table II-4, which is taken from the work of Hall and Algie.[80] For Fe-Cr systems, the exchange factor is 0, so sigma phase formation is favorable.
2. Similarity in crystal structure also favors sigma formation. For example, ferrite is BCC and sigma is BCT. Therefore, a little distortion of the BCC ferrite phase may generate a BCT sigma phase.[12,16]

In austenitic stainless steels, especially in welds, some amount of ferrite is always present to minimize hot cracking tendency of the

TABLE II-4

EXCHANGE FACTOR OF SOME ALLOY SYSTEMS

System (A-B)	Exchange Factor*	Comment
Fe-Cr	0.0	σ-favorable
Mn-Cr	-5.5	
Co-Cr	2.3	
Mn-Mo	3.6	
Fe-Mo	8.6	
Co-Mo	10.7	σ-less favorable
Mn-V	0.0	σ-favorable
Fe-V	5.2	
Co-V	7.4	
Ni-V	8.1	

*Exchange Factor (EF) expressed as % = $(r_A - r_B / r_A) \times 100$ where r_A and r_B = the atomic radii of the elements A and B in the system A-B, respectively.

Source: E. A. Hall and S. H. Algie, "The Sigma Phase," Review No. 104, J. Inst. Metals, Vol. 94, p. 94 (1966).

weld. When such is the case, the ferrite easily transforms to sigma phase because of the following reasons:

1. Atomic mobility is greater in ferrite than in austenite since austenite (FCC) is a more closely packed structure (four atoms per unit cell) as compared to ferrite (two atoms per unit cell).
2. The preferential precipitation of carbides in the ferrite sites concentrates the alloying elements locally or distorts the ferrite lattice and thereby facilitates the formation of sigma phase.
3. The segregation of chromium in ferrite in preference to austenite tends to produce ferrite areas which are considerably higher in chromium than the nominal alloy composition would indicate.
4. Due to the presence of some carbon in stainless steels, carbide $Cr_{23}C_6$, or in general, $M_{23}C_6$ is formed, where M is a carbide forming element. Once $M_{23}C_6$ is formed, sigma forms around the $M_{23}C_6$ carbide which provides nucleating sites. However, Blenkinshop and Nutting[11] oppose this theory.
5. In commercial stainless steels, there are trace elements, such as titanium and silicon. The precipitation of sigma phase upon prolonged aging may be interpreted in terms of the effect of Ti and Si upon the ECC (equivalent chromium content[14] expressed as ECC = Cr (wt.%) - 0.226 Ni (wt.%)) of the matrix.

Such elements, particularly Ti, have a stabilizing effect on sigma, as found by Grot and Spruiell.[91]

6. In stainless steel, carbides are formed due to the presence of carbon. This carbide, $M_{23}C_6$, may be decarburized, which could result in a topochemical transformation to sigma phase, as suggested by Goldschmidt.[60] This theory is in agreement with that of Sims,[39] who postulated that "if all carbon atoms are removed from an $M_{23}C_6$ lattice, then a slight shift in atom relationship would be needed for the structure to become that of sigma." However, it should be noted that decarburization is not always necessary for sigma phase to occur in stainless steels.

2. EFFECT OF SIGMA PHASE ON PROPERTIES OF STAINLESS STEEL

Physical Properties of Sigma Phase

Little experimental work has been done to determine the physical properties of sigma phases. However, some conclusions will be made from the available literature.

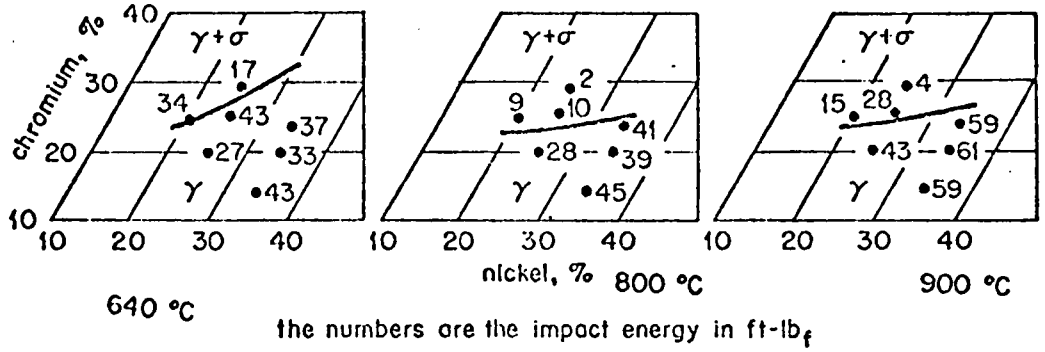
Magnetic properties. At room temperature, most sigma phases are nonmagnetic, but Beck[87] found ferromagnetism at liquid-nitrogen temperature in certain cases. This low-temperature ferromagnetism was confirmed and proved to be the general case, at least for the first long "Periodic Table of the Elements" transition-metal sigma phases--in particular, (Fe-Co-Cr)σ, (Fe-Cr-Mo)σ, and (Co-Cr-Mo)σ.

Electronic and electric properties. Sigma phase may be a full-zone structure, as indicated by Kazantsev,[88] who found that during the transition of ferrite (α) to sigma (σ) the conductivity was reduced by a factor of 1/40 or 0.025. It was suggested that during the alpha ferrite to sigma transition, a transfer of electrons between the 3d and 4sp shells was necessary to explain Kazantsev's results. Sigma phase also shows negative temperature coefficient of resistivity. The room temperature resistivity for a Co-V sigma has been reported to be of the order of 320 micro-ohm ($\mu\Omega$) cm.[80]

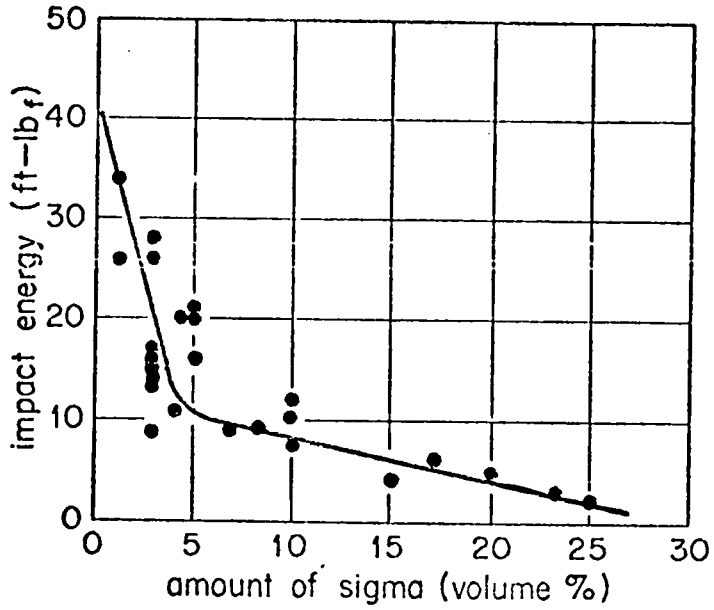
Hardness of sigma phase. The sigma phase is very hard (and brittle) at room temperature. Bain and Griffiths[59] have reported the hardness for (Fe-Cr)σ to be Rockwell "C" 68 (940 Diamond Pyramid Hardness, DPH). However, in (Fe-Cr-Ni)σ, the hardness was determined to be 750 DPH (Rc62) by Dulis and Smith.[36] The brittleness is such that Bain and Griffiths found the sigma phase to fracture into pieces during hardness testing. It has been suggested that the brittleness of (Fe-Cr)σ at room temperature was attributed to the difficulties of generating dislocations in an ordered lattice[80] such as sigma.

Effect of Sigma Phase on Properties (Mechanical, Chemical, etc.) of Stainless Steels

In stainless steels, the presence of sigma decreases ductility and impact strength at room temperature.[67] The detrimental effect of sigma on mechanical properties, such as impact energy, in austenitic stainless steel is shown in Figure II-10.



(a) Isothermal sections of the Fe-Cr-Ni ternary phase diagram illustrating the influence of the presence of sigma on the 20°C impact energy. (The steels were solution-annealed for one hour at ~1060°C, water-quenched, then aged at the indicated temperatures for 3000 hours.)



(b) Relation between the amount of sigma present and the 20°C impact energy.

Figure II-10. Relationship Between the Impact Energy at 20°C and Sigma Formation in Austenitic Stainless Steels. (Ni content between 20 and 35%; Cr content between 14 and 29%.)

Source: C. R. Brooks, The University of Tennessee, Knoxville, Tennessee (1976). (Adapted from A. M. Talbot and D. E. Furman, "Sigma Formation and Its Effect on the Impact Properties of Iron-Nickel-Chromium Alloys," Transactions of the American Society for Metals, Volume 45, p. 429 (1953).

The room temperature tensile and yield strengths, which are shown in Table II-5, do not indicate any recognizable trend with increasing amounts of sigma phase. It is, therefore, postulated that relatively small amounts of sigma in a ductile matrix do not affect the room temperature tensile and yield strengths significantly.[34,36]

The effect of aging temperature on room temperature impact values and ductility for a 25Cr-20Ni alloy steel after Emmanuel[36] are represented in Figures II-11 and II-12, respectively. A more definite trend was exhibited by the elongation and reduction of area (RA) values, both of which reach a minimum in samples aged between 1400-1600°F (760-870°C) as shown in Figure II-11. This range was found to be the one in which sigma formation was a maximum. The room temperature ductility after exposure to 1700°F (930°C), at which no sigma was generated, is markedly improved. Likewise, the impact values of the aged specimens follow a similar trend, as shown in Figure II-12. Again, minimum room temperature impact strength is noted in the said temperature range where sigma formation is said to be maximum in the 25Cr-20Ni alloy steels.

Data on low-temperature (cryogenic temperatures) mechanical properties for the aged stainless steels are lacking in the literature. However, K. G. Brickner and J. D. Defilippi (U.S. Steel Corporation Research Laboratory), on p. 24 of the 1977 Handbook of Stainless Steels, report that types 304, 304L, 310, and 347 wrought (annealed) austenitic stainless steels exhibit good ductility and excellent toughness even at -253°C (-428°F). They further conclude that although there are differences in the energy absorbed in impact tests by the various austenitic

TABLE II-5

ROOM TEMPERATURE TENSILE AND YIELD STRENGTH PROPERTIES OF TYPE 310 ALLOY AGED AT VARIOUS TIMES AND TEMPERATURES

Condition of Sample	Yield Strength, 2% Offset (psi)	Tensile Strength (psi)
Annealed	46,200	92,000
48 hr. at 1000°F	48,100	90,700
500 hr. at 1000°F	41,100	92,200
1000 hr. at 1000°F	47,300	91,600
100 hr. at 1200°F	55,500	89,000
300 hr. at 1200°F	54,800	88,000
500 hr. at 1200°F	64,500	89,300
1000 hr. at 1200°F	40,500	87,800
1 hr. at 1400°F	45,800	91,600
3 hr. at 1400°F	46,300	90,800
24 hr. at 1400°F	43,600	89,200
48 hr. at 1400°F	40,500	79,500
500 hr. at 1400°F	39,750	89,600
1000 hr. at 1400°F	34,800	90,200
1 hr. at 1600°F	42,400	90,200
3 hr. at 1600°F	39,900	89,800
48 hr. at 1600°F	54,000	88,000
100 hr. at 1600°F	42,000	87,000
500 hr. at 1600°F	45,900	87,200
1000 hr. at 1600°F	42,700	87,100
1 hr. at 1700°F	47,500	89,300
3 hr. at 1700°F	48,000	88,500
100 hr. at 1700°F	57,000	84,750
200 hr. at 1700°F	43,500	81,100
500 hr. at 1700°F	37,300	76,500
1000 hr. at 1700°F	36,800	77,000

Source: G. N. Emmanuel, Symposium on the Nature, Occurrence, and Effects of Sigma Phase, ASTM STP No. 110, American Society of Testing and Materials, Philadelphia, Pennsylvania, p. 82 (1950).

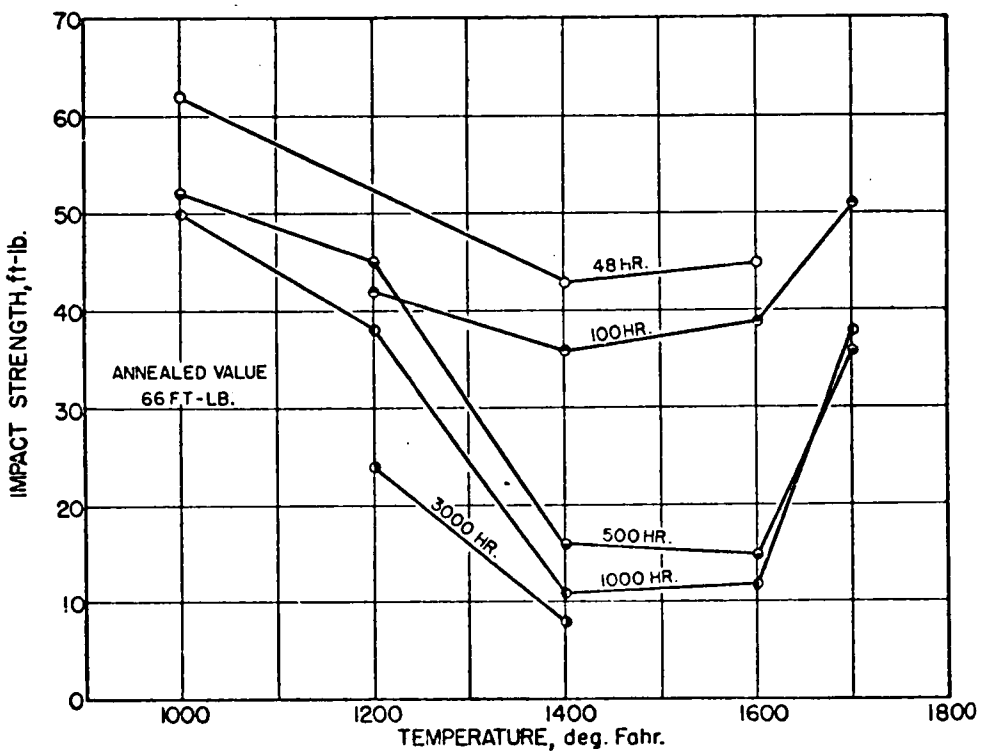


Figure II-11. Effect of Time and Temperature on Room Temperature Impact Values of 25Cr-20Ni Alloy.

Source: G. M. Emmanuel, Symposium on the Nature, Occurrence, and Effects of Sigma Phase, ASTM STP No. 110, American Society of Testing and Materials, Philadelphia, Pennsylvania, p. 86 (1950).

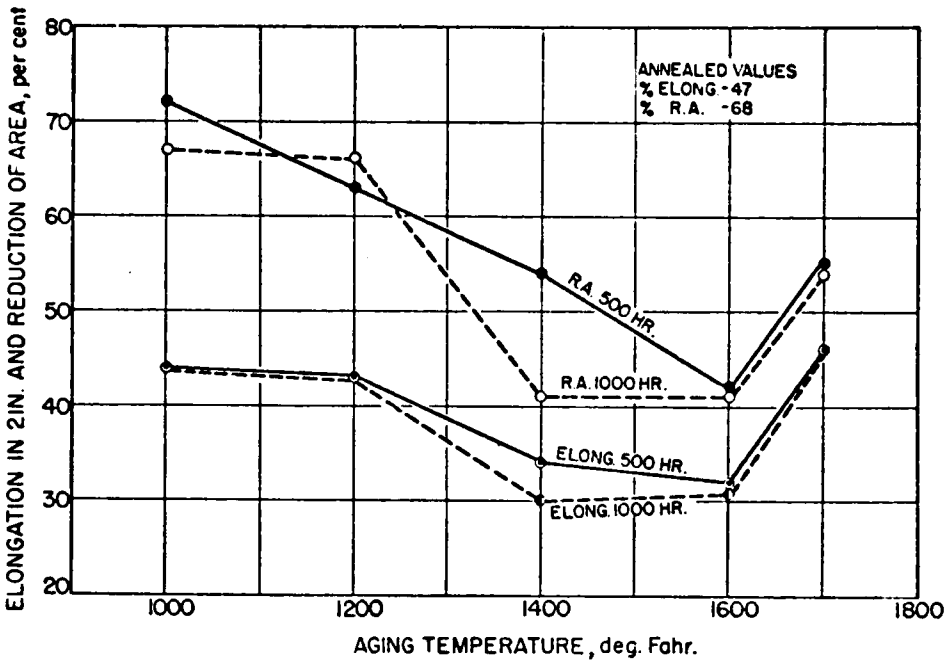


Figure II-12. Effect of Time and Temperature on the Ductility of 25Cr-20Ni Alloy Steel.

Source: G. M. Emmanuel, Symposium on the Nature, Occurrence, and Effects of Sigma Phase, ASTM STP No. 110, American Society of Testing and Materials, Philadelphia, Pennsylvania, p. 86 (1950).

stainless steels, these differences may not significantly affect their engineering performance.

Although room temperature mechanical properties, such as toughness, of the aged austenitic stainless steels rapidly fall off with the increase of sigma content of the specimen, tests conducted at high temperatures show relatively little adverse effects.[36,80] (See Table II-6.) It may be seen from the data that increasing temperature will restore a certain amount of toughness to a previously sigmatized 25Cr-20Ni alloy steel.

The effect of sigma on high-temperature mechanical properties[80,112] are:

1. Sigma may increase creep strength up to 760°C for short-term applications involving deformation of the order of 1% per hour.
2. At a slow rate of strain, sigma decreases creep strength.
3. Sigma increases short-term tensile and creep strengths.
4. If conditions of formation are such that the sigma is finely dispersed within the grains, an increase in both ambient and elevated temperature strength can result.[112]

Hills and Harries[100] have carried out indepth studies of the effect of sigma on mechanical properties at room and elevated temperatures in Fe-Ni-Cr alloys containing 0.07-0.14% carbon. They also found that the effect of sigma (up to 14% sigma) is more severe on the room temperature mechanical properties (such as % RA, impact energy, UTS, and % elongation)

TABLE II-6

EFFECT OF SIGMA ON TOUGHNESS AT ELEVATED TEMPERATURES FOR AN Fe-25Cr-20Ni ALLOY STEEL

Initial Condition (Aging)	Sigma Content After Aging	Testing Temperature	Impact Strength (ft-lb)
1000 hr. at 1200°F (650°C)	4-8%	77°F (25°C)	38
		1200°F (650°C)	36
		1400°F (760°C)	44
1000 hr. at 1400°F (760°C)	>8%	77°F (25°C)	11
		1200°F (650°C)	18
		1400°F (760°C)	19
1000 hr. at 1600°F (870°C)	>8%	77°F (25°C)	12
		1200°F (650°C)	19
		1400°F (760°C)	22
1000 hr. at 1700°F (930°C)	0-4%	77°F (25°C)	38
		1200°F (650°C)	50
		1400°F (760°C)	53

Source: G. N. Emmanuel, Symposium on the Nature, Occurrence, and Effects of Sigma Phase, ASTM STP No. 110, American Society of Testing and Materials, Philadelphia, Pennsylvania, p. 82 (1950).

than at elevated temperatures. Their elevated test temperatures varied from 540-980°C (1000-1800°F).

One of the most important chemical effects of sigma phase on stainless steel is related to corrosion in acid media. This will be briefly discussed.

Sigma phase, when present in fine dispersions, particularly around the grain boundaries, does markedly reduce the resistance to attack by nitric acid and sulphuric acid. This is shown in Figure II-13. However, when sigma phase occurs as large particles, corrosion resistance did not decrease significantly.(80) Since sigma phase is a compound that contains chromium, it is expected that when sigma phase forms, the chromium level in the matrix will be reduced and will thereby decrease the corrosion resistance of the alloy.

Chemically, sigma phase itself is not resistant to strongly oxidizing media like hot concentrated nitric acid. In such a medium, an alloy with intergranular sigma will undergo intergranular corrosion.(112)

3. SEMI-QUANTITATIVE PREDICTION OF SIGMA PHASE FORMATION IN AUSTENITIC STAINLESS STEEL ALLOYS

Earlier Concepts--Theory of Gow and Harder

Prediction of sigma phase in the simple Fe-Cr system or in Fe-Cr-Ni multicomponent systems is difficult if one relies solely on the so-called "equilibrium" diagrams (or constitution diagrams) because of the sluggishness of the reactions where "true" equilibrium is rarely achieved. Sigma became a problem during World War II in aircraft engines utilizing iron-base austenitic alloys with 15-25% chromium. One such

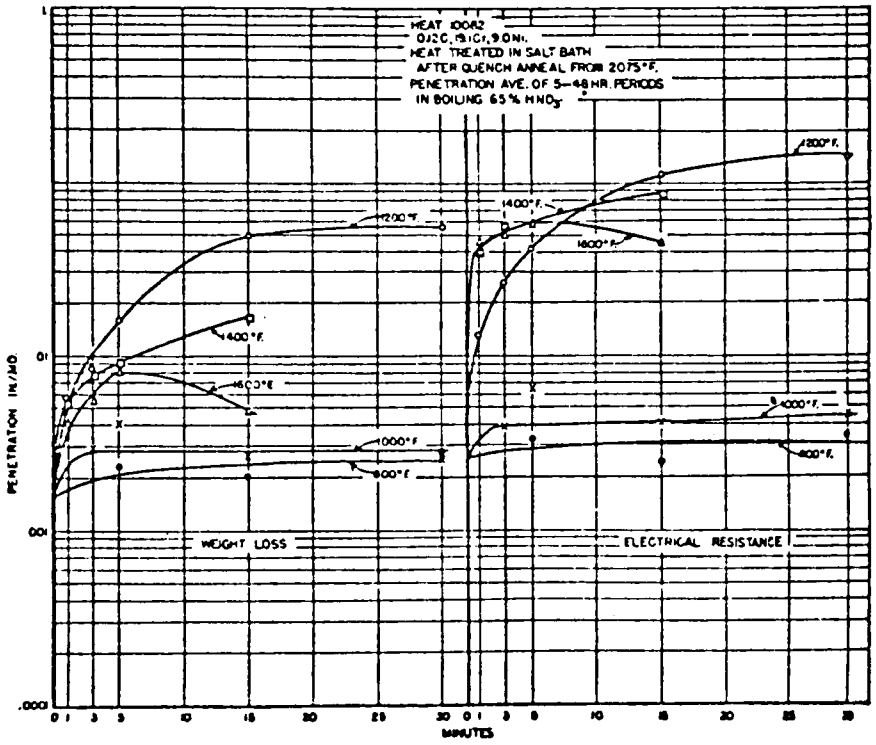


Figure II-13. Corrosion Rates of a 0.12% C, 19.1% Cr, and 9.0% Stainless Casting in Nitric Acid After Sensitization at 800-1600°F (425-870°C) for One to Three Minutes.

Source: E. O. Hall and S. H. Algie, "The Sigma Phase," Review No. 104, J. Inst. Metals, Vol. 94, pp. 61-88 (1966).

alloy is type HH alloy (Fe base, cast 16% Cr-12% Ni), which is prone to sigma formation upon aging. The question was whether the alloy was safe for elevated-temperature application. To tackle this problem, in 1942 Gow and Harder[38] proposed the empirical equation (called "ratio factor" or simply RF):

$$RF = \frac{(\%\ Cr - 16\%\ C)}{\%\ Ni} = 1.7 \qquad \text{(II-1a)}$$

to define the approximate boundary between the phase which contained sigma or ferrite (or both) and the wholly austenitic phase. They postulated that only those alloys with ratio factors of less than 1.7 could be wholly austenitic and, thus, less prone to sigma formation.

Qualitatively, this equation makes sense because increasing the carbon or nickel content of the alloy will have a tendency to decrease the RF and, thus, make the alloy less susceptible to embrittlement by sigma formation, as carbon and nickel are austenite stabilizers. On the other hand, increase of Cr content (ferrite stabilizer) will have just the opposite effect by increasing the RF.

Despite the merit of Gow and Harder's equation, the relationship ran into problems because it only applied to a single alloy, and the relationships are too qualitative to be useful in alloy development. For example, the alloy did not account for the effect of silicon, which invariably occurs in the Fe-Cr-Ni alloys. Jackson[36] proposed a modified RF to accommodate for the effect of silicon, as follows:

$$RF = \frac{[\%\ Cr + 3(\%Si-1) - 16\%\ C]}{\%Ni} \qquad \text{(II-1b)}$$

From this relationship, one can see that silicon is important, but not anywhere near so effective as carbon, in affecting sigma or ferrite formation.

Because of problems associated with the RF concepts in predicting sigma in Fe-Cr-Ni alloys, other semi-empirical approaches, such as equivalent chromium content and electron vacancy number theories, were developed, as shall be seen next.

Theory of Equivalent Chromium Content (ECC)

Like Gow and Harder,[38] Hull[14] (Westinghouse Research Laboratories, Pittsburgh, Pennsylvania) realized that austenitic stainless steels are complex, multicomponent alloys and that prediction of sigma phase by the application of rigorous thermodynamic approaches or kinetic theories (to be discussed in a separate section) in these alloys was virtually intractable for all practical purposes. Therefore, he felt that it was necessary to consider semi-empirical or semi-quantitative approaches to tackle the problem. Therefore, in 1973 he conducted a series of charpy notched-impact bend ductility tests[95] on his chill-cast 16Cr-20Ni-10Mn-2.25Mo-Fe Kromarc* alloys after exposing these alloys for long aging time (1000 hours) at 816°C (1500°F). Hull studied chill-cast samples of various alloys (where sigma formed) and developed the element coefficients by multiple regression analysis. His expression is:

---

*Kromarc alloy is the registered trademark of the Westinghouse Electric Company.

$$\begin{aligned} ECC = {} & Cr\ (wt.\%) + 0.31\ Mn\ (wt.\%) + 1.76\ Mo\ (wt.\%) \\ & + 0.97\ W\ (wt.\%) + 2.02\ V\ (wt.\%) + 1.58\ Si\ (wt.\%) \\ & + 2.44\ Ti\ (wt.\%) + 1.70\ Nb\ (wt.\%) + 1.22\ Ta\ (wt.\%) \\ & - 0.226\ Ni\ (wt.\%) - 0.177\ Co\ (wt.\%). \end{aligned} \qquad \text{(II-2)}$$

Thus, by knowing the chemical composition of an austenitic stainless steel alloy, one can compute the ECC merely by substituting the chemical composition into Equation (II-2). The lower the computed ECC, the less susceptible the alloy to embrittlement by the formation of intermetallic sigma phase. Conversely, the higher the ECC, the more susceptible the alloy to sigma formation. Hull never arrived at an absolute number for ECC above which sigma will form, but looking at his results (Figure II-14 and Table II-7), sigma forming alloys are those where the ECC values are approximately 17 or higher. Note that there was a large scattering of data in Hull's test, as one can see from Table II-7. This was partly attributed to the sub-size Charpy impact test (Figure II-15) (based on the ASTM E23-72[95]), which used only small, 25-gm (1/4-inch-diameter) tapered pins where reading of the bend angles is more susceptible to human error than for standard Charpy tests. Nevertheless, Hull's results and their interpretation seem to be in agreement with the expected embrittlement behavior of the alloys. For example, the coefficient -0.226 for nickel in Equation (II-2) is qualitatively correct since nickel is an austenite stabilizer, and its tendency is to increase the bend angle (see Figure II-16) with the increase of nickel content of the alloys and, thus, produce less susceptibility to sigma formation upon aging. On the other hand, Cr, which is known to promote sigma formation upon aging, has a negative slope in

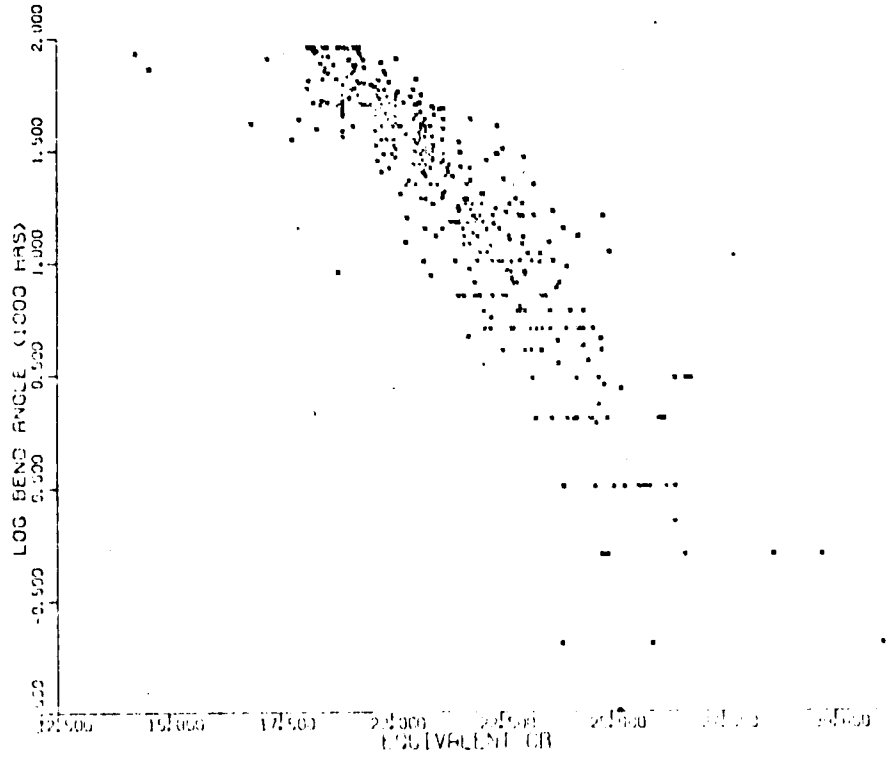


Figure II-14. Bend Angles Vs. Equivalent Cr Content of Kromarc Alloys After Aging for 1000 Hours at 816°C (1500°F).

Source: F. C. Hull, "Effects of Composition on Embrittlement of Austenitic Stainless Steels," Welding Journal, Vol. 52, p. 104-S (1973).

TABLE II-7

ESTIMATES OF COEFFICIENTS, STANDARD ERRORS, F-RATIOS, AND CHROMIUM EQUIVALENTS IN MODELS RELATING IN θ TO COMPOSITION FOR CAST STAINLESS STEELS AGED AT 1500°F (816°C)

Estimates of Coefficients, Standard Errors, F-Ratios and Chromium Equivalents in Models Relating ln θ to Composition for Cast Stainless Steels Aged at 1500 F (816 C) in Data Set I

	As cast				Aged 17 hr at 1500 F				Aged 100 hr at 1500 F				Aged 1000 hr at 1500 F			
Term	Coeff.	Std Er	F-Ratio	Cr Equiv.	Coeff	Std Er.	F-Ratio	Cr Equiv.	Coeff	Std Er.	F-Ratio	Cr Equiv.	Coeff	Std Er.	F-Ratio	Cr Equiv
Constant	8 733	.75			13 052	.73			15 722	.60			18 896	44		
Cr	-.183	.029	40	1 00	-.395	.031	161	1.00	-.554	.027	428	1 00	-.742	.021	1275	1 00
Mn	-.064	.018	13	.35	-.118	.015	61	.30	-.181	014	165	.33	-.236	011	457	32
Mo	-.352	.050	50	1.92	-.605	.053	233	2 03	-.975	.039	620	1.76	-1.215	028	1832	1 64
W	—	—	—	—	-.306	.050	37	.77	-.526	.042	154	.95	-.639	.034	342	66
V	-.333	044	56	1 82	-.673	.053	161	1 70	-.925	.048	372	1 67	-1.278	051	622	1 72
Si	-.325	.098	11	1 77	-.733	.11	44	1 85	-.831	.096	76	1 50	-.855	077	123	1 15
Ti	-.327	.108	9	1.78	-1.101	.12	91	2.79	-1.228	.104	138	2 22	-1 272	.085	225	1 72
Cb	-.507	052	95	2.77	-1.043	.061	291	2 64	-.913	053	301	1.64	-.720	042	288	97
Ta	-.210	.047	20	1.16	-.490	.055	80	1.24	-.501	.048	109	.90	-.432	039	123	58
Ni	.0277	.0051	29	-.151	.076	.0061	154	-.192	.114	.0048	551	-.205	.137	.0036	1421	-.185
Co	.0077	.012	0.4	-.042	.073	.013	34	-.185	.086	.0068	160	-.156	.120	.0045	707	-.162
No of observations	=	72				113				178				218		
F-ratio of regression	=	12.8				40				94				256		
Standard error	=	.313				.398				.390				.335		
Coeff of determination, R^2	=	.677				.813				.862				.932		

Source: F. C. Hull, "Effects of Composition on Embrittlement of Austenitic Stainless Steels," Welding Journal, Vol. 52, p. 104-S (1973).

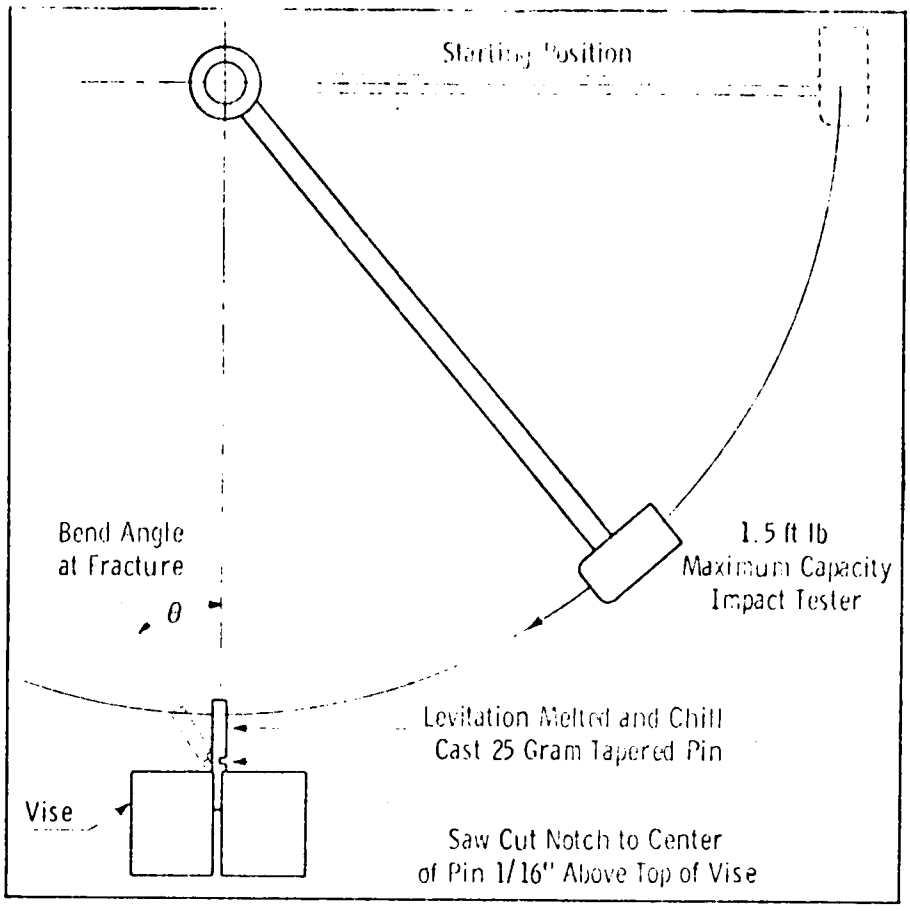
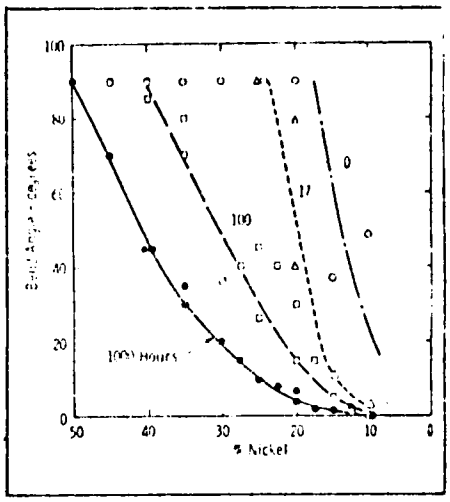


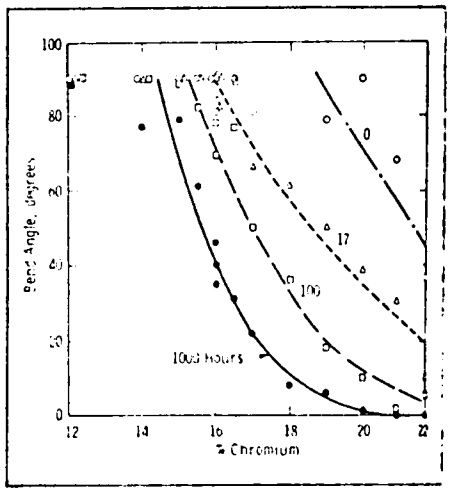
Figure II-15. Simple Impact Test to Evaluate the Embrittlement of Cast Stainless Steel Pins on Aging.

Source: F. C. Hull, "Effects of Composition on Embrittlement of Austenitic Stainless Steels," Welding Journal, Vol. 52, p. 104-S (1973).



Effect of aging at 1500 F (816 C) on the notched impact bend angle of 1/4 in. diam cast pins of steels containing 16% Cr, 10-50% Ni, 10% Mn, 5% Mo, balance Fe

(A)



Effect of aging at 1500 F (816 C) on the notched impact bend angle of 1/4 in. diam cast pins of steels containing 12-22% Cr, 20% Ni, 10% Mn, 0.1% Si, 3% Mo, balance Fe

(B)

Figure II-16. Bend Angles Vs. Compositions of the Kromarc Alloys (1/4-Inch-Diameter) Upon Aging for 1000 Hrs. at 816°C (1500°F).

Source: F. C. Hull, "Effects of Composition on Embrittlement of Austenitic Stainless Steels," Welding Journal, Vol. 52, p. 104-S (1973).

Figure II-16, meaning, thereby, that increase of Cr content of the alloy decreases the bend angle of the aged specimens and makes them more susceptible to embrittlement by sigma precipitation.

One of the objectives of Hull's experiment was to determine how much of various alloying elements could be added to a fully austenitic steel without the steel becoming susceptible to embrittlement during long-time service at elevated temperatures. It appears that Hull did achieve his objective in the as-cast stainless steel alloys which are prone to chemical segregation. Hull's semi-quantitative approach also has received good reviews recently by Grot and Spruiell[91] and Leitnaker and Bentley,[113] who mentioned that "Hull's equation is a good approximation" because higher chromium content makes a steel more susceptible to sigma formation. In essence, it is just a convenient method to account for the shift in the $\sigma+\gamma/\gamma$ phase boundary on addition of other alloying elements and the consequent change in driving force or free energies for sigma to form.

However, there are several important points that must be addressed in order to fully assess the theory of equivalent chromium content. First, the theory was applied only to fully austenitic, as-cast alloys. How valid this approach would be for solution-treated (wrought-annealed) stainless steel alloys is not known. Second, Hull did not take the effect of carbon into account to compute the ECC of the alloy. Carbon is a very strong austenitic stabilizer. In order that the theory of ECC be valid, correction due to carbide precipitation upon aging should have been taken into account. Although Hull mentions that his alloys had only 0.002-0.005% carbon, in actual practice, many alloys would have

carbon content greater than this value, where the effect of carbon on ECC (and, hence, sigma) would be more significant by the formation of carbides reducing the chromium content of the austenite matrix. Finally, Hull actually measured "embrittlement" rather than sigma content. It is not clear to what extent this may bias his results.

Theory of the Electron Vacancy Number (EVN)

Another semi-empirical or semi-quantitative approach to the prediction of sigma phase formation in austenitic stainless steel alloys is referred to as "the theory of electron vacancy number," or simply EVN or $\bar{N}v$ theory. This theory, originally due to Pauling[97] and later developed by Beck,[87] is based upon the assumption by Sully and Heal[116] that the intermetallic compound sigma phase is also an electron compound which forms in the alloy systems at certain fixed valence electron to atom ratios.[118] This approach, which is based upon the theory of alloy phases, was successfully applied by Woodyatt et al.[117] to the complex nickel-based austenitic super alloys. Woodyatt et al.[117] indicated that the average electron vacancy number, $\bar{N}v$, is given by:

$$\begin{aligned}\bar{N}v = {} & 4.66\ \text{Cr (At.\%)} + 10.00\ \text{Mo (At.\%)} + 4.66\ \text{W (At.\%)} \\ & + 5.66\ (\text{V} + \text{Nb} + \text{Ta};\ \text{At.\%}) + 6.66\ (\text{Ti} + \text{Zr} + \text{Si};\ \text{At.\%}) \\ & + 0.66\ \text{Ni (At.\%)} + 1.71\ \text{Co (At.\%)} \\ & + 2.66\ \text{Fe (At.\%)} + 3.66\ \text{Mn (At.\%)} + 7.66\ \text{Al (At.\%)}.\end{aligned} \qquad \text{(II-3)}$$

According to Woodyatt et al., if $\bar{N}v$ is above 2.52, the alloy should form sigma phase. Woodyatt et al. calculated $\bar{N}v$ for type 310 stainless steel to be 2.88, which agrees with the sigma-forming behavior of the alloy.

However, according to an unpublished work of deBarbadillo mentioned in the 1977 Handbook of Stainless Steels, the $\overline{Nv}$ value for Fe-Cr-Co-Ni-Mo alloys was found to be in the range of 2.95-3.05. Data for pure Fe-Cr-Ni alloys are not available in the literature.

The actual computation of $\overline{Nv}$ is complicated because it involves atomic percent of elements instead of weight percents, and it also involves orbital electrons s, p, d, or hybrid electron calculations. The detail procedures which involve computer programs such as PHACOMP, etc. have been beautifully illustrated by Sims[39] in the book The Superalloys. Wallace,[62] Brewer,[96] Woodyatt et al.,[117] Greenfield and Beck,[105,106] and Pauling[97] all have made significant contributions to refine or calculate the average electron vacancy number $\overline{Nv}$ as shown in Equation (II-3). For example, Woodyatt et al.[117] pointed out that the loss of matrix composition due to pre-precipitation of phases such as carbide must be taken into account. The essential important steps and assumptions to compute the average electron vacancy number $\overline{Nv}$ are shown below:

$$\overline{Nv} = \sum_{i=1}^{n} f_i \, (Nv)_i \qquad \text{(II-4)}$$

where: $\overline{Nv}$ = the average electron vacancy number,

f_i = atom fraction of the i^{th} element in the austenite (γ) matrix,

$(Nv)_i$ = electron vacancy number of the i^{th} element of the system, and

n = number of elements in the matrix.

When interstitial elements, such as carbon or nitrogen, are present in the alloy, its stability at the equilibrium aging temperature must be known or calculated in order to compute $\bar{N}v$ successfully and accurately. The solubility of carbon with temperature in austenitic stainless steels containing 18% Cr is available in the literature.[25,26]

The electron vacancy number $\bar{N}v$ for most of the important alloying elements based upon the work of Wallace[62] is shown in Table II-8. Note that the effect of Mo is much higher than Cr because it increases tendencies toward sigma formation in the alloys more than Cr.

In the calculation of the average electron vacancy number $\bar{N}v$, the following assumptions, according to Sims and Hagel,[39] are essential so that prediction for the sigma phase occurrence could be made. The assumptions that must be made are:

1. All other phases expected in the alloy have formed, and the alloy is close to equilibrium.
2. The sigma phase or other topologically closed-packed (TCP) phase which might precipitate will form entirely from the austenite (γ) alloy matrix.
3. The $\bar{N}v$ will be a linear function of the matrix composition.

Upon reviewing ECC Equation (II-2) and electron vacancy number ($\bar{N}v$) Equation (II-3), it is found that there is considerable parallelism between both theories. Both theories require correction due to prior precipitation, which, in many cases, reduces the minor alloying elements such as Ti and Nb. Also, the effect of Cr or Mo seems to be positive in both equations in the formation of sigma since both these elements are

TABLE II-8

ELECTRON VACANCY NUMBERS ($\bar{N}v$) FOR THE ELEMENTS COMMONLY FOUND IN AUSTENITIC STAINLESS STEEL ALLOY MATRICES

Elements	($\bar{N}v$)	Atomic Radius (Å)
Cr	4.66	1.28
Mo	10.00*	1.40
W	4.66	1.41
V	5.66	1.36
Nb	5.66	1.47
Ta	5.66	1.47
Ti	6.66	1.47
Zr	6.66	1.61
Ni	0.66	1.25
Co	1.71	1.26
Fe	2.66	1.26
Mn	3.66	1.12
Al	7.66	1.43
Si	6.66	1.17

*Revised value by Sims and Hagel.[39] Original assigned number by Wallace[62] was 4.66.

Source: W. Wallace, Metal Science, Vol. 9, p. 547 (1975).

known to promote sigma phase precipitation upon aging. A critical discussion of both the theories is presented in Chapter V.

4. KINETICS OF SIGMA PHASE FORMATION--THE EFFECTS OF VARIABLES ON SIGMA PHASE FORMATION

The kinetics of phase transformation--austenite to sigma--are considered in this section. The rate of nucleation of sigma phase (and the number of nucleating sites) and their growth rate will control the austenite to sigma transformation. This is obviously a diffusion-controlled process because an entirely new equilibrium phase must be formed from the austenite matrix by motion of the atomic species such as Fe, Cr, and Ni.

Due to the slow diffusion rate of chromium and nickel in iron in the solid state, the process is obviously slow, having a large activation energy. In the ternary and multicomponent systems, the reaction rate is often much slower compared to binary Fe-Cr systems because of the slower diffusion rate of the species like Cr, Ni, Mo, etc. in iron (Fe).

Kinetics of sigma phase formation in stainless steel alloys have been considered by Spruiell,[5] Grot and Spruiell,[91] Blenkinsop and Nutting,[11] Duhaj et al.,[36] Weiss and Stickler,[16] and Marshall and Hooper.[34] Observations show that sigma does not nucleate homogeneously in the austenite matrix and that it always requires a high-energy interface for nucleation. High-energy interfaces such as stacking faults, twin boundaries, dislocations, grain boundaries, triple point junctions, and often foreign particles such as oxide or sulphide inclusions provide favorable nucleating sites for sigma.

The rate of growth of sigma phase, once it nucleates, is governed by the time, temperature, and composition of the alloy. The kinetics of sigma phase formation are best represented by time-temperature-precipitation (TTP) or time-temperature-transformation (TTT) diagrams, as shown in Figure II-17, which is for a commercial grade 316 stainless steel. In Figure II-17, the bulk extracts of the various phases that form in type 316 stainless steel are shown. It is clear from the figure that formation of $M_{23}C_6$ carbide takes place much earlier than the sigma phase. This is explained on the basis that diffusion rate of carbon* in the austenite matrix is much higher compared to the diffusion of Cr, Ni, or Mo (sigma-forming elements) in the austenite. Further, if the structure is fully austenitic, the transformation rate of sigma directly from austenite is extremely small, if not negligible.[18] On the other hand, if the structure is a duplex alloy such as $\gamma+\alpha$, the rate of sigma phase formation is much higher[115] (compared to a single-phase austenite matrix) because of available γ/α high-energy boundaries where sigma nucleates. There may also be direct transformation of BCC ferrite (α) to BCT sigma (σ).[80] Grot and Spruiell[91] have determined TTT diagrams for austenitic stainless steel alloys containing titanium and concluded that sigma formation was higher in titanium-modified alloys compared to type 316 alloys. The compositions of alloys used by Spruiell[91] and Stickler[16] are given in Table II-9.

Another novel way of presenting the effect of time and temperature on the rate of sigma formation after Emmanuel[36] is shown in Figure II-18,

---

*Necessary to form carbide.

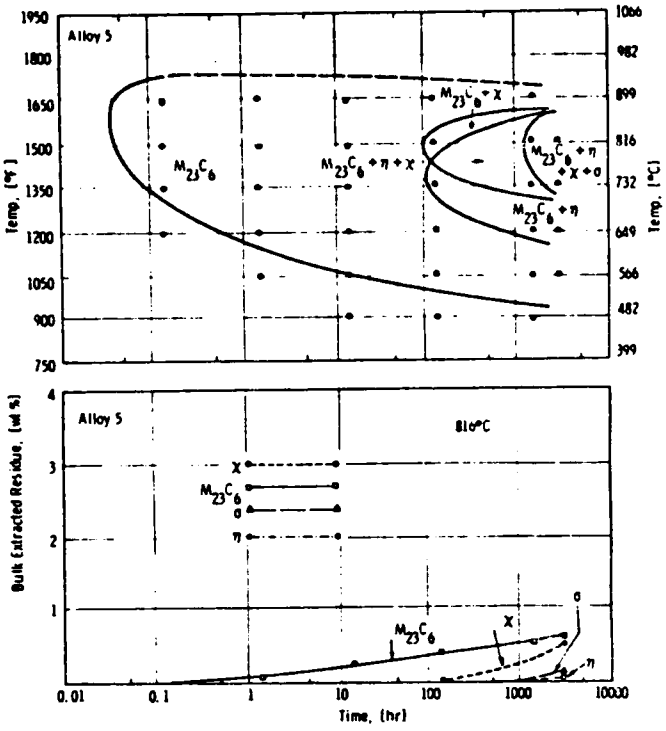


Figure II-17. Time-Temperature-Precipitation Diagram of 316 Stainless Steel Solution-Treated at 1260°C for 1.5 Hour and Water-Quenched.

Source: B. Weiss and R. Stickler, "Phase Instabilities During High Temperature Exposure of 316 Austenitic Stainless Steel," Met. Trans., Vol. 3, p. 851 (1972).

TABLE II-9

ALLOY COMPOSITIONS USED BY GROT AND SPRUIELL AND WEISS AND STICKLER

Alloy Grade	Chemical Analysis (wt.%)											Reference
	C	Cr	Ni	Mo	Ti	Mn	Si	P	S	N	Fe	
316Ti Mod.	0.057	17.52	13.96	2.51	0.29	1.41	0.03	0.005	0.004	0.004	Balance	91
321	0.06	17.48	9.58	----	0.50	1.69	0.54	0.012	0.006	0.006	Balance	91
316L	0.023	17.3	13.1	2.66	----	1.74	0.73	----	----	----	Balance	16
316	0.066	17.4	12.3	2.05	----	1.57	0.21	----	----	----	Balance	16

Source: A. S. Grot and J. E. Spruiell, Met. Trans. A, Vol. 6A, p. 2023 (1975); B. Weiss and R. Stickler, Met. Trans., Vol. 3, p. 851 (1972).

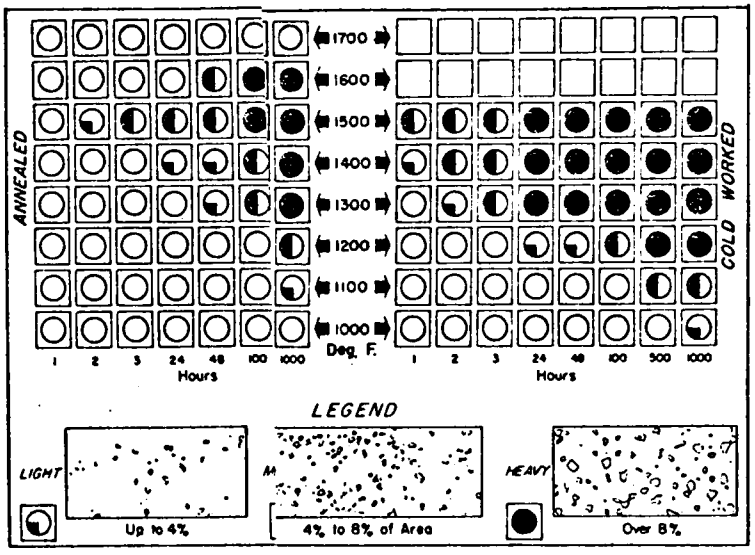


Figure II-18. Time and Temperature Conditions Conducive to Sigma Phase Formation in 25Cr-20Ni Steel (Fe Base).

Source: G. N. Emmanuel, "Symposium on the Nature, Occurrence, and Effects of Sigma Phase," ASTM STP 110, American Society for Testing and Materials, Philadelphia, Pennsylvania, p. 82 (1950).

which is more or less self-explanatory. The aging characteristics of the annealed type 310 material between 110-1600°F (600-870°C) are presented in Figure II-18. It will be noted that at 1600°F (870°C), the rate of sigma formation begins to decrease, and no sigma was apparent after 1000 hours at 1700°F (930°C). From the evidence, it is concluded that the rate of sigma formation in type 310 material increases with temperature up to 1500°F (815°C) and then rapidly decreases to the vanishing point at 1700°F (930°C). Such observations seem to be generally in agreement with classical phase precipitation theory.

Cold Work

Cold work of the matrix generates dislocations and dislocation density is increased with the increase of cold work of the alloy. This enhances the rate of diffusion of the species such as Cr and Ni and thereby favors sigma formation, which has general composition of formula $[(CrMo)x\ (FeNi)y]$[5] where x and y are numbers close to unity[16] in many instances. Since cold working may also generate stacking faults, which are, in general, high-energy interfaces, sigma nucleation may also be increased.

Recrystallization

When recrystallization occurs during aging, sigma phase formation is further enhanced because of ready sigma nucleation at slow-moving recrystallizing grain boundaries. Diffusion is enhanced due to rapid diffusion paths at the grain boundaries[5] which induce high growth rate of sigma phase.

Spruiell et al.[5] found that when recrystallization was absent, sigma phase formation was not much accelerated due to cold work.[34] Further, limited information on 18Cr-12Ni niobium-stabilized steel suggests that stressing the alloy at 650°C increases the rate of sigma formation.[34] However, recent studies by Andress[108] did not find any effect of stress in type 316L weld metal.

As-Cast Structure Vs. Wrought Alloy

As-cast structures are more prone to sigma formation than solution-treated material because of chemical segregation, especially chromium, in the matrix. This fact is illustrated in Figure II-19, which shows that sigma formation occurs much earlier in as-cast alloys as compared to a wrought structure under similar conditions of composition and temperature.

Solution Treatment Temperature

Increase of solution treatment temperature decreases the rate of sigma formation, as concluded by Weiss and Stickler.[16] This effect was attributed to the increased grain size caused by increased solution treatment temperatures and the longer diffusion paths of sigma-forming elements to the grain boundaries. It must be mentioned that increasing solution treatment temperature decreases dislocation density and thereby decreases the rate of sigma formation by providing fewer nucleation sites for sigma.

Grain Size Effect

Fine grain size enhances phase instability by providing additional nucleating sites and shorter diffusion paths for precipitate-forming

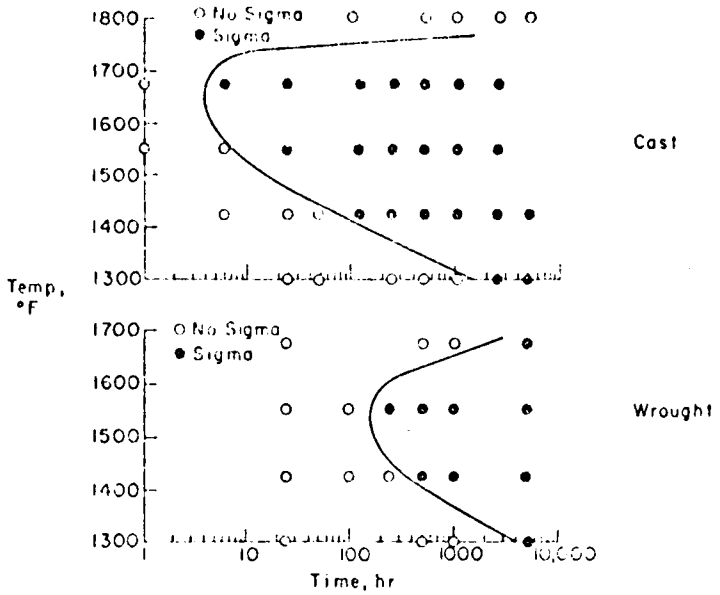


Figure II-19. Occurrence of Sigma in Fine-Grained, Unstressed IN-100.

Source: C. T. Sims, The Superalloys (C. T. Sims and W. C. Hagel, Editors), John Wiley and Sons, New York, p. 259 (1972).

elements. However, Spruiell[5] found that in the grain size* range ASTM 3.5-13, the effect is not as significant as the effect of cold work, particularly when recrystallization occurs during the aging treatment.

Effect of Composition on Sigma

The effects of alloying elements on the composition limits for the formation of phases in stainless steels are broadly summarized by stating that ferrite stabilizers, such as Cr, Si, Mo, Al, Ti, and Nb, promote sigma. On the other hand, the austenite stabilizers, C, N, Ni, and Mn, generally retard the rate of sigma formation.[34] This statement is supported by Spruiell and Grot's findings,[91] who observed that titanium enhanced the rate of sigma formation. That is, the elements which increase the ECC are, in general, ferrite stabilizers and have a tendency to increase the rate of sigma formation. Elements which have negative effect on ECC of the alloy generally retard sigma formation.

Effect of Carbon on Sigma Formation in Austenitic Stainless Steels

Carbon in stainless steels retards sigma formation as reported by many investigators.[5,18,22] It has been suggested that soluble carbon has an inhibiting effect on sigma formation, partly because nucleation of sigma phase is impaired in the presence of dissolved carbon. The sigma structure has no room for carbon to be dissolved, as reported by Wiegand and Doruk[24] and, hence, carbon must be segregated out before sigma forms.

---

*ASTM grain size number N is defined as $n = 2^{N-1}$ where N = ASTM grain size number as said, and n = number of grains per square inch at 100X magnification.

The effect of excessive carbon beyond equilibrium solubility limit dictated by temperature and composition[25,26] ends up as carbide because of the strong carbide-forming tendencies of the transition elements such as Cr. As a result, the ECC of the alloy is decreased, and, correspondingly, sigma, an intermetallic compound which contains a large amount of Cr, is inhibited.[16] It should be noted that 1 wt.% carbon can remove as much as 17 wt.% Cr from the matrix by forming chromium carbide.

The effects of carbon on sigma formation have been reported qualitatively by Thielsch,[18] who observed that a 26Cr-20Ni heat-resisting alloy containing over 0.20 wt.% carbon required exposure of 14 days at 1600°F (870°C) to produce any evidence of sigma formation. Further, the crucial effect of carbon on sigma phase formation in a cast 25Cr-20Ni steel have been quantitatively cited by Marshall and Hooper,[34] as shown below:

$$\text{Volume \% } \sigma = 11 \times \% \text{ Si} + 4.5\% \text{ Cr} - 58\% \text{ C} - 3.5\% \text{ Mn} - 1.1\% \text{ Ni} - 70. \qquad \text{(II-5)}$$

Since Hull[14] and Sticha[15] did not take carbon into account in their ECC theory, Spruiell[5] and Grot and Spruiell[91] have suggested that the original ECC theory of Hull be modified to take carbon into consideration. The modified theory is called "the Effective Equivalent Chromium Theory."

CHAPTER III

EXPERIMENTAL PROCEDURE

In this chapter, a brief description of the experimental procedure used in this research is presented.

1. MATERIALS, ALLOY PREPARATION, AND CHARACTERIZATION

All alloys used in this investigation were prepared at The University of Tennessee, Knoxville Chemical and Metallurgical Engineering Department Laboratory. Nine special alloys were prepared in a High-Vacuum Balzer Induction Furnace using high-purity raw materials such as iron (Fe), chromium (Cr), nickel (Ni), and graphite (C). Each raw material will be individually described regarding its purity, as each is an important variable of the alloys.

1. Iron--Purity 99.95%+, electrolytic grade. Trace oxides such as Fe_2O_3 were reduced in hydrogen atmosphere at 925°C (1700°F) for one hour. The reduced iron was then cleaned by dipping it in a mixture of phosphoric acid (H_3PO_4) and hydrogen peroxide (H_2O_2), followed by rinsing in methanol (CH_3OH).
2. Chromium--Purity 99.9%+, electrolytic grade. Supplier: Atomergic Chemetals Co., Carle Place, New York.
3. Nickel--Purity 99% minimum on nickel shots, and 99%+ on zone-refined nickel bars. Nickel bars were provided by Dr. Ben F. Oliver, Professor, The University of

Tennessee, Knoxville. Nickel shots were purchased from International Nickel Company. The nickel shots had 0.4% Fe and 0.15% C, but vacuum melting removed part of the existing impurities, such as carbon, present in the raw material.

4. Graphite--Electrolytic grade, high purity. Supplier: United Aircraft Company.

Selection of alloy compositions, as shown in Table III-1, was based upon the equivalent chromium content (ECC) desired, the carbon content of the alloy, and the ferrite number, FN[19] (the approximate volume percent of ferrite in the alloy matrix) (based upon the Schoefer Diagram,[92] which correlates chromium and nickel equivalents with ferrite number in as-cast stainless steel alloys). The ECC, based upon overall chemical compositions, was expressed as

$$ECC = Cr\ (wt.\%) - 0.226\ Ni\ (wt.\%)^{(14)}$$

for pure alloys. Please note: Hereafter, all percentages of elements shall be referred to as wt.%, unless specified differently.

The melting operation was performed using a 30-KV TOCCO power source. A stabilized zirconia ceramic crucible with composition 95% ZrO_2 - 5% CaO (melting point 2600°C) from N.L. Industries was used to hold the hot molten alloy.

The molten alloy was held in the molten state for a minimum time (~10 minutes) consistent with obtaining a homogeneous melt. During this time, the alloy was constantly stirred by convection induced by electromagnetic induction. Then, after ten minutes, the alloy was poured into

TABLE III-1

CHEMICAL COMPOSITIONS OF THE SPECIAL AUSTENITIC STAINLESS STEEL ALLOYS PREPARED FOR THIS STUDY[a]

Alloy Composition Number	% C	% Cr	% Ni	% Fe	As-Cast FN
3[b]	0.019	18.3	15.0	66.681	0
5[b]	0.006	19.8	14.2	66.0	0
8[c]	0.40	25.5	14.3	59.80	0.5
9[c]	0.014	26.1	14.6	59.30	20.5
10[c]	0.18	25.9	14.0	59.92	3.5
14[c]	0.20	22.2	15.1	62.50	0.5
17[c]	0.05	24.7	17.5	57.75	3.0
18[c]	0.19	24.5	17.5	57.81	0
19[c]	0.38	26.2	17.2	56.22	0

[a]All elements are in wt.%. All alloys were wrought annealed for chemical analysis.

[b]Melted under vacuum (10^{-2}-10^{-3} atmosphere).

[c]Melted in an atmosphere of 40 cm Argon (inert gas).

a water-cooled chemically cleaned copper mold (conductor) with internal dimensions of 3.75x0.75x2.25 inches. The alloy was allowed to cool to room temperature before removing from the mold. Each casting weighed approximately 500 grams, or a little over a pound.

Two alloys, number 3 and number 5, were melted using a vacuum of $\sim 10^{-2}$-10^{-3} atmosphere (1 mm Hg = 1 torr; 760 mm (torr) Hg = 1 atm.). The other seven alloys (numbers 8, 9, 10, 14, 17, 18, and 19) were melted using 40-cm pressure, high-purity argon gas to prevent the loss of carbon from the molten alloys.

Chemical analysis was performed by Oak Ridge National Laboratory, Oak Ridge, Tennessee, and by Galbraith Laboratories, Knoxville, Tennessee. Chemical compositions of the alloys are shown in Table III-1.

The ferrite measurements [107] were performed using a Magne-Gage manufactured by the American Instrument Co., Silver Springs, Maryland. A minimum of three readings were taken, and the arithmetic average of the three represents the FN for the alloy. This is shown in the last column of Table III-1.

2. SAMPLE PREPARATION

In this section, the techniques employed to prepare the samples for the aging study are briefly described. The aging study is discussed in Section 3.

The original stainless steel casting from the water-cooled copper mold was cleaned, and any slivers or fins on the casting were dressed out. The casting was then cut into three pieces, with each weighing ~150 grams. The pieces are identified as No. 1, No. 2, and No. 3.

The No. 1 piece was used in its as-cast condition. The No. 2 piece was used in its as-cast, but cold-worked, state. The No. 3 sample was used in a solution-treated condition with somewhat controlled austenite grain size.

Since the initial state of the alloy greatly affects the physical and mechanical properties, the preparation given to each sample piece will be described in depth.

1. No. 1 Sample (As-Cast State)--This piece was cut into ten pieces with a mechanical water-cooled saw. The first piece was used for microstructural analysis of the as-cast structure. The remaining nine pieces were used for aging studies at various temperatures for different lengths of (aging) time. This is described in Section 3.
2. No. 2 Sample (As-Cast Plus Cold-Worked State)--The second piece of the as-cast alloy, cut from the original casting, was given ~50% cold work. An 8-inch-diameter manually fed rolling mill, located in the Mechanical Laboratory, Metallurgical Engineering Department, The University of Tennessee, Knoxville, was used for the cold working (rolling) operations. The actual amount of cold work given to each sample is shown in Table III-2. Each cold-worked sample was cut into ten small pieces. One piece was used for microstructural analysis, and the remaining nine pieces were used for the aging study.

TABLE III-2

AMOUNT OF COLD WORK GIVEN TO EACH ALLOY

Alloy Composition Number	% Cold Work (C.W.)* Given By Rolling	Average (Mean) % C.W.
3	49.43	
5	47.50	
8	54.50	50.54
9	50.32	
10	54.12	
14	47.75	
17	50.83	
18	50.93	
19	49.17	

*Based upon reduction in thickness. % C.W. = $(t_o - t/t_o) \times 100$, where t_o = original thickness, and t = final thickness of the sample after rolling.

3. No. 3 Sample (As-Cast Plus Cold-Worked Plus Solution-Treated Alloy)--The third piece of the material, cut from the original casting, was homogenized at 1050°C (1920°F) for two days (48 hours) in a high-purity argon atmosphere followed by water quench. This was done to ensure uniform chemical composition of the alloy by diffusion process. Then the alloy, after homogenization, was given a nominal 50% c.w. and then solution treatment (anneal) at 1050°C (1920°F) for one hour followed by water quench. This cold-working and solution-treating process was repeated until a desired grain size (generally, fine grain size, ASTM 5-8) of the alloy was obtained. However, for higher carbon (for example, alloy number 8) or duplex alloys, such as alloy number 9 with ferrite + austenite microstructure, a higher solution treatment temperature, 1150°C (2100°F) was employed to get the desired grain size. This process of repeated cold-working and solution treatment eliminated the "as-cast" inhomogeneous structure and redissolved carbon into solid solution. However, all ferrite present in the original cast structure was not dissolved back into solid solution into the parent austenite matrix. The grain sizes (ASTM) of the homogenized and solution-treated material are shown in Table III-3.

TABLE III-3

FINAL ASTM GRAIN SIZES* OF THE NINE SPECIAL ALLOYS
AFTER HOMOGENIZATION AND SOLUTION TREATMENT

Alloy Number	Grain Sizes	Comments
3	6-7	Fine (F)
5	9	Very Fine (VF)
8	9-10	VF
9	9	VF
10	9	VF
14	8	F
17	7	F
18	8	F
19	10	VF

*The ASTM grain size is determined by using the equation $n = 2^{N-1}$ where n = number of grains at 100X magnification per square inch, and N = ASTM grain size number. For simplicity and convenience, standard ASTM charts are available for comparison.

The procedure described above for solution treatment was repeated for all nine special (experimental) alloy compositions.

3. HEAT TREATMENT

Three 30-inch-long tubular electric furnaces (resistance type) were chosen for long-term (1000 hours and 2000 hours) aging treatments. The treatments were carried out at 650°C, 750°C, and 850°C. These furnaces were equipped with temperature control devices, so that the desired temperatures could be maintained with an accuracy of ± 5°C over six inches of working length in the tubular furnaces. The temperature distribution within each furnace is presented in Appendix E, Figures A-E-1 through A-E-3. The temperature of each furnace was periodically checked with a Leeds and Northrup potentiometer (accuracy ± 0.1°C) to ensure that the furnaces were in compliance with the above mentioned prescribed tolerances.

For short-term heat treatments (one, ten, and 100 hours at 650°C, 750°C, and 850°C), another tubular furnace was selected with controlled argon flowing atmosphere to prevent oxidation of the samples. The same temperature tolerance (± 5°C) was maintained in this furnace as well. After the heat treatments, the samples were water quenched to room temperature to suppress further phase transformation. Surface trace oxides, if present, were removed with the help of sandpaper before attempting any further metallurgical examination on the samples.

For long-term aging treatments, vacuum encapsulation was used. This was accomplished by using 1.375-inch-internal-diameter x 3-inch-long inconel tubes where the samples were placed and sealed by welding

under 1-micron vacuum to minimize oxidation. The inconel tubes containing the samples (which were all marked by proper "identification numbers") were placed in the furnaces in the constant temperature zones as shown in Appendix E.

After the aging treatments were completed, the inconel tubes containing the samples were water quenched in cold water to suppress phase transformation, and the samples were removed from the tubes for metallurgical examination.

Each sample was cut into four pieces for the following examination:

1. First piece--for optical microscopy.
2. Second piece--for scanning electron microscopy (SEM).
3. Third piece--for transmission electron microscopy (TEM).
4. Fourth piece--for bulk extraction of phases formed.

Each method is described in subsequent sections.

4. SAMPLE NOMENCLATURE

The following nomenclature was used in order to keep track of the many samples examined (270 samples).

1. The "first" number of the specimen refers to the original chemical compositions as shown in Table III-1, page 70. For example, if the number starts with a number 3, it means composition number 3.
2. The "second" number following the first refers to the treatment given to the sample prior to aging. The numbers 0, 1, and 2 were used to specify this pretreatment condition as follows:

a. 0--as-cast alloy

b. 1--as-cast alloy plus ~50% c.w. as shown in Table III-2, page 73.

c. 2--as-cast alloy was diffusion annealed (homogenized) at 1050°C (1920°F), ~50% c.w., and then solution treated at 1050°C or higher for a desired grain size as shown in Table III-3, page 75.

3. The "third" number refers to the aging time and temperature the alloy received as shown in Table III-4. For example, if the third number is 1, it means that the alloy was aged for one hour at 650°C, the number 7 means the alloy was aged 1000 hours at 750°C, and so on.

To give a complete example, sample number 3-2-1 means that the alloy composition is number 3 (see Table III-1, page 70). The alloy was ~50% c.w. (Table III-2, page 73) and then was solution treated at 1050°C or higher long enough to achieve the desired grain size (Table III-3, page 75). Finally, the solution-treated alloy was aged for one hour at 650°C (see Table III-4).

5. OPTICAL METALLOGRAPHY

Small samples of about 1-gram weight were mounted using DuPont Lucite or Buehler* bakelite using heat and pressure in a mounting press.

---

*Buehler Ltd., Evanston, Illinois.

TABLE III-4

SAMPLE NOMENCLATURE FOR THE AGING TIME AND TEMPERATURE

	Third Number								
Condition	1	2	3	4	5	6	7	8	9
Aging Temperature	←←←←←←← 650°C →→→→→→→				←←←←← 750°C →→→→→			←←← 850°C →→	
Aging Time (hours)	1	10	100	1000	10	100	1000	100	1000

Explanations: 1 means aging time of one hour at 650°C, 7 means aging time of 1000 hours at 750°C, and so on.

In some cases, Buehler plastic expoxide (five parts by weight) and Buehler expoxide hardener (one part by weight) were mixed together and were used for sample mounting. After mounting, the specimens were rough-polished on a coarse emery paper, making sure that the sample was flat enough for the next stage of polishing operation. Additional grinding was done using four grades of emery paper--Grit I (240-mesh silicon carbide); Grit 0 (320-mesh); Grit 00 (400-mesh); and Grit 000 (600-mesh)--using Varsol as lubricant. The final polishing operation was carried out on "Syntron" vibratory polishers with 1-micron (10^{-4}-cm) and 0.06-micron alumina (Al_2O_3) powder using distilled water as lubricant.

The use of tap water was never permitted because of pitting problems on samples. In many cases, a 50% glycerol and 50% H_2O mixture was used to minimize pitting corrosion. Further, glycerol acted as a lubricant during polishing for a better surface finish.

Five etchants (chemical and electrolytic) were used to reveal the microstructural details as described in this section. For the electrolytic etchant, a direct current (DC) power source with variable voltage was used. A 3/16-inch-diameter hole was drilled on the back of each plastic mount (which contained the alloy specimen) for good electrical contact between the specimen (which acted as an anode) and the electrolyte which had a platinum foil serving as a cathode. The many etchants used are described in tabular form in Table III-5.

After etching, the specimens were dried with methanol or isopropyl alcohol. Then the specimens were examined under a Leitz optical microscope.

TABLE III-5

RECOMMENDED CHEMICAL AND ELECTROLYTIC ETCHANTS FOR OPTICAL METALLOGRAPHY OF STAINLESS STEEL ALLOYS

Etchant Number*	Chemical Composition	Type of Etch	Objective
1	54% HCl 8% HNO_3 38% H_2O	Chemical-- Etch at 150°F and rinse with hot running water.	To reveal general, all-purpose microstructure. No color.
2	45 gm KOH (solid) 60 ml H_2O	Electrolytic-- Use 2.5-4 V DC, 30-50 mA/cm^2 current density.	To reveal sigma phase. Stains sigma yellow to reddish brown in color.
3	10% oxalic acid (solid) 90% H_2O	Electrolytic-- 3 V DC, 30-50 mA/cm^2	Stains sigma and carbide phase. No color.
4	Murakami's Reagent $K_3Fe(CN)_6$--10 gm NaOH--10 gm	Electrolytic-- 3-6 V DC, 50 mA/cm^2	Etches carbide first, then sigma.
5	chromic acid (CrO_3)-- 25 gm glacial acetic acid--133 ml (CH_3COOH) 7 ml H_2O	Electrolytic-- 9 V DC	To reveal ferrite and general microstructure.

*Source: Etchants 1, 2, 3, and 4--Metals Handbook (8th Edition), Volume 8, ASM, p. 291 (1973); ASTM STP-110[36]; K. W. Andrews[30,32,33]. Etchant 5 courtesy of Dr. C. D. Lundin, The University of Tennessee, Knoxville.

The Leitz microscope used in our research had a capability of up to 1000X magnification with good resolution. Selected areas of the specimens were photographed using a Polaroid 4x5-inch instant film with negative. The negatives were quickly developed and dried for future enlargments or reproduction of desired photomicrographs.

6. SCANNING ELECTRON MICROSCOPY (SEM)

The microstructures of the chemically or electrolytically etched specimens were examined by a scanning electron microscopy, Model AMR-900. An energy dispersive x-ray detector was used in order to perform x-ray fluorescence analysis of the matrix composition, the carbide particles composition, and the hard sigma phase particles composition. The detector and the energy dispersive multichannel analyzer were manufactured by ORTEC. The electron beam was limited to the desired spot of the metallurgical specimen during image analysis (partial field technique). The emitted spectra were collected for 400 seconds with a tilt angle of 26°. The accelerating voltage for the electron beam was 21 KV. Typical examples of the Intensity vs. Energy (KeV) plots for the austenite and sigma (σ) and for the matrix and carbide phase ($M_{23}C_6$) are shown in Appendix F.

It should be noted here that no gold coating was used on the metal specimen itself for the SEM work. However, since the metal specimen was mounted on lucite plastic, which is a nonconductor of electicity, the lucite area was coated with a silver paint to make the specimen conductive to the stage of the specimen in the microscope. This operation was necessary to protect the electron microscope itself, as well,

because plastic with no metal paint has a tendency to overheat when an electron beam is aimed at the specimen.

7. TRANSMISSION ELECTRON MICROSCOPY (TEM)

The specimens from composition number 9 which had high equivalent chromium content (ECC) were examined under a Philips Model EM300 transmission electron microscope in order to identify the phases present in the alloy. The transmission electron microscopy involved two stage operations: first, sample preparation and second, examination of the prepared samples in the electron microscope at 100 KV.

The sample preparation technique used here was similar to the one developed by DuBose and Stiegler.[101] The heat-treated (aged) specimens of composition 9 were cut into 90-mil square plates with a thickness between 15-20 mils (1 mil = 10^{-3} inches). Then, a 3-mm-diameter disk sample was punched. Extreme care (and caution) were exercised during the punching operation to minimize severe c.w. condition in the metal specimen because such a condition may affect the internal structure of the sample.

The prepared disk was jet-polished (referred to here as "dimpling") by an acid jet which consisted of 60% H_3PO_4 (phosphoric acid) and 40% H_2SO_4 (sulphuric acid) at 100°C at 200 volts DC and a current of 100 mA. The jet diameter was approximately 1 mm and produced a region in the center of the disk of reduced thickness. The specimen was rinsed in H_2O and then in methyl alcohol. The dimpled specimen was then electropolished at room temperature (25°C or 77°F) in a 5% perchloric acid-95% ethanol solution by passing a 400-mA current. This procedure was

continued until a hole was created in the specimen. Such a hole in the specimen was detected by a photosensitive cell geared with a controller and an alarm system. The specimens then went through the rinsing procedure in the following sequence:

distilled water ↠ distilled water plus versene ↠ distilled water ↠ methanol.

The specimens were then loaded to the sample holding device of the transmission electron microscope for metallurgical examination. Photomicrographs were taken on a KODAK* projector on slide plates especially manufactured for electron microscopy. By switching the transmission electron microscopy from TEM to diffraction mode, diffraction patterns could be obtained.

8. MICROHARDNESS MEASUREMENTS

Measurement of the hardness of the second phase (sigma phase) and of the matrix phase was accomplished by using a Kentron Hardness Tester. A diamond pyramid indenter was used with an applied load of 10 gm. The reliability of the measurements was checked using standard hardness test blocks. Such tests fell within the specified variation for the test blocks.

---

*Registered trademark of the Eastman Kodak Company.

9. BULK EXTRACTION OF PRECIPITATES--QUALITATIVE AND QUANTITATIVE ANALYSIS

After prolonged and short-term aging treatments of the alloys at various times and temperatures, the alloys were subjected to electrochemical treatments to selectively dissolve the matrix phase. The effort was concentrated on the long-term aging samples because of the greater quantity of the second phase in these samples.

In the electrolytic dissolution process, the heat-treated sample, weighing approximately 1 gm, was placed in a 10% HCl-90% CH_3OH solution. The sample was made the anode, and a platinum foil was used as cathode. A current density of 175-255 mA/cm^2 was passed through the sample by adjusting the variable resistance of the circuit.

Prior to the electrolytic extraction process, all specimens were descaled by passing a DC current of 0.2 ampere (200 mA) per square centimeter for two minutes in a solution which consisted of the following composition:

HCl --	9% (volume)
HF --	4%
H_2O --	87%
Total --	100%

The sample was then rinsed in distilled water, followed by rinsing in methanol (CH_3OH).

The extracted particles were centrifuged for about five minutes. This process achieved two things: first, the precipitates were settled

down at the bottom of the test tube, and second, the clear liquid on top of the precipitate was physically separated.

The clear liquid (which was green) was discarded by decanting process with extreme care to make sure that the particles at the bottom of the tube were not disturbed. The mixture was then diluted with fresh methanol, and the centrifugal process was repeated several times until a reasonably colorless solution was obtained. The mixture of methanol and extracted powder (or precipitates) was finally dried under vacuum in a desiccator or over a constant temperature (about 80°C or 176°F) water bath. The powder was then weighed to calculate the weight percent extract which was subsequently used in the x-ray diffraction analysis. The accuracy of weighing by an Electronic Balance* was 0.0001 gm.

Some difficulties, especially dissolution of sigma phase in the present solution, were encountered. Therefore, a new solution recommended by Dulis and Smith[36] was used. The solution had the following composition:

150 gm citric acid

100 gm potassium iodide

20 ml hydrochloric acid

150 ml water

The specimens were dissolved with applied voltage of about 4 volts DC and 400-mA current.

---

*Mettler Instrument Corp, Hightstown, New Jersey.

10. X-RAY DIFFRACTION FOR PHASE IDENTIFICATION

Two methods were used to obtain x-ray diffraction patterns. Either a Philips x-ray diffractometer or a Debye-Scherrer powder camera was used. In each case, CuK_α radiation (λ^* = 1.542 Å) was used (1 Å = 10^{-8} cm).

In the Philips diffractometer, the extracted powder was placed on a silicon single-crystal so as to provide a very low background scattering. A diffracted beam was used to eliminate other extraneous scattering and further reduce the background. The pattern was recorded in the range of 70-30° (2Θ). In one instance, for composition number 9, the chemically etched specimen was directly exposed to the CuK_α radiation to get diffraction of the sigma phase, as well as of the austenite matrix phase.

The sample preparation for the Debye-Scherrer patterns began with the extracted dry powder. This was ground to very fine particles and was then fed to a 0.5-mm-diameter low melting glass tube. After compacting the powder in the funnel, the tube was sealed off by heat. The final specimen size was 0.5-mm diameter x 1 cm.

The specimen was mounted and centered on the camera for x-ray diffraction. The type of film used was 3.5-cm-wide, Kodak NS-392T. The camera diameter (ID) was 115 cm. The x-ray source, once again, was CuK_α radiation (λ = 1.542 Å) with a nickel filter.

After exposing the film to CuK_α radiation for about ten hours, x-ray patterns of the extracted powder were developed. Qualitative phase identifications were carried out by comparing the d-spacings (distance between planes) computed from the diffraction angle using Bragg's

---

*Wavelength of radiation.

law* against available standard patterns expected to occur in austenitic stainless steels.

11. QUANTITATIVE MICROSCOPY

A point count method, as described by Blank and Gladman[70] was used to calculate the volume fraction of sigma (σ) phase. A 5x5-inch transparent grid with 100 small square grids per square inch was constructed with pencil and straight edge. The grid was placed directly on each optical micrograph at random. All micrographs were for alloys aged at 750°C for 1000 hours, because this time-temperature combination had the maximum amount of sigma phase precipitation.

By counting the total number of grid intersections that lie within the sigma phase particles and dividing this number by the total number of grid points covering the photomicrograph, the point fraction ($\Delta P/P$) was calculated which is equal to the area fraction ($\Delta A/A$) or volume fraction ($\Delta V/V$) of that phase.[70]

The point count method was used as opposed to lineal analysis as recommended by Blank and Gladman.[70] However, for composition number 9, which exhibited coarser polygonal structure, lineal analysis was applied.

---

*Bragg's law $\rightarrow\rightarrow$ $n\lambda = 2d \sin\theta$

where: n = order of reflection

λ = wavelength of radiation

d = spacing of the planes

2θ = Bragg angle.

CHAPTER IV

CHARACTERIZATION OF UNAGED MATERIALS

1. CHEMICAL COMPOSITION

Results

The chemical composition of the nine prepared alloys was shown in Table III-1, page 70. The table includes carbon, chromium, nickel, and iron contents of the alloys.

Table IV-1 shows the equivalent chromium content (ECC) of the relatively pure alloys based upon their overall chemical compositions. The ECC is defined as % Cr - 0.226% Ni.[14] The ECC's were used as a variable in this study. Likewise, the electron vacancy number (EVN or $\bar{N}v$), another variable, is also shown in Table IV-1 based upon the chemical compositions. The EVN is computed from EVN = 4.66 Cr (At.%) + 0.66 Ni (At.%) + 2.66 Fe (At.%).[62,94]

Discussion

The composition range of the nine experimental alloys varied as follows:

Carbon (C) -- 0-0.40%

Chromium (Cr) -- 18.3-26.2%

Nickel (Ni) -- 14.0-17.5%

Iron (Fe) -- Balance.

TABLE IV-1

EQUIVALENT CHROMIUM CONTENT (ECC) AND THE AVERAGE ELECTRON VACANCY NUMBER (EVN OR $\bar{N}v$) OF THE LABORATORY-PREPARED ALLOYS

Alloy Number	ECC[a]	EVN[b]	Wt.% Carbon
3	14.9	2.76	0.019
5	16.6	2.81	0.006
8	22.3	2.84	0.40
9	22.8	2.94	0.014
10	22.7	2.91	0.18
14	18.8	2.80	0.20
17	20.8	2.84	0.05
18	20.6	2.81	0.19
19	22.3	2.80	0.38

[a]Based upon overall chemical compositions. ECC = % Cr - 0.226% Ni.[14]

[b]EVN corrected for carbide precipitation at 750°C. EVN = 4.66 Cr (At.%) + 0.66 Ni (At.%) + 2.66 Fe (At.%)[62,94]

The ECC of the alloys, expressed as % Cr - 0.226% Ni,[14] varied from 14.9-22.8%. The EVN (or $\overline{Nv}$) varied from 2.76-2.94 (see Table IV-1). The ECC's were calculated based upon overall compositions of the alloys, as mentioned before, but corrections were made due to carbide precipitation at 750°C (1380°F) to compute the average EVN's ($\overline{Nv}$'s).

Nickel was primarily selected as an austenite stabilizer. The objective was to keep the nickel content at a reasonably constant level to allow for studying the effect of other variables on sigma formation.

Selection of chromium content was based on the work of Hull.[14] Hull found significant amounts of sigma formation after long-term aging (1000 hours at 816°C or 1500°F) in his as-cast stainless steel alloys with ECC between 17.5 and 26.0.

In the present study, the ECC's of the alloys based upon overall chemical compositions were classified into three groups, as shown in Table IV-2. The average EVN's ($\overline{Nv}$'s) of the alloys were not selected; they were simply calculated by the equation:

$$\overline{Nv} = 4.66\ Cr\ (At.\%) + 0.66\ Ni\ (At.\%) + 2.66\ Fe\ (At.\%).$$

Please see Table IV-1, where the EVN's of the nine experimental alloys are given.

Carbon content was used as a major variable in this study. It was desired to study the effect of carbon with respect to sigma formation at a given equivalent chromium content of the alloys. For example, alloy numbers 9 and 10 have similar ECC's (Table IV-1) but different carbon content. Likewise, alloys 17 and 18 have similar ECC's but different carbon content.

TABLE IV-2

CLASSIFICATION OF THE NINE EXPERIMENTAL ALLOYS BASED UPON THEIR OVERALL CHEMICAL COMPOSITIONS

Alloy Group Number	Average ECC*	Alloy Composition Number	Comments
I	22.5	8, 9, 10, 18	Number 9 alloy was duplex (austenite + ferrite).
II	20.7	17, 18	Number 17 was duplex.
III	<20	3, 5, 14	All fully austenitic.

*ECC = Cr (wt.%) - 0.226 Ni (wt.%). Please see Table IV-1 for the actual ECC's of the alloys.

Greater carbon content (more than 0.4%) in the alloys could not be reached during vacuum melting. Possible reasons for this include incomplete dissolution of carbon in the melt, oxidation of carbon to CO or CO_2 and loss through the vacuum system, etc. The fact that carbon is a very strong austenite stabilizer was readily apparent in the alloys, as will become obvious in the next section, where the measurement of ferrite in the alloys is discussed.

2. FERRITE MEASUREMENTS

Results

The ferrite content of the alloys was measured by Magne-Gage* following procedures recommended by DeLong.[107] The ferrite content, expressed as ferrite number (FN), of as-cast and as-cast plus cold-worked (c.w.) alloys is shown in Table IV-3. The actual amount of c.w. given to each alloy is shown in Table III-3, page 73.

Discussion

The ferrite contents varied from 0 (alloys 3 and 5, for example) to as much as 20% for alloy number 9. Upon c.w., the ferrite number increased somewhat. This is because some unstable austenite might have been converted to BCT martensitic structure. Martensite, like ferrite, is magnetic in nature and contributes to ferrite number increments when measured by Magne-Gage. However, the austenite to martensite transformation was considered small, and, for all practical purposes, this effect on sigma formation could be neglected.

---

*More correctly put as Aminco-Brenner Magne Gage.

TABLE IV-3

FERRITE NUMBERS (FN) OF AS-CAST, COLD-WORKED (c.w.), AND SOLUTION-TREATED ALLOYS PRIOR TO AGING

Alloy Composition Number	FN of As-Cast Alloys	FN After 50% c.w.	FN After Solution Treatment	Comments
3	0	0.6	1.4	Austenitic
5	0	0.6	1.2	Austenitic
8	0.5	0.2	0.5	Austenitic
9	20.5	21.6	9.0	Duplex*
10	3.5	4.8	1.0	Duplex
14	0.5	0.5	0.4	Austenitic
17	3	3.7	0.8	Duplex
18	0	0.2	0	Austenitic
19	0	0.2	0	Austenitic

*Austenite + delta ferrite.

3. MICROSTRUCTURES OF AS-CAST, COLD-WORKED, AND SOLUTION-TREATED ALLOYS

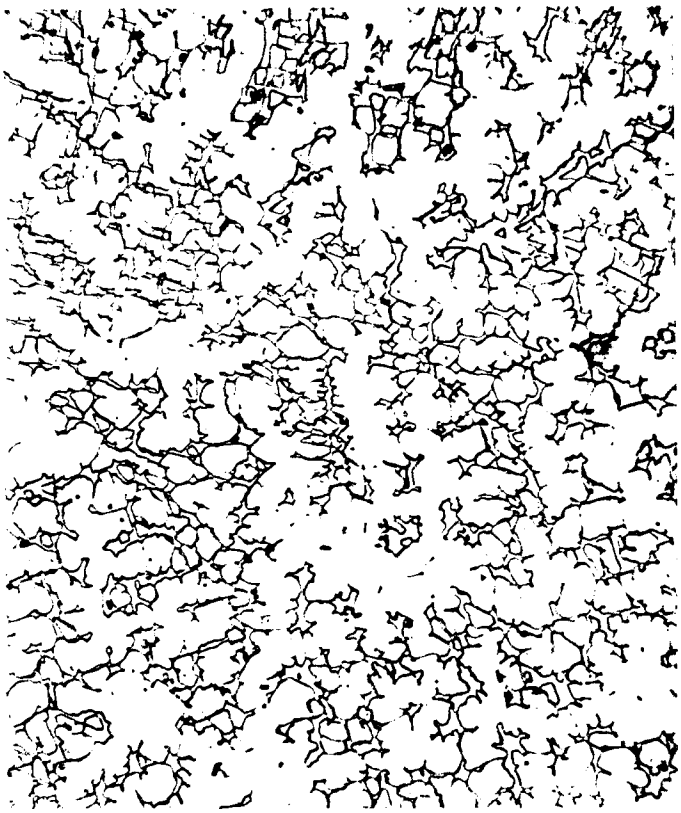
In this section, a general description and explanation of microstructures of the as-cast, cold-worked, and solution-treated (annealed) alloys is presented.

As-Cast Alloys

The important microstructures of the as-cast alloys covering the low-carbon (almost 0%) to high-carbon (~0.4%) range are shown in Figures IV-1, IV-2, and IV-3. For the purpose of this discussion, 0.2% carbon is referred to as medium carbon content.

Low-carbon alloy. The microstructure of a low-carbon, as-cast alloy (composition number 9) is shown in Figure IV-1. The structure shows a large amount of ferrite in the austenite matrix, with no evidence of free carbide ($M_{23}C_6$). The ferrite content of the alloy was about 20% based on the Magne-Gage test. The large amount of ferrite in the alloy was attributed to the relatively high Cr content (Cr being a ferrite former) and the presence of very little austenite stabilizer such as carbon.[1,92] Table III-1 (page 70) shows that this composition had 26.1% Cr and only 0.014% C. The structure is quite non-uniform (heterogeneous), which is typical for as-cast alloys. Lack of carbides in the structure is attributed to the availability of very little carbon for carbide formation and to the lack of a low-temperature precipitation treatment.

SAMPLE NUMBER 9-0



0.014% C, ECC = 22.8

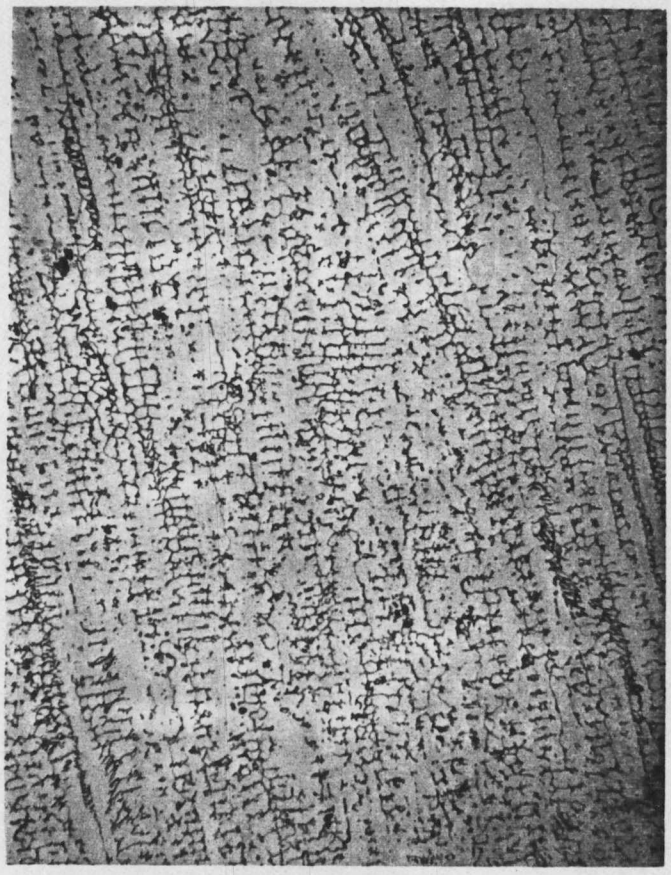
200X Magnification

Chromic Acid Etch
(Electrolytic)

Photomicrograph shows ferrite in
austenite matrix (duplex structure).

Figure IV-1. As-Cast Structure for Steel Composition Number 9.

SAMPLE NUMBER 10-0



0.18% C, ECC = 22.7

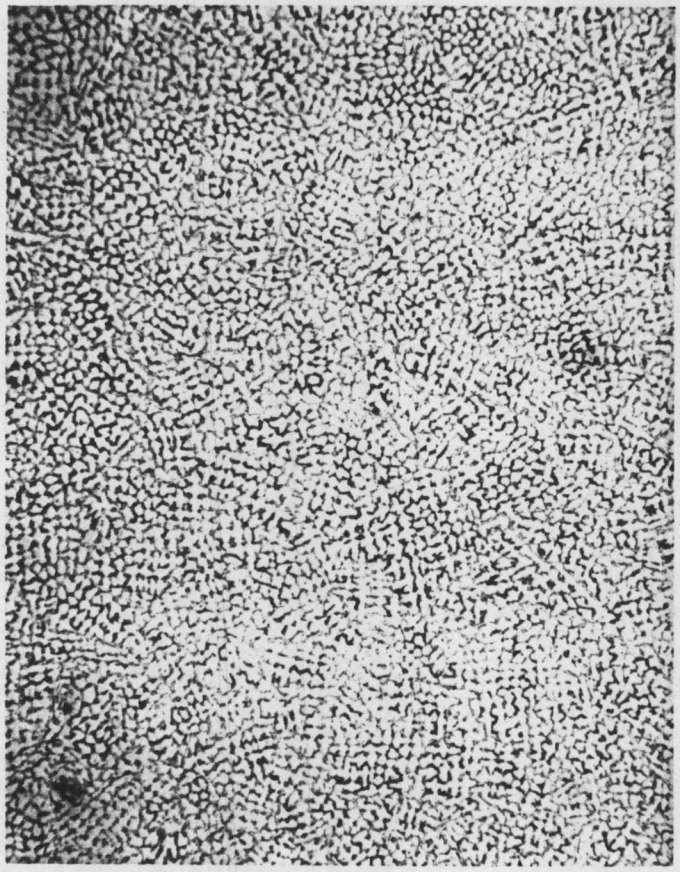
100X Magnification

Chromic Acid Etch
(Electrolytic)

A small amount of ferrite and carbide particles are observable in the dentritic structure.

Figure IV-2. As-Cast Structure for Alloy Composition Number 10.

SAMPLE NUMBER 19-0



0.38% C, ECC = 22.3

200X Magnification

Chromic Acid Etch
(Electrolytic)

Photomicrograph reveals a large amount of carbides in the interdentric channels.

Figure IV-3. As-Cast Structure for Composition Number 19.

Medium-carbon alloy. A typical microstructure of an as-cast medium-carbon alloy is presented in Figure IV-2. This alloy had 0.18% C. The alloy (composition number 10) was almost austenitic in its as-cast state, with only 3.5% ferrite. This result from the Magne-Gage test was in agreement with the Schaeffer diagram[1] because of the similarity between welding conditions (which Schaeffer predicted) and the as-cast conditions of the alloy. The carbon, which is about 30 times stronger than Ni in stabilizing austenite, was responsible for making this cast structure nearly austenitic.

The microstructure reveals a dentritic pattern which is controlled by chemical composition and growth conditions[103] such as cooling rate, etc. The structure shows a notable amount of carbide particles which appear as fine dots in the photomicrograph.

High-carbon alloy. A high-carbon as-cast microstructure is presented in Figure IV-3. The photomicrograph represents alloy composition number 19 with carbon content 0.38%.

According to Magne-Gage test, this as-cast alloy contains no ferrite. The lack of ferrite in the microstructure is attributed to the high carbon content of the alloy, which is a strong austenite stabilizer. The microstructure does not exhibit any noticeable ferrite.

The microstructure reveals a large amount of carbides compared to both Figures IV-1 (low-carbon structure) and IV-2 (medium-carbon structure). The carbides are trapped in the interdentritic channels of the solidified as-cast structure.

In general, alloys which exhibit as-cast structures are more brittle, exhibit chemical segregation in localized regions, and show typical dentritic structures compared to wrought alloys.

Upon examination of the solidified structures, which could have an influence on sigma formation, it is found that they are not the same. For example, Figure IV-1, page 96, shows the structure of low-carbon as-cast alloy number 9 to have a semi-continuous ferrite network. Likewise, Figure IV-2, page 97, shows dentritic structure for medium-carbon (0.18% C) alloy number 10, and Figure IV-3, page 98, represents the solidified structure of high-carbon (0.38% C) alloy number 19, whose microstructure is interdentritic.

The microstructures of the as-cast alloys are hard to control because, as Chalmers[103] has pointed out, they are dependent upon the G/R ratio,* where G is the temperature gradient in the liquid metal, and R is the rate of heat removal away from the mold wall during cooling. Chalmers pointed out that depending upon the G/R ratio, which controls the growth conditions of the metal, a dentritic, lamellar, cellular, or mixed microstructure could result in the solidified metal. Andress,[108] who studied ferrite measurements of 316L weld metal, similar to the as-cast alloys, found wide variations of ferrite numbers in the solidified structures. The ferrite numbers varied lengthwise, as well as in cross-section. Andress attributed these variations to cooling and freezing rates, segregation in the metal, and other variables such as nitrogen pick-up by the hot metal.

---

*Also, by $G/\sqrt{R}$ ratio and chemical composition of the liquid metal.

Thus, the local chemistry variations (segregations) or microstructural variations in the same casting or from casting to casting are unavoidable unless the G/R ratio is strictly controlled. In the alloys in this study, such variations probably did exist and therefore could, to some extent, affect the sigma formation--qualitatively or quantitatively. However, it was felt that the overall chemical compositions would have the strongest effect on sigma formation. Because of complexities associated with microstructure, morphology, or segregations associated with the as-cast structures, their effects, in depth, on sigma formation will not be presented in this investigation.

Cold-Worked Alloys

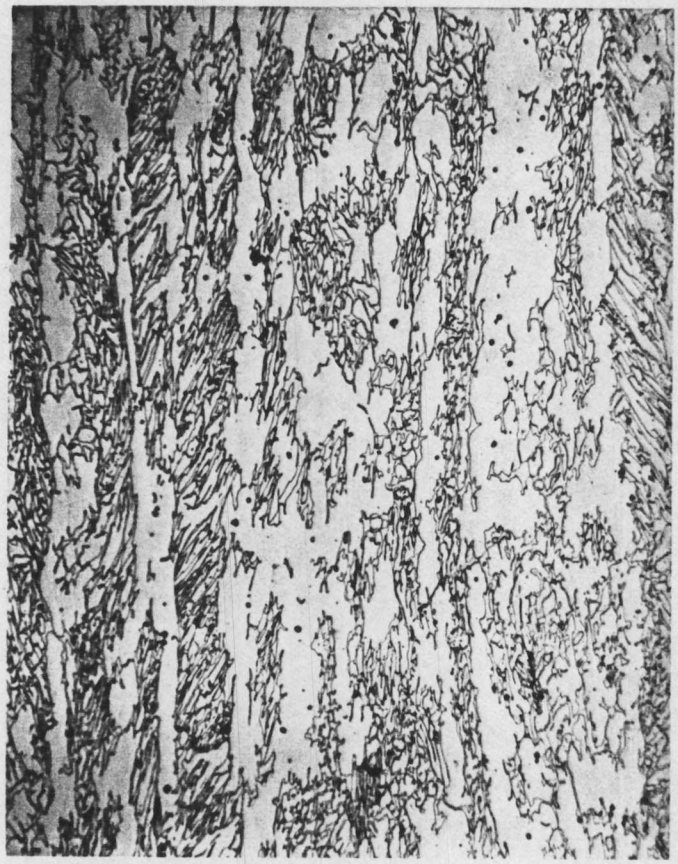
Microstructures of the typical cold-worked alloys are presented in Figures IV-4 and IV-5. Figure IV-4 is for a low-carbon (0.014% C) alloy, and Figure IV-5 is for a high-carbon (0.40% C) alloy.

Low-carbon alloy. The microstructure of the low-carbon alloy number 9, after giving 50.3% cold work by rolling, is shown in Figure IV-4. The rolling direction is shown in the photomicrograph. The ferrite grains are seen to be elongated in the rolling direction, while becoming thinner in the thickness direction. The matrix is austenitic.

High-carbon alloy. The photomicrograph of a high-carbon (0.40%) alloy (composition number 8) is presented in Figure IV-5. This microstructure shows elongated structure aligned mostly in the rolling direction. There is no evidence of any ferrite in the structure, but carbide particles are present in the austenite matrix.

Cold work was given to the as-cast alloys to break up the as-cast dentritic structure for structural homogeneity and to realize uniform

SAMPLE NUMBER 9-1



←←← Rolling Direction →→→

0.014% C, ECC = 22.8

200X Magnification

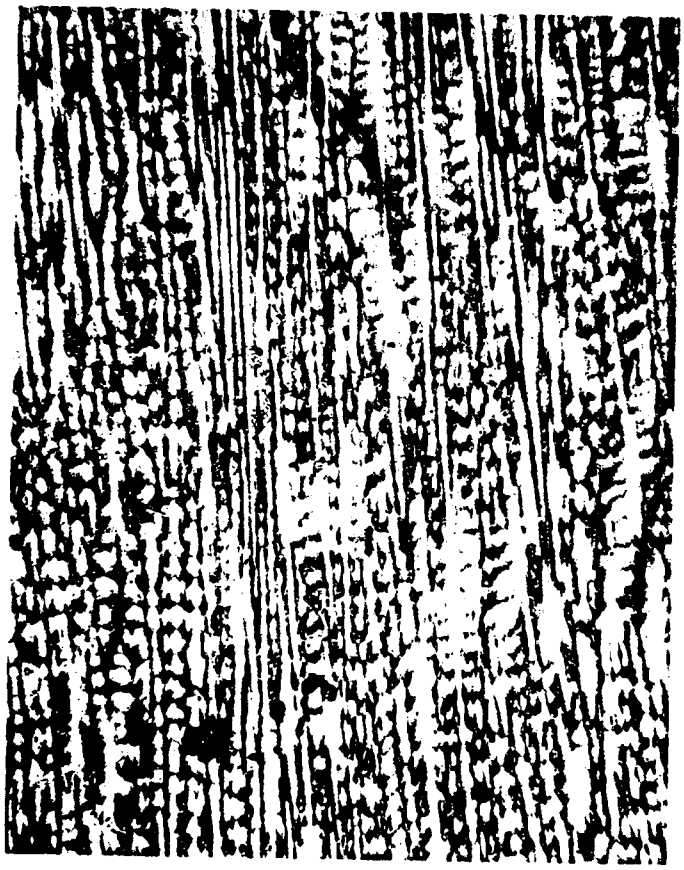
Chromic Acid Etch
(Electrolytic)

The microstructure reveals elongated ferrites primarily in the rolling direction.

Figure IV-4. Optical Photomicrograph for Alloy Number 9 Given 50.3% Cold Work By Rolling.

CRANESE CREST

SAMPLE NUMBER 8-1



0.40% C, ECC = 22.3

100X Magnification

Chromic Acid Etch
(Electrolytic)

←←← Rolling Direction →→→

The photomicrograph shows elongated structure in the direction of rolling.

Figure IV-5. Optical Micrograph for Alloy Composition Number 8 After Cold Working (~50%).

chemical compositions throughout the structure following subsequent heat treatments. This is presented in the next chapter. It is also known that cold work has a significant effect on the rate of sigma formation in wrought-annealed grades of stainless steel.

Solution-Treated Alloys

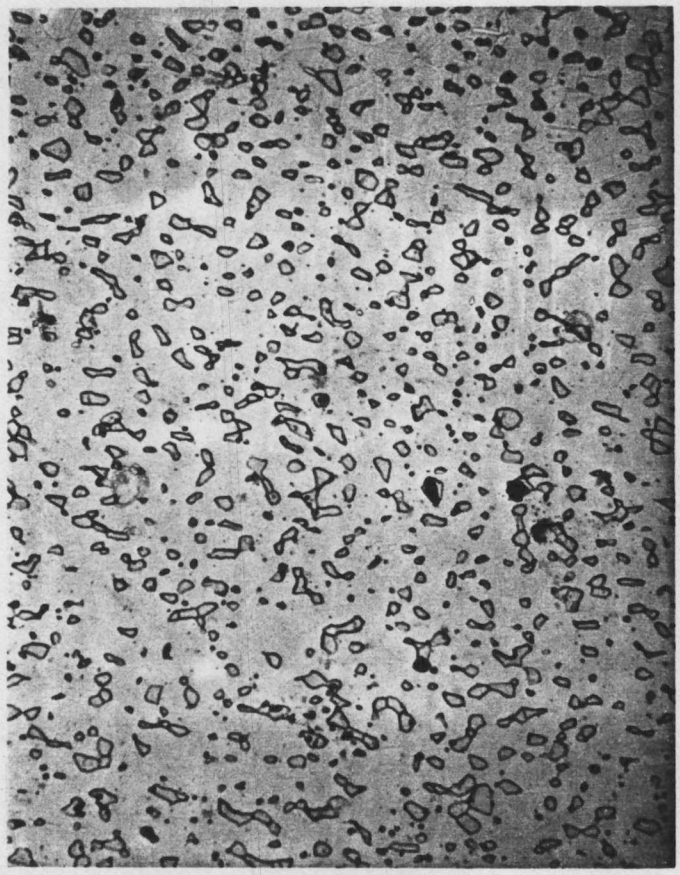
Three important microstructures of group I alloys (with average ECC of 22.5) in their solution-treated conditions are presented in Figures IV-6, IV-7, and IV-8.

Low-carbon alloy. An optical micrograph for the low-carbon alloy (number 9) after solution treatment is presented in Figure IV-6. The microstructure shows about 9% isolated islands of ferrite, some annealing twins, and little or no carbides in the austenitic matrix. The ASTM austenitic grain size was estimated to be between 6 and 7 (fine grain). The structure is completely recrystallized and exhibits polygonal (equiaxed) structure unlike the cold-worked structure (Figure IV-4, page 102) or as-cast structure (Figure IV-1, page 96). The annealing twins, as mentioned, are characteristic of wrought-annealed FCC structures such as austenitic stainless steels.

The ferrite content of the alloy was reduced down from its original 20.5% to its present 9.0%. This indicates that about 50% of the original ferrite went into (solid) solution by the solution treatment.

Medium-carbon alloy. A photomicrograph for the medium-carbon alloy (number 10) after solution treatment is presented in Figure IV-7. This alloy, which had the same ECC as number 9, shows a uniform, predominantly austenitic structure with some annealing twins, carbides, and

SAMPLE NUMBER 9-2



0.014% C, ECC = 22.8

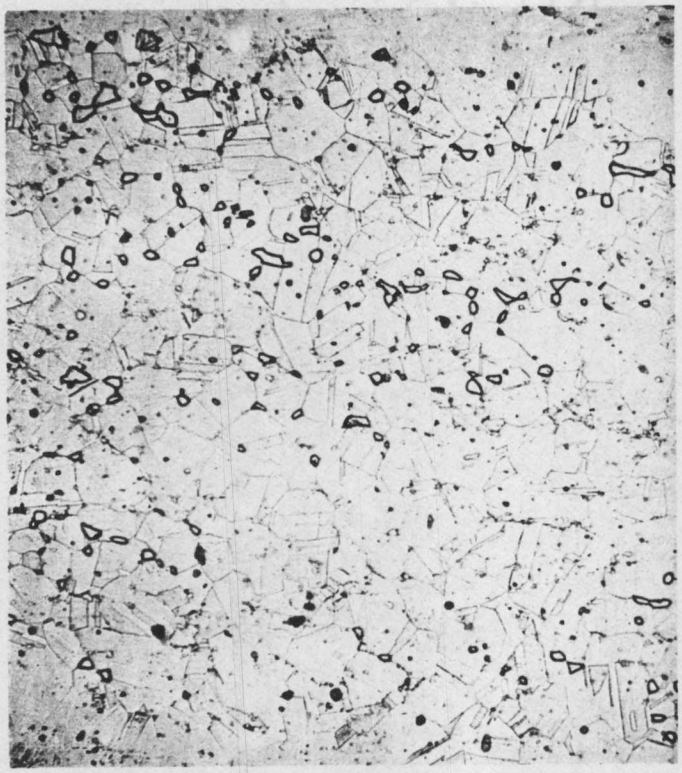
200X Magnification

Chromic Acid Etch
(Electrolytic)

The small islands are ferrite in an austenitic matrix. The austenite grain size was ASTM 6-7 (fine grain).

Figure IV-6. Optical Photomicrograph for a Low-Carbon Solution-Treated Alloy.

SAMPLE NUMBER 10-2



0.18% C, ECC = 22.7

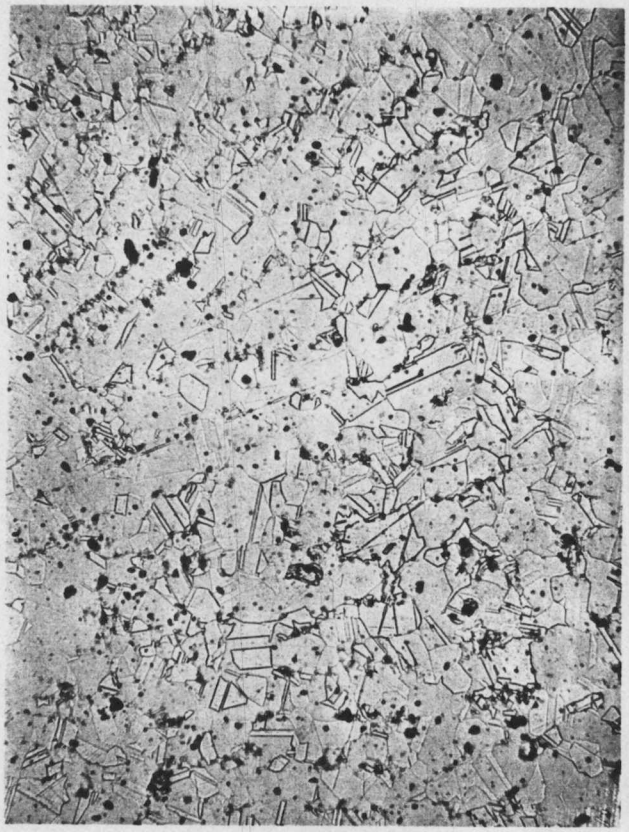
200X Magnification

Chromic Acid Etch
(Electrolytic)

The photo shows uniform austenite grains, annealing twins, and carbides. Estimated austenitic grain size was ASTM 9 (fine grain).

Figure IV-7. Optical Photomicrograph of a Medium-Carbon Solution-Treated Alloy.

SAMPLE NUMBER 18-2



0.19% C, ECC = 20.6

100X Magnification

Chromic Acid Etch
(Electrolytic)

The photo shows annealing twins, uniform austenitic grain size (ASTM 8), some carbides, and etch pits in an austenitic matrix.

Figure IV-8. Optical Photomicrograph of a Medium-High Carbon Solution-Treated Alloy.

ferrite grains. The ferrite content of the alloy was reduced to 1% from 3.5% in its as-cast state, indicating that some ferrite went to solid solution.

The alloy exhibits equiaxed polygonal structure unlike its counterpart as-cast structure (Figure IV-2, page 97). The austenite grain size of the alloy was very fine and was estimated to be ASTM 9.

Medium-high alloy. A typical microstructure for a medium-high carbon (number 18) after solution treatment is shown in Figure IV-8. This photomicrograph reveals uniform austenitic grains with annealing twins. Some carbides are also visible. The grain size of the structure was estimated to be ASTM 8, which was considered fine grain. The microstructure shows no ferrite and was in agreement with the Magne-Gage test (see Table IV-3, page 94).

General Discussion

Metals or alloys in their cold-worked state (structure) are considered more thermodynamically unstable than their solution-treated (annealed) counterparts because of their high internal stored energy. Cold work generates defects in them such as slip bands, dislocation clusters, stacking faults, and a highly distorted structure.(109) Therefore, the diffusion distances between heterogeneities is reduced. Further, the dislocations and other defects of a cold-worked structure provide additional nucleation sites for sigma phase formation during aging, as shall be seen later. All cold-worked structures lead to recovery, recrystallization, and grain growth during solution treatment.(109)

The solution-treated alloys, in general, are considered to have been in thermodynamic equilibrium at the solution treatment temperature of 1050°C (1920°F). On quenching, this structure is retained. Thus, the solution-treated samples possess a high degree of chemical homogeneity and equiaxed grain structure compared to their as-cast or cold-worked counterparts. Such uniformity in chemical compositions and structure is considered very essential to study the effects of independent or dependent variables on sigma phase formation. The presence of ferrite grains (islands) in alloy number 9, for example, in the solution-treated material would allow for studying the effect of ferrite on sigma formation. In the present study, the ferrite content was considered a secondary variable.

CHAPTER V

CHARACTERIZATION OF THE AGED MATERIALS

This chapter presents brief descriptions of the effects of aging on the alloy compositions prepared for this study. Of particular interest is the amount and rate of sigma formation. Microstructural changes associated with such variables as aging temperature and time constitute a major portion of this chapter because of their importance in examining the sigma formation. Evidence will be presented for identification of the sigma phase and other microconstitutents present in the structure using such techniques as x-ray diffraction, microhardness measurements, optical metallography, electron microscopy, etc.

Finally, the aging behaviors of the prepared as-cast, cold-worked, and solution-treated (annealed) alloys will be analyzed. Analyses will include interpretation of data, comparison with the results of other investigations, and an evaluation of various methods of predicting the existence of sigma phase. The latter relates especially to the evaluation of methods. The theory of equivalent chromium content (ECC) and the theory of electron vacancy number (EVN or $\overline{Nv}$) applied to austenitic stainless steels to predict sigma phase formation will be discussed. Suggestions will be made for better analysis in case of discrepancies.

1. OPTICAL METALLOGRAPHY AND MICROHARDNESS MEASUREMENTS

Optical Metallography

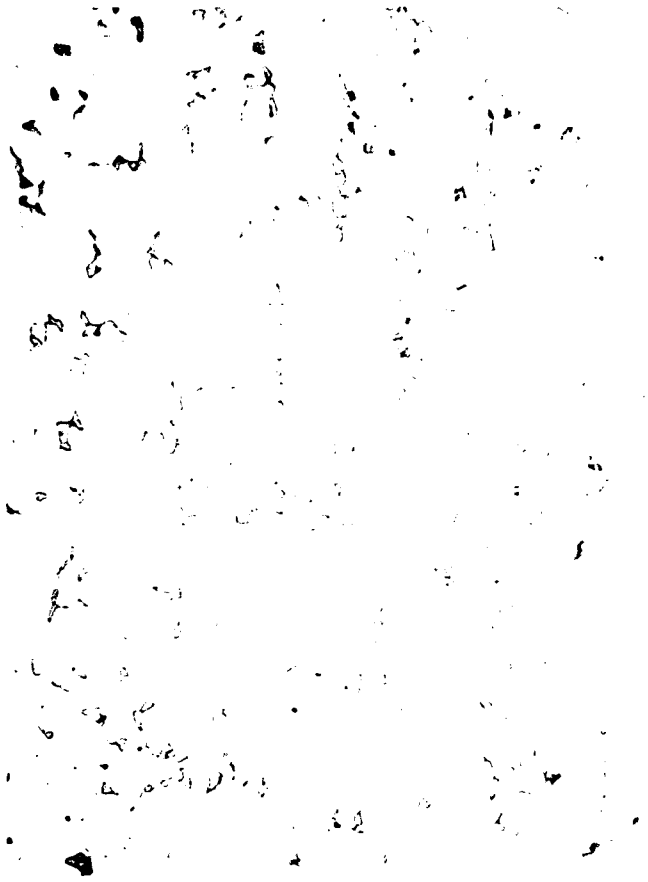
In this section, relevant optical micrographs of selected aged samples of as-cast, cold-worked, and solution-treated materials are presented. Aging was carried out at 650°C, 750°C, and 850°C for various lengths of time. Because of the large number of samples, it is convenient to present the micrographs in four groups, as described below:

1. Group A--Consists of microstructures after aging and the changes due to variation of chemical compositions. See Figures V-1 and V-2.
2. Group B--Consists of microstructural changes in aged alloys due to variations of aging temperature. See Figures V-3, V-4, and V-5. Graphical representation is presented in Figure V-6.
3. Group C--Consists of microstructural changes after aging associated with the initial conditions of the alloys such as as-cast, cold work, and solution treatment. See Figure V-7.
4. Group D--Consists of microstructural changes after aging due to variations of aging time. See Figures V-8, V-9, V-10, and V-11.

Group A Photomicrographs--Composition Effects

This group of photomicrographs is primarily concerned with the effect of chemical composition, especially chromium and carbon content, on the amount and rate of sigma formation. Chromium and carbon were the

(a) SPECIMEN NUMBER 10-2-7



CR = 25.9 Wt.%, Group I
(Ave. ECC = 22.5, 0.18% C)

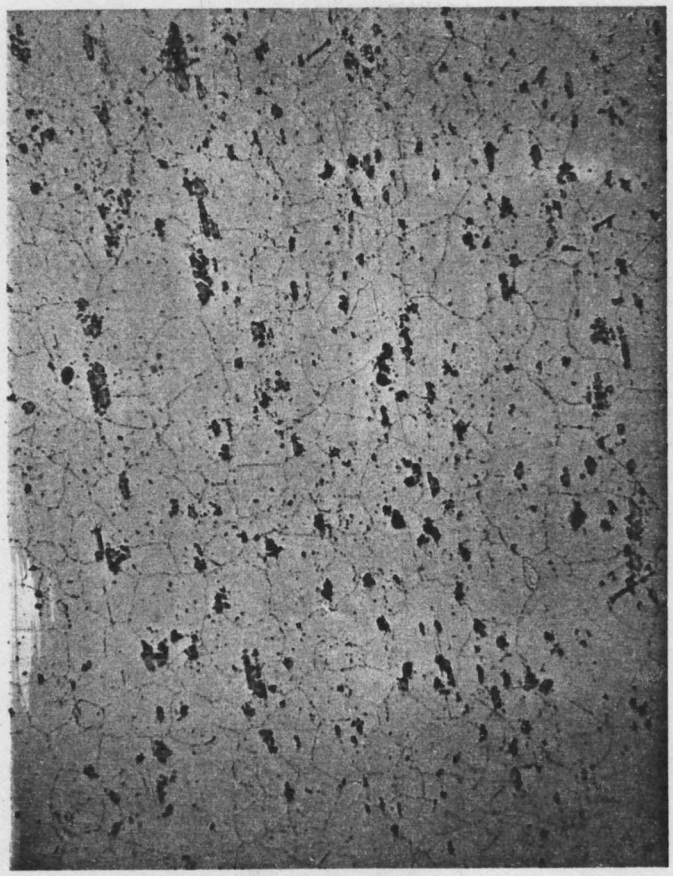
200X Magnification

Etchant--KOH-H_2O
(Electrolytic)

Microstructure of the alloy with ECC = 22.7 showing 10% sigma after aging for 1000 hours at 750°C.

Figure V-1. Effect of Chromium on Sigma Formation.

(b) SPECIMEN NUMBER 18-2-7



CR = 24.5 Wt.%, Group II
(Ave. ECC = 20.7, 0.19% C)

200X Magnification

Etchant--KOH-H_2O
(Electrolytic)

Microstructure with ECC = 20.6 showing only 3% sigma under similar aging conditions as (a).

Figure V-1. (Continued)

CRANES CREST

(a) SPECIMEN NUMBER 10-2-7



Group I, 0.18% C
(Ave. ECC = 22.5)

200X Magnification

Etchant--KOH-H_2O
(Electrolytic)

Microstructure of the 0.18% C alloy
(ECC - 22.7) showing 10% sigma phase.
Aging temperature 750°C, 1000 hours.

Figure V-2. Effect of Carbon on Sigma Formation.

CRANE CREST

(b) SPECIMEN NUMBER 19-2-7



Group II, 0.38% C
(Ave. ECC = 22.5)

200X Magnification

Etchant--KOH-H_2O
(Electrolytic)

Optical microstructure of the 0.38% C alloy (ECC = 22.3) showing only 4% sigma. Aging temperature 750°C, 1000 hours. Compare the morphology of sigma shown here with (a)

Figure V-2. (Continued)

(a) SPECIMEN NUMBER 8-2-4



0.40% C, ECC = 22.3

200X Magnification

650°C, 1000 Hours

0% Sigma

Mostly reveals carbides in austenitic matrix.

Figure V-3. Effect of Aging Temperature on the Rate of Sigma Formation On a High-Carbon (0.4% C) Alloy.

(b) SPECIMEN NUMBER 8-2-7



0.40% C, ECC = 22.3

200X Magnification

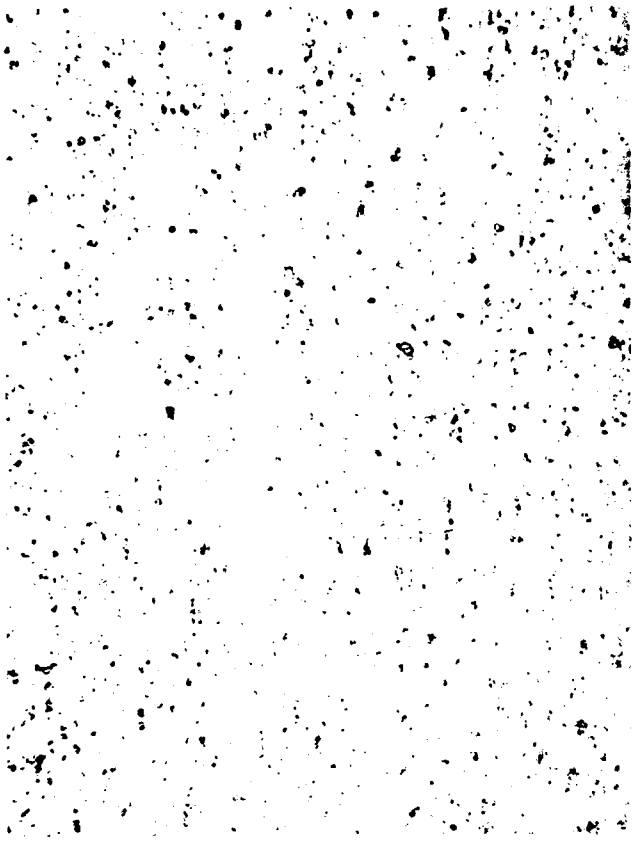
750°C, 1000 Hours

6% Sigma

Note sigma which stains dark after etching with KOH-H_2O electrolytic etchant. Also reveals carbides in austenitic matrix.

Figure V-3. (Continued)

(c) SPECIMEN NUMBER 8-2-9



0.40% C, ECC = 22.3

200X Magnification

850°C, 1000 Hours

0% Sigma

Figure V-3. (Continued)

(a) SPECIMEN NUMBER 9-2-4



0.014% C, ECC = 22.8

200X Magnification

650°C, 1000 Hours

Sigma ≃ 5%

Phases not stained dark are ferrite particles in an austenitic matrix. The same is true for (b) and (c).

Figure V-4. Effect of Aging Temperature On a Low-Carbon (0.014% C) Alloy.

(b) SPECIMEN NUMBER 9-2-7



0.014% C, ECC = 22.8

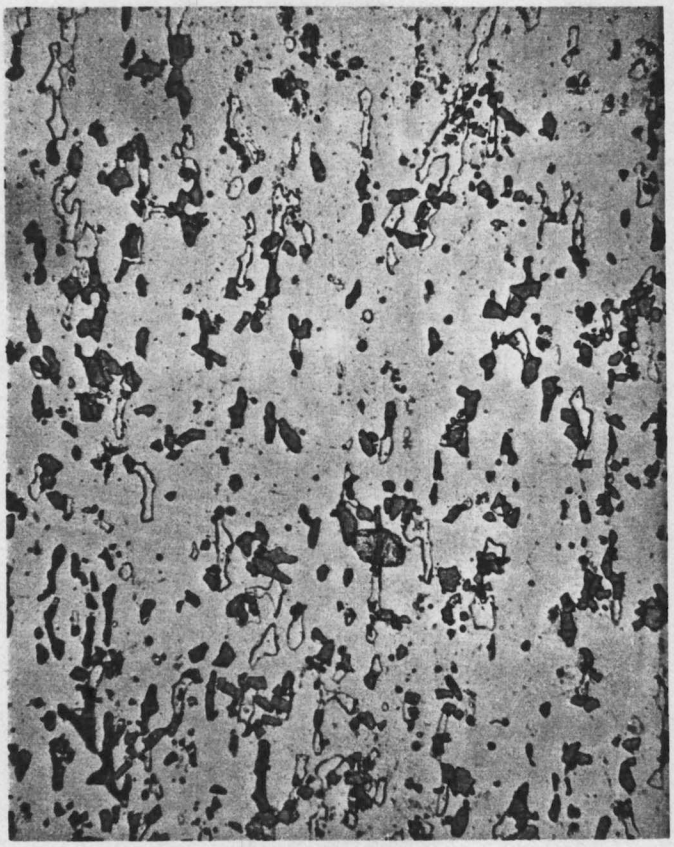
200X Magnification

750°C, 1000 Hours

Sigma ≃ 20%

Figure V-4. (Continued)

(c) SPECIMEN NUMBER 9-2-9



0.014% C, ECC = 22.8

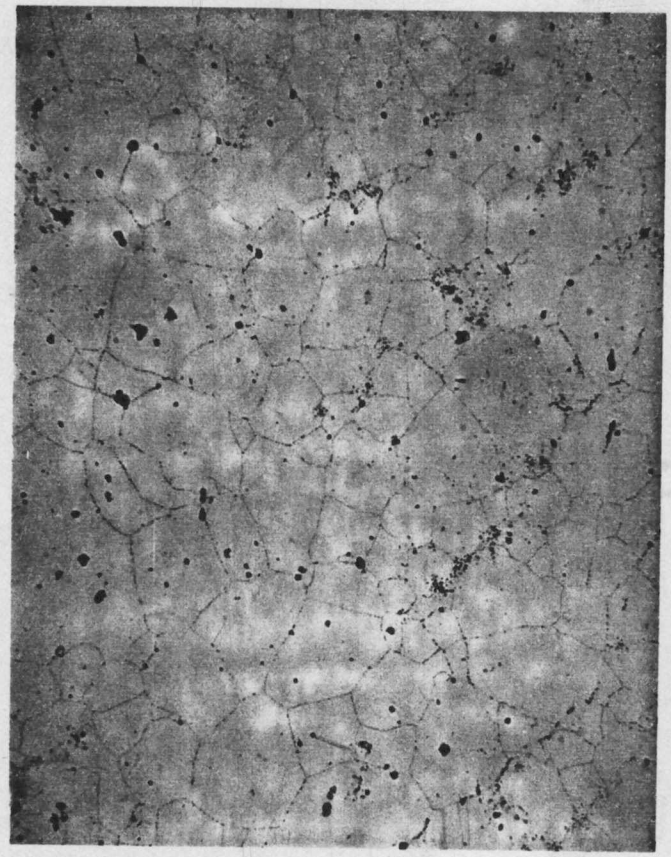
200X Magnification

850°C, 1000 Hours

Sigma ≃ 9%

Figure V-4. (Continued)

(a) SPECIMEN NUMBER 18-2-4



0.18% C, ECC = 20.6

200X Magnification

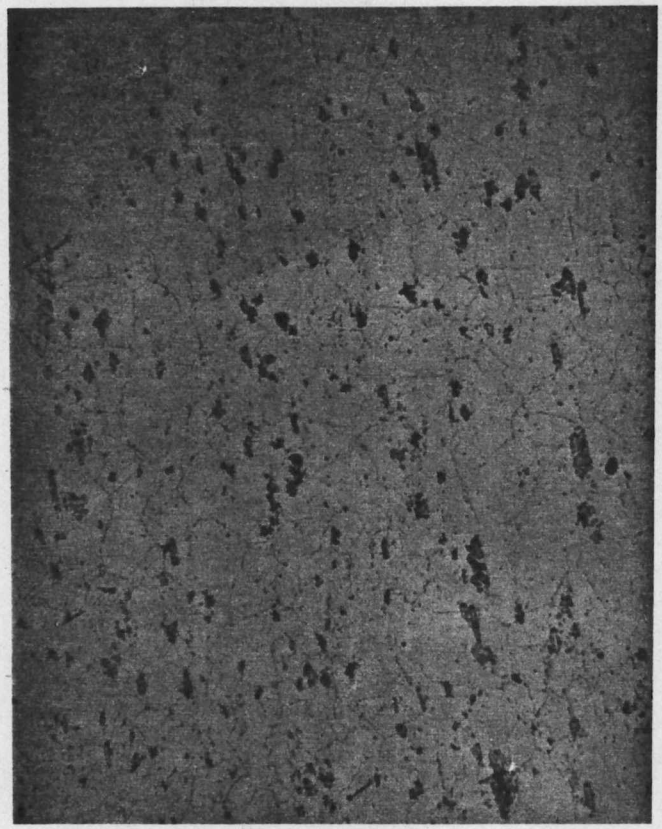
650°C, 1000 Hours

0% Sigma

Reveals only precipitation of carbides
and presence of no sigma phase.

Figure V-5. Effect of Aging Temperature On Sigma Formation for a Medium-Carbon (0.18% C) Alloy.

(b) SPECIMEN NUMBER 18-2-7



0.18% C, ECC = 20.6

200X Magnification

750°C, 1000 Hours

3% Sigma

Reveals only precipitation of carbides and presence of 3% sigma phase.

Figure V-5. (Continued)

(c) SPECIMEN NUMBER 18-2-9



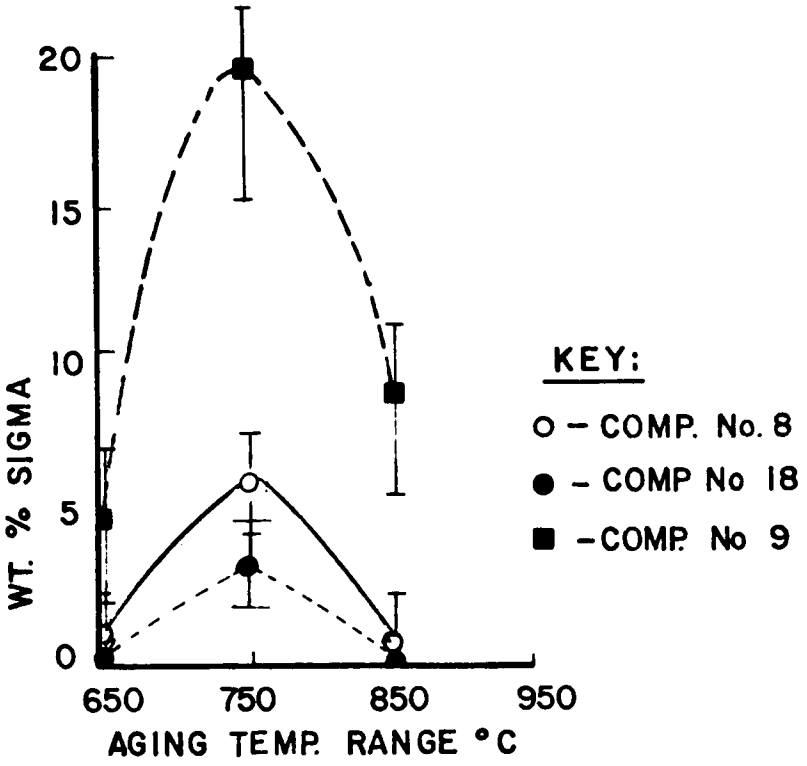
0.18% C, ECC = 20.6

100X Magnification

850°C, 1000 Hours

<3% Sigma

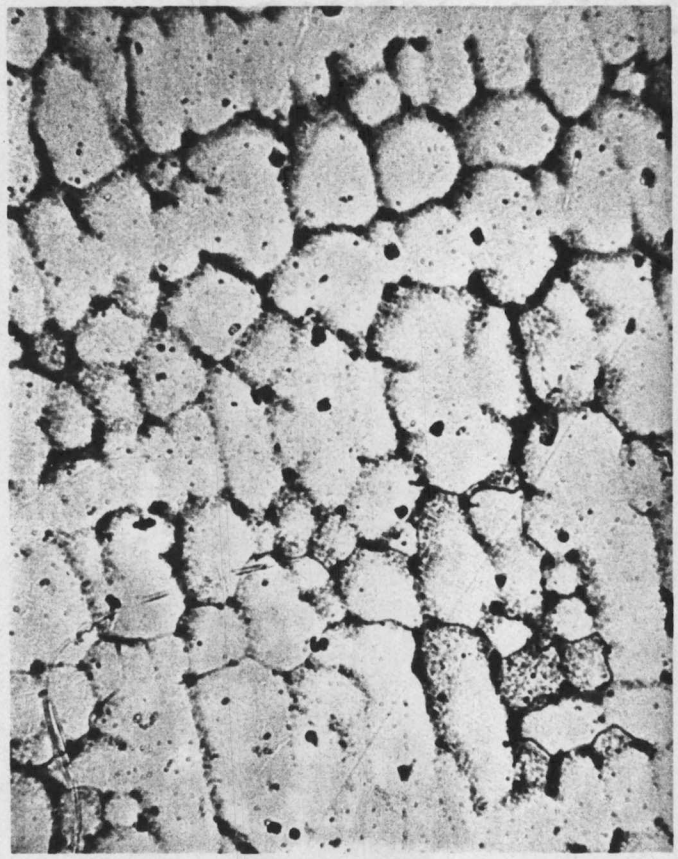
Figure V-5. (Continued)



ALLOY No.	%C	ECC (%Cr - 0.226 %Ni)		GROUP No
8	0.40	22.3		I
9	0.014	22.8		I
18	0.19	20.6		II

Figure V-6. Effect of Aging Temperature for 1000 Hours in the Range of 650-850°C (1200-1560°F) On the Rate of Sigma Formation in Three Solution-Treated Alloys.

(a) SPECIMEN NUMBER 18-0-4



0.19% C, ECC = 20.6

200X Magnification

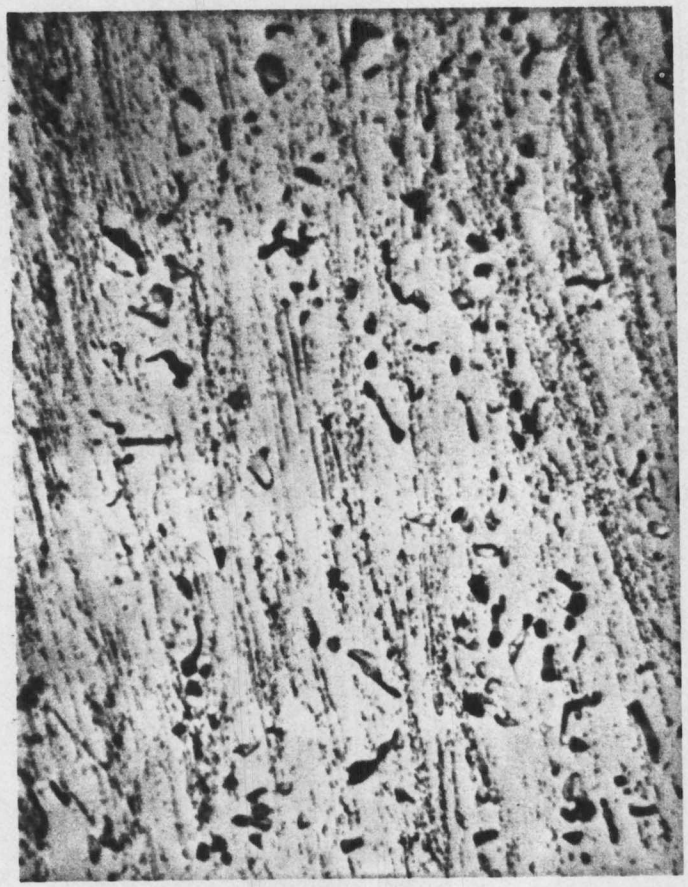
Etchant--KOH-H_2O
(Electrolytic)

0% Sigma

As-cast alloy. Mostly reveals carbides and little sigma in austenitic matrix.

Figure V-7. Effects of Initial Pre-Aging Treatments on Sigma Formation After Aging for 1000 Hours at 650°C.

(b) SPECIMEN NUMBER 18-1-4



0.19% C, ECC = 20.6

1000X Magnification

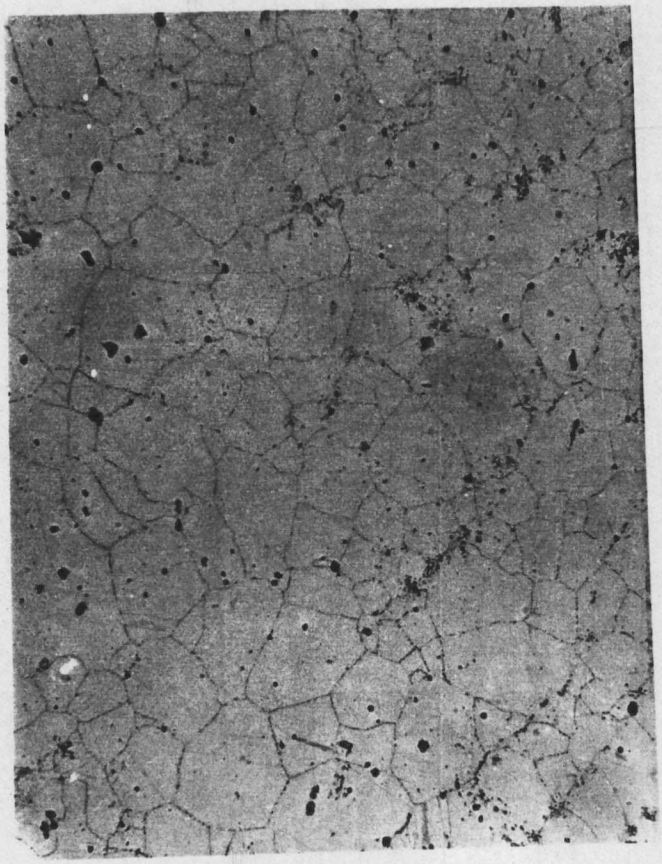
Etchant--KOH H_2O
(Electrolytic)

~7% Sigma

Cold-Worked (51%) alloy. Shows sigma (and carbides) along the slip bands in an austenitic matrix.

Figure V-7. (Continued)

(c) SPECIMEN NUMBER 18-2-4



0.19% C, ECC = 20.6

200X Magnification

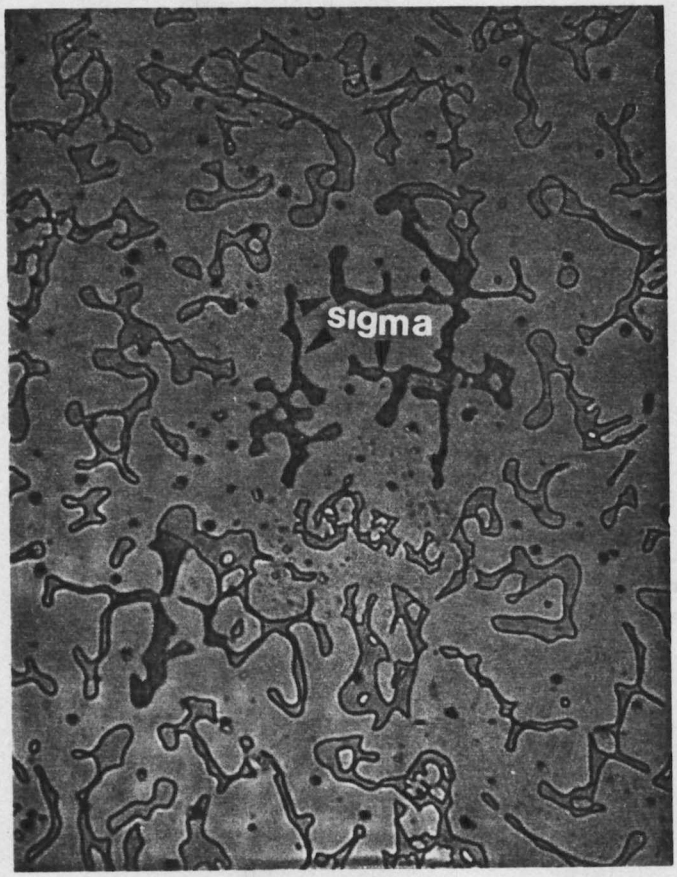
Etchant--KOH H_2O
(Electrolytic)

0% Sigma

Solution-Treated alloy. Mostly reveals carbides and little sigma in austenitic matrix.

Figure V-7. (Continued)

(a) SPECIMEN NUMBER 9-0-1



0.014% C, ECC = 22.8

200X Magnification

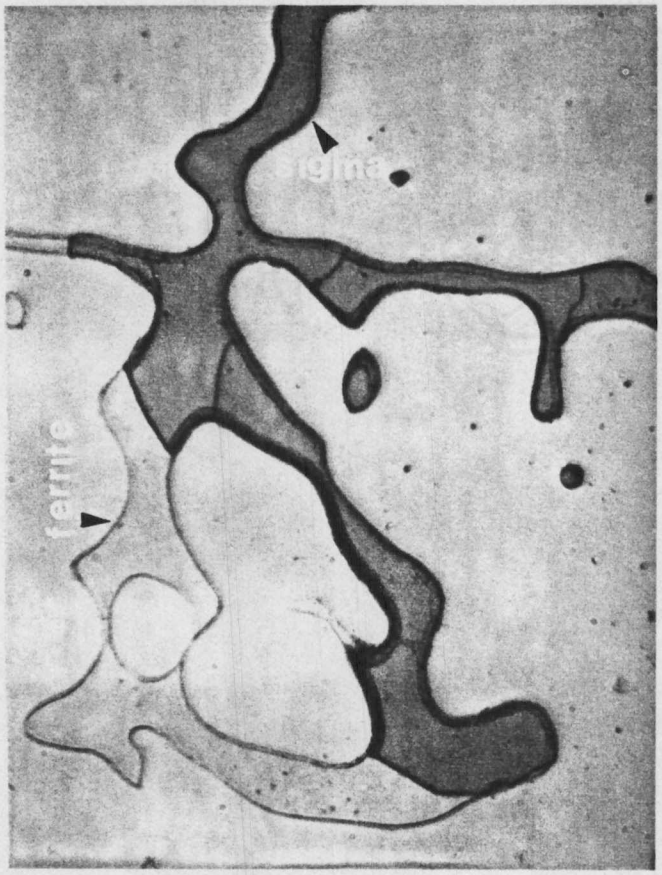
Etchant--KOH H_2O
(Electrolytic)

650°C, 1 Hour

Trace of sigma (dark phase).

Figure V-8. Optical Photomicrographs Showing the Effect of Aging Time (at 650°C) on Sigma Phase Transformation on a Low-Carbon (0.014% C) As-Cast Alloy.

(b) SPECIMEN NUMBER 9-0-1



0.014% C, ECC = 22.8

1000X Magnification

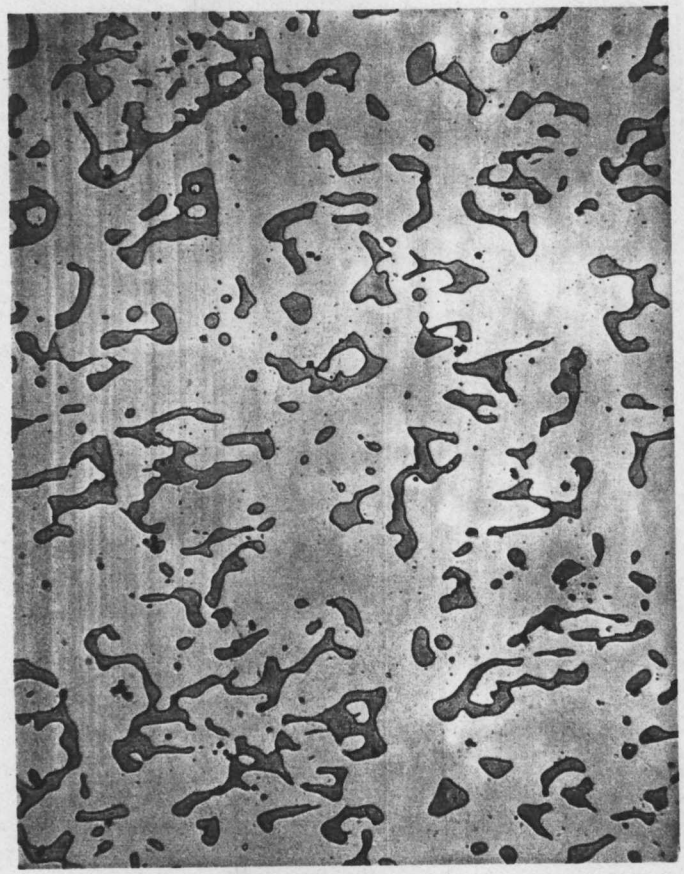
Etchant--KOH H_2O
(Electrolytic)

650°C, 1 Hour

Some sigma. (Same as (a) but with 1000X magnification.)

Figure V-8. (Continued)

(c) SPECIMEN NUMBER 9-0-2



0.014% C, ECC = 22.8

200X Magnification

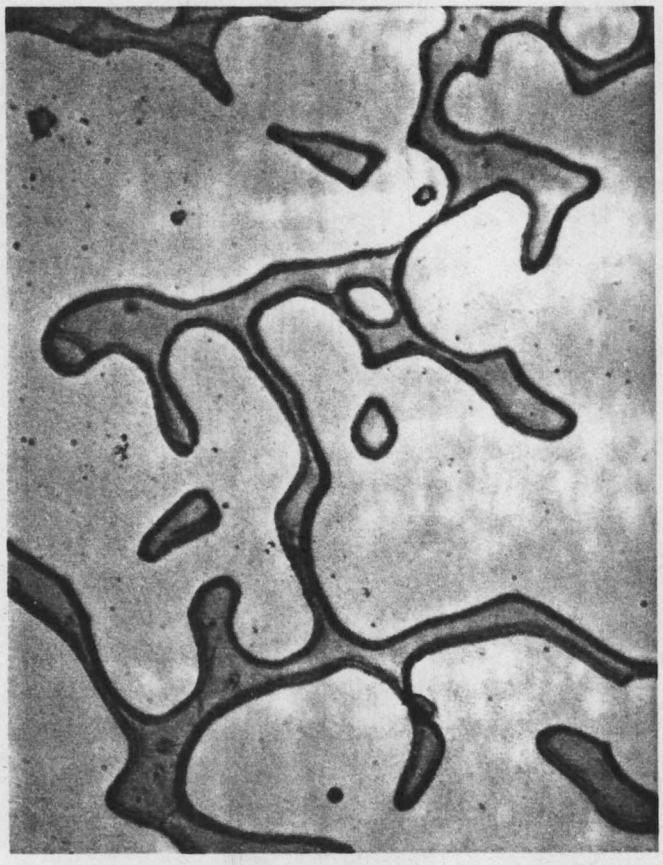
Etchant--KOH H_2O
(Electrolytic)

650°C, 10 Hours

About 90% transformed.

Figure V-8. (Continued)

(d) SPECIMEN NUMBER 9-0-3



0.014% C, ECC = 22.8

1000X Magnification

Etchant--KOH-H_2O
(Electrolytic)

650°C, 100 Hours

Approximately complete transformation.

Figure V-8. (Continued)

(a) SPECIMEN NUMBER 9-1-1



0.014% C, ECC = 22.8

200X Magnification

Etchant--KOH-H_2O
(Electrolytic)

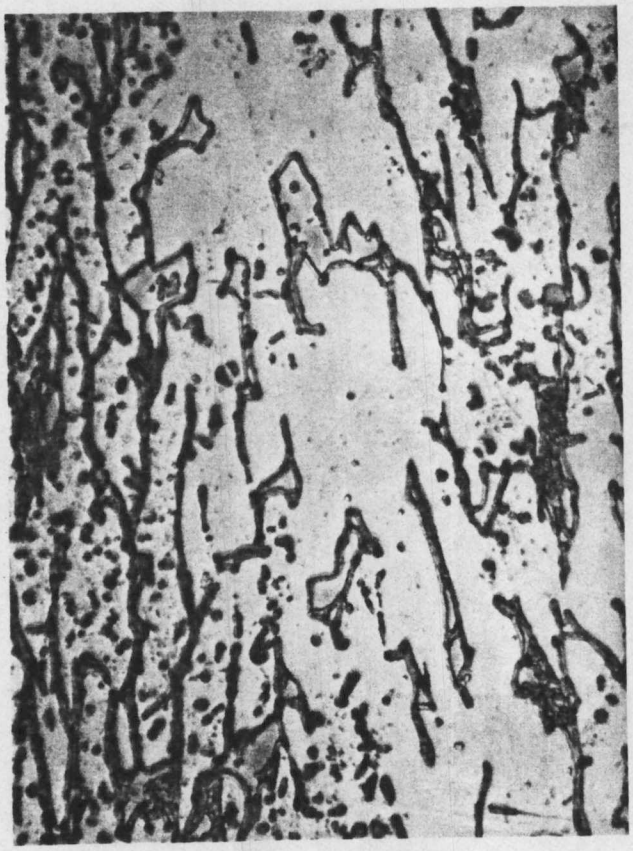
650°C, 1 Hour

~50% c.w.

Sigma phase is etched dark.

Figure V-9. Effect of Aging Time (at 650°C) on Sigma Phase Transformation for Alloy 9, Which Was Cold-Worked Prior to Aging.

(b) SPECIMEN NUMBER 9-1-3



0.014% C, ECC = 22.8

1000X Magnification

Etchant--KOH-H O
(Electrolytic)

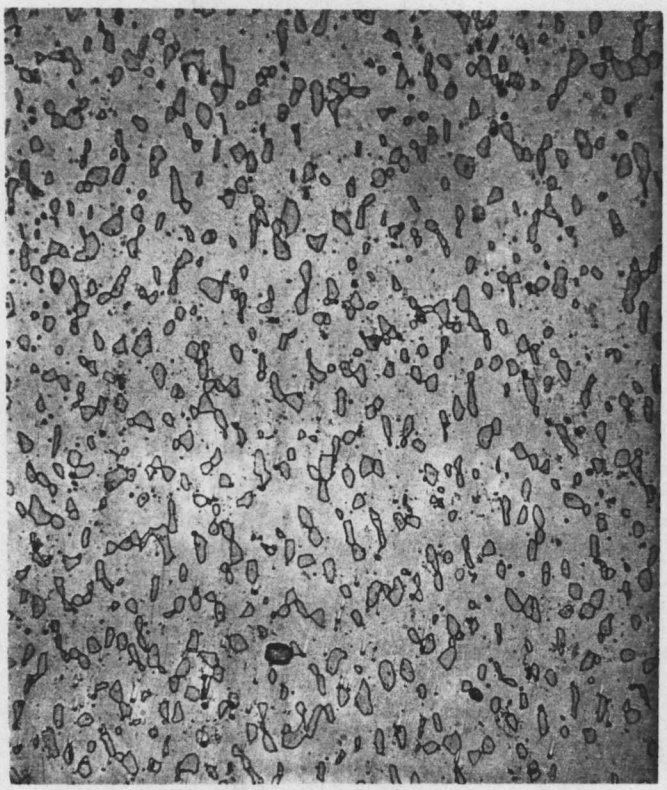
650°C, 100 Hours

~50% c.w.

Sigma phase is etched dark. Note partial recrystallization.

Figure V-9. (Continued)

(a) SPECIMEN NUMBER 9-2-1



0.014% C, ECC = 22.8

200X Magnification

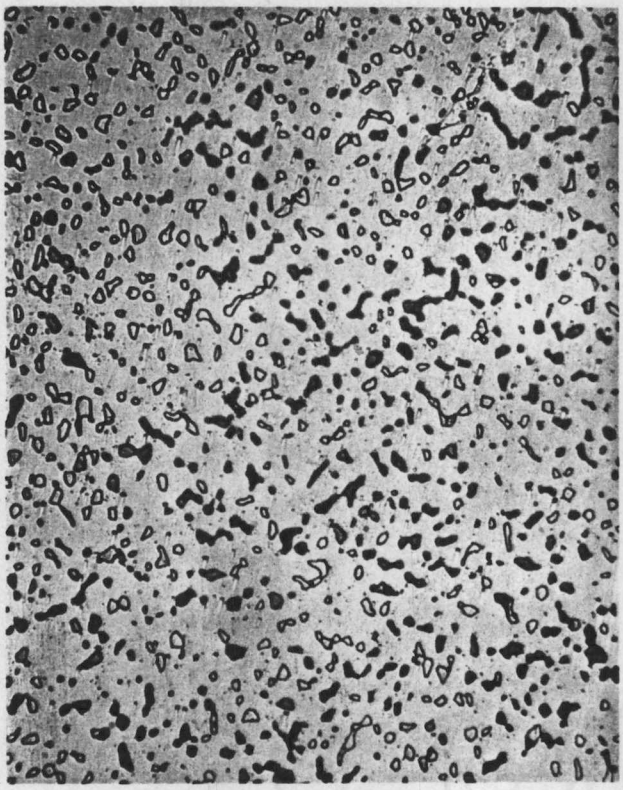
Etchant--KOH-H_2O
(Electrolytic)

650°C, 1 Hour

No sigma.

Figure V-10. Photomicrographs Illustrating the Effect of Aging Time (at 650°C) on Sigma Transformation for a Low-Carbon (0.014% C) Alloy Which Was Solution-Treated Prior to Aging.

(b) SPECIMEN NUMBER 9-2-2



0.014% C, ECC = 22.8

200X Magnification

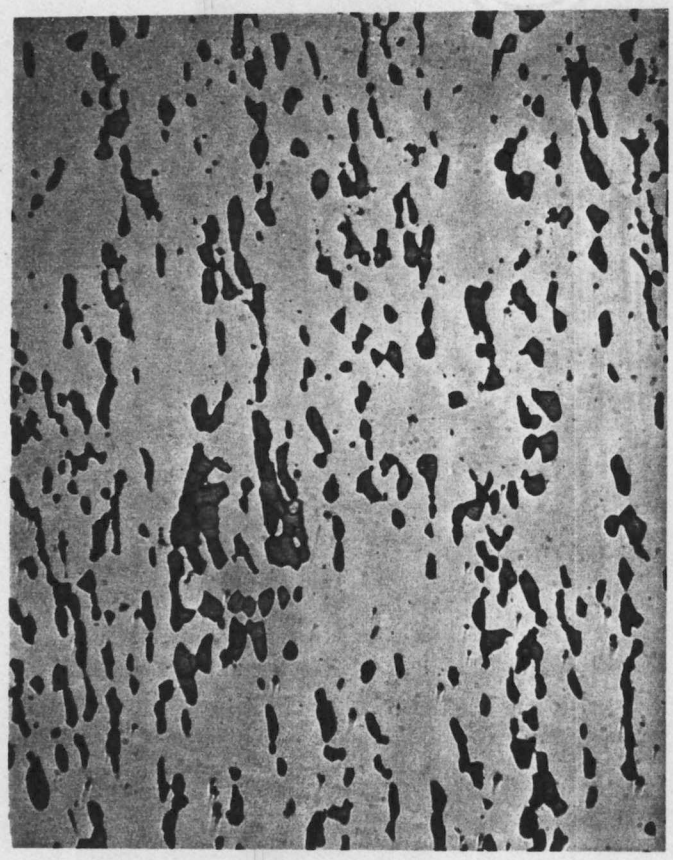
Etchant--KOH-H_2O
(Electrolytic)

650°C, 10 Hours

Some sigma (see dark particles).

Figure V-10. (Continued)

(c) SPECIMEN NUMBER 9-2-3



0.014% C, ECC = 22.8

200X Magnification

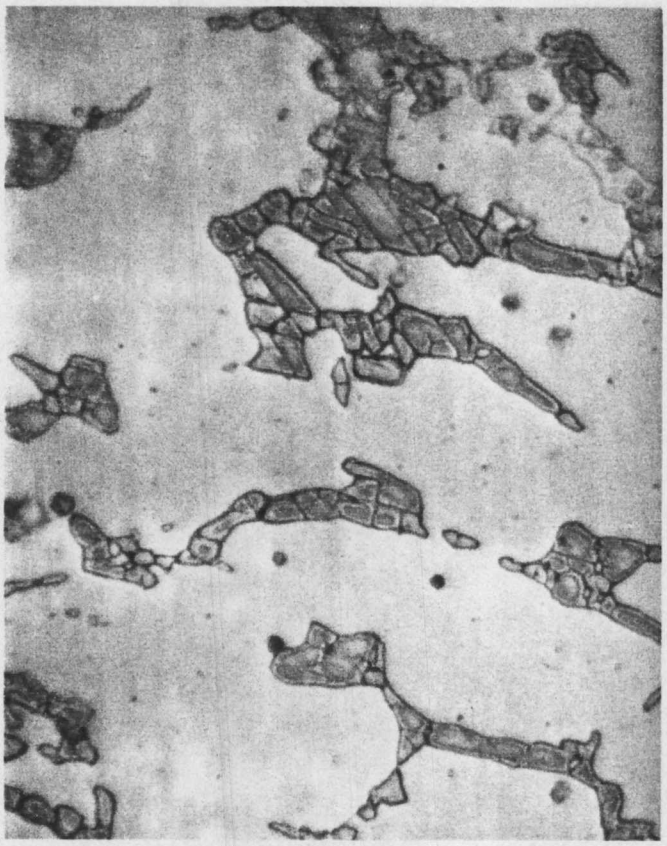
Etchant--KOH-H_2O
(Electrolytic)

650°C, 100 Hours

Approximately 100% sigma (dark phase).

Figure V-10. (Continued)

(d) SPECIMEN NUMBER 9-2-4-X



0.014% C, ECC = 22.8

1000X Magnification

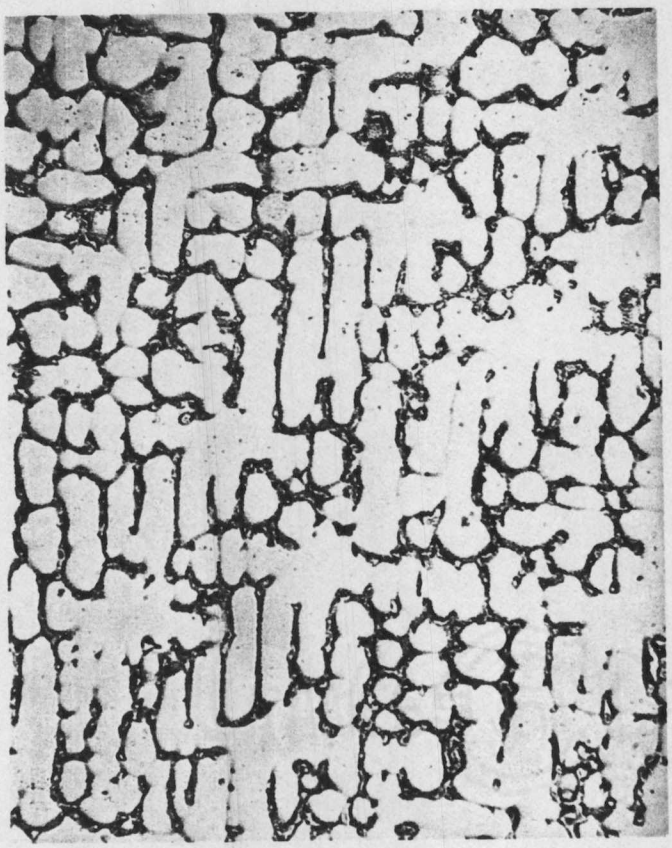
Etchant--KOH H_2O
(Electrolytic)

650°C, 2000 Hours

Note the morphology of sigma, which has a characteristic "dog-bone" appearance.

Figure V-10. (Continued)

(a) SPECIMEN NUMBER 8-0-2



0.40% C, ECC = 22.3

200X Magnification

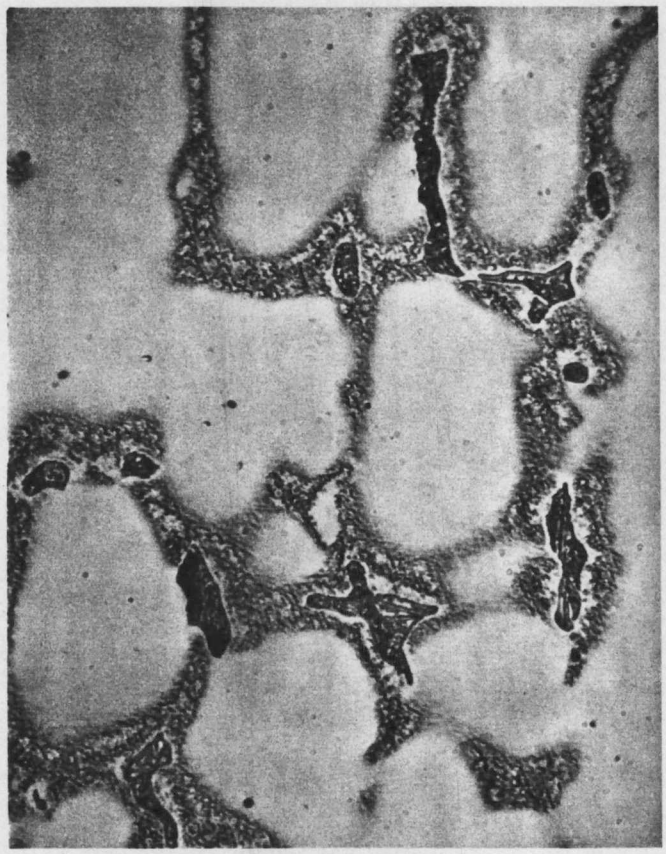
Etchant--KOH-H_2O
(Electrolytic)

650°C, 10 Hours

As-cast. No sigma.

Figure V-11. Photomicrographs Showing the Effect of Time and Cold Work on Sigma Phase Transformation.

(b) SPECIMEN NUMBER 8-0-2



0.40% C, ECC = 22.3

1000X Magnification

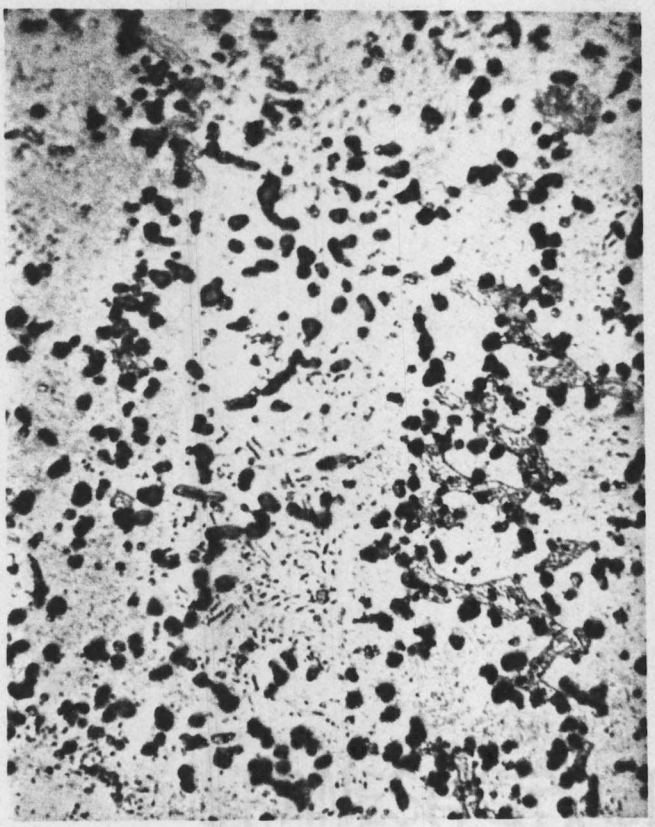
Etchant--KOH H_2O
(Electrolytic)

650°C, 10 Hours

As-cast. No sigma. (Same as (a) but with 1000X magnification.)

Figure V-11. (Continued)

(c) SPECIMEN NUMBER 8-1-3



0.40% C, ECC = 22.3

1000X Magnification

Etchant--KOH-H_2O
(Electrolytic)

650°C, 100 Hours

Approximately 50% c.w. Substantial amount of sigma (dark). Note "globular" massive morphology.

Figure V-11. (Continued)

principal composition variables in the Fe-Cr-Ni alloys used in this investigation. The effect of chromium on sigma formation is of interest because it is well known that an increase of Cr in commercial grades of stainless steels generally has a tendency to increase sigma formation after aging at 600-900°C (1100-1650°F). It is important to verify that this same behavior is observed in this study's Fe-Cr-Ni alloys. Further, no studies have been published that deal with the austenitic stainless steel alloys containing about 0.20-0.40% carbon. Because of the well known "sensitization effect," stainless steel such as AISI 304, 308, 316, etc. generally contain about 0.08% carbon (maximum).

The effect of Cr content on sigma formation is readily observed in Figure V-1, pp. 112-113. Two alloys containing different Cr content but nearly identical carbon levels are shown. The nickel content of these alloys results in a lowering of the ECC compared to the actual Cr content in accordance with the equation

$$ECC = Wt.\% Cr - 0.226 (Wt.\%) Ni.$$

In Figure V-1, both the actual Cr content and the ECC are higher in (a) than in (b), and there is clearly a greater amount of precipitated phases in (a) than in (b). A variety of techniques to be described in more detail in subsequent sections showed that the precipitates consisted of $M_{23}C_6$ carbides and sigma phase. The larger particles in greater abundance in (a) are sigma. The carbides are generally the smaller "dot-like" particles.

The sigma particles can be stained a reddish-brown by using the electrolytic etching and staining technique described in Chapter III.

This made it possible to use quantitative metallographic techniques to estimate the relative amount of sigma phase present in the microstructures.

Figure V-1(a), page 112, which had 25.9% Cr (0.18% C) and represents alloy number 10, shows 10% sigma after aging, whereas Figure V-1(b), page 113, with 24.5% Cr (0.19% C) representing alloy number 18, shows only 3% sigma. Both alloys were solution-treated (with controlled austenite grain size) and then aged for 1000 hours at 750°C. Thus, it is clear that Cr has a strong effect on sigma formation. Generally, the higher the Cr, the higher the sigma content. This is expected because in sigma, with its prototype composition (Fe-Cr), about half of its composition is chromium.[36,113] Further, increase of Cr content of the alloy provides a greater driving force for sigma formation as governed by the phase equilibria of the Fe-Cr-Ni system. Generally, this driving force is decreased somewhat by increased nickel content, and this is the effect which is apparently being accounted for in the ECC concept.

Metallographs of the specimens aged at 750°C for 1000 hours were typically chosen and presented in Figure V-1 because it was found that the rate of sigma formation was maximum at 750°C as compared to 650°C or 850°C. It is also hoped that 1000 hours aging time should be sufficient to produce the maximum amount of sigma phases in this study's Fe-Cr-Ni alloys.

The effect of Cr content is also shown in Table V-1. Upon examination of this table, it is found that both group I (average Cr = 25.9%) and group II (average Cr = 24.6%) alloys did form sigma upon aging, but group II was considerably less, as expected. Group III alloys (average Cr = <20.1%), on the other hand, did not form any noticeable amount of

TABLE V-1

PERCENT SIGMA[a] VS. % CARBON AND % Cr FOR THE SOLUTION-TREATED ALLOYS AFTER AGING FOR 1000 HOURS AT 750°C

Alloy Number	Specimen Number	% Carbon	Wt.% Cr	% Sigma	ECC[b]	ECC[c]	Comments
			GROUP I (Ave. ECC[d] = 22.5)				
8	8-2-7	0.40	25.5	6	18.5	22.3	Austenitic
9	9-2-7	0.014	26.1	20	22.6	22.8	Duplex[e]
10	10-2-7	0.18	25.9	10	20.6	22.7	Austenitic
19	19-2-7	0.38	26.2	4	18.8	22.3	Austenitic
			GROUP II (Ave. ECC[d] = 20.7)				
17	17-2-7	0.05	24.7	6	20.3	20.8	Austenitic
18	18-2-7	0.19	24.5	3	18.8	20.6	Austenitic
			GROUP III (Ave. ECC[d] <20.0)				
3	3-2-7	0.019	18.3	0	14.7	14.9	Austenitic
5	5-2-7	0.006	19.8	0	16.6	16.6	Austenitic
14	14-2-7	0.20	22.2	0	16.9	18.8	Austenitic

[a]Estimated by matallographic examination at 100X.[(70)] Etchant used--45 gm KOH-60 ml H_2O, 2.5 V DC (30 mA/cm^2).[(71)]

[b]ECC after correcting for carbide precipitation at 750°C.

[c]ECC based upon overall chemical composition.

[d]ECC = Cr (wt.%) - 0.226 Ni (wt.%) (arithmetic average of the ECC's).

[e]Austenite + ferrite.

sigma after 1000 hours at 750°C because, perhaps, the Cr content relative to nickel content was not high enough. However, although some sigma phase was expected in alloy 14 (based upon phase equilibria in the Fe-Cr-Ni ternary system), no sigma was found. This is probably because the alloy had 0.20% carbon, which significantly reduced the matrix chromium available for sigma formation. The effect of carbon on sigma formation will be discussed later.

Most of the present alloys were austenitic except number 9, which had about 9% ferrite after solution treatment. Some sigma in this composition could have come from the direct ferrite to sigma transformation with relative ease because of close similarity of their crystal structures (ferrite is BCC, sigma, BCT). The existence of ferrite in the initial microstructure is known to enhance the rate of sigma formation,[14,16] but the equilibrium amount of sigma should be controlled by the overall alloy composition.

Photomicrographs of representative samples showing the effect of carbon content are presented in Figure V-2, pp. 114-115. Results for all the alloys after aging are shown in Table V-1.

Figure V-2(a), page 114, shows the microstructure of the medium-carbon (0.18% C) alloy, number 10, which was solution-treated and then aged for 1000 hours at 750°C (1380°F). Ten percent sigma is noticed in this photomicrograph. Figure V-2(b), page 115, on the other hand, shows the microstructure of the high-carbon (0.38% C) alloy, number 19, which was also solution-treated and received identical aging. The sigma content of this microstructure was estimated to be only 4%. Thus, it is seen that carbon reduces the amount of sigma formation after such aging

treatments. This is attributed to the loss of the matrix chromium by the formation of carbides ($M_{23}C_6$) and, thus, the lowering of the available Cr for sigma formation. These findings are well in accord with the proposals of Gow and Harder[38] and Marshall and Hooper.[34]

Note that both the alloys had comparable austenite grain size (see Table III-3, page 75) prior to aging, and both alloys, belonging to group I, had nearly identical Cr content and ECC (see Table V-1, page 144).

Similar results to those shown in Figure V-2, pp. 114-115, were observed when comparing compositions 8 and 9 and 9 and 10 (see Table V-1). Alloy number 9, with low carbon content, had about 9% ferrite prior to aging, which, as noted above, increases the rate of sigma formation upon aging. However, this should be irrelevant to the equilibrium amount of sigma.

Group II alloys (average ECC = 20.7) also indicate that increase of carbon content decreases the amount of sigma phase (see Table V-1).

No conclusions could be made for group III alloys (average ECC < 20.0) because no sigma formed in these alloys after aging at 750°C for 1000 hours. It is believed that group III alloys did not have enough chromium to begin with for sigma phase formation.

The results of aging at 750°C for 1000 hours have been presented because, as mentioned before, the other two aging temperatures--namely 650°C and 850°C--showed substantially less sigma phase (even after 1000 hours) compared to the 750°C aging treatments. This will be described in more detail later.

Group B Photomicrographs--Effect of Aging Temperature on Sigma Formation

The effect of aging temperature on sigma formation is presented in Figures V-3, pp. 116-118, V-4, pp. 119-121, and V-5, pp. 122-124. A graphical representation of the results is shown in Figure V-6, page 125. All the samples were aged for 1000 hours and were aged at various temperatures: 650°C (1200°F), 750°C (1380°F), and 850°C (1560°F). Also, all the samples were solution-treated to produce a homogeneous austenite of controlled grain size. Note that all alloys were fully austenitic after this treatment except alloy 9, which contained 9% ferrite.

Micrographs of alloy 8 of group I are presented in Figure V-3, pp. 116-118. One can see that the 750°C sample shown in (b) has the maximum amount of sigma phase, but the 650°C (a) and 850°C (c) photomicrographs show no sigma phase at all, even though all samples received 1000 hours aging at the given temperatures. Note that (a) and (c) reveal mostly carbides in the austenitic matrices because the alloy had a high carbon content (0.40% C).

Similarly, the effect of aging temperature on sigma formation for alloy 9 (which had only 0.014% C) is presented in Figure V-4, pp. 119-121. Again, a maximum amount of sigma phase (20%) is observed at the 750°C (b) aging temperature as compared to only 5% at 650°C (a) or 9% at 850°C (c). Note that the lighter particles are ferrite, while only the particles stained dark (actual color--reddish brown, under optical microscope) by the KOH-H_2O electrolytic etchant are sigma phase particles.

Figure V-5, pp. 122-124, demonstrates the effect of aging temperature on sigma formation in alloy 18, which belongs to group II (average ECC = 20.6). This alloy was fully austenitic and is considered a

medium-carbon sample (0.18% C). Once again, sigma phase formation was maximum at 750°C (b). In Figure V-5, (a), page 122 (650°C), and (c), page 124 (850°C) reveal mostly intergranular and transgranular precipitation of carbides throughout the austenitic matrix.

In Figure V-6, page 125, the sigma content (%) is shown as a function of aging temperature in graphical form for alloy compositions 8, 9, and 18. There is not much difference between 8 and 18, but alloy 9 shows substantially larger amount of sigma compared to 8 or 18. The exact nature of the curves is not known, but there appears to be a maximum (for each composition) between 650°C and 850°C.

The present finding--namely maximum sigma transformation at 750°C--was expected, because sigma is known to form most readily at 750°C in austenitic stainless steels.[16] Grot and Spruiell,[91] for example, who worked on a 316 titanium-modified stainless steel, found similar results. Likewise, Marshall and Hooper[34] and Weiss and Stickler[16] have also reported that sigma formation was maximum at 750°C (1380°F) in their alloys after long aging periods.

Sigma formation, like any other phase, is controlled by nucleation and growth conditions and thermodynamic equilibrium. At low temperature, namely 650°C (1200°F), the diffusion of elements like Cr, Ni, etc. in the austenitic matrix is slow and sluggish. Since sigma phase is an intermetallic compound which consists of elements like Fe, Cr, and Ni, very long aging would be required for thermodynamic equilibrium. Likewise, at higher temperature such as 850°C (1560°F), even though diffusion rate is high, the relative amount of sigma phase is lower. This is presumably caused by shift in phase equilibria of Fe-Cr-Ni-C systems.

Emmanuel,[36] who worked on Fe-25Cr-20Ni alloys, reported that sigma phase increases with temperature up to 1500°F (815°C) and then rapidly decreases to a vanishing point at 1700°F (930°C). The present findings closely resemble those of Emmanuel.

Group C Photomicrographs--Effect of Pretreatments

Although the initial sample conditions should have no effect on the equilibrium amount of sigma formed in an alloy of given composition, it was deemed important to briefly examine their effect on the rate of sigma phase formation in the prepared alloys. This is presented in Figure V-7, pp. 126-128.

In Figure V-7, (a), page 126, shows the microstructure of the as-cast alloy, number 18 (0.19% C), after aging for 1000 hours at 650°C (1200°F). No sigma could be found in this optical micrograph, which was developed after etching electrolytically in a KOH-H_2O solution. The structure reveals a fine dispersion of carbides ($M_{23}C_6$) in an austenitic matrix. It is believed that the growth conditions for sigma were not favorable. The alloy had no ferrite in its as-cast state prior to aging. Note that the dentritic or lamellar patterns (after solidification) have been partially eliminated by some diffusion occurring during aging. A mild cellular structure is still observable.

The effect of cold work on sigma phase formation is presented in (b), page 127, of Figure V-7. This photomicrograph shows about 7% sigma after aging for 1000 hours at 650°C. Notice that both samples representing (a) and (b) had the same chemical composition--0.19% C (with ECC = 20.6), but different amounts of cold work prior to aging--(a) had 0% and (b) had 51%. Thus, the positive effect of cold work on sigma formation is

demonstrated in this illustration. A cold-worked structure is considered thermodynamically unstable and is prone to sigma formation, because the cold work provides a driving force for sigma formation at the defects such as slip bands, stacking faults, etc.[16,111] Spruiell et al.[5] have pointed out the enhancement of diffusion of elements because of the decrease of diffusion distance in a cold-worked structure. Further, the enhancement of sigma phase could be related to ease of nucleation at slow-moving recrystallizing boundaries, together with enhanced growth rate due to diffusion along the boundary. This effect was first discussed by Spruiell, Scott, Ary, and Hardin.[5]

Note that sigma phases shown in (b), page 127, of Figure V-7 are extremely small--typically about 10^{-3} x 10^{-4} cm diameter--and seem to reside primarily in the recrystallized regions of the austenitic matrix. This is in general agreement with the observations of Spruiell et al.[5]

Figure V-7(c), page 128, shows the microstructure of the same alloy (18), which was solution-treated prior to aging and etched under similar conditions as (a) and (b). This photomicrograph shows little or no sigma. A uniform distribution of carbides in an austenitic matrix is revealed. The growth conditions for sigma phase were not favorable in this structure, as in the cold-worked alloy, although the chemical composition was the same.

Similar effects of initial sample condition were observed for each of the alloy compositions.

Group D Photomicrographs--Effect of Aging Time

The changes in microstructure with aging time were found to be strongly dependent on alloy composition and initial microstructure. The

progressive changes occurring in the microstructure of alloy composition number 9 (0.014% C, ECC = 22.8) with aging time at 650°C (1200°F) are shown in Figures V-8, pp. 129-132, V-9, pp. 133-134, and V-10, pp. 135-138. Figure V-8 shows the effect of aging the as-cast alloy, Figure V-9 shows the effect of aging the 50% cold-worked alloy, and Figure V-10 shows the effect of aging the solution-treated alloy. It should be recalled that this alloy (9) had about 20% ferrite in the as-cast condition and about 9% ferrite in the solution-treated condition.

For each initial condition in this alloy, sigma first nucleated in the ferrite (or at the boundary with austenite) and then grew until all the ferrite was eliminated. In Figures V-8 to V-10, the sigma particles are stained dark and have the same shape as the white ferrite regions embedded in the austenitic matrix. Cold working increased the rate of sigma formation compared to the as-cast alloy, while solution treatment reduced it as previously discussed.

The morphology of sigma varied with initial pretreatment also. The as-cast sample developed an "island-like" or semi-continuous sigma morphology, which has been found to be more detrimental to toughness than the globular-type sigma.[16,17] Sigma developed in the cold-worked sample, Figure V-9, exhibits a smaller particle size, a greater number density of particles, and a somewhat more globular morphology. In the solution-treated samples, the sigma phase is discontinuous clusters of globular particles.

The progression of changes shown in Figures V-8 to V-10 were not observed in the case of samples which contained little or no ferrite in the initial microstructure.

Alloy number 8, which belonged to the same group as number 9 (group I, ECC = 22.5) but contains more carbon (0.40% C) and almost no ferrite, was studied concerning the effect of aging time on sigma formation. The microstructures are presented in Figure V-11, pp. 139-141. Aging time varied from 10-100 hours at 650°C. In one case (part (c), page 141), the alloy was ~50% cold-worked and then aged for 100 hours at 650°C to learn the effect of cold work on sigma formation for this alloy.

Figure V-11(a), page 139, shows the as-cast aged sample at 650°C for 10 hours, with very little sigma phase. Mostly carbides (trapped in interdentritic channels) in the austenitic matrix are revealed. This figure is worth comparing with Figure V-8(c), page 131 (composition 9, 10 hours, 0.014% C), which shows a substantial amount of sigma, indicating once again the effect of carbon on sigma formation.

Figure V-11(b) is the same as (a) but at higher magnification (1000X), which reveals only carbides in the austenitic matrix and no sigma.

A microstructure of the cold-worked (~50%) and aged sample of the alloy (8) is shown in Figure V-11(c), page 141. The alloy was aged for 100 hours at 650°C. The photomicrograph exhibits a substantial amount of sigma phases with massive globular morphology and dispersion of carbides in the austenitic matrix. Once again, it is seen that cold work has an accelerating effect on sigma formation.

Microhardness Measurements

Another method which aids in the identification of sigma phase in the austenitic stainless steel alloys is the microhardness measurements

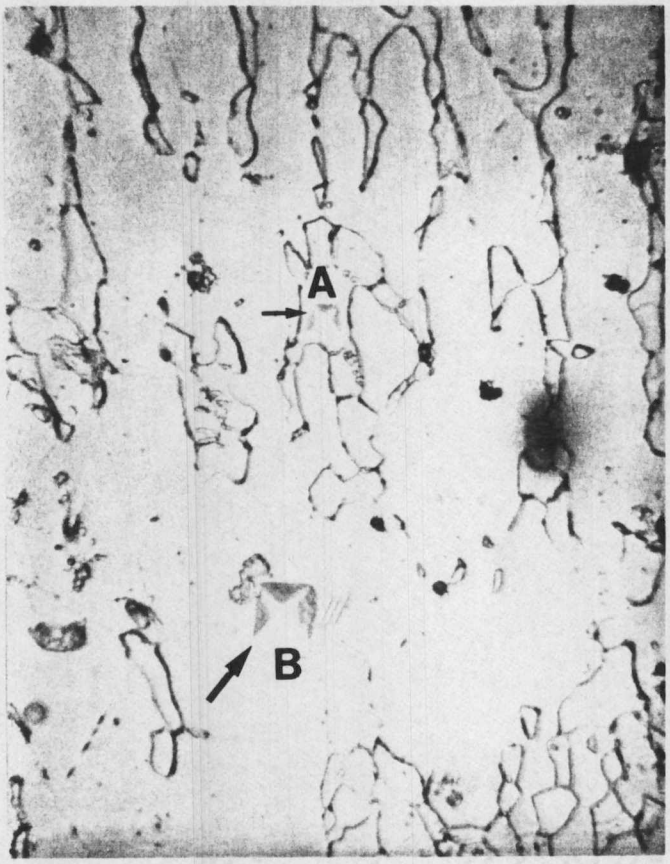
on the phase itself using suitable applied load. It is known that sigma phase is much harder than both the austenite phase and the ferrite phase.[56]

Microhardness measurements were attempted on alloy number 9, which had the highest amount of sigma phase, as revealed by the optical metallographic technique. The alloy was aged for 1000 hours at 650°C. The results of the investigation are shown in Figure V-12. This figure shows a much larger indentation on the austenitic matrix (B) but a much smaller indentation on the sigma phase (A) under the same applied load of 10 gm. This clearly indicates that sigma phase is much harder than the austenite phase (sigma phase 674 DPH vs. 148 DPH for the austenitic matrix). A comparative hardness data for the various phases under different conditions is presented in Table V-2, which indicates that sigma phase is harder than the cold-worked or annealed austenitic matrix. These findings are slightly lower than those of Dulis and Smith.[56] who reported sigma hardness to be ~750 DPH in a Fe-18Cr-8Mo steel after aging for 3000 hours at 1500°F (815°C). They used a 1-gm load and 2000X magnification. Such variation of hardness could be attributed to the variation of chemical composition of the sigma phase in the alloy system or to experimental errors resulting from the different loads.

Although this method gives an idea of the presence of sigma phase in the system, it is by no means 100% accurate because another phase--namely $M_{23}C_6$ carbide--which also occurs in the austenitic stainless steel alloys upon aging, is also considerably harder than the austenitic matrix. However, alloy number 9 had very little carbon and, therefore,

COMPOSITION NUMBER 9

SPECIMEN NUMBER 9-2-4



1000X Magnification

650°C, 1000 Hours

Oxalix Acid Etch
(Electrolytic)

Load Applied--10 gm

Microhardness data showing diamond pyramid indentations on the sigma phase (A) in an austenitic matrix (B). The hardness of the sigma phase was 674 DPH (R_C59), whereas the austenitic matrix hardness was only 148 DPH (R_B79).

Figure V-12. Diamond Pyramid Hardness Numbers (Microhardness) for Sigma and Austenite.

TABLE V-2

HARDNESS OF VARIOUS PHASES IN AUSTENITIC STAINLESS STEEL

Alloy Number	Specimen Number	Alloy Treatment	Measured Hardness Values		Comments
9	9-0	As-cast	(153 DPH)	R_B80	Bulk hardness on matrix.
9	9-1	As-cast + 50% c.w.	(294 DPH)	R_C29	Matrix hardness.
9	9-2	Solution-treated, 1050°C, 1 hour, then water-quenched	(147 DPH)	R_B78	Matrix hardness.
9	9-2-4	Aged 1000 hours, 650°C	674 DPH	(R_C59)	Microhardness* data on sigma phase.
9	9-2-4	Aged 1000 hours, 650°C	148 DPH	(R_B79)	Microhardness* data on austenite matrix.

*Load applied--10 gm.

little or no carbides. Therefore, it is not believed that the hardness values were from the carbide phase.

Because the size and shape of sigma particles were alike in many of this study's alloys, it is felt that microhardness measurements in one sample (number 9) should be sufficient to give an idea of the magnitude of the sigma hardness. Later, the unknown phases in alloy 9 were further confirmed to be sigma phase by x-ray diffraction and transmission electron microscopy experiments.

2. FERRITE MEASUREMENTS

The ferrite numbers of the solution-treated alloys before and after aging for 1000 hours are given in Table V-3. The experimental procedure was described in Chapter III.

The table indicates that all the original ferrite content of the solution-treated alloys disappeared after 1000 hours at 650°C, 750°C, or 850°C. The microstructural analyses previously described in this chapter showed that the ferrite was gradually transformed to sigma phase. The ferrite number measurements by Magne-Gage indicate that this transformation is complete at all temperatures studied after 1000 hours of aging.

Andress[108] studied such transformation extensively on his 316L weld metal and found similar results. However, he found that a small amount (less than 0.2%) of ferrite was present even after 2000 hours of aging at 650°C, which he attributed to sluggishness of the reaction at low ferrite levels. Andress reported that ferrite decay followed a sigmoidal transformation.

TABLE V-3

FERRITE MEASUREMENTS* OF THE AGED SOLUTION-TREATED ALLOYS

Alloy Number	Initial FN Solution-Treated Sample	FN After Aging 1000 Hrs.			Comments
		650°C	750°C	850°C	
3	1.4	0	0	0	Complete ferrite to sigma transformation
5	1.2	0	0	0	"
8	0.5	0	0	0	"
9	9.0	0	0	0	"
10	1.0	0	0	0	"
14	0.4	0	0	0	"
17	0.8	0	0	0	"
18	0	0	0	0	"
19	0	0	0	0	"

*Measured with a Magne-Gage.

3. BULK EXTRACTION AND X-RAY DIFFRACTION-- QUANTITATIVE RESULTS

The phases formed in the aged samples were identified by x-ray diffraction patterns from the extracted residues and by direct diffraction on the bulk aged sample of composition number 9 samples aged for 1000 hours at 650°C, 750°C, and 850°C used in this study.

The weight percent (wt.%) of extracted precipitates from the aged samples are presented in Tables V-4 and V-5. Table V-4 shows the results using a 10% HCl-90% methanol extraction solution. Table V-5 is the result of extraction from composition 9 using a different electrolytic solution, the composition of which is given below:

150 gm citric acid

100 gm KI

20 ml HCl

150 ml H_2O.

This was done because of dissolution of sigma phase in the widely used 10% HCl-90% CH_3OH solution.

For most samples, the weight percent extracted residues in the next-to-last column of Table V-4 appear to be mostly $M_{23}C_6$ carbide. This statement is based, in part, on the x-ray diffraction results (to be described later in this section) and, in part, on the agreement obtained between the measured amount of extract and the results of calculations used to compute the percent carbide based upon the carbon content of the alloys and their solid solubility limits at the aging temperatures. The principle used was that carbide forms only from the excess carbon

TABLE V-4

BULK ELECTROLYTIC EXTRACTION RESULTS USING
10% HCl-90% CH_3OH SOLUTION[a]

Sample Number	%C	Aging Temperature (°C)	Aging Time (Hours)	Wt.% Extract	Calculated Wt.% Carbide[b]
3-0-4	0.019	650	1000	0.2023	0.2983
3-1-4	0.019	650	1000	0.2823	0.2983
3-2-4	0.019	650	1000	0.2516	0.2983
3-2-7	0.019	750	1000	0.6530	0.3335
3-2-9	0.019	850	1000	0.7014	0.3384
5-0-4	0.006	650	1000	0.1391	0.0942
5-1-4	0.006	650	1000	0.3192	0.0942
5-2-4	0.006	650	1000	----	----
5-2-7	0.006	750	1000	0.0714	0.1053
5-2-9	0.006	850	1000	0.2633	0.1069
8-0-4	0.40	650	1000	2.9333	6.28
8-1-4	0.40	650	1000	4.5706	6.28
8-2-4	0.40	650	1000	6.1143	6.28
8-2-7	0.40	750	1000	6.1240	7.02
8-2-9	0.40	850	1000	5.4065	7.124
9-0-4	0.014	650	1000	0.3296	0.2198
9-1-4	0.014	650	1000	0.4804	0.2198
9-2-4	0.014	650	1000	0.2927	0.2198
9-2-7	0.014	750	1000	0.2889	0.2457
9-2-9	0.014	850	1000	0.902	0.2493
10-0-4	0.18	650	1000	1.0649	2.826
10-1-4	0.18	650	1000	2.5560	2.826
10-2-4	0.18	650	1000	2.6775	2.826
10-2-7	0.18	750	1000	2.6930	3.159
10-2-9	0.18	850	1000	3.8944	3.2058
14-0-4	0.20	650	1000	0.6942	3.14
14-1-4	0.20	650	1000	2.8203	3.14
14-2-4	0.20	650	1000	2.5932 (3.1432)	3.14

TABLE V-4 (Continued)

Sample Number	%C	Aging Temperature (°C)	Aging Time (Hours)	Wt.% Extract	Calculated Wt.% Carbide[b]
14-2-7	0.20	750	1000	2.9663	3.51
14-2-9	0.20	850	1000	2.8943	3.562

[a]Solution used--10% HCl-90% CH_3OH at 600 mA/cm^2. This current density was considered too high because of dissolution of sigma phase, it was found later. 175-225 mA/cm^2 is preferred.

[b]Formula used to calculate % carbide:

Temperature	Carbide Formula	Comments
650°C	$[Cr_{15.70}\ Fe_{7.30}]C_6$	1 wt.% C ≡ 15.70% carbide
750°C	$[Cr_{17.55}\ Fe_{5.45}]C_6$	1 wt.% C ≡ 17.55% carbide
850°C	$[Cr_{19.05}\ Fe_{3.95}]C_6$	1 wt.% C ≡ 17.81% carbide

TABLE V-5[a]

BULK ELECTROLYTIC[b] EXTRACTION RESULTS USING 150 gm CITRIC ACID-100 gm KI-20 ml HCl-150 ml H_2O SOLUTION

Experiment Number	Sample Number	Wt.% Extract	Average Wt.% Extract
1	9-0-4[c]	9.02	
2		4.71	
3		2.31	
4		3.35	4.85

[a]Composition number 9, as-cast sample, aged for 1000 hours at 650°C (1200°F).

[b]Courtesy of Mr. Thomas M. Andress, Jr., The University of Tennessee, Knoxville, Tennessee (1968) (now with the American Electric Power Service Corporation of Canton, Ohio).

[c]Solution used:

150 gm citric acid
100 gm KI
20 ml HCl
150 ml H_2O

voltage--4 V DC (approx.)
current--400 mA

Source: E. J. Dulis and G. V. Smith, Symposium on the Nature, Occurrence, and Effects of Sigma Phase, ASTM STP No. 110, American Society for Testing and Materials, Philadelphia, Pennsylvania, p. 1 (1950).

above the solubility limit and that the stoichiometry of the carbide, generally accepted as approximately $M_{23}C_6$, takes different forms depending upon the aging temperature at equilibrium or nearly equilibrium conditions. The details of these calculations are shown in Appendix C and Appendix D.

The results in Table V-4 did not agree well with metallography with respect to the amount of sigma present in the alloys. At this point, it was concluded that the 10% HCl-90% CH_3OH solution was dissolving the sigma particles and it would be necessary to verify the presence of sigma by another means. One such approach was changing the extraction solution to that listed under Table V-5.

The percent residue extracted from composition 9 using this new solution is shown in Table V-5. This is substantially above the value extracted using the HCl-methanol solution, confirming the fears expressed above.

Qualitative Identification of Phases--Sigma Phase

The powder x-ray diffraction on the residues described in Table V-5 from composition number 9 after aging for 1000 hours at 650°C are presented in Table V-6. Results of direct diffraction on the bulk aged sample are shown in Table V-7. The bulk sample was aged at 650°C for 1000 hours. The bulk sample was then electrolytically etched for ten seconds at 35 mA/cm^2 current density in a 90 ml H_2O-10 ml oxalic acid solution. The relative intensities given in Table V-7 are considered approximate only because of the fact that the sample might have preferred orientation in the metal.

TABLE V-6

d-SPACINGS OF THE RESIDUE OBTAINED FROM COMPOSITION 9 (SAMPLE 9-0-4) AFTER AGING FOR 1000 HOURS AT 650°C[a]

2Θ (°)	Relative Intensities (I/I_o)	d (Å) (Calculated)	d (Å) From File	(hkl)	Comments
83.2	12	1.16	1.01	(414)	Sigma
79.7	15	1.20	1.22	(720)	"
77.3	18	1.23	1.25	(413)	"
76.0	17	1.25	1.27	(532)	"
52.3	14	1.75	1.78	(312)	"
50.1	16	1.82	1.85	(222)	"
48.7	25	1.87	1.90	(331)	"
47.5	49	1.91	1.95[b]	(411)	"
46.4	30	1.96	1.99[b]	(212)	"
44.1	21	2.05	2.04 2.09	(202) (330)	"
42.8	35	2.11	2.15	(410)	"
40.0	19	2.25	2.30	(002)	"

[a]Extraction solution used:

150 gm citric acid
100 gm KI
20 ml HCl
150 ml H_2O

voltage--4 V DC
current--400 mA

[b]d values used to compute c_o, a_o, and c_o/a_o ratio.

Source: E. J. Dulis and G. V. Smith, Symposium on the Nature, Occurrence, and Effects of Sigma Phase, ASTM STP No. 110, American Society for Testing and Materials, Philadelphia, Pennsylvania, p. 3 (1950).

TABLE V-7

DIRECT X-RAY DIFFRACTION RESULTS ON BULK COMPOSITION 9 (SAMPLE 9-1-4) AFTER AGING FOR 1000 HOURS AT 650°C[a]

Peak Number	2Θ (°)	Relative Intensities[b] (I/I_o)	d (Å) (Calculated)	d (Å) From File	(hkl)	Comments
1	50.70	>100	1.81	1.80	(200)	Austenite
2	49.40	50	1.84	1.85	(222)	Sigma
3	48.10	60	1.89	1.90	(331)	Sigma
4	46.85	98	1.94	1.95	(411)	Sigma
5	45.75	94	1.98	1.98	(420)	Sigma
6	44.50	81	2.04	2.04	(202)	Sigma
7	43.50	>100	2.08	2.08	(111)	Austenite
8	42.15	95	2.14	2.15	(410)	Sigma
9	39.20	65	2.30	2.30	(002)	Sigma
10	37.70	60	2.39	2.39	(311)	Sigma

[a]Prior to x-ray diffraction, the specimen was micropolished to 0.06 micron and then electrolytically etched. Bath used: 90 ml H_2O, 10 ml oxalic acid, 2.5 V DC (35 mA/cm^2 current density); etched for ten seconds.

[b]May vary from data in x-ray powder data file because of preferred orientation.

Table V-6 confirmed that the peaks of the residue from composition 9 were from the sigma phase. Using the (hkl) planes to be (411) where $d_{(411)}$ = 1.94691 Å, and (212) where $d_{(212)}$ = 1.98917 Å, c_o value was calculated to be 4.600 Å, a_o to be 8.860 Å, and the c_o/a_o ratio 0.52. These values agree well with that of Weiss and Stickler[16] who reported sigma phase with the parameters (shown in Table V-8) in their 316 and 316L austenitic stainless steels. For details of these calculations, see Appendix A.

The small variations in the lattice parameters were attributed to variations of chemical composition of the sigma phase itself and the equilibrium conditions that may vary depending upon aging time, temperature, and the chemistry of the alloy used.

No carbide was detected by x-ray diffraction from the extract from sample number 9. This is assumed due to the small amount of such carbide present relative to the amount of sigma phase.

Tables V-7 and V-8 confirm the presence of sigma phase in an austenitic matrix for alloy composition 9 after aging for 1000 hours at 650°C (1200°F).

Identification of Carbide(s)

The results of x-ray diffraction from the residues extracted from composition 8 (0.4% C) are presented in Tables V-9 and V-10. Table V-9 is the result of x-ray diffraction after the alloy sample was aged for 1000 hours at 650°C. This result was obtained after placing the powder sample on a silicon single crystal mounted on an x-ray diffractometer. Table V-10, however, is the result of powder diffraction using a Debye-Scherrer camera. The sample was aged for 1000 hours at 850°C.

TABLE V-8

LATTICE PARAMETERS FROM X-RAY DIFFRACTION DATA--
c_o, a_o, and c_o/a_o RATIO FOR SIGMA PHASE

Parameters	This Investigation[a]	Weiss and Stickler[16] Data[b]
c_o	4.600 Å	4.597 Å
a_o	8.860 Å	8.828 Å
c_o/a_o Ratio	0.52	0.52

[a]Composition 9, as-cast alloy, 26.1% Cr, 14.6% Ni, 0.014% C, Fe base. Aging conditions--650°C (1200°F), 1000 hours.

[b]System--316 and 316L stainless steels. Composition--17.3-17.4% Cr, 12.3-13.1% Ni, 2.05-2.66 Mo, C = 0.023-0.066% C, Fe base. Aging conditions--815°C (1500°F), 3000 hours.

Source: B. Weiss and R. Stickler, Met. Trans., Vol. 3, p. 851 (1972).

TABLE V-9

RESULTS BY X-RAY DIFFRACTOMETER ON POWDER RESIDUE FROM COMPOSITION 8 (SAMPLE 8-2-4) AGED FOR 1000 HOURS AT 650°C*

Peak Number	2Θ (°)	Relative Intensities (I/I_o)	d (Å) (Calculated)	d (Å) From File	(hkl)	Comments
1	37.90	25	2.37	2.38	(240)	$Cr_{23}C_6$
2	41.70	33	2.17	2.18	(242)	"
3	44.30	100	2.05	2.05	(333) (151)	"
4	48.40	28	1.88	1.89	(440)	"

*Radiation used--CuK_α = 1.54178 Å. Composition 8 had 0.40% C.

TABLE V-10

IDENTIFICATION OF $M_{23}C_6$ CARBIDE[a] BY DEBYE-SCHERRER METHOD[b]

Line Number	Observed "d" Values (in Å)	d (Å) From Card File (Standard)	Relative Intensities[c]	(hkl) Planes	Comments
1	2.65	2.669	VW	(040)	$Cr_{23}C_6$
2	2.36	2.3872	M	(240)	
3	2.16	2.1792	M+	(242)	"
4	2.04	2.0546	VS	(333)	"
5	1.87	1.8873	M	(440)	"
6	1.79	1.8046	M	(351)	"
7	1.76	1.7793	M-	(442)	"
8	1.60	1.6095	W	(262)	"
9	1.285	1.2947	VW	(464)	"
10	1.25	1.2580	M (diffuse)	(660)	"
11	1.225	1.2246	M-	(662)	"
12	1.185	1.1936	W	(480)	"
13	1.165	1.1718	W	(191)	"
14	1.115	1.1192	VW	(391)	"
15	1.082	1.0896	M-	(484)	"
16	1.068	1.0730	W	(393)	"
17	0.970	0.9746	W	(4 10 2)	"
18	0.957	0.9626	W	(1 11 1) (775)	"
19	0.93	0.9328	W	(595)	"
20	0.91	0.9155	W	(686)	"
21	0.90	0.9023	W	(6 10 2)	"
22	0.840	0.8440	W	(4 12 0)	"
23	0.838	0.8337	W	(4 12 2)	"
24	0.82	0.8237	W	(8 10 2)	"
25	0.812	0.8337	S	(4 12 3)	"
26	0.810	0.8164	M-	(993)	"
27	0.794	0.7980	W	(797)	"
28	0.792	0.7957	M-	(6 12 0)	"
29	0.790	0.7875	W	(6 12 2)	"
30	0.7754	0.7705	W	(888)	"

[a] Extracted by electrochemical dissolution technique.

[b] Sample 8-2-4, aged for 1000 hours at 850°C (1560°F).

[c] Intensity classification: VS = Very Strong; S = Strong; M = Medium; VW = Very Weak; M+ = Above Medium; M- = Below Medium.

Both tables indicate the presence of carbides with no evidence of any sigma phase. This result is in agreement with that of the optical metallography described before.

The bulk residues obtained using 10% HCl-90% CH_3OH shown in Table V-4, page 159, were examined by x-ray diffraction--both by Debye-Scherrer camera and the x-ray diffractometer technique using a silicon single crystal. The residues which were obtained after aging the samples at 650°C, 750°C, and 850°C for 1000 hours showed only $M_{23}C_6$ carbides, with no evidence of sigma or any other phases, including the other intermetallic compounds. These results lead to the conclusion that the solution with a current density of 600 mA/cm^2 dissolved most of the sigma or other phases except the $M_{23}C_6$ carbides. It was later discovered that with a current density of 175-225 mA/cm^2 in the 10% HCl-90% CH_3OH solution or using a different solution (see experimental procedure suggested by Dulis and Smith[56]), a considerable amount of sigma was observed in alloy 9 after aging for 1000 hours at the aging temperature.

4. ELECTRON MICROSCOPY

In this section, identification of the phases present in the microstructures by electron microscopy will be presented. The two types of electron microscopy employed in this investigation are "scanning electron microscopy" (SEM) and "transmission electron microscopy" (TEM). The experimental procedure was described in Chapter III for both types of work and the techniques used.

Results of Scanning Electron Microscopy

X-ray fluorescence spectra from the sigma phase (A), the austenitic matrix (B), and the carbide phase (C) were obtained. See Figure V-13 for the selected precipitates to be identified and Figures V-14 (sigma vs. austenite) and V-15 (carbide vs. austenitic matrix) for the spectra, which shows the plot of emitted intensity vs. energy (KeV). The specimen of composition 9 was solution-treated and then aged for 1000 hours at 750°C (1380°F).

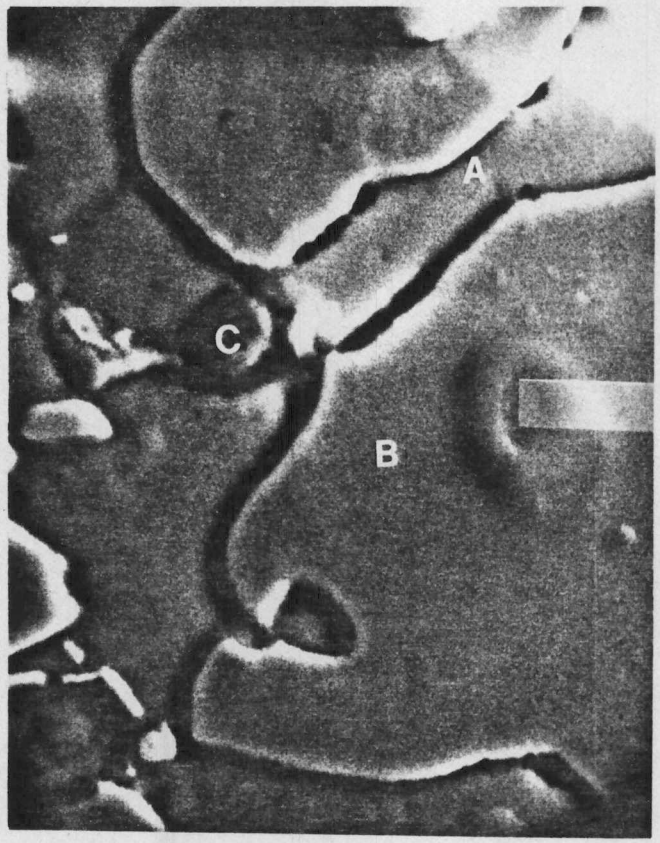
From Figures V-14 and V-15, it is seen that the precipitates are comparatively richer in chromium than the austenitic matrix, as both the carbide and sigma phases have higher Cr counts than the matrix. It is, however, not possible to readily distinguish the carbide from sigma by this technique.

Results of Transmission Electron Microscopy

Figure V-16 shows a photomicrograph. Figure V-17 shows the actual diffraction pattern from a selected area of the alloy composition number 9, which was aged for 1000 hours at 650°C. Such electron diffraction patterns were used to identify the phases present based on lattice parameters of the phases to be identified.

Appendix A clearly explains how to calculate the lattice parameters--namely, c_o, a_o, c_o/a_o ratio, and the angles between the selected known crystallographic planes (of BCT lattice to which sigma belongs). The measured angles were compared with calculated angles for the BCT system. The results are summarized in Table V-11, which lists the angles and the c_o, a_o, and c_o/a_o ratio for three samples studied.

SAMPLE NUMBER 9-2-4



A--Sigma Particle

B--Austenitic Matrix

C--Carbide

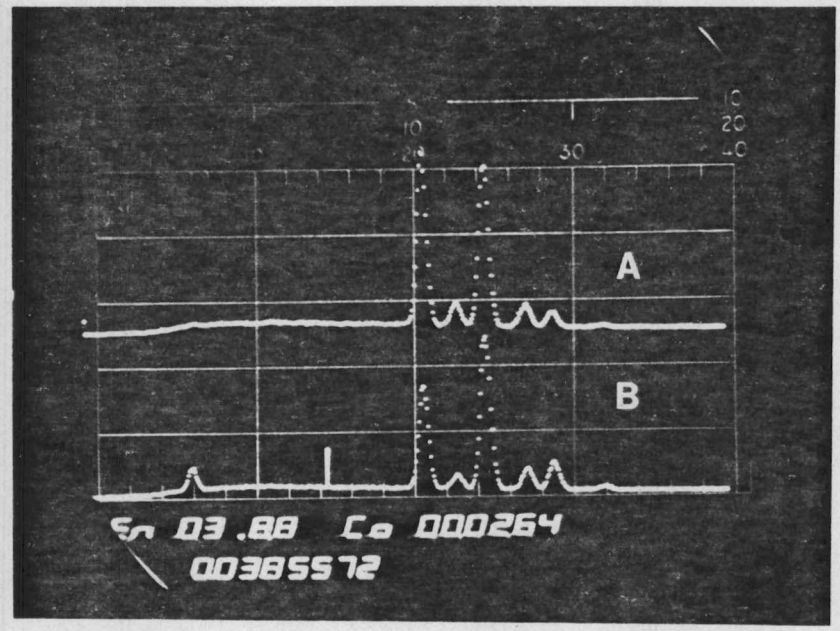
5000X Magnification

Oxalic Acid Etch
(Electrolytic)

Figure V-13. SEM of the Solution-Treated Alloy Composition (9) After Aging for 1000 Hours at 650°C.

CRANES CREST

SAMPLE NUMBER 9-2-4



Tilt Angle = 26°

Solution-Treated

Intensity normalized for Fe peaks.

Aged 1000 Hours, 650°C

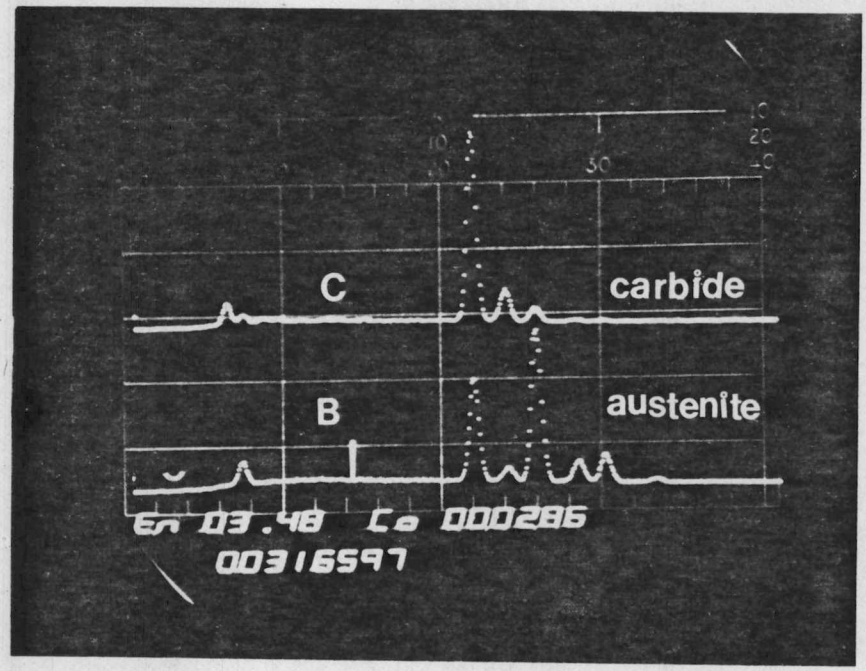
PEAKS: (Elements/energy in KeV)

Intensities (Counts)	Si	Cr_1 (5.41)	Cr_2 (5.95)	Fe_1 (6.40)	Fe_2 (7.06)	Ni_1 (7.47)	Ni_2 (8.26)
Sigma (A)	292	5451	880	5018	820	567	182
Matrix (B)	858	3277	576	4761	769	948	203

Note: Cr_1 means Cr Kα peak, Cr_2 means Cr Kβ peak, etc.

Figure V-14. X-Ray Fluorescence Spectra (Intensity Vs. Energy in KeV) from Sigma Phase (A) and the Austenitic Matrix (B).

SAMPLE NUMBER 9-2-4



Tilt Angle = 26°

Solution-Treated

Intensity normalized for Fe peaks.

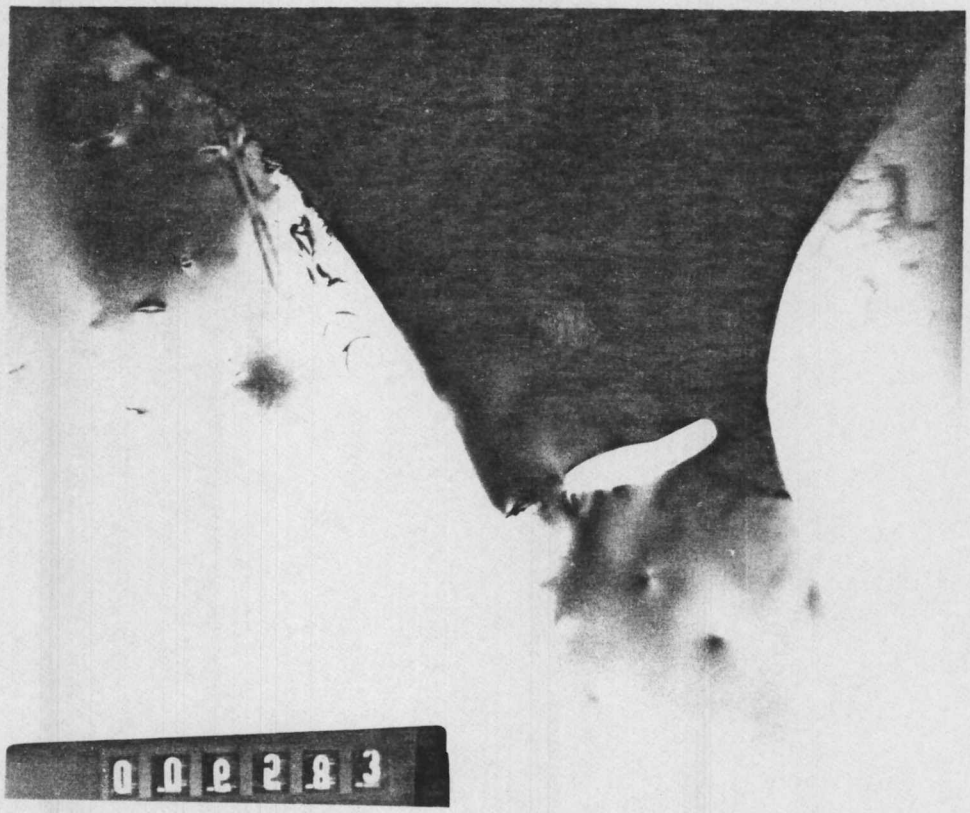
Aged 1000 Hours, 650°C

PEAKS: (Elements/energy in KeV)

Intensities (Counts)	Al	Si	$Cr_{K\alpha}$ (5.41)	$Cr_{K\beta}$ (5.95)	$Fe_{K\alpha}$ (6.40)	$Fe_{K\beta}$ (7.06)	$Ni_{K\alpha}$ (7.47)	$Ni_{K\beta}$ (8.26)
Carbide (C)	1080	961	8000	1414	737	71	137	---
Matrix (B)	---	962	5649	985	8000	1255	1522	343

Figure V-15. X-Ray Fluorescence Spectra (Intensity Vs. Energy in KeV) from the Carbide (C) and the Austenitic Matrix (B).

SAMPLE NUMBER 9-2-4



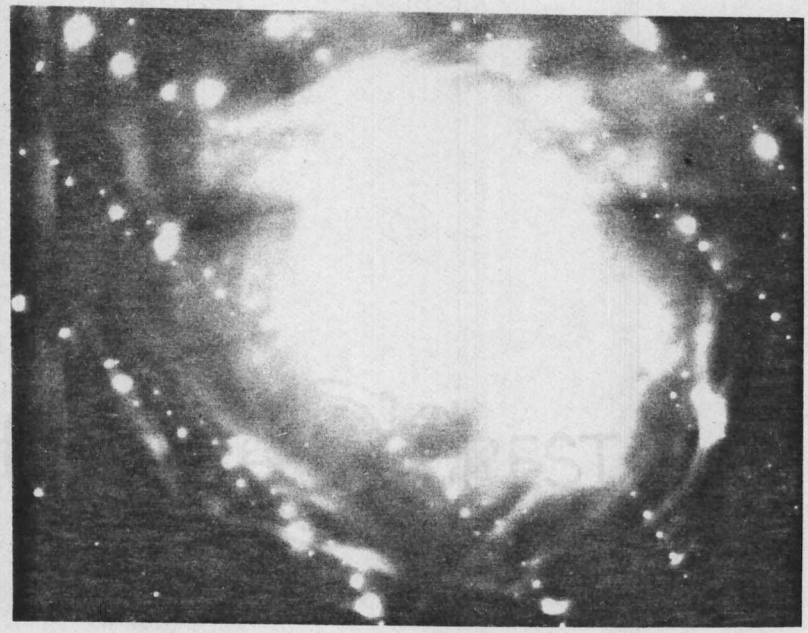
TEM Plate No. 006583

26900X Magnification

Aged 1000 Hours, 650°C

Figure V-16. Sigma Phase in Composition 9 as Revealed by Transmission Electron Microscope. (The photomicrograph reveals dislocations.)

SAMPLE NUMBER 9-2-4



TEM Plate No. 006582

26900X Magnification

Aged 1000 Hours, 650°C

Figure V-17. Electron Diffraction Pattern from the Sigma Phase. (The actual sigma particle from which the diffraction was taken is shown in Figure V-16, Plate No. 006583.)

TABLE V-11

LATTICE PARAMETERS OF SIGMA PHASE FROM TEM DIFFRACTION DATA[a]

TEM Plate Number	c_o (A)	a_o (A)	c_o/a_o Ratio	Angle[b] $\Theta_{R_1R_2}$ (°) Calc.	Meas.	$\Theta_{R_2R_4}$ (°) Calc.	Meas.	Comments
006582	4.60	8.86	0.52	---	---	---	---	Alloy 9, 26Cr-15Ni
006578	---	---	---	22.45	22.5	---	---	Alloy 9, 26Cr-15Ni
006580	4.64	9.30	0.50	136	136	18.64	18.30	Alloy 9, 26Cr-15Ni
Weiss and Stickler[c] Stickler	4.60	8.83	0.52	---	---	---	---	Type 316, aged 3000 hours, 815°C
Spruiell et al.[d]	4.58	8.86	0.52	---	---	---	---	Type 316, aged 3250 hours, 710°C

[a]For sample 9-2-4, solution-treated, aged 1000 hours at 650°C.

[b]See Appendix A for technique used to calculate the angles.

[c]B. Weiss and R. Stickler, Met. Trans., Vol. 3, p. 851 (1972).

[d]J. E. Spruiell et al., Met. Trans., Vol. 4, p. 1533 (1973).

It is clearly seen from Table V-11 that the c_o, a_o, and c_o/a_o ratio agree well with those of published results[5,12,16] for sigma phase in similar systems. Therefore, the phases present in composition 9 after aging were successfully identified as "sigma phase (σ)."

It is important to know that like composition 9, the other alloy compositions (8, 10, 17, 18, and 19) also had similar intermetallic phases in morphology, as well as in color (under optical microscope) after KOH-H_2O electrolytic etching. Although they were not verified as sigma by TEM diffraction data, the intermetallic phase present in alloy compositions 8, 10, 17, 18, and 19 were also assumed to be sigma phase.

5. ANALYSIS OF AGING BEHAVIOR

In this section, a critical discussion of the results will be presented. Emphasis will be given to the correlation of the sigma formation results obtained on the aged alloys to the results predicted by employing the semi-empirical theories or approaches that have been discussed in the literature.

Kinetic Effects

Formation of sigma phase in the austenitic stainless steels is quite complex. This is because most of them are multicomponent alloys. The stable austenite boundary in the system is often difficult to establish because of the slow rate of approach to equilibrium. Consequently, the thermodynamic driving force for precipitation of phases from austenite is generally unknown. The kinetics are a function of this unknown driving force through its effect on the rate of nucleation. However, the kinetics also involve the rate of growth which is largely

diffusion controlled. In the present study, the effects of nucleation were not specifically separated out from the effects of growth. Only the overall kinetics were studied.

Various types of pretreatments were given to the experimental alloys, and they were then aged for various lengths of time at different aging temperatures. It was found that the pretreatments given or microstructure of the alloys had a significant effect on the amount, size, distribution, and morphology, in general, of the sigma phase formation. For example, the as-cast alloys showed a more rapid formation of sigma compared to the solution-treated alloys. It is believed that this is because the as-cast structure is associated with chemical concentration gradients and segregation during rapid cooling, whereas the solution-treated alloy is relatively free from such chemical inhomogeneities. In regions of high concentration of Cr, the sigma phase is nucleated more rapidly than in the alloy of uniform concentration. There may also be effects due to microstructure differences.

In the present investigation, it was also found that cold work accelerated the amount of sigma phase formation in the austenitic stainless steels. Such findings agree well with those of Spruiell,[5] Weiss and Stickler,[16] and Marshall and Hooper,[34] who mostly worked on commercial grades of 316 stainless steels. It is believed that introduction of cold work in the alloy creates defects in the metals such as dislocations, slip bands, etc., which may act as potential nucleation sites for sigma to form. Further, the structure is more refined, implying that the diffusion distance would be shorter compared to an annealed

structure, and, therefore, sigma would grow more favorably from the thermodynamically unstable cold-worked structure.

It was also found that the amount of sigma is enhanced by recrystallization occurring in the aging temperature range. Spruiell et al.[5] related phase enhancement to ease of nucleation at slow-moving recrystallizing boundaries together with enhanced growth rates due to diffusion along the boundary. Cold work alone, with no recrystallization, is not very effective in the enhancement of sigma formation, it was suggested.[5]

Many austenitic stainless steels in their as-cast or wrought states contain ferrite. In particular, austenitic weld metals contain ferrite (~3-7%) in order to help prevent hot-cracking.[17,18,19] It was found that sigma nucleated readily in structures containing some ferrite in the austenitic matrix. This is probably because sigma can nucleate easier at the ferrite-austenite boundary or interface because of difference in interfacial energy. It is expected that cold work would further enhance the rate of sigma formation.

It was found that the morphology of sigma phase varied depending upon pretreatments. In the as-cast alloys containing some initial ferrite, it had an "island-like" or semi-continuous, "dog-bone" type morphology, whereas in many cold-worked and solution-treated alloys, the morphology of sigma varied from "globular" massive type to "needle-like." Such variations of sigma morphology were also found by Leitnaker and Bentley,[113] who studied aging behavior of type 321 stainless steel which was aged for 17 years at ~600°C (1100°F). Leitnaker and Bentley[113] also found no definite correlation between the habit planes of sigma and its parent austenitic matrix phase and concluded that

sigma phase grew wherever there is room and growth conditions exist. Thus, one can appreciate the complexities associated with the kinetics of sigma phase formation.

Prediction of Sigma-Forming Tendencies

Evidence was presented that the kinetics of sigma phase formation in the austenitic stainless steels can vary significantly with changes in their initial microstructure or pretreatments. However, the thermodynamic approach neglects the effect of initial microstructure on sigma formation. Thermodynamics assumes that all steels, regardless of their structures, with the same overall chemical composition should have the same relative amounts of phases if alloys are aged for a very long time to achieve thermodynamic equilibrium. Because of the slow kinetics of sigma formation due to the relatively low temperature of interest, thermodynamic equilibrium is rarely attained in stainless steels. Thus, the application of rigorous thermodynamic approaches to predict phase stability or phase instability in stainless steels was considered beyond present capabilities. This made it necessary to consider semi-empirical theories or approaches.

A primary goal of this investigation was the establishment of a quantitative semi-empirical relationship which should be capable of predicting the occurrence of sigma phase in austenitic stainless steels as a function of chemical composition of the alloys. While previous investigators had considered this problem for several alloying elements, little discussion of the role of carbon was available, and much of the present effort was aimed at understanding this rate.

There are two well known semi-empirical theories currently available on this subject. The first is the theory of equivalent chromium content (ECC), and the second is the theory of electron vacancy number (EVN or $\bar{N}v$).

The ECC theory was developed by Hull[14] about a decade ago. Studying the equilibrium diagram[71] (see Figure II-1, page 12), one finds that about 18% Cr by weight is necessary to form sigma. Hull[14] and Sticha[15] argued that the effect of other alloying elements like Mo, Ni, Si, etc. could be expressed in terms of a single-variable ECC to predict the embrittlement tendencies of the alloy. According to this theory, a minimum ECC would be necessary to induce sigma in the Fe-Cr-Ni system, and the higher the ECC of a steel, the higher the chance of that steel to be embrittled by the formation of sigma.

One of the objectives of Hull's[14] investigation was to determine how much of various alloying elements could be added without causing the steel to be susceptible to embrittlement during long-time service at elevated temperatures. Hull worked on a series of Kromarc stainless steels and used Charpy notched impact tests to find the embrittlement tendencies of the alloys by noting the bend angles of the aged specimens. Using regression analysis (taking the effect of Cr as unity), he devised an equation for ECC:

$$\begin{aligned} \text{ECC} = {} & \text{Cr (wt.\%)} + 0.31\ \text{Mn (wt.\%)} + 1.76\ \text{Mo (wt.\%)} \\ & + 0.97\ \text{W (wt.\%)} + 2.02\ \text{V (wt.\%)} \\ & + 1.58\ \text{Si (wt.\%)} + 2.44\ \text{Ti (wt.\%)} \\ & + 1.70\ \text{Cb (wt.\%)} + 1.22\ \text{Ta (wt.\%)} - 0.226\ \text{Ni (wt.\%)}. \end{aligned}$$

Thus, this approach is just a convenient method to account for the shift in the $\sigma+\gamma$ and γ (gamma) phase boundary depending upon the alloying elements added to the system which produce a change in the driving force for sigma precipitation.

The EVN (or $\bar{N}v$) theory, originally due to Pauling[97] and later developed by Beck[87] is based upon the assumption that the intermetallic compound sigma phase is also an electron compound. The electron compounds are intermetallic phases which form in alloy systems at certain electron-to-atom (e/a) ratios.[119] The compounds form from elements with similar crystal structure with comparable atomic diameters and have loose (valence) electrons or holes. Beck[87] realized that it might be possible to characterize the sigma phase range by calculating an average hole number ($\bar{N}v$) for the solid solution matrix from its composition. Thus, one could predict the occurrence of sigma phase depending upon the average number of electron vacancies in the alloy. Such calculations, which take into account the orbital electrons such as s, p, d, etc. are beautifully illustrated by Sims and Hagel[39] in The Superalloys.

For alloying elements occurring in superalloys and stainless steels, the $\bar{N}v$ is given by the equation:

$$\begin{aligned}\bar{N}v = {} & 4.66\ \text{Cr (At.\%)} + 10.00\ \text{Mo (At.\%)} \\ & + 4.66\ \text{W (At.\%)} + 5.66\ (\text{V} + \text{Nb} + \text{Ta, At.\%}) \\ & + 6.66\ (\text{Ti} + \text{Zr} + \text{Si, At.\%}) + 0.66\ \text{Ni (At.\%)} \\ & + 1.71\ \text{Co (At.\%)} + 2.66\ \text{Fe (At.\%)} \\ & + 3.66\ \text{Mn (At.\%)} + 7.66\ \text{Al (At.\%)}.\end{aligned}$$

This equation was developed by Woodyatt.[117]

Beck[87] characterized sigma phase by $\bar{N}v$ values from 3.35-3.68 in the Cr-Co-Fe, Cr-Co-Mo, and Cr-Ni-Mo superalloys. Woodyatt[117] further pointed out that the loss of matrix composition due to the precipitation of carbides or nitrides must be taken into account. Also, in the calculation of $\bar{N}v$, it was assumed that the alloy has reached equilibrium; sigma phase forms entirely from the single-phase austenitic matrix; and that $\bar{N}v$, the average electron vacancy number, will be a linear function of the matrix composition.

Investigated here is the application of both these semi-empirical approaches to the relatively pure laboratory-prepared Fe-Cr-Ni alloys in the present study and to commercial alloys studied by other research workers of The University of Tennessee, Knoxville under the direction of Spruiell.[22] The results for the nine prepared alloys are presented in Table V-12, and results of commercial grades of stainless steels are presented in Table V-13.

The effect of ECC computed from overall composition is shown graphically in Figure V-18. It is clear that an increase of ECC has a strong effect on sigma formation, and it appears that a minimum ECC of about 18 is necessary before an appreciable amount of sigma is formed after aging the alloys for 1000 hours at 750°C. The correlation between sigma and ECC seems to be nonlinear.

The effect of carbon content on sigma formation can be ascertained from Figure V-19, which shows the relative amount of sigma as a function of carbon content at three levels of ECC. These data clearly indicate that increasing carbon content decreases the relative amount of sigma phase at a given ECC.

TABLE V-12

WT.% SIGMA VS. COMPOSITIONS FOR GROUP I, II, AND III EXPERIMENTAL ALLOYS[a] AFTER AGING FOR 1000 HOURS AT 750°C (1380°F)

Alloy Number	Specimen Number	% Carbon	Wt.% Cr	ECC[b]	ECC[c]	EVN[d]	Observed % Sigma[e]	Comments
GROUP I (Ave. ECC[b] = 22.5)								
8	8-2-7	0.40	25.5	22.3	18.5	2.84	6	Austenitic
9	9-2-7	0.014	26.1	22.8	22.6	2.94	20	Duplex
10	10-2-7	0.18	25.9	22.7	20.6	2.91	10	Austenitic
19	19-2-7	0.38	26.2	22.3	18.8	2.80	4	Austenitic
GROUP II (Ave. ECC[b] = 20.7)								
17	17-2-7	0.05	24.7	20.8	20.3	2.84	6	Austenitic
18	18-2-7	0.19	24.5	20.6	18.8	2.81	3	Austenitic
GROUP III (Ave. ECC[b] < 20.0)								
3	3-2-7	0.019	18.3	14.9	14.7	2.76	0	Austenitic
5	5-2-7	0.006	19.8	16.6	16.6	2.81	0	Austenitic
14	14-2-7	0.20	22.2	18.8	16.9	2.80	0	Austenitic

[a]All alloys were solution-treated and had controlled microstructure prior to aging (see Chapter III). For complete chemical analyses of the other commercial grades of stainless steels, see Table V-13.

[b]ECC based upon overall chemical composition = Cr (wt.%) - 0.226 Ni (wt.%).

[c]ECC corrected for carbide precipitation at 750°C.

[d]EVN corrected for carbide precipitation at 750°C. EVN (or $\bar{Nv}$) = 4.66 Cr (At.%) + 0.66 Ni (At.%) + 2.66 Fe (At.%).

[e]Estimated by metallographic examination ($KOH-H_2O$ electrolytic etch).

TABLE V-13

COMPARISON OF EXPERIMENTAL OBSERVATIONS OF SIGMA FORMATION WITH PREDICTIONS BASED ON ECC AND EVN SEMI-EMPIRICAL THEORIES FOR COMMERCIAL-GRADE STAINLESS STEELS AND WELD METALS

Sample[a]	Chemical Composition,[b] Wt.%							ECC[c]	ECC[d]	EVN[e]	Observed Sigma %
	C	Cr	Ni	Mo	Mn	Si	Ti				
A 304	0.04	18.2	8.75	---	1.36	0.32	---	17.2	16.6	2.88	0
A 316	0.06	17.3	13.30	2.33	1.72	0.40	---	19.6	19.0	2.88	2.5
A 321	0.06	17.48	9.58	---	1.69	0.54	0.50	17.9	17.3	2.86	<0.5
A 316 TiM	0.06	17.52	13.96	2.51	1.41	0.03	0.29	20.1	19.6	2.89	3.2
W 16-8-2	0.07	15.48	7.34	1.77	1.63	0.10	---	17.6	16.9	2.94	1.0
W 16-8-2	0.06	16.50	8.92	1.70	1.36	0.39	0.02	18.6	18.0	2.95	1.2
W 316	0.04	18.90	13.00	2.20	1.75	0.44	0.02	21.1	20.8	2.96	3.4
W 316	0.06	18.55	11.28	2.12	1.86	0.49	0.01	21.1	20.6	2.98	2.6
W 308-A	0.052	18.18	10.95	---	1.64	0.35	---	16.8	16.2	2.85	0.2
W 308-D	0.060	19.30	9.89	---	1.65	0.37	---	18.1	17.6	2.92	1.5
W 308L-A	0.020	18.40	10.80	---	1.62	0.38	---	17.1	16.9	2.89	0.2
W 308L-D	0.022	19.09	10.32	---	1.66	0.41	---	17.9	17.8	2.92	1.7
W 316-A	0.065	17.79	12.30	2.22	1.92	0.46	---	20.2	19.7	2.94	1.7
W 316-D	0.069	19.38	11.78	2.12	1.96	0.52	---	21.9	2.13	2.99	7.5

TABLE V-13 (Continued)

Sample[a]	Chemical Composition,[b] Wt.%							ECC[c]	ECC[d]	EVN[e]	Observed Sigma %[f]
	C	Cr	Ni	Mo	Mn	Si	Ti				
W 316-A	0.035	17.88	13.07	2.15	1.85	0.40	---	19.9	19.6	2.93	1.3
W 316-D	0.037	18.60	11.64	2.12	1.87	0.46	---	21.0	20.7	2.98	4.3
W 316L	0.025	19.12	13.60	2.17	1.84	0.38	---	19.9	19.6	2.95	3.21-4.64[g]
W 316L	0.025	19.12	13.60	2.17	1.84	0.38	---	19.9	19.6	2.95	1.0-1.2[h]

[a] The prefix "A" indicates wrought-annealed samples, while "W" indicates weld metal.

[b] Iron-base alloys (balance is Fe in wt.%).

[c] ECC based on overall chemical composition = Cr (wt.%) + 1.76 Mo (wt.%) - 0.226 Ni (wt.%).

[d] ECC corrected for carbide precipitation at 750°C.

[e] EVN corrected for precipitation at 750°C = 4.66 Cr (At.%) + 10 Mo (At.%) + 0.66 Ni (At.%) + 2.66 Fe (At.%).

[f] Estimated amounts after aging 1000 hours at 750°C, wt.% by metallographic examination.[70]

[g] Aged 2000 hours, 650°C in argon atmosphere.[108]

[h] Aged as above but in argon + N_2 atmosphere.[108]

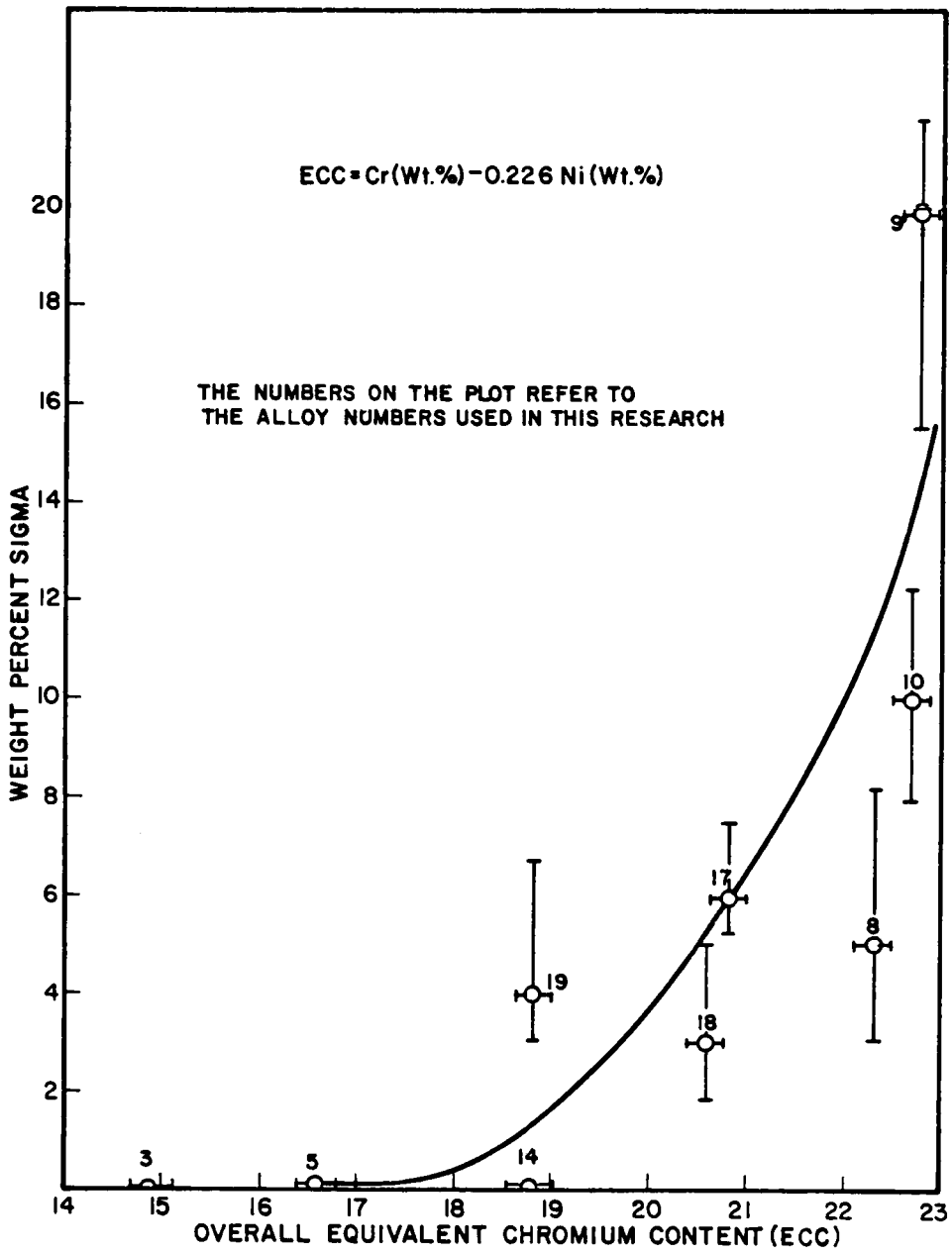


Figure V-18. Wt.% Sigma (Optical Metallographic Method) Vs. Overall ECC of the Nine Experimental Alloys Aged 1000 Hours at 750°C.

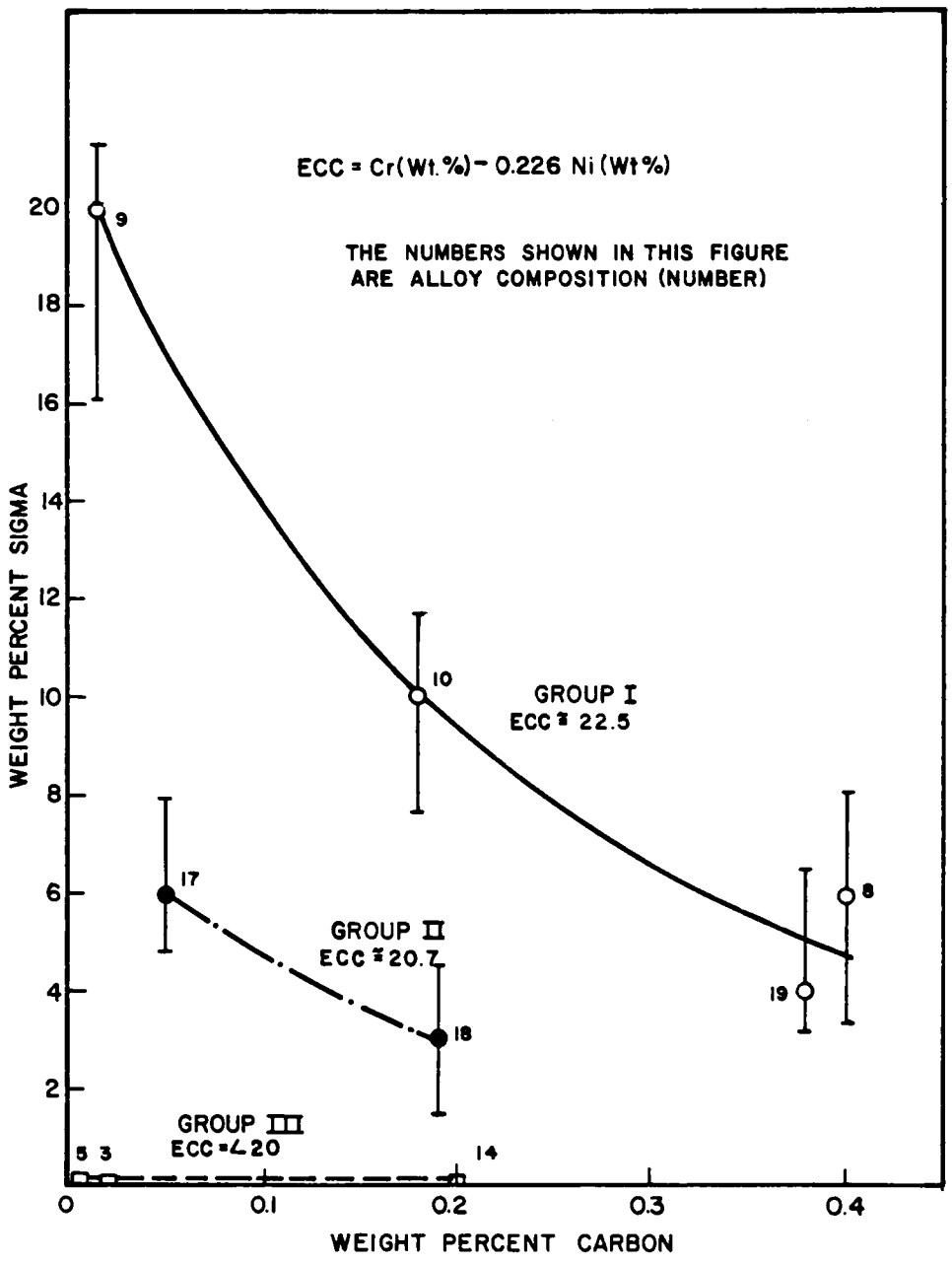


Figure V-19. Wt.% Sigma (Optical Metallographic Method) Vs. % Carbon of the Nine Experimental Alloys, Solution-Treated After Aging 1000 Hours at 750°C.

The reason for the effect of carbon on the relative amount of sigma was further investigated by applying a correction to the ECC for the alloying elements removed by precipitation of carbide at the aging temperature. This is shown in Figure V-20. The correlation shown in Figure V-20 appears better than that shown in Figure V-18, suggesting that removal of alloying elements from solution by precipitation is the main cause of the effect of carbon content on sigma formation shown in Figure V-19.

Marshall and Hooper[34] have also noted a significant effect of carbon content on the amount of sigma formed. The effect noted was in the same direction observed here and of similar magnitude.

The effect of ECC based upon overall chemical composition for the 18 research alloys and weld metals studied under the direction of Spruiell[22] is graphically shown in Figure V-21. Most of the alloys and the weld metals were aged for 1000 hours at 750°C. However, one weld metal, W 316L, which was studied by Andress[108] was aged for 2000 hours at 650°C in different atmospheres. All the relative amount of sigma was obtained by electrochemical extraction in a 10% HCl-90% CH_3OH solution under identical current densities--namely, 175-225 mA/cm^2. The same results are also plotted in Figure V-22 but only after corrections were made to ECC values for carbide precipitation at 750°C.

The results show a positive trend--namely, the higher the ECC, the higher the percentage of sigma. Further, the spread of data seems to be less when a correction was made for carbide precipitation, as shown in Figure V-22.

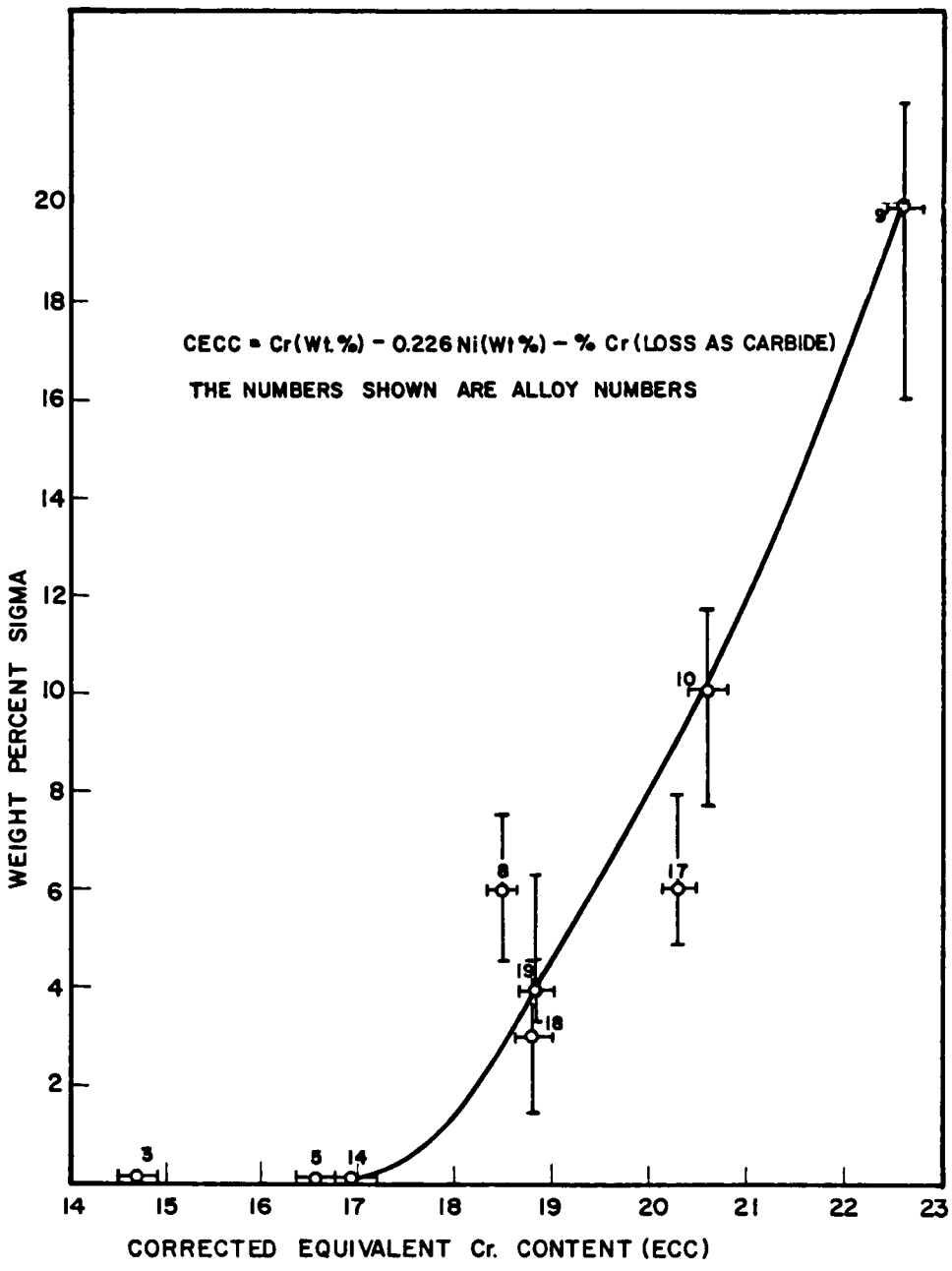


Figure V-20. Wt.% Sigma (Optical Metallographic Method) Vs. ECC of the Nine Experimental Alloys After Correcting for Carbide Precipitation and When Aged 1000 Hours at 750°C.

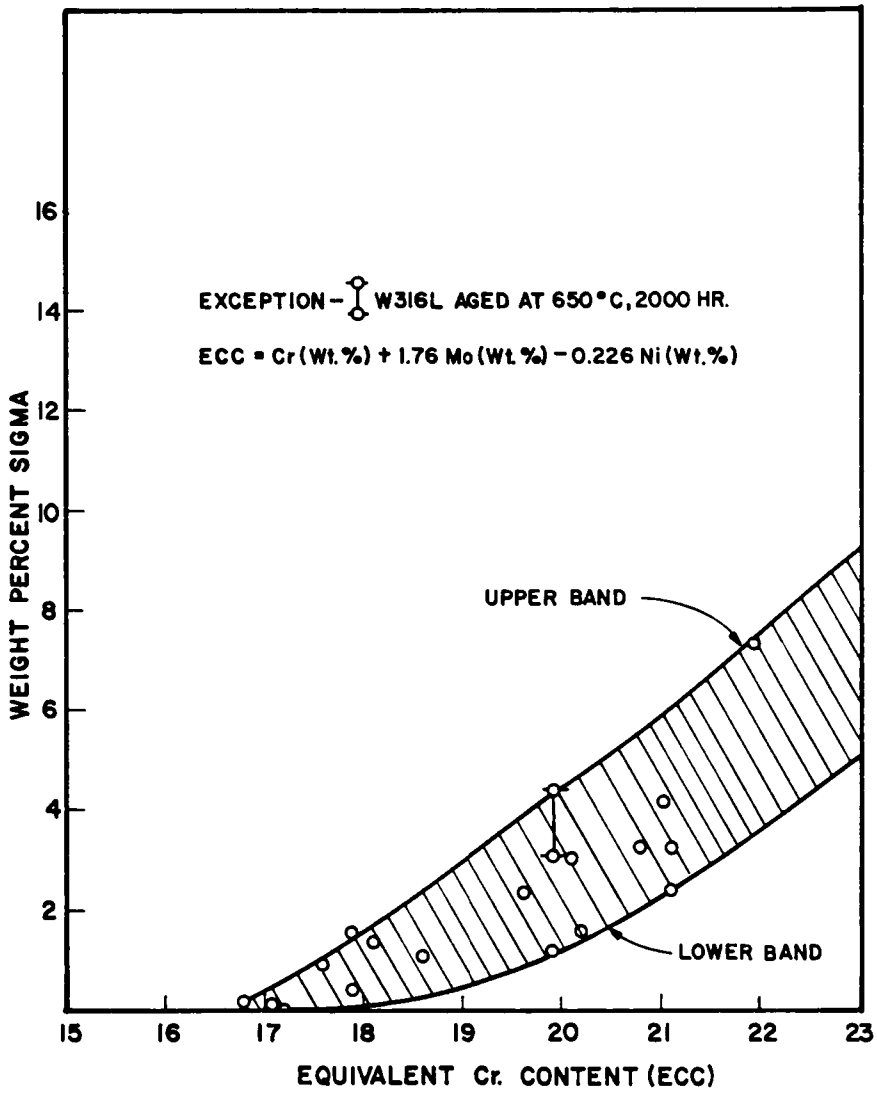


Figure V-21. Wt.% Sigma (Bulk Extraction Method) Vs. Overall ECC for Commercial-Grade Stainless Steel Alloys and Weld Metals Aged 1000 Hours at 750°C.

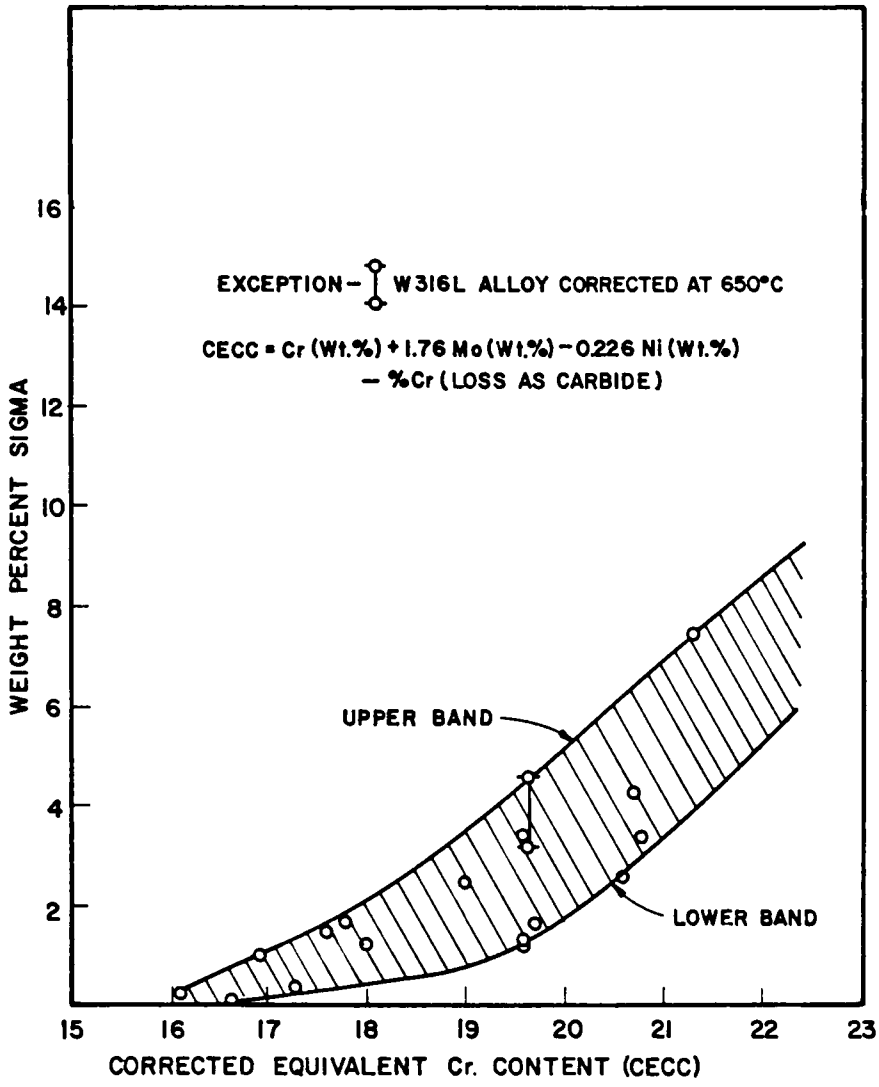


Figure V-22. Wt.% Sigma (Bulk Extraction Method) Vs. ECC for Commercial-Grade Stainless Steel Alloys After Correcting for Carbide Precipitation at 750°C.

As pointed out before, under certain experimental conditions there seems to be dissolution of sigma phase in the widely used 10% HCl-90% CH_3OH solution. A concern for this possibility was also expressed by many other research workers.[16,94,108] Therefore, the results shown in Figures V-21 and V-22 may be somewhat in error due to dissolution of sigma. However, the trend seems to be similar to the results for the experimental pure alloys (where optical metallography was used to compute sigma phase count).

It should be noted that in the commercial grades of austenitic stainless steel alloys and weld metals, sigma seems to form even at an ECC of 17, compared to 18 or higher for the nine experimental alloys used in this investigation. This difference may be a result of the fact that many commercial-grade stainless steels and weld metals contain 3-8% delta (δ) ferrite, which accelerates sigma phase formation for the reasons explained previously. Similarly, in his 316L weld metal, Andress[108] found sigma following aging with relative ease, and chemical segregation was said to be another cause for sigma formation with little difficulty. In an 18-8 weld metal containing ferrite, Wegrzyn and Klimpel[115] found sigma after only 30 seconds following aging at 750°C (1380°F). This demonstrates the strong effect of ferrite upon sigma formation.

The effect of EVN of alloys on sigma formation for the nine experimental alloys (relatively pure) and for commercial grades of stainless steels and weld metals is now graphically presented. In Figure V-23, the effect of EVN (or $\overline{Nv}$) on sigma content for the nine prepared alloys is presented after aging the solution-treated alloys for

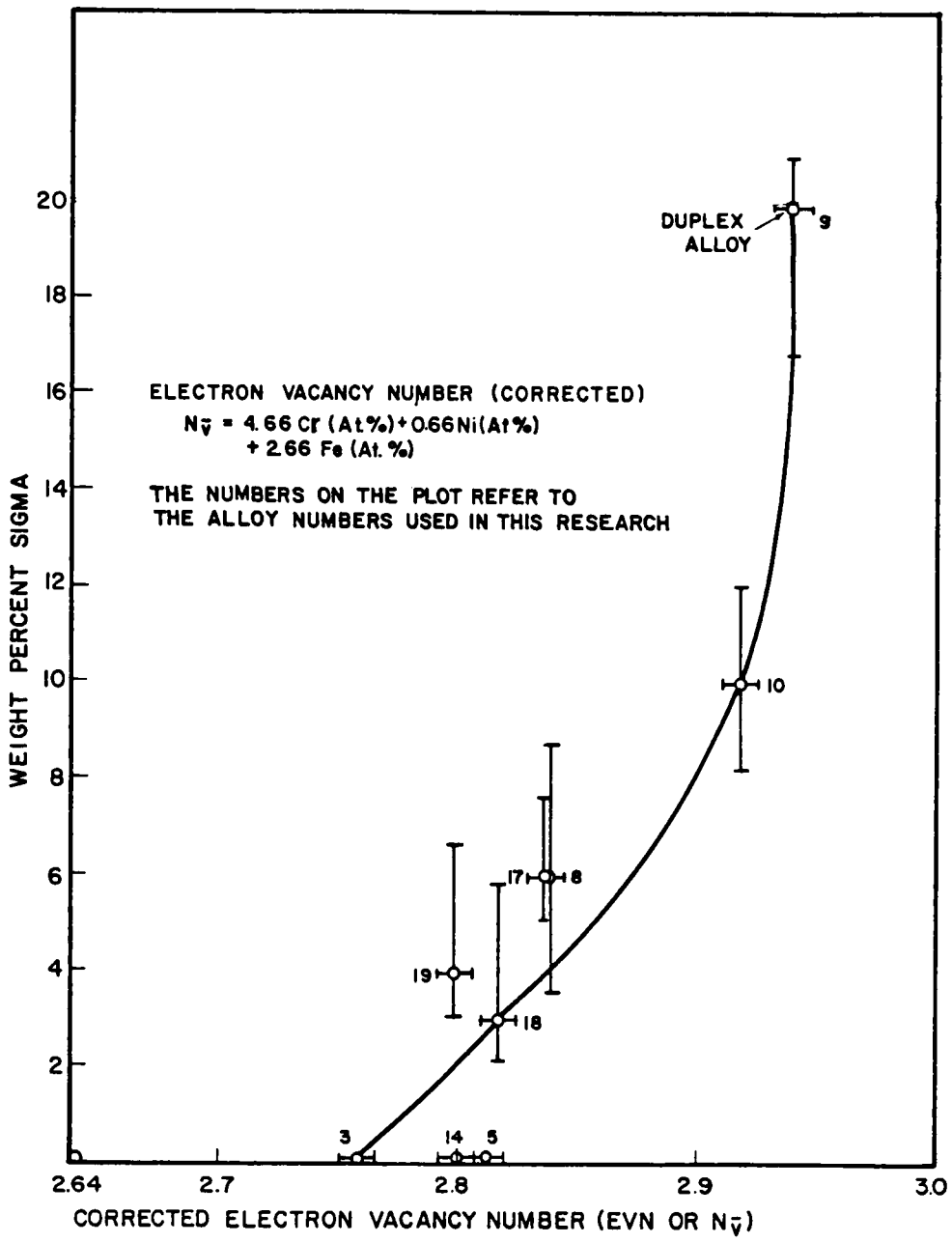


Figure V-23. Wt.% Sigma (Optical Metallographic Method) Vs. EVN for the Pure Nine Laboratory Alloys After Correcting for Precipitation of $M_{23}C_6$ Carbide and Aging 1000 Hours at 750°C.

1000 hours at 750°C. Note that correction was made due to carbide precipitation in the computation of $\bar{N}v$. It appears that the results are in accord with the prediction, but sigma is seen when $\bar{N}v$ is about 2.80 or greater. The average EVN's ($\bar{N}v$'s) for sigma-forming steels are considerably below the range of 3.3 suggested by Beck.[87] However, it is seen that the results here agree better with the suggestion of Woodyatt,[117] who worked on superalloys in 1966. He suggested that if $\bar{N}v$ is above 2.52, the alloy should form sigma. Referring back to Table V-12, page 184, and Figure V-23, it is seen that a maximum amount of sigma formed in alloy 9, which had a duplex (ferrite + austenite) structure and $\bar{N}v$ = 2.94. This result agrees well with that of deBarbadillo[112] (unpublished work) cited in the 1977 Handbook of Stainless Steels. de Barbadillo[112] extensively worked on Fe-Cr-Co-Ni stainless steels and found sigma in alloys which had $\bar{N}v$ numbers in the range of 2.95-3.05.

Upon examination of Figure V-24, which shows wt.% sigma vs. the EVN of commercial grades of stainless steels and many weld metals (after correction was made for carbide precipitation at 1000 hours, 750°C), one finds that most of the alloys with $\bar{N}v$ of around 2.85 form sigma phase.

There seems to be some scattering of data in the plots shown in Figures V-23 and V-24 even after correction was made for precipitation of carbides. This could be attributed to the incorrect or not precisely known coefficients in the equations used to calculate the EVN of the alloys. For example, in the equation to compute $\bar{N}v$ proposed by Woodyatt et al.,[117]

$$\bar{N}v = 4.66\ Cr\ (At.\%) + 10\ Mo\ (At.\%) + 0.66\ Ni\ (At.\%) + 2.66\ Fe\ (At.\%),$$

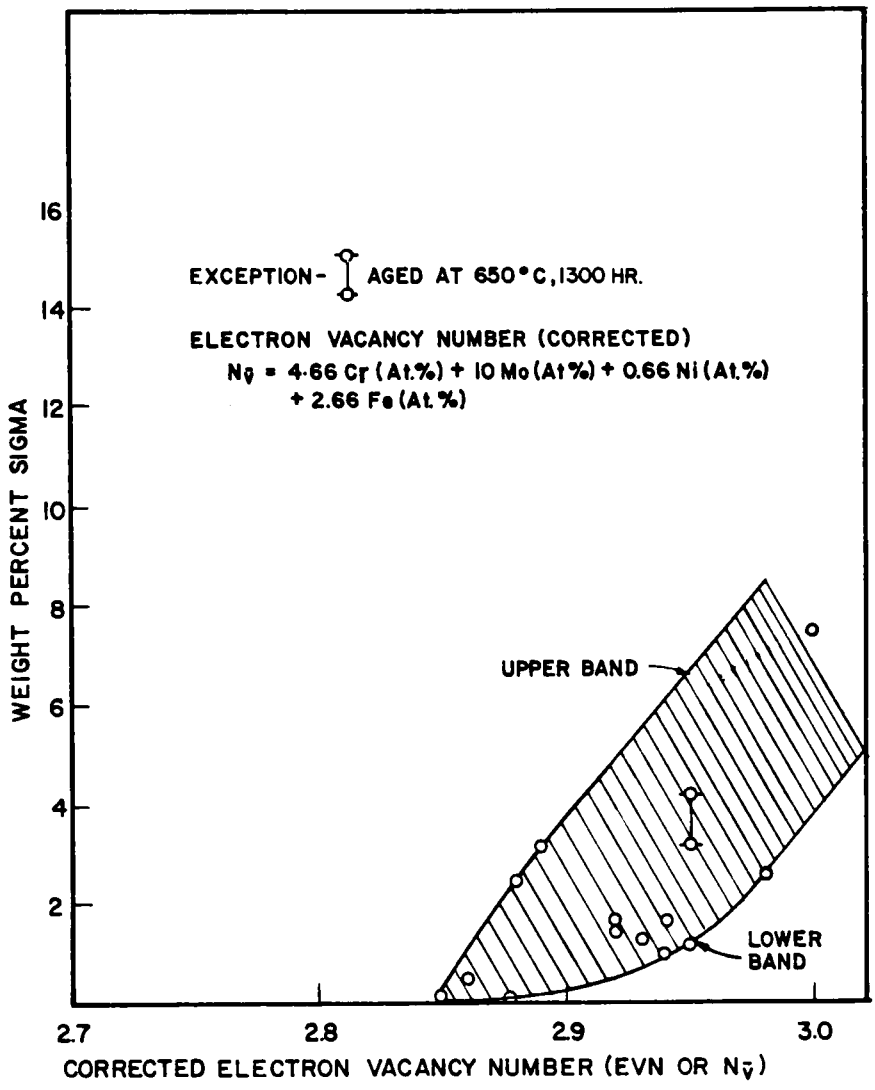


Figure V-24. Wt.% Sigma (Bulk Extraction Method) Vs. EVN for Commercial Alloys After Correcting for Carbide Precipitation at 750°C.

the coefficient for Mo was originally assigned 4.66, but later, Mihalisin[112] assigned a number 9.66. However, a number 10 was assigned by Sims and Hagel[39] because of the abnormal contribution of Mo in sigma formation. However, Biss et al.[114] thought that a number higher than 10 may have to be assigned to Mo because of the effectiveness of Mo in forming sigma.

Similar uncertainties also exist for other elements, as well. Thus, one can appreciate the problem while attempting to compute $\bar{N}v$ using the above equation.

Likewise, scattering of data is also noticed in the wt.% sigma vs. ECC plots (after correcting for carbide precipitation at 750°C) shown in Figures V-20, page 190, and V-22, page 192. This might be attributed to the interaction of one element on another in Hull's equation:[14]

$$ECC = Cr\ (wt.\%) - 0.226\ Ni\ (wt.\%) + 1.76\ Mo\ (wt.\%).$$

That is, the effect of sigma formation by Mo addition may vary not only with Mo content itself, but also its interactions with other elements, as pointed out by Leitnaker and Bentley.[113] Hull[14] treated each element independently in his regression analysis without considering the effects of other elements. Also, Hull did not consider the effects of carbon in his aged samples (1000 hours, 816°C), which would also introduce errors in the ECC results.

As discussed before, the errors in the estimation of sigma phase by the bulk chemical extraction technique (which has a tendency to dissolve sigma in the 10% HCl-90% CH_3OH) solution) could also contribute

to the error bands of the plots of sigma content vs. $\bar{Nv}$ or sigma % vs. ECC. However, it was assumed that in our metallographic estimation of sigma phase by KOH-H_2O electrolytic etching, the error was kept to a minimum. Sources of error in this technique arise due to nonuniform distribution of the sigma phase or size and shape variation, together with human error encountered while estimating sigma phase by the lineal intercept or point count methods used.

Careful consideration of the data and the sources of error lead to the conclusion that sigma phase was observed after aging the alloys for 1000 hours at 750°C, with a minimum ECC (based upon Hull's equation) of 17 $\pm$ 0.5% or an average EVN of 2.85 $\pm$ 0.05. This result agrees better with the findings of deBarbadillo[112] than with other previous investigators.[87,117]

A comparison of the two semi-empirical approaches for predicting sigma formation will now be addressed. In the absence of minor alloying elements in the austenitic stainless steels, the ECC is given by

$$\text{ECC} = \text{Cr (wt.\%)} + 1.76\ \text{Mo (wt.\%)} - 0.226\ \text{Ni (wt.\%)},$$

and the average EVN ($\bar{Nv}$) is given by

$$\bar{Nv} = 4.66\ \text{Cr (At.\%)} + 10\ \text{Mo (At.\%)} + 0.66\ \text{Ni (At.\%)} + 2.66\ \text{Fe (At.\%)}.$$

Reviewing the above equations, it appears that both approaches are parallel, because an increase of either ECC or $\bar{Nv}$ generally increases the tendency toward sigma formation.

An increase of Cr content will increase ECC and $\bar{N}v$, and, thus, more sigma will precipitate out. An increase of Ni content, an austenite stabilizer, reduces ECC and $\bar{N}v$. It should be noted that while one may be tempted to think that an increase of Ni will increase $\bar{N}v$, it does not because when Ni is increased, Fe content (%) of the alloy will decrease. Since the contribution of Fe on $\bar{N}v$ is greater (2.66) than that of Ni (0.66), $\bar{N}v$ will decrease with the increase of Ni content of the alloy.

Both theories require correction due to pre-sigma precipitates such as carbides or nitrides which form during aging in the presence of interstitial elements such as carbon or nitrogen, respectively.

A discrepancy arises between these equations when both Cr and Ni concentration are increased in the proportion of Ni/Cr = 4.4. Although the ECC values show little change, the $\bar{N}v$ values drop sharply. Careful examination of such alloys has not been carried out.

Unless careful experimental research is carried out for such alloys, it cannot be ascertained which theory or approach is better in predicting the sigma-forming tendency for the alloys in the system of stainless steels. This research indicates that within experimental error encountered, both semi-empirical theories satisfactorily predict the sigma-forming tendencies of the stainless steels studied.

CHAPTER VI

CONCLUSIONS AND RECOMMENDATIONS

Throughout the course of this experimental research program, the objective was to learn the effect of carbon content on the amount, rate, and nature of sigma phase formation in austenitic stainless steels which were prepared in a laboratory using high-purity raw materials. Another goal was to test the validity of the two semi-empirical methods of predicting the formation of sigma phase in the general class of austenitic stainless steel alloys. Most austenitic stainless steels generally involve multicomponent systems, and, therefore, by their nature, they make things more complicated to understand or study than the simple systems. Nevertheless, in the limited time span and with the equipment and facilities available for this study such as electron microscopy, optical metallography, x-ray diffraction, and microhardness measurements, the goals of the study were attainable. Conclusions and recommendations are presented in this chapter.

1. CONCLUSIONS

1. An increase of carbon content of the alloys in the range of 0-0.40 wt.% retards sigma phase formation at a given ECC.
2. The major source of the effect of carbon was the removal of carbide-forming (and sigma-forming) elements from solution by precipitation of carbides.

3. With an increase of either the ECC or EVN, more sigma seems to form, and the trend was upward for the laboratory-prepared alloys, as well as commercial grades of austenitic stainless steels. Some sigma was observed after 1000 hours of aging at 750°C in alloys having an ECC (based upon Hull's equation) of more than 17 $\pm$ 0.5 wt.% or an EVN of 2.85 $\pm$ 0.05. In both cases, these values are based on the austenite matrix composition after correction for precipitation of phases such as carbides which precipitate earlier than sigma. It was not possible in the present investigation to establish which of the two semi-empirical approaches is the more accurate for predicting sigma phase formation. The ECC approach seemed to have a slight edge based on the data scatter, but this may reflect only the effect of errors in the coefficients of the equations used to compute ECC or EVN than the approach itself. Generally, the two methods give very similar results and may actually be more or less equivalent measures of sigma-forming tendencies.

4. The following sequence, in <u>decreasing</u> order, of sigma-forming tendencies were noted so far as the effect of initial conditions on sigma formation is concerned:

As-cast cold-worked samples $\rightarrow\rightarrow\rightarrow$ as-cast structures $\rightarrow\rightarrow\rightarrow$ solution-treated alloys.

This was attributed to the favorable nucleation and growth conditions for cold-worked or as-cast structures as compared to the solution-treated samples. As-cast structures show segregation which serves as potential sites (such as Cr-rich regions) for sigma formation. The defects created in the metal by cold work may serve as potential sites for sigma nucleations, but it is believed that recrystallization occurring during aging and consequent nucleation at slowly moving austenite grain boundaries is another important mechanism for the increased rate of sigma formation. These observations support the research of Spruiell et al.[5] and Weiss and Stickler,[16] who found similar correlations in their austenitic stainless steels.

5. The existence of ferrite in the initial microstructure also enhanced the rate of sigma formation. This seemed clearly to be associated with nucleation of sigma at ferrite-austenite interfaces.
6. Sigma phase formation was found to be maximum at 750°C when the nine solution-treated special alloys were aged for 1000 hours. Much lesser quantities were found at 650°C or 850°C aging temperatures.

7. Chemical extraction of the precipitates indicate that carbides form with relative ease at the aging temperatures--namely 650°C, 750°C, or 850°C. Whether precipitation of carbides was a prerequisite for sigma formation or sigma phase formed directly from the parent austenite matrix was not established in this investigation.
8. The most successful etchant for the sigma phase identification was an electrolytic etchant using KOH-H_2O solution with controlled (DC) current density and the etchant time. This solution preferentially etched the sigma phase (relative to the austenite grain boundaries) whose color varied from yellow to reddish-brown under optical microscope. Such characteristic colors and contrast made sigma phase identification easier. Chromic acid also was used, but only as a general etchant (electrolytic). Chemical etchants used for general use in revealing stainless steel microstructure were found to be unsuitable for identification of sigma phase.
9. Optical metallographic technique was found to be more suitable to obtain the wt.% sigma phase in the aged microstructures than the bulk electrolytic extraction method because it was discovered that sigma phase was being dissolved in the solution.

10. This study shows that the morphology of sigma phase varied depending upon where and how it grew. For example, sigma formed in an austenite-ferrite as-cast structure were "dog-bone" like present in a semi-continuous network. On the other hand, the sigma which formed in a wrought-annealed structure were both globular and dog-bone shaped with random distribution. Such variations in sigma morphology have also been reported by Leitnaker and Bentley.[113] The particle size of sigma was typically 0.0001 cm (0.00004 inch) diameter x 0.005 cm (0.002 inch) long.

2. RECOMMENDATIONS

The following recommendations are offered for future research:

1. More attention should be given to the establishment of the coefficients in the equations used to compute both the ECC and the average EVN ($\overline{Nv}$).
2. Simple algebraic computations show that when one increases both chromium and nickel concentration in the proportion of Ni/Cr $\simeq$ 4.4, the ECC shows little change, whereas the average EVN drops considerably. It is not known how such alloys will behave upon aging. An investigation of such alloys would help to establish which of the

two semi-empirical approaches is better for prediction of sigma phase formation.

3. Experiments using longer aging times should also be considered in order to better establish the minimum number for $\bar{N}v$ at which sigma will form. While the results of this study showed a value of 2.85 ± 0.05 as this minimum, previous investigators[39,112] have quoted values ranging from 2.52-3.3.

LIST OF REFERENCES

LIST OF REFERENCES

1. D. M. Hadrill and C. Humphries, Stainless Steels, British Welding Research Association Publication Bulletin, September and November (1964); January (1965).

2. Metal Progress Databook, Vol. 108(1), p. 192 (1975).

3. H. R. Brager, J. Nuclear Material, Vol. 57, p. 103 (1975).

4. C. F. Cheng, J. Nuclear Material, Vol. 56, p. 11 (1975).

5. J. E. Spruiell, J. A. Scott, C. S. Ary, and R. L. Hardin, Met. Trans., Vol. 4, p. 1533 (1973).

6. Republic Enduro Stainless Steels, Republic Steel Corporation, Alloy Steel Div., Massillon, Ohio, p. 103 (1951).

7. D. C. Ludwigson and H. S. Link, "Further Studies on the Formation of Sigma Phase in 12 to 16 Percent Chromium Steels," ASTM Special Technical Publication No. 369, American Society for Testing and Materials, Philadelphia, PA, p. 299 (1963).

8. J. H. G. Monypenny, Stainless Iron and Steel, Vol. 2 (Microstructure and Constitution), Chapman and Hall Limited (London), p. 104 (1954).

9. L. K. Singhal and M. L. Vaidya, Trans. A.S.M., Vol. 62, p. 879 (1969).

10. M. E. Nicholson and C. H. Samans, Trans. A.S.M., Vol. 44, p. 601 (1952).

11. P. A. Blenkinsop and J. Nutting, Journal of Iron and Steel Inst., Vol. 205, p. 953 (1967).

12. P. Duhaj, J. Ivan, and E. Makovicky, Journal of Iron and Steel Inst., Vol. 206, p. 1245 (1968).

13. L. K. Singhal and J. W. Martin, Journal of Iron and Steel Inst., Vol. 205, p. 947 (1967).

14. F. C. Hull, Welding Journal, Vol. 52, p. 104-S (1973).

15. E. A. Sticha, Structural stability of commercial wrought austenitic steels for power plant piping to 1450°F, Proc. American Power Conf., I.I.T., Chicago, Illinois, Vol. 22, p. 288, March (1960).

16. B. Weiss and R. Stickler, Met. Trans., Vol. 3, p. 851 (1972).

17. R. W. Emerson and M. Morrow, Welding Journal, Vol. 30, p. 15-S (1951).

18. H. Thielsch, Welding Journal, Vol. 29, p. 577-S (1950).

19. W. T. DeLong, Welding Journal, Vol. 53, p. 273-S (1974).

20. H. Thielsch, Welding Journal, Vol. 29, p. 361-S (1950).

21. F. C. Hull, Welding Journal, Vol. 46, p. 399-S (1967).

22. J. E. Spruiell, Studies on Microstructure--Property Relationship in Austenitic Stainless Steels, Energy Research and Development Administration Contract No. AT-(40-1)-4044, The University of Tennessee, Knoxville, Tennessee, February (1975).

23. Metals Handbook (8th Edition), Volume I, "Properties and Selection," American Society for Metals, Metals Park, Ohio, p. 419 (1961).

24. H. Wiegand and M. Doruk, Arch. Eisenhuttenwesen, Vol. 8, p. 559 (1962).

25. H. Tuma, M. Vyklicky, and K. Lobel, Carbon Activity and Solubility in Austenitic Chromium-Nickel Steels with about 18% Cr, BNWL-TR (1973), an English Translation from Arch. Eisenhuttenwesen, Vol. 41(10), pp. 983-988 (1970).

26. H. Tuma, M. Vyklicky, and K. Lobel, Carbon Activity and Solubility in Stainless Chromium-Nickel Steels with about 18% Cr and 9% Ni, an English Translation from Arch. Eisenhuttenwesen, Vol. 40(9), pp. 727-731 (1969).

27. L. S. Darken and R. W. Gurry, Physical Chemistry of Metals, McGraw-Hill Book Co., New York, p. 304 (1953).

28. L. R. Woodyatt, Met. Trans., Vol. 7A, p. 983 (1976).

29. E. E. Thum (Editor), The Book of Stainless Steels, American Society for Metals, Chapters 1, 2, 3, and 14 (1935).

30. R. E. Lismer, L. Pryce, and K. W. Andrews, Journal of Iron and Steel Inst., Vol. 171, p. 49 (1952).

31. R. Ergang, G. Gunther, and H. Weik, Stahl Eisen, Vol. 79, p. 46 (1959).

32. L. Pryce, H. Hughes, and K. W. Andrews, Journal of Iron and Steel Inst., Vol. 184, p. 289 (1956).

33. L. Pryce and K. W. Andrews, Journal of Iron and Steel Inst., Vol. 195, p. 415 (1960).

34. P. Marshall and A. J. Hooper, "Sigma Phase Formation in Stainless Steels," Central Electricity Generating Board Research Department, Report No. 7044, Berkeley (England), April (1975).

35. E. R. Jette and A. G. H. Andersen, Trans. A.S.M., Vol. 24, p. 375 (1936).

36. Symposium on the Nature, Occurrence, and Effects of Sigma Phase, ASTM Special Technical Publication No. 110 (1950).

37. P. A. Krammer, K. Masubuchi, and R. E. Monroe, "Cracking in High-Strength Steel Weldments--A Critical Review," DMIC Report No. 197, Battelle Memorial Research Institute, February (1964).

38. J. T. Gow and O. E. Harder, Trans. A.S.M., Vol. 30, p. 855 (1942).

39. C. T. Sims, "The Occurrence of Topologically Close-Packed Phases," in The Superalloys, C. T. Sims and W. C. Hagel (Editors), John Wiley and Sons, p. 259 (1972).

40. Symposium on Evaluation Tests for Stainless Steels, ASTM Special Technical Publication No. 93, pp. 146-183 (1950).

41. J. G. Parr and A. Hanson, An Introduction to Stainless Steel, American Society for Metals, Metals Park, Ohio (1965).

42. C. A. Zapffe, Stainless Steels, American Society for Metals, Metals Park, Ohio (1949).

43. Stainless Steel Handbook, Allegheny Ludlum Steel Corporation, Pittsburgh, Pennsylvania (1951).

44. M. Hansen, Constitution of Binary Alloys, McGraw-Hill Book Company, New York (1958).

45. B. D. Cullity, Elements of X-Ray Diffraction, Addison-Wesley Publishing Co., Inc., Reading, Massachusetts, p. 388 (1956).

46. C. R. Brooks, Manuscript on Stainless Steels, The University of Tennessee, Knoxville, Tennessee (1976).

47. V. A. Phillips, Modern Metallographic Techniques and Their Applications, Wiley-Interscience, New York (1971).

48. I. S. Brammar and M. A. P. DeWey, Special Preparation for Electron Metallography, American Elsevier Publishing Company, New York (1966).

49. J. L. McCall and W. M. Mueller, Metallographic Specimen Preparation, Optical and Electron Microscopy, Plenum Press, New York (1973).

50. R. E. Smallman and K. H. G. Ashbee, Modern Metallography, Pergamon Press, New York (1966).

51. D. G. Brandon, Modern Techniques in Metallography, Butterworths and Co., London, p. 223 (1966).

52. H. Modin and S. Modin, Metallurgical Microscopy, Butterworths and Co., London, p. 148 (1973).

53. M. H. Lewis, Acta. Met., Vol. 14, p. 1421 (1966).

54. S. Nenno, Trans. Jap. Inst. Metals, Vol. 3, p. 82 (1962).

55. H. J. Goldschmidt, Journal of Iron and Steel Inst., Vol. 162, p. 294 (1949).

56. E. T. Dulis and G. V. Smith, Symposium on the Nature, Occurrence, and Effects of Sigma Phase, ASTM Special Technical Publication No. 110 (cited in Reference 36), p. 1 (1950).

57. R. E. Lismer, Journal of Iron and Steel Inst., Vol. 171, p. 49 (1952).

58. F. B. Pickering, "Precipitation Process in Steels," I.S.I. Special Report No. 64, pp. 118-126 (1959).

59. E. G. Bain and W. E. Griffiths, Trans. A.I.M.E., Vol. 75, p. 166 (1927).

60. H. Goldschmidt, Interstitial Alloys, Plenum Press, New York, pp. 109-143 (1967).

61. R. M. Brick, R. B. Gordon, and A. Phillips, Structure and Properties of Alloys, 3rd Edition, McGraw-Hill Book Co., New York, pp. 339-358 (1965).

62. W. Wallace, Metal Science, Vol. 9, pp. 547-551 (1975).

63. C. DaCasa, Journal of Iron and Steel Inst., Vol. 207, pp. 1325-1332 (1962).

64. J. W. Edington, Practical Electron Microscopy in Materials Science, Monograph No. 2, "Electron Diffraction in Electron Microscope," McMillan, Philips Technical Library, pp. 94-104 (1975).

65. L. W. Murr, Electron Optical Systems in Materials Science, McGraw-Hill Book Co., New York, p. 237 (1970).

66. K. G. Brickner, "Stainless Steels for Room Temperatures," in Source Book on Stainless Steels, American Society for Metals, Metals Park, Ohio, pp. 25-53 (1976).

67. A. M. Talbott and D. E. Furman, Trans. A.S.M., Vol. 45, p. 429 (1953).

68. A. S. Grot, Time-Temperature-Precipitation Studies of Titanium Modified Type 316 and Type 321 Stainless Steels," M.S. Thesis, The University of Tennessee, Knoxville, Tennessee, p. 98 (1974).

69. E. E. Bloom and J. O. Stigler, Trans. Am. Nuclr. Soc., Vol. 15.1, pp. 253-254 (1972).

70. J. R. Blank and T. Gladman, "Quantitative Metallography," in Tools and Techniques in Physical Metallurgy, Vol. 1 (F. Weinberg, Editor), Marcel Dekker, Inc., New York, pp. 265-327 (1970).

71. Metals Handbook (8th Edition), Vol. 8, "Metallography, Structures, and Phase Diagrams," American Society for Metals, Metals Park, Ohio, p. 291 (1973).

72. F. B. Pickering, "Physical Metallurgy of Stainless Steel Developments," Review No. 211, International Metals Reviews (Publication), pp. 227-268, December (1976).

73. H. E. McGannon (Editor), "Steels for Elevated-Temperature Service," in The Making, Shaping, and Treating of Steels (9th Edition), U.S. Steel Corporation, Herbick and Held Pub., Pittsburgh, Pennsylvania, pp. 1163-1202 (1971).

74. J. H. Wernick, "Topologically Closed-Packed Structures," in Intermetallic Compounds (J. H. Westbrook, Editor), John Wiley and Sons, New York, pp. 204-209 (1967).

75. W. Hume-Rothery, Phase Stability in Metals and Alloys (P. S. Rudman, J. Stinger, and R. I. Jaffee, Editors), McGraw-Hill Book Co., New York, pp. 14-23 (1967).

76. International Tables for "Symmetry Groups," X-Ray Crystallography, Vol. I, Kynoch Press, Birmingham, England, p. 48 (1952).

77. Metals Handbook (8th Edition), Volume I, "Properties and Selection" (cited in Reference 23), American Society for Metals, Metals Park, Ohio (1961) (used as a general reference).

78. W. Treischke and G. Tamman, Z. Anorg. Allg. Chem., Vol. 55, p. 402 (1907).

79. R. E. Reed-Hill, Physical Metallurgy Principles (2nd Edition), D. Van Nostrand Company, New York, p. 726 (1973).

80. E. O. Hall and S. H. Algie, "The Sigma Phase," Review No. 104, J. Inst. Metals, Vol. 94, pp. 61-88 (1966).

81. B. Hattersley and W. Hume-Rothery, Journal of Iron and Steel Inst., Vol. 204, pp. 683-701 (1966).

82. A. J. Cook and F. W. Jones, Journal of Iron and Steel Inst., Vol. 148, pp. 217-226 (1943).

83. A. J. Bradley and H. J. Boldschmidt, Journal of Iron and Steel Inst., Vol. 144, pp. 273-283 (1941).

84. H. P. Stuwe, Trans. Met. Soc. A.I.M.E., Vol. 215, p. 408 (1959).

85. J. S. Kasper and R. M. Waterstrat, Acta. Cryst., Vol. 9, p. 289 (1956).

86. J. S. Kasper, "Theory of Alloy Phases," American Society for Metals, Metals Park, Ohio (1956).

87. P. A. Beck, Trans. A.I.M.E., Vol. 194, p. 420 (1952).

88. V. Kazantsev, Doklady Adak. Nauk, Vol. 101, p. 477 (1955).

89. D. S. Clark and W. R. Varney, Physical Metallurgy for Engineers, D. Van Nostrand Co., New York, pp. 318-347 (1962).

90. A. J. Cook and B. R. Brown, Journal of Iron and Steel Inst., Vol. 171, pp. 345-353 (1952).

91. A. S. Grot and J. E. Spruiell, Met. Trans. A, Vol. 6A, pp. 2023-2030 (1975).

92. L. J. Schwartzendruber, L. H. Bennett, E. A. Schoefer, W. T. DeLong, and H. C. Campbell, Welding Journal, Vol. 53, pp. 1-S-18-S (1974).

93. Metal Progress Data Book, A.S.M., p. 161 (1977).

94. S. W. Yang, A Study of Cold Worked State and Annealing Behavior of the Austenitic Stainless Steels, Ph.D. Thesis, The University of Tennessee, Knoxville, Tennessee, August (1977).

95. Standard Methods for Notched Bar Impact Testing of Metallic Materials, ASTM Specification No. E23-72, American Society for Testing and Materials, Philadelphia, Pennsylvania (1972).

96. L. Brewer, "Prediction of High-Temperature Metallic Phase Diagrams," in High-Temperature Materials, V. F. Zackay (Editor), John Wiley and Sons, New York, pp. 12-103 (1965).

97. L. Pauling, Phys. Review, Vol. 54, p. 899 (1938).

98. C. S. Barrett and T. B. Massalski, Structure of Metals (3rd Edition), McGraw-Hill Book Co., New York, pp. 266, 492 (1966).

99. H. J. Goldschmidt, "The Structure of Carbides in Alloy Steels," Part I--General Survey, Journal of Iron and Steel Inst., Vol. 160, pp. 356-362 (1948).

100. R. F. Hills and D. R. Harries, Chemical Process Engineering, pp. 391-396, September (1960).

101. C. K. H. DuBose and J. O. Stiegler, "Semi-Automatic Preparation of Specimens for Transmission Electron Microscopy," Report No. ORNL-4066, Oak Ridge National Laboratory, Oak Ridge, Tennessee, February (1967).

102. V. Clhal and M. Prazak, Journal of Iron and Steel Inst., Vol. 193, pp. 360-367 (1959).

103. B. Chalmers, Principles of Solidification, John Wiley and Sons, New York (1964).

104. Metals Handbook (8th Edition), Volume I, p. 1226 (cited in Reference 77).

105. P. Greenfield and P. A. Beck, Trans. A.I.M.E., Vol. 200, p. 253, (1954).

106. P. Greenfield and P. A. Beck, Trans. A.I.M.E., Vol. 206, p. 256, (1956).

107. W. T. DeLong, Welding Journal, Vol. 52, pp. 69-S-72-S (1973).

108. T. M. Andress, Jr., "Some Aspects of the Thermal Stability of 316L Weld Metal," M.S. Thesis, The University of Tennessee, Knoxville, Tennessee, December (1980).

109. G. Dieter, Mechanical Metallurgy (2nd Edition), McGraw-Hill Book Co., New York, p. 133 (1976).

110. C. R. Brooks, Heat Treatment of Ferrous Alloys, McGraw-Hill Book Co., New York, p. 205 (1979).

111. F. Garofalo, Trans. A.S.M., Vol. 54, p. 430 (1961).

112. C. J. Novak, Handbook of Stainless Steels (D. Peckner and I. M. Bernstein, Editors), McGraw-Hill Book Co., New York, pp. 4-60-4-78 (1977).

113. J. M. Leitnaker and J. Bentley, Met. Trans. A, Vol. 8A, pp. 1605-1613 (1977).

114. V. Biss, G. N. Kirby, and D. L. Sponseller, Met. Trans. A, Vol. 7A, p. 1251 (1976).

115. J. Wegrzyn and A. Klimpel, Welding Journal, Vol. 60, pp. 146-S-154-S (1981).

116. A. H. Sully and T. J. Heal, Research, Vol. 1, p. 228 (1948).

117. L. R. Woodyatt, C. J. Sims, and H. J. Beattie, Trans. A.I.M.E., Vol. 236, p. 519 (1966).

118. A. H. Cottrell, Theoretical Structural Metallurgy, Edward Arnold, London, p. 131 (1959).

APPENDICES

APPENDIX A

APPENDIX A

IDENTIFICATION OF SIGMA PHASE BY ELECTRON DIFFRACTION

In this section, attempts will be made to identify the phases, especially sigma phase, from electron diffraction patterns. The objective is to identify (hkl) planes and the lattice to spot distances. The latter was calculated from a knowledge of camera constant, λL, where λ = wavelength of radiation used and L = distance between the sample and the photographic screen (see Figure A-A-1).

First, an explanation will be given as to how to calculate the camera constant, and then the (hkl) plane will be determined for each photographic plate. The camera constant was found to be about 2.50 for the present case.

After knowing d(hkl), the lattice constant c_o (z axis) and a_o (x,y axis) will be determined. Since c_o/a_o ratios for sigma phase are known for the Fe-Cr-Ni system, a knowledge of c_o/a_o ratios will be helpful in identifying the phase from which the diffraction patterns were taken.

Further, the angles measured and calculated[45] between any two planes (such as $(h_1k_1l_1)$ and $(h_2k_2l_2)$) were another way of identifying the sigma phase qualitatively. In all cases, they agreed well.

1. DETERMINATION OF CAMERA CONSTANT

In Figure A-A-1, the symbols (shown) have the following meaning:

L = Distance from diffracting sample to photographic plate.

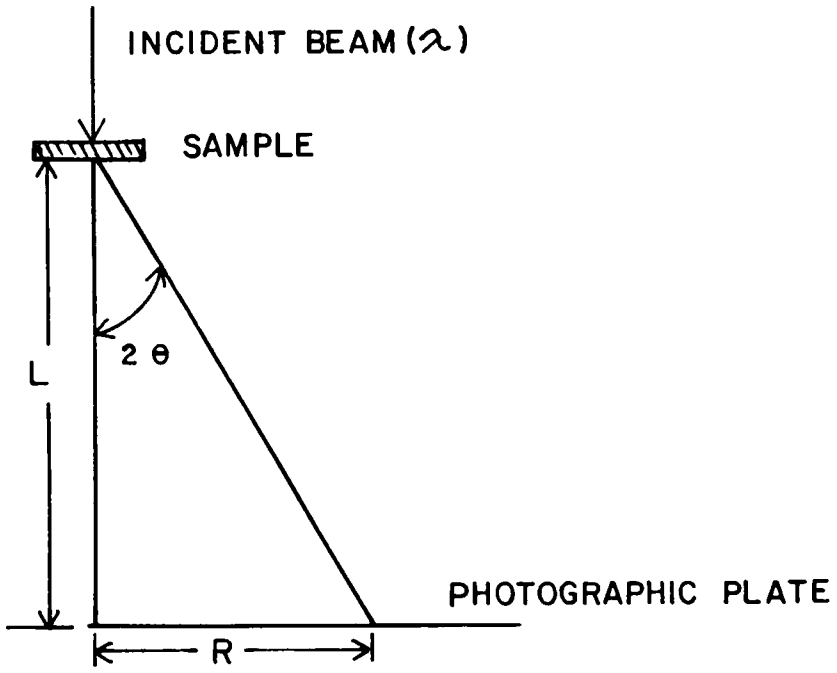


Figure A-A-1. A Simple Electron Diffraction Camera.

R = Distance from incident beam to diffraction spot.

λ = Wavelength of incident beam.

From the geometry of the camera:

$$\tan 2\Theta = R/L,$$

and as the angle, Θ, is small,

$$2\Theta = R/L \qquad \text{(A-A-1)}$$

From Bragg's Law:

$$2d \sin \Theta = 2d\,\Theta = \lambda \quad (\text{for } n = 1, \Theta \text{ small}). \qquad \text{(A-A-2)}$$

By substituting Equation (A-A-2) in Equation (A-A-1):

$$R/L = \lambda/d \quad \text{or} \quad \lambda d = L/R. \qquad \text{(A-A-3)}$$

Ao, the camera constant (CC) is:

$$CC = \lambda L = dR. \qquad \text{(A-A-4)}$$

From Equations (A-A-3) and (A-A-4), it is seen that inverses of the distances measured in an electron diffraction pattern are related to the magnitudes of the interplanar spacings of the diffracting crystal multiplied by a scale factor. This constant of proportionality, λL, is called the camera constant. For each diffraction pattern, there is only one camera constant. The different values of R measured on the diffraction pattern reflect the various different interplanar spacings d(hkl) in a crystal. Thus, once the camera constant is precisely known, the

interplanar spacings can be calculated from the distances measured on the diffraction pattern by using Equations (A-A-3) and (A-A-4).

2. ACTUAL GEOMETRIC CALCULATIONS FOR CC FROM THE DIFFRACTION PATTERN OF THE AUSTENITE (γ) PHASE

The austenite phase (of alloy composition 9, which was solution-treated and then aged for 1000 hours at 650°C (1200°F)) and its diffraction pattern are respectively shown in Figures A-A-2 and A-A-3. From the pattern (Figure A-A-3) and the vector diagram shown in Figure A-A-4, the CC is computed (see Figure A-A-4 and the computations and explanations pertaining to Figure A-A-4).

The sigma phase was identified by knowing the d(hkl) values and the angles between $(h_1k_1l_1)$ and $(h_2k_2l_2)$ planes of the diffraction patterns. See Figures A-A-4 through A-A-7 and the subsequent pages for explanations. Note that in actual computation, the knowledge of CC = d x R was used. Also, sigma was further identified (qualitatively) by calculating the c, a, and c/a ratios and comparing the values against standard published lattice parameters for sigma in the Fe-Cr-Ni systems. See Figure V-16, page 174, and Figure V-17, page 175, for sigma phase and its characteristic diffraction patterns, respectively. These photomicrographs are shown in Chapter V.

SAMPLE NUMBER 9-2-4



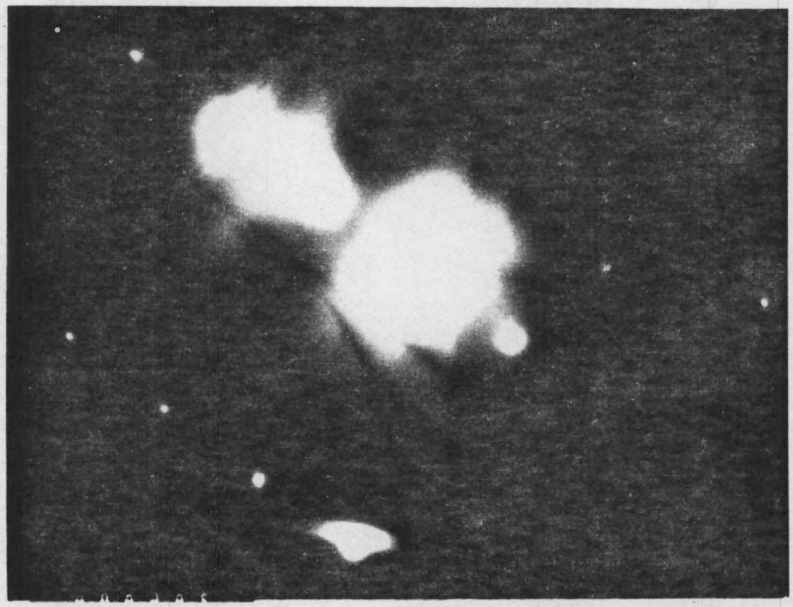
26900X Magnification

TEM Photomicrograph

Plate No. 006577

Figure A-A-2. Austenite (γ) Phase Showing Typical Annealing Twins.

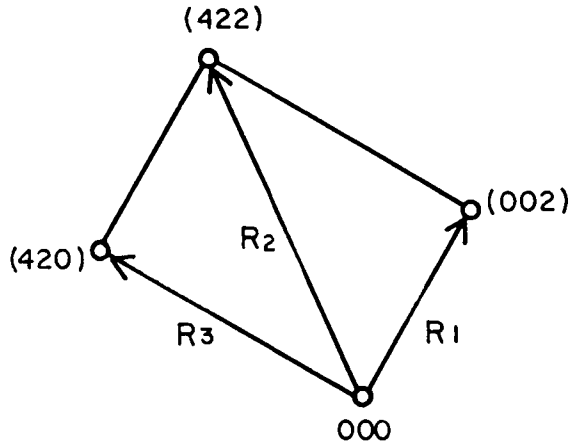
SAMPLE NUMBER 9-2-3



26900X Magnification

Plate No. 006584

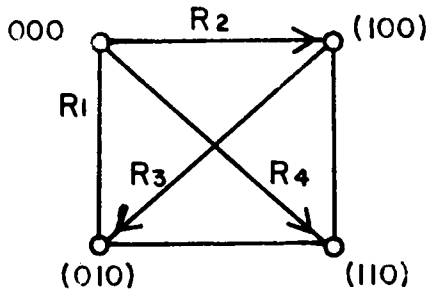
Figure A-A-3. Diffraction Pattern from the Austenite Phase as Shown in Figure A-A-2.



Note that planes appear as points in reciprocal lattice system.

Figure used for TEM Plate No. 006584.

Figure A-A-4. Vector Diagram Showing (hkl) Planes in FCC Systems.

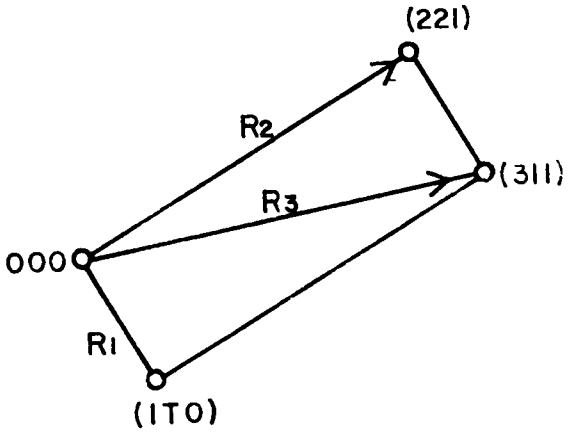


SAMPLE NUMBER 9-2-7

TEM Plate No. 006582 (sigma diffraction pattern)

TEM Plate No. 006583 (sigma particle)

Figure A-A-5. Vector Diagram for Sigma Identification.

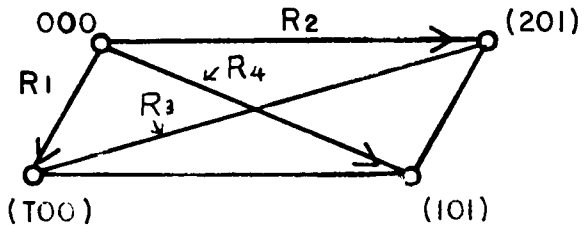


SAMPLE NUMBER 9-2-7

TEM Plate No. 006578 (sigma phase)

TEM Plate No. 006579 (diffraction pattern)

Figure A-A-6. Vector Diagram to Calculate the Angles Between Planes of Sigma Phase.



SAMPLE NUMBER 9-2-7

TEM Plate No. 006580 (sigma diffraction pattern)

TEM Plate No. 006581 (sigma particle)

Figure A-A-7. Vector Diagram to Compute Angles Between Planes for Sigma Phase.

Diffraction Pattern for Austenite (γ) Matrix

Sample 9-2-4, Plate No. 006584:

For the austenite matrix photomicrograph, see Figure A-A-2. For the diffraction pattern, see Figure A-A-3. From the pattern:

$R_1 = 3.35$ cm

$R_2 = 8.15$ cm

$R_3 = 7.40$ cm

$\text{Magnification Factor} = M = 2.40$

Diffraction Spots for Matrix (γ)

$$\frac{R_2}{R_1} = \frac{d_1}{d_2} = 2.433 \qquad \frac{R_2}{R_3} = \frac{d_3}{d_2} = 1.101 \qquad \frac{R_3}{R_1} = 2.209$$

Attached Tables A-A-1 and A-A-2 imply that

$$\frac{R_2}{R_1} = \frac{R_{422}}{R_{002}} \qquad \frac{R_3}{R_1} = \frac{R_{420}}{R_{002}}$$

Upon checking, it is seen that

$$\vec{422} = \vec{420} + \vec{002}$$

i.e., $h_1 + h_2 = h_3$

$k_1 + k_2 = k_3$

$l_1 + l_2 = l_3$

From Table A-A-1:

$d_{002(FCC)} = 1.795$ Å

TABLE A-A-1

INTERPLANAR SPACINGS OF AUSTENITE

Crystal Structure: Face-Centred Cubic

Unit Cell: a = 3.59Å

hkl	d-spacing Å
111	2.073
200	1.795
220	1.269
311	1.082
222	1.036
400	0.898
331	0.824
420	0.803
422	0.733
511,333	0.691
440	0.635
531	0.607
600,442	0.598
620	0.568
533	0.548
622	0.541
444	0.518
551,711	0.503

Source: A. S. Grot, "Time-Temperature-Precipitation Studies of Titanium Modified Type 316 and 321 Stainless Steels," M.S. Thesis, The University of Tennessee, Knoxville, Tennessee, p. 98 (1974).

TABLE A-A-2

RATIOS OF d-SPACINGS IN FACE-CENTERED CUBIC SYSTEMS

hkl	111	200	220	311	222	400	311	420	422	511 333	440	531	442 600
111	1	1.15	1.64	1.92	2.00	2.31	2.52	2.58	2.83	3.00	3.266	3.416	3.464
200	0.866	1	1.41	1.66	1.73	2.00	2.18	2.24	2.449	2.598	2.828	2.958	3.000
220	0.612	0.707	1	1.17	1.22	1.41	1.54	1.58	1.732	1.837	2.000	2.092	2.121
311	0.522	0.604	0.854	1	1.05	1.21	1.31	1.35	1.477	1.567	1.706	1.784	1.809
222	0.500	0.578	0.817	0.957	1	1.15	1.26	1.29	1.414	1.500	1.633	1.708	1.732
400	0.433	0.500	0.707	0.830	0.866	1	1.09	1.12	1.225	1.299	1.414	1.479	1.500
311	0.397	0.459	0.649	0.760	0.795	0.917	1	1.03	1.124	1.192	1.298	1.357	1.376
420	0.387	0.446	0.632	0.740	0.774	0.894	0.975	1	1.095	1.162	1.265	1.323	1.342
422	0.354	0.408	0.577	0.677	0.707	0.816	0.890	0.913	1	1.061	1.155	1.208	1.225
511,333	0.333	0.385	0.544	0.638	0.667	0.770	0.839	0.861	0.943	1	1.089	1.339	1.155
440	0.306	0.354	0.500	0.586	0.612	0.707	0.771	0.791	0.866	0.919	1	1.046	1.061
531	0.293	0.338	0.478	0.561	0.586	0.679	0.737	0.756	0.828	0.878	0.956	1	1.014
442,600	0.289	0.333	0.471	0.553	0.577	0.667	0.726	0.745	0.816	0.866	0.943	0.986	1

Source: A. S. Grot, "Time-Temperature-Precipitation Studies of Titanium Modified Type 316 and 321 Stainless Steels," M.S. Thesis, The University of Tennessee, Knoxville, Tennessee, p. 98 (1974).

$$\text{Camera Constant (CC)} = (R_{002} \times d_{002})/M = \frac{3.35 \times 1.795}{2.40} = 2.5055$$

$$\text{or } (R_{422} \times d_{422})/M = \frac{8.15 \times 0.734}{2.40} = 2.4925$$

$$\text{or } (R_{420} \times d_{420})/M = \frac{7.40 \times 0.803}{2.40} = 2.4759$$

Average CC = 2.50.

Diffraction Pattern Picture for Sigma (σ)

Sample 9-2-7:

See Figure V-16, page 194,
Plate No. 006583.

See Figure V-17, page 195,
Plate No. 006582.

Magnification Factor = M = 2.36

Total Magnification = 26900X

750°C, 1000 Hours

CC = 2.50

From Figure A-A-5:

$R_1 = 0.63/2.36 = 0.2669$ cm	$d_1 = CC/R_1 = 9.3651$ Å
$R_2 = 0.62/2.36 = 0.2627$ cm	$d_2 = CC/R_2 = 9.5161$ Å
$R_3 = 0.82/2.36 = 0.3475$ cm	$d_3 = CC/R_3 = 7.1951$ Å
$R_4 = 0.92/2.36 = 0.3898$ cm	$d_4 = CC/R_4 = 6.4130$ Å

$\Theta_{R_1R_2}$ calculated = 90°, $\Theta_{R_1R_2}$ measured = 89°

$\Theta_{R_2R_4}$ calculated = 45°, $\Theta_{R_2R_4}$ measured = 44°

$\Theta_{R_1R_4}$ calculated = 45°, $\Theta_{R_1R_4}$ measured = 45°

Since 110 = 100 + 010 and the angles (Θ's) measured and calculated agree, this pattern has been identified.

For BCT crystal structure, the angle ϕ between planes $(h_1k_1l_1)$ and $(h_2k_2l_2)$ is given by the following relation. According to Cullity,[45]

$$\cos = \frac{\left(\frac{h_1h_2 + k_1k_2 + l_1l_2}{a^2}\right) + \left(\frac{l_1l_2}{c^2}\right)}{\left(\frac{h_1^2 + k_1^2}{a^2} + \frac{l_1^2}{c^2}\right)^{1/2} \left(\frac{h_2^2 k_2^2}{a^2} + \frac{l_2^2}{c^2}\right)^{1/2}}$$

where c and a are the lattice parameters of BCT crystal in (z) and (x,y) directions, respectively.

For a BCT crystal (σ),

$c = 4.60$ Å

$a = 8.86$ Å

c/a ratio = 0.52

where $1\text{Å} = 10^{-8}$ cm.

Identification of Sigma By Electron Diffraction

Sample 9-2-7:

Plate No. 006578
(sigma)

Plate No. 006579
(picture)

Magnification = 27930X

750°C, 1000 Hours

CC = 2.50

M = 2.45

From Figure A-A-6:

$R_1 = 0.95/2.45 = 0.39$ cm	$d_1 = 2.50/0.39 = 6.41$ Å
$R_2 = 2.27/2.45 = 0.93$ cm	$d_2 = 2.50/0.93 = 2.69$ Å
$R_3 = 2.50/2.45 = 1.02$ cm	$d_3 = 2.50/2.45 = 2.45$ Å

Upon inspection, $311 = 221 + 1\bar{1}0$,

$$\Theta_{R_1R_2 \text{ calculated}} = 90°, \Theta_{R_1R_2 \text{ measured}} = 90°$$

$$\Theta_{R_2R_3 \text{ calculated}} = \Theta_{R_2R_3 \text{ measured}} = 22.45°.$$

So the pattern has been identified to be sigma.

Identification of Sigma Phase By Electron Diffraction

Sample 9-2-7:

Plate No. 006580
(sigma diffraction pattern)

Plate No. 006581
(sigma particle)

Magnification Factor = M = 2.36

CC = 2.50

CC = 2.50 = d X R, so d = CC/R = 2.50/R. From Figure A-A-7:

$R_1 = 0.64/2.36 = 0.27$ cm	$d_1 = 2.50/0.27 = 9.26$ Å
$R_2 = 1.80/2.36 = 0.76$ cm	$d_2 = 2.50/0.76 = 3.29$ Å
$R_3 = 2.33/2.36 = 0.99$ cm	$d_3 = 2.50/0.99 = 2.53$ Å
$R_4 = 1.42/2.36 = 0.60$ cm	$d_4 = 2.50/0.60 = 4.15$ Å

$$\Theta_{R_2R_4 \text{ calculated}} = 18.64, \Theta_{R_2R_4 \text{ measured}} = 18.30°$$

$$\Theta_{R_1R_2 \text{ calculated}} = \Theta_{R_1R_2 \text{ measured}} = 136°.$$

Since 101 = 201 + $\bar{1}00$ and measured Θ's agree with calculated Θ's, this diffraction pattern has been identified to be sigma phase.

Calculation for c and a for Sigma

For BCT (Cullity[45]) (T.E.M. Data):

$$d = \frac{1}{\left(\frac{h^2 + k^2}{a^2} + \frac{l^2}{c^2}\right)^{1/2}}$$

or $$\left(\frac{1}{d}\right)^2 = \frac{h^2 + k^2}{a^2} + \frac{l^2}{c^2}$$

or $$\left(\frac{1}{d_{\bar{1}00}}\right)^2 = \left(\frac{1}{a}\right)^2, \quad \text{or} \quad d_{\bar{1}00} = a = 9.26 \text{ Å}.$$

Again,

$$\left(\frac{1}{d_{201}}\right)^2 = \frac{4}{a^2} + \frac{1}{c^2} = \left(\frac{1}{3.24}\right)^2 \qquad \text{(A-A-5)}$$

$$\left(\frac{1}{d_{100}}\right)^2 = \frac{1}{a^2} + \frac{1}{c^2} = \left(\frac{1}{4.15}\right)^2 \qquad \text{(A-A-6)}$$

From Equations (A-A-5) and (A-A-6),

$$\frac{3}{a^2} = \left(\frac{1}{3.29}\right)^2 - \left(\frac{1}{4.15}\right)^2$$

or $$a = 9.35 \text{ Å}$$

$$\text{Average } a = 9.30 \text{ Å}$$

$$\frac{1}{c^2} = \left(\frac{1}{4.15}\right)^2 - \left(\frac{1}{9.30}\right)^2$$

$$c = 4.64 \text{ Å}.$$

So, for sigma in composition 9,

$$a_o = 9.30 \text{ Å}$$

$$c_o = 4.64 \text{ Å}$$

$$c_o/a_o = 0.50.$$

These results agree well with the published lattice parameters for sigma in the Fe-Cr-Ni system, so the phase is identified as sigma.

Calculation of c_o – a_o, and c_o/a_o Ratios for Sigma from X-Ray Diffraction Results

See Table V-6, page 163, and consider two (hkl) planes from the table:

$(h_1k_1l_1) = (411)$, $(I/IO) = 49$, and

$(h_2k_2l_2) = (212)$, $(I/IO) = 30$.

For (411), using the equation $\frac{h^2 + k^2}{a^2} + \frac{l^2}{c^2}$ (for BCT crystal):

$$\frac{1}{d^2_{(411)}} = \frac{16 + 1}{a_o^2} + \frac{1}{c_o^2} = \frac{17}{a_o^2} + \frac{1}{c_o^2} \qquad \text{(A-A-7)}$$

and

$$\frac{1}{d^2_{(212)}} = \frac{4+1}{a_o^2} + \frac{4}{c_o^2} = \frac{5}{a_o^2} + \frac{4}{c_o^2} \qquad \text{(A-A-8)}$$

From simultaneous Equations (A-A-7) and (A-A-8),

$$a_o = 8.860 \text{ Å}$$

$$c_o = 4.600 \text{ Å}$$

$$c_o/a_o = 0.52.$$

These values agree well with the lattice parameters for sigma in Fe-Cr-Ni systems published in the literature.

APPENDIX B

APPENDIX B

COMPUTER PROGRAM TO CALCULATE At.% Cr, Fe, Ni, ETC. AND THE AVERAGE EVN, $\bar{Nv}$, FOR Fe-Cr-Ni ALLOYS

A computer program (in FORTRAN language) showing how to calculate the average electron vacancy number ($\bar{Nv}$) in approximately single-phase austenitic stainless steel alloys is shown in Figure A-B-1.

From a knowledge of chemical compositions of the alloys, At.% of the alloys were calculated from their atomic weights. For composition number 9, for example, this is shown in Figure A-B-2. The average electron vacancy number concentration was calculated based upon the following equation:

$$\bar{Nv} = 4.66 \times \% \text{ Cr} + 2.22 \times \% \text{ Fe} + 0.61 \times \% \text{ Ni}$$

(for pure alloys).

The percent of elements expressed in this equation are in At.%. The solubility of carbon assumed was 0.03 % (weight) at 750°C.

In Appendix C, carbon solubility was assumed to vary with temperature. Such calculations as variation of $\bar{Nv}$ with temperature are also shown in Appendix C.

```
      REAL NI
40    WRITE(4,10)
10    FORMAT(///5X,37HENTER WT.% OF CR,NI,C  IN FORMAT 10.4 )
20    FORMAT(F10.4)
      READ(4,20)CR
      READ(4,20)NI
      READ(4,20)C
C *** CONVERT TO ATOMIC PER CENT
      FE=100.-CR-NI-C
      CR=CR/51.996
      NI=NI/58.71
      C=C/12.0
      FE=FE/55.847
      CALL RESC(CR,FE,NI,C)
      WRITE(4,25)
      WRITE(4,30)CR,NI,C,FE
25    FORMAT(//5X,15HATOMIC PER CENT,10X,2HCR,10X,2HNI,11X,1HC,10X,2HFE)
30    FORMAT(//,22X,F10.4,2X,F10.4,2X,F10.4,2X,F10.4)
C *** SOLUBILITY OF C IS ASSUMED
      CS=0.02
      C=C-CS
      FE=FE-1.*C
      CR=CR-17./6.*C
      CALL RESC(FE,CR,NI,0.0)
      AV=4.66*CR+2.22*FE+0.61*NI
      WRITE(4,90)AV
90    FORMAT(///5X,25HTHE AV. ELECTR. VAC. NO. :,F10.4)
      GO TO 40
      STOP
      END

F4S \12A
>BL_RESC

END PASS1

      SUBROUTINE RESC(A,B,C,D)
      TL=A+B+C+D
      TL=TL/100.0
      A=A/TL
      B=B/TL
      C=C/TL
      D=D/TL
      RETURN
      END
```

Figure A-B-1. FORTRAN IV Program to Calculate Average Electron Vacancy Number, Nv.

Source: Computer program written by S. W. Yang, The University of Tennessee, Knoxville, Tennessee (1977). (Mr. Yang is now with G.E. Research Lab, Schenectady, New York.) The equation to compute Nv is based upon the work of W. Wallace, Metal Science, Vol. 9, pp. 547-551 (1975). (See Reference 62.)

```
 ENTER WT.% OF CR,NI,C  IN FORMAT 10.4

24.10
14.22
0.06

   ATOMIC PER CENT          CR           NI           C           FE

                        25.5500      13.3516      0.2756      60.8228

   THE AV. ELECTR. VAC. NO. :  261.6304
```

Note 1: Divide the output by 100 to get the average EVN; i.e., 2.616.

Note 2: The actual average EVN ($\overline{Nv}$) for alloy 9 after correction for carbide precipitation is 2.94. The original EVN calculated as shown above (2.616) is not correct. The inaccuracies in Nv resulted due to an error in the original chemical analysis. Nevertheless, the principle of computing $\overline{Nv}$ remains the same.

Figure A-B-2. Computer Printout for Electron Vacancy Concentration for Composition 9 (Solution-Treated Alloy).

APPENDIX C

APPENDIX C

SOLUBILITY OF CARBON WITH TEMPERATURE IN Fe-Cr-Ni ALLOYS

The solubility of carbon with respect to temperature is exponential.[25,26] Since carbon solubility in the austenitic matrix does affect the electron vacancy number ($\bar{N}v$) as discussed previously and in Appendix B, the carbon solubility limit using equilibrium condition is calculated in this section.

Results of carbon solubility vs. temperatures at 650°C, 750°C, and 850°C are shown in Table A-C-1. Results are explained in subsequent paragraphs of this appendix.

The original carbon added was known (see Table III-1, page 70). Knowing the solubility limit at a given temperature (Table A-C-1), the available carbon content could be calculated simply by subtracting the soluble carbon from the original carbon content of the alloy. The results appear in Table A-C-2.

The carbon solubility in equilibrium with the austenite matrix at 650°C, 750°C, and 850°C was calculated using the following equation based upon the work of Tuma:[25,26]

$$\log_{10} N_C = \frac{(-6800 + 4500\ N_{Ni})}{T} - 4.0\ N_{Ni} + 2.93 \qquad \text{(A-C-1)}$$

where: N_C = mole fraction of carbon

N_{Ni} = mole fraction of nickel

T = aging temperature in °K.

TABLE A-C-1

EFFECT OF TEMPERATURE ON SOLUBILITY OF CARBON IN Fe-Cr-Ni-C ALLOYS

Temperature (°C)	Wt.% Carbon
650	0.0010
750	0.00473
850	0.01627

Note:

$$\text{Log}_{10} N_C = \frac{(-6800 + 4500\ N_{Ni})}{T} - 4.0\ N_{Ni} + 2.93$$

where: N_C = mole fraction of carbon

N_{Ni} = mole fraction of nickel

T = temperature in °K.

	Cr	Ni	Fe	C
Atomic Weight	51.996	58.71	55.847	12.01

Source: H. Tuma, M. Vyklicky, and K. Lobel, English Translation from Arch. Eisenhuttenwesen: BNWL-TR (1970), Vol. 41(10), p. 983 (see Reference 25); Vol. 40(9), pp. 727-731 (1969) (see Reference 26).

TABLE A-C-2

AVAILABLE CARBON (FOR CARBIDE FORMATION) FOR ALLOYS AT 650°C, 750°C, and 850°C

Alloy Number	Original Wt.% Carbon	Wt.% Available Carbon at Aging Temperatures (°C)			Mole Fraction Ni (N_{Ni})
		650	750	850	
3	0.019	0.018	0.0143	0.0027	0.1415
5	0.006	0.0050	0.0013	0	0.1415
8	0.40	0.3990	0.3953	0.3837	0.1312
9[a]	0.06	0.0590	0.0553	0.0437	0.1335
10	0.18	0.1790	0.1753	0.1637	0.1386
14[b]	0.19	0.1890	0.1853	0.1737	0.1464
17	0.05	0.0490	0.0453	0.0337	0.1642
18	0.19	0.1890	0.1853	0.1737	0.1641
19	0.38	0.3790	0.3753	0.3637	0.1592

[a]New analysis, C = 0.014%.

[b]New analysis, C = 0.20%.

Equation (A-C-1) is valid for a stainless steel having 18 wt.% chromium. Since in our alloys (see Table III-1) the Cr content was more than 18%, Equation (A-C-1) is approximate for alloys having more than 18% Cr. In the absence of other work for alloys having more than 18% Cr, the wt.% carbon at 650°C, 750°C, and 850°C was calculated using Equation (A-C-1). Results are shown in Table A-C-1.

APPENDIX D

APPENDIX D

VARIATION OF STOICHIOMETRY VARIATIONS OF $M_{23}C_6$ CARBIDE WITH AGING TEMPERATURE AND CALCULATION OF ELECTRON VACANCY NUMBER, $\bar{N}v$

In this section, the popularly assumed $M_{23}C_6$ carbide in a system is also assumed to vary in its chemical formula where the carbides general chemical formula is represented as

$$(Cr_x\ Fe_y)C_6$$

where $x + y = 23$ based upon the work of DaCasa.[63]

The carbides stoichiometry significantly affects the amount of elements consumed (such as Cr, Fe, C) by formation of carbides. Therefore, the available elements in solid solution can vary, and thereby the electron vacancy number ($\bar{N}v$) and the equivalent chromium content (ECC) values change. Since both these variables--$\bar{N}v$ and ECC--in an alloy can significantly affect the tendency of an alloy to embrittlement by forming sigma, such calculations are extremely important. Precisely, therefore, the calculations appear in the following pages.

The nature of $M_{23}C_6$ carbide and its variation or deviation from the norm are shown in Tables A-D-1 and A-D-2. Variation of ECC with temperature for various alloys is shown in Table A-D-3. Variation of $\bar{N}v$ with aging temperature for various alloys is shown in Table A-D-4.

The first step is to compute x and y for the carbide $(Cr_x\ Fe_y)C_6$ where $x + y = 23$ based upon the work of DaCasa.[63] Then, the amount of

TABLE A-D-1

EFFECT OF TEMPERATURE ON STOICHIOMETRY (CHEMICAL FORMULA) OF $M_{23}C_6$* $(Cr_x\ Fe_y)C_6$

Temperature (°C)	Cr/Fe Ratio	$(Cr_x\ Fe_y)C_6$	Time
650	2.0	$(Cr_{15.70}\ Fe_{7.30})C_6$	1000 Hours
750	3.0	$(Cr_{17.55}\ Fe_{5.45})C_6$	1000 Hours
850	4.5	$(Cr_{19.05}\ Fe_{3.95})C_6$	1000 Hours

*It is assumed that solubility of nickel in $M_{23}C_6$ is insignificant.

Source: C. DaCasa, JISI, Vol. 207, 1969, pp. 1325-1332.

TABLE A-D-2

AMOUNT OF $M_{23}C_6$ FORMATION BASED UPON $(Cr_x\ Fe_y)C_6$ FORMULA FOR ALLOYS AT VARIOUS TEMPERATURES

	650°C,[a] $(Cr_{15.70}\ Fe_{7.30})C_6$		750°C,[b] $(Cr_{17.55}\ Fe_{5.45})C_6$		850°C,[c] $(Cr_{19.05}\ Fe_{3.95})C_6$	
Alloy Number	Wt.% Available Carbon	Wt.% Carbide	Wt.% Available Carbon	Wt.% Carbide	Wt.% Available Carbon	Wt.% Carbide
3	0.018	0.32	0.0143	0.26	0.0027	0.05
5	0.0050	0.09	0.0013	0.02	0	0
8	0.3990	7.18	0.3953	7.07	0.3837	6.83
9	0.0590	1.06	0.0553	0.99	0.0437	0.78
10	0.1790	3.22	0.1753	3.14	0.1637	2.92
14	0.1890	3.40	0.1853	3.31	0.1737	3.09
17	0.0490	0.88	0.0453	0.81	0.0337	0.60
18	0.1890	3.40	0.1853	3.31	0.1737	3.09
19	0.3790	6.82	0.3753	6.71	0.3637	6.48

[a] 650°C, 1 gm C ≡ 15.70 gm carbide; 11.3286 gm Cr; 5.6576 gm Fe.

[b] 750°C, 1 gm C ≡ 17.55 gm carbide; 12.6635 gm Cr; 4.2238 gm Fe.

[c] 850°C, 1 gm C ≡ 17.81 gm carbide; 13.7458 gm Cr; 3.0613 gm Fe.

TABLE A-D-3

ELEMENTS IN SOLID SOLUTION WITH THE MATRIX AT 650°C, 750°C, AND 850°C AFTER CARBIDE FORMATION

Alloy Number	Original Composition		Final Chemical Composition					
			650°C		750°C		850°C	
	Wt.%	ECC	Wt.%	ECC	Wt.%	ECC*	Wt.%	ECC
3	C = 0.019 Cr = 18.38 Ni = 14.98 Fe = Balance	15.0	C = 0.0010 Cr = 18.18 Ni = 14.98 Fe = Balance	14.79	C = 0.00473 Cr = 18.20 Ni = 14.98 Fe = Balance	14.81	C = 0.01627 Cr = 18.34 Ni = 14.98 Fe = Balance	4.95
5	C = 0.006 Cr = 18.48 Ni = 14.99 Fe = Balance	15.1	C = 0.0010 Cr = 18.42 Ni = 14.99 Fe = Balance	15.03	C = 0.0047 Cr = 18.46 Ni = 14.99 Fe = Balance	15.07	C = 0.006 Cr = 18.46 Ni = 14.99 Fe = Balance	15.09
8	C = 0.40 Cr = 23.94 Ni = 14.14 Fe = Balance	20.74	C = 0.0010 Cr = 19.42 Ni = 14.14 Fe = Balance	16.22	C = 0.0047 Cr = 18.93 Ni = 14.14 Fe = Balance	15.73	C = 0.0163 Cr = 18.67 Ni = 14.14 Fe = Balance	15.47
9	C = 0.06 Cr = 24.10 Ni = 14.22 Fe = Balance	20.93	C = 0.0010 Cr = 23.43 Ni = 14.22 Fe = Balance	20.22	C = 0.0047 Cr = 23.40 Ni = 14.22 Fe = Balance	20.19	C = 0.0163 Cr = 23.50 Ni = 14.22 Fe = Balance	20.29

TABLE A-D-3 (Continued)

Alloy Number	Original Composition		Final Chemical Composition					
			650°C		750°C		850°C	
	Wt.%	ECC	Wt.%	ECC	Wt.%	ECC*	Wt.%	ECC
10	C = 0.18 Cr = 25.63 Ni = 14.84 Fe = Balance	22.28	C = 0.0010 Cr = 23.60 Ni = 14.84 Fe = Balance	20.25	C = 0.0047 Cr = 23.41 Ni = 14.84 Fe = Balance	20.06	C = 0.0163 Cr = 23.38 Ni = 14.84 Fe = Balance	20.03
14	C = 0.19 Cr = 23.92 Ni = 15.65 Fe = Balance	20.38	C = 0.0010 Cr = 21.78 Ni = 15.65 Fe = Balance	18.24	C = 0.0047 Cr = 21.57 Ni = 15.65 Fe = Balance	18.03	C = 0.0163 Cr = 21.53 Ni = 15.65 Fe = Balance	17.99
17	C = 0.05 Cr = 24.69 Ni = 17.46 Fe = Balance	20.74	C = 0.0010 Cr = 24.13 Ni = 17.46 Fe = Balance	20.18	C = 0.0047 Cr = 24.12 Ni = 17.46 Fe = Balance	20.17	C = 0.0163 Cr = 24.23 Ni = 17.46 Fe = Balance	20.28
18	C = 0.19 Cr = 24.47 Ni = 17.54 Fe = Balance		C = 0.0010 Cr = 22.33 Ni = 17.54 Fe = Balance		C = 0.0047 Cr = 22.12 Ni = 17.54 Fe = Balance		C = 0.0163 Cr = 22.08 Ni = 17.54 Fe = Balance	

TABLE A-D-3 (Continued)

Alloy Number	Original Composition		Final Chemical Composition					
			650°C		750°C		850°C	
	Wt.%	ECC	Wt.%	ECC	Wt.%	ECC*	Wt.%	ECC
19	C = 0.38 Cr = 26.19 Ni = 17.15 Fe = Balance	22.31	C = 0.0010 Cr = 21.90 Ni = 17.15 Fe = Balance	18.02	C = 0.0047 Cr = 21.44 Ni = 17.15 Fe = Balance	17.56	C = 0.0163 Cr = 21.19 Ni = 17.15 Fe = Balance	17.31

*Recalculated values by Spruiell in "Final Report on Studies of Microstructure--Property Relationships in Austenitic Stainless Steels," The University of Tennessee, Knoxville, Tennessee, Report No. ORO-4044-7 (1977):

ECC:	Alloys: 3	5	8	9	10	14	17	18	19
Overall Composition	14.9	16.6	22.3	22.8	22.7	18.8	20.8	20.6	22.3
After Carbide Precipitation Correction at 750°C	14.7	16.6	18.5	22.6	20.6	16.9	20.3	18.8	18.8

TABLE A-D-4

ELECTRON VACANCY NUMBER ($\bar{Nv}$) AT ROOM TEMPERATURE (RT), 650°C, 750°C, AND 850°C

	$\bar{Nv} \times 10^2$			
Number	RT	650°C	750°C[a]	850°C
3	246.7285	246.7033	246.6531	246.6996
5	247.3273	247.3083	247.3110	247.2756
8	252.3053	251.1691	249.8069	248.8234
9[b]	261.6304	261.3546	261.1871	261.1590
10[b]	261.6949	260.8631	260.2845	259.9204
14	255.6432	254.9761	254.3403	253.9365
17[b]	258.5114	258.3003	258.1818	258.1731
18	254.1704	253.5526	252.9152	252.5081
19	254.2743	253.0316	251.7492	250.7965

[a]Shows large amount of sigma phase after aging.

[b]Recalculated values by Spruiell in "Final Report on Studies of Microstructure--Property Relationships in Austenitic Stainless Steels," The University of Tennessee, Knoxville, Tennessee, Report No. ORO-4044-7 (1977):

$\bar{Nv}$:	Alloys: 3	5	8	9	10	14	17	18	19
After Carbide Precipitation Correction at 750°C	2.76	2.81	2.84	2.94	2.91	2.80	2.84	2.81	2.80

of $M_{23}C_6$ carbide is computed based upon $(Cr_x\ Fe_y)C_6$ formula for Fe-Cr-Ni alloys at 650°C, 750°C, and 850°C from a knowledge of carbon solubility in austenite matrix and knowing the values for x and y. Finally, an explanation is given as to how to calculate the amounts of elements (Cr, C, Fe) which remain in solid solution at various temperatures--namely 650°C, 750°C, and 850°C. From this knowledge, the parameters $\bar{N}v$ and ECC at any temperature could be calculated.

1. EFFECT OF TEMPERATURE ON STOICHIOMETRY OF $M_{23}C_6$

The general form of carbide $M_{23}C_6$ in austenitic stainless steel is $(Cr_x\ Fe_y)C_6$, and the value of x and y are dependent upon equilibrium aging temperature and time. This fact has been verified by DaCasa.[63] Based upon his work, the (Cr wt.%/Fe wt.%) ratio was taken to be 2.0 at 650°C, 1000 hours; 3.0 at 750°C, 1000 hours; and 4.5 at 850°C, 1000 hours. Taking the atomic weights 51.996 (≃52) for Cr and 55.847 for Fe,

$$\frac{51.996x}{55.847y} = 2.0 \text{ at } 650°C,\ 1000 \text{ hours} \qquad \text{(A-D-1)}$$

and

$$x + y = 23. \qquad \text{(A-D-2)}$$

From Equations (A-D-1) and (A-D-2), the values for x and y are solved, and the results are given in Table A-D-1.

In the calculations above, it is assumed that solubility of nickel in $M_{23}C_6$ is insignificant.

2. AMOUNT OF $M_{23}C_6$ FORMATION BASED UPON $(Cr_x\ Fe_y)C_6$ FORMULA FOR ALLOYS AT 650°C, 750°C, and 850°C

Based upon the chemical formula for $(Cr_x\ Fe_y)C_6$ shown in Table A-D-1 and knowing the available carbon (from Table A-C-2, page 243), the weight percent carbides $(Cr_{15.70}\ Fe_{7.3})C_6$ at 650°C (1000 hours); $(Cr_{17.55}\ Fe_{5.45})C_6$ at 750°C (1000 hours); and $(Cr_{19.05}\ Fe_{3.95})C_6$ at 850°C (1000 hours) were calculated. The results are shown in Table A-D-2. The weight percent carbides were later used from Table A-D-3 to calculate the amount of elements in the carbide and the elements remaining in equilibrium with the austenite (solid solution) matrix.

3. ELEMENTS (Cr, C, Fe) IN SOLID SLUTION WITH AUSTENITE AT 650°C, 750°C, AND 850°C

From a knowledge of the carbides formation at 650°C, 750°C, and 850°C (see Table A-D-2), the amount of Cr and Fe in $(Cr_x\ Fe_y)C_6$ carbides are calculated. Since the original chemical composition is known, the amount of Cr and Fe in solid solution with austenite is calculated simply by subtracting the tied-in Cr and Fe (with carbides) from the original Cr and Fe. Nickel composition stays the same. The amount of carbon in solid solution was already calculated (see Table A-C-1, page 242). The elements in solid solution will later be used to calculate electron vacancy numbers and equivalent chromium contents as shown in Tables A-D-3 (for ECC) and A-D-4 (for $\bar{N}v$).

It was later discovered that the $\bar{N}v$ and ECC values were somewhat in error due to errors in chemical analyses of the alloys. However, the

principles used to compute $\bar{N}v$'s and ECC's are correct. The ECC and $\bar{N}v$ values were later recalculated by Spruiell* and were used in this research. The new results are shown in Tables A-D-3 and A-D-4.

---

*J. E. Spruiell, "Final Report on Studies of Microstructure--Property Relationships in Austenitic Stainless Steels," The University of Tennessee, Knoxville, Tennessee, Report No. ORO-4044-7 (1977).

APPENDIX E

APPENDIX E

TEMPERATURE PROFILES FOR TUBULAR FURNACES

Temperature profiles for the tubular furnaces are shown in Figures A-E-1 through A-E-3.

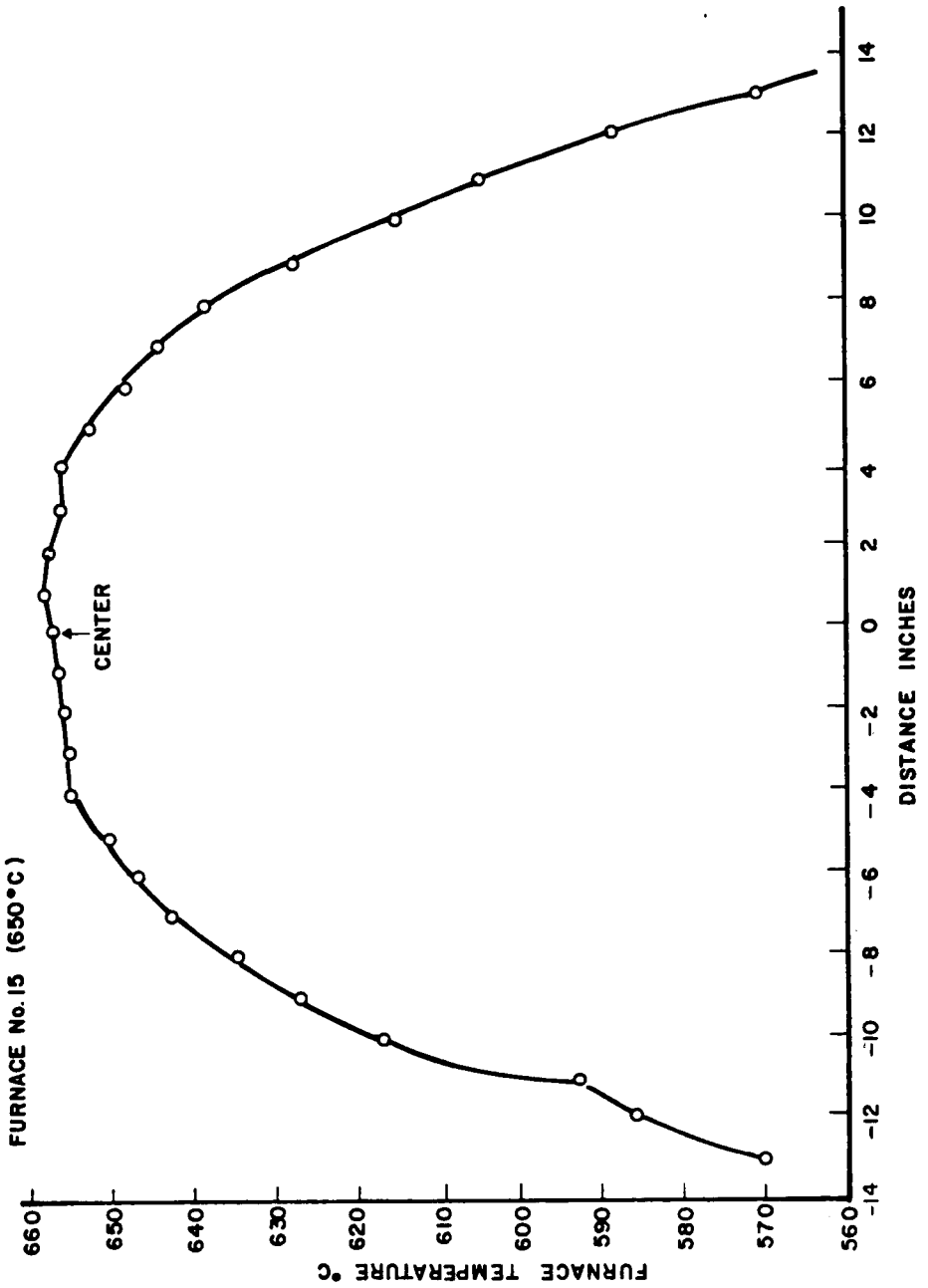


Figure A-E-1. Temperature Profile for Furnace No. 15 (650°C).

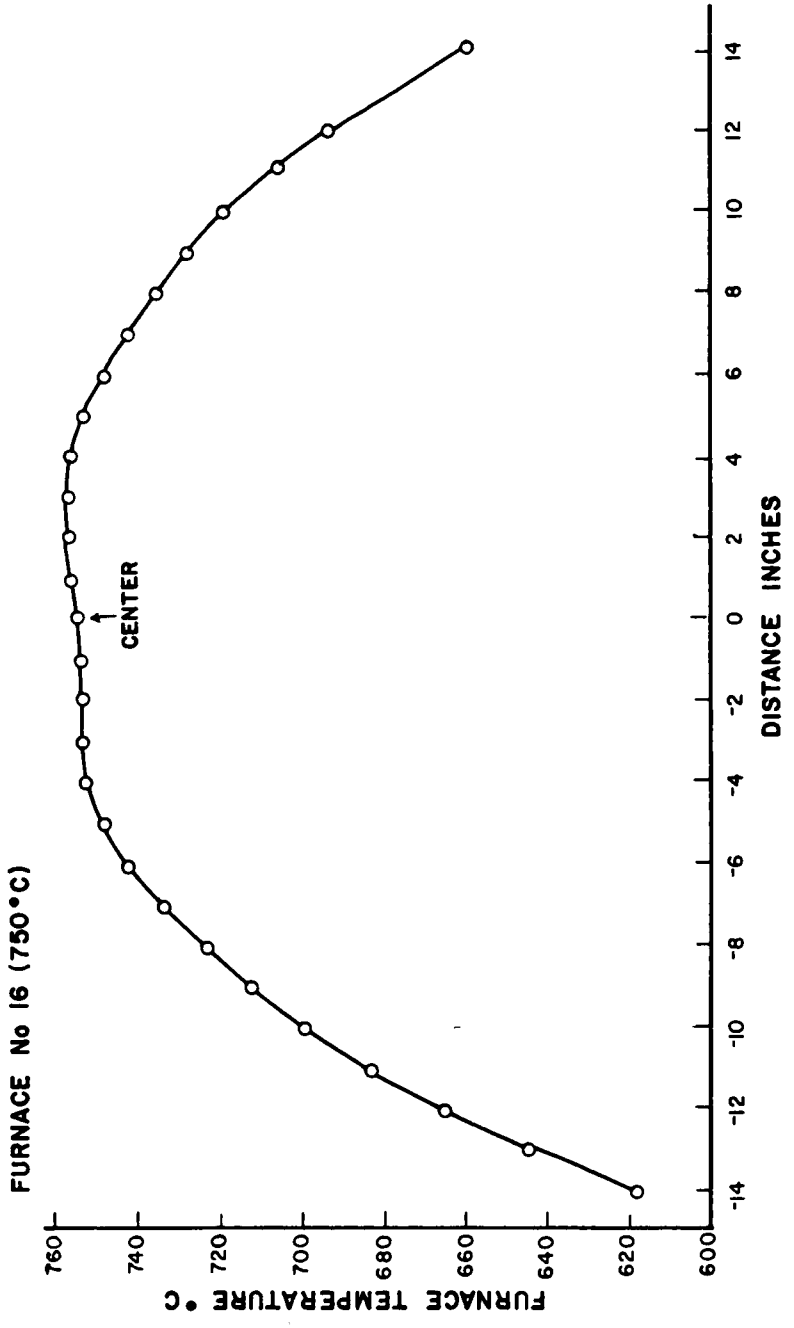


Figure A-E-2. Temperature Profile for Furnace No. 16 (750°C).

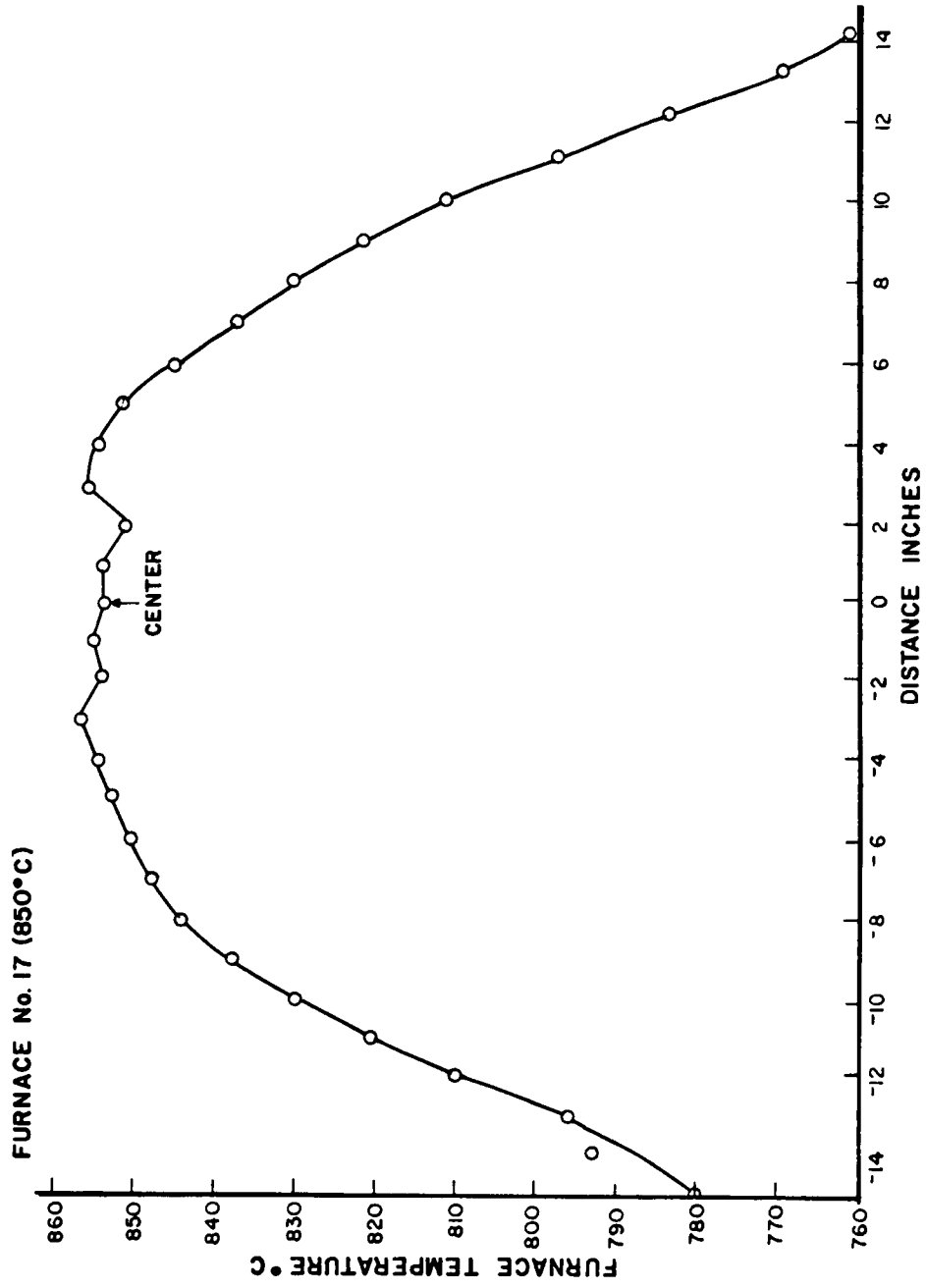


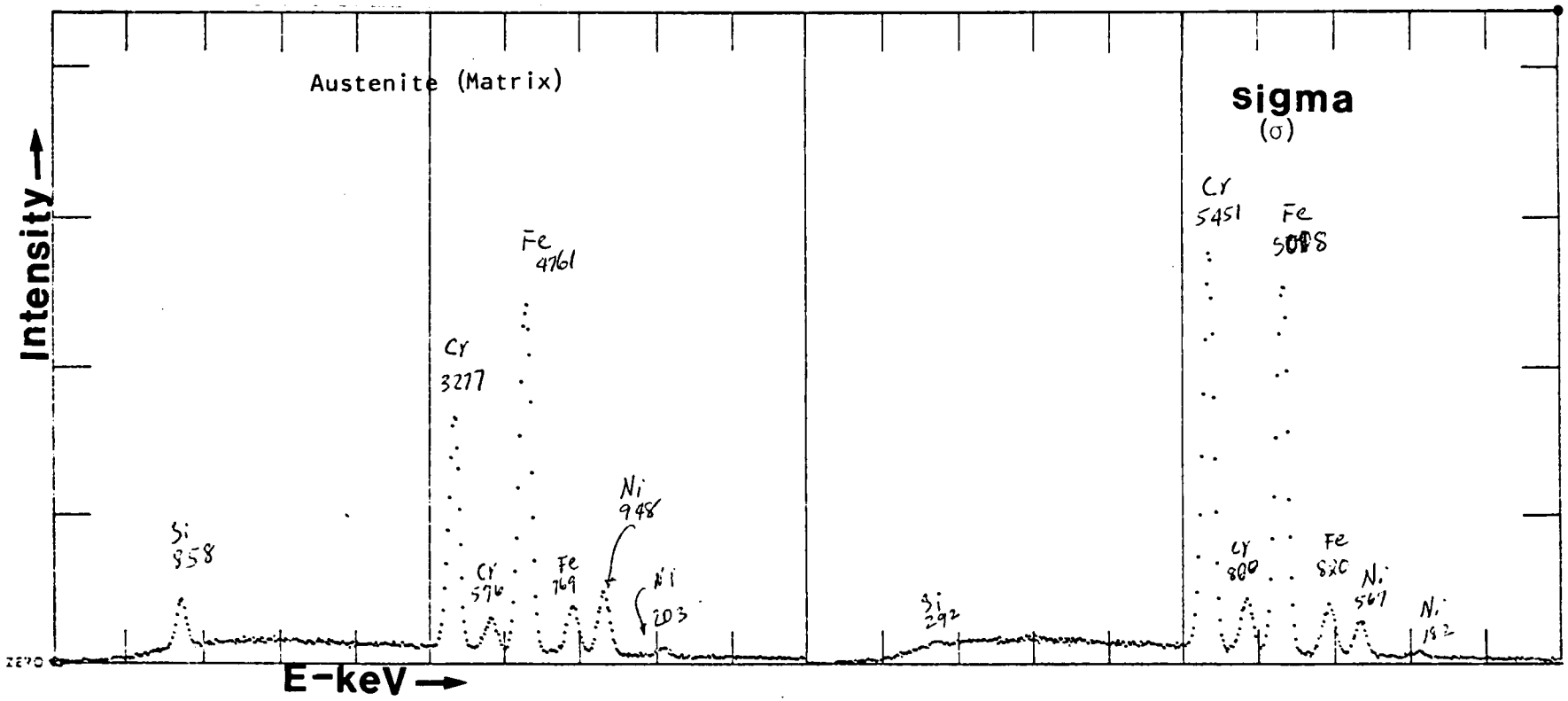
Figure A-E-3. Temperature Profile for Furnace No. 17 (850°C).

APPENDIX F

APPENDIX F

INTENSITY VS. ENERGY PLOTS FOR SIGMA, AUSTENITE, AND CARBIDE PHASES

The intensity vs. energy plots for austenite and sigma phase are shown in Figure A-F-1. The intensity vs. energy plots for austenite matrix and $M_{23}C_6$ carbide are shown in Figure A-F-2. The plots were obtained with the help of scanning electron microscope energy dispersive analyzer.



Note: The intensity scale is actually arbitrary; it was normalized for the (Fe) peak.

SAMPLE NUMBER 9-2-4

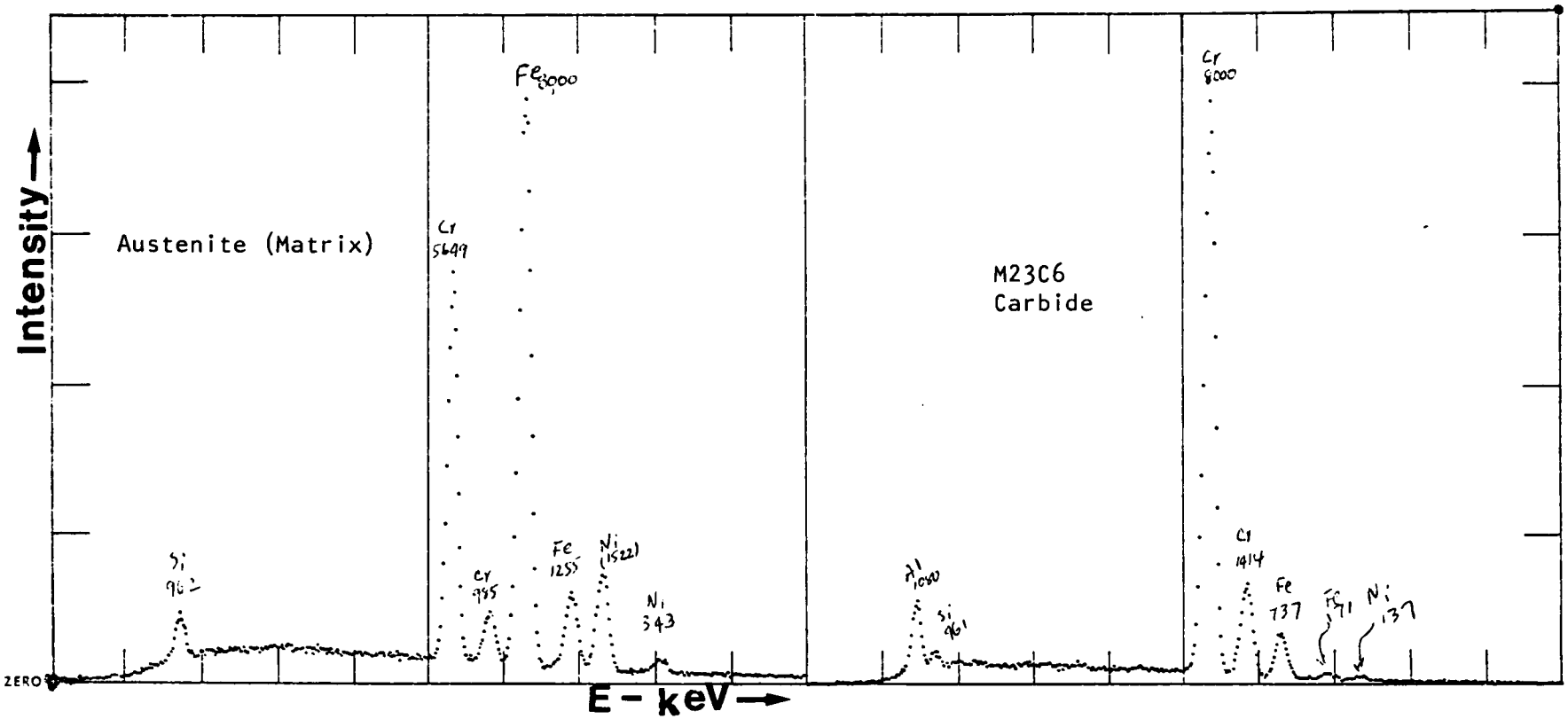
Tilt Angle = 26°

Partial Field

5000X Magnification

KEY:	KeV	Intensity (Counts)
Fe	Kα 6.40	(150)
	Kβ 7.06	(15)
Cr	Kα 5.41	(150)
	Kβ 5.95	(30)
Ni	Kα 7.47	(150)
	Kβ 8.26	(15)

Figure A-F-1. SEM Energy Dispersive Analyses for Austenite Matrix (Left) and Sigma Phase (Right).



Note: The intensity scale is actually arbitrary; it was normalized for the (Fe) peak.

SAMPLE NUMBER 9-2-4

Tilt Angle = 26°

Partial Field

5000X Magnification

KEY:

KeV	Intensity (Counts)
Fe Kα 6.40	(150)
Kβ 7.06	(15)
Cr Kα 5.41	(150)
-Kβ 5.95	(30)
Ni Kα 7.47	(150)
-Kβ 8.26	(15)

Figure A-F-2. SEM Energy Dispersive Analyses for Austenite Matrix (Left) and $M_{23}C_6$ Carbide (Right).

APPENDIX G

APPENDIX G

PERIODIC TABLE OF THE ELEMENTS

Periodic tables of the elements are shown in Figures A-G-1 through A-G-3.

Figure A-G-1 shows crystal structures of the elements, and, thus, one can predict sigma phase formation between elements of similar properties. Likewise, Figure A-G-2 clearly shows the transition metals which are also prone to sigma formation. Figure A-G-3, on the other hand, is primarily useful for ferrous metallurgists and clearly shows favorable size factor and unfavorable size factor of elements, and, thus, one can predict sigma formation. The atomic sizes shown are based largely on the work of Hume-Rothery[75] and Pauling.[97]

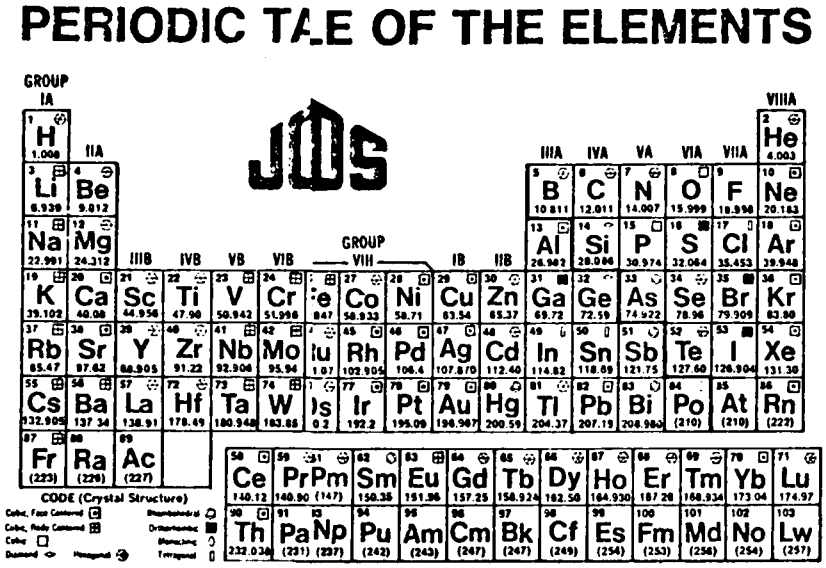
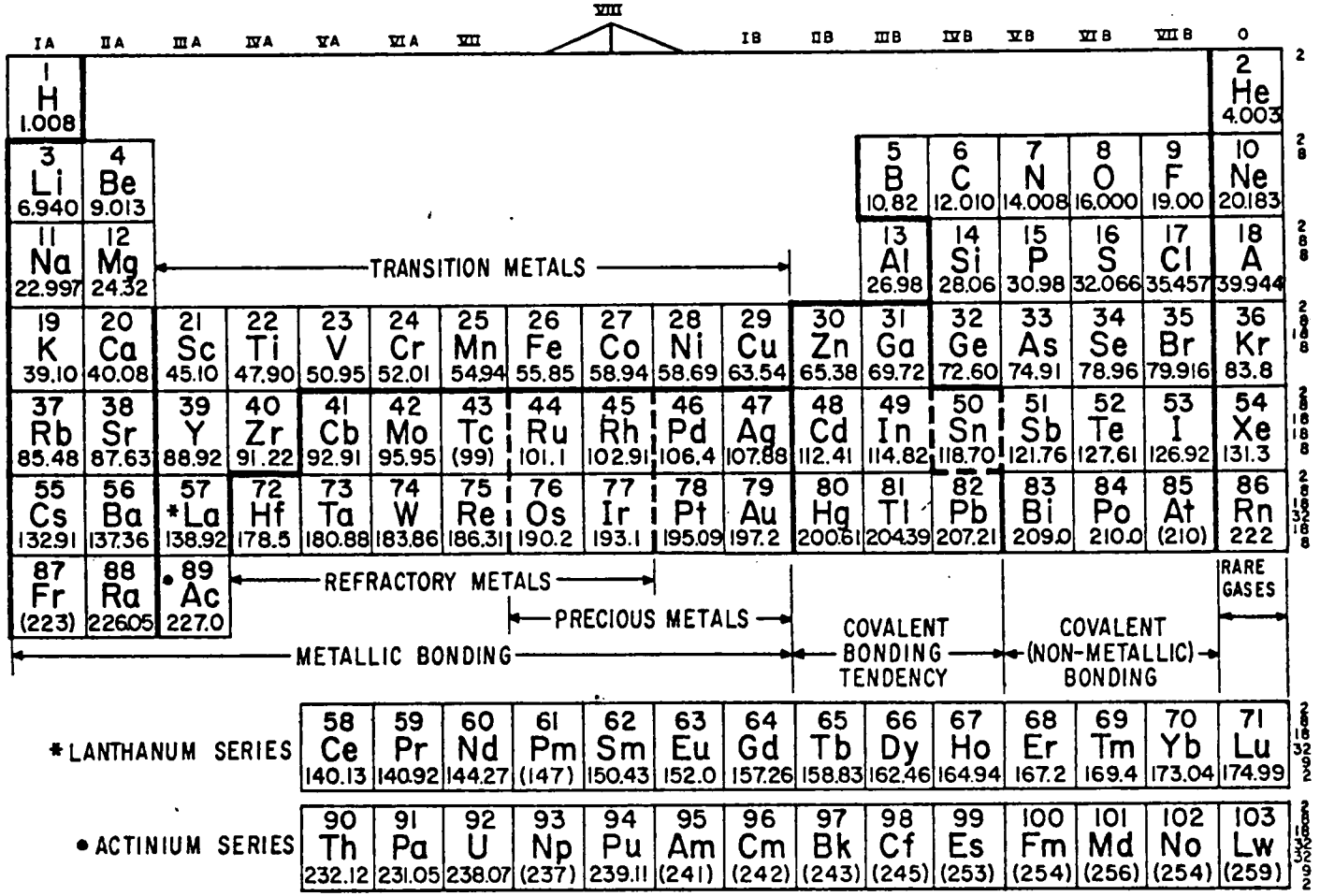


Figure A-G-1. Periodic Table of the Elements Showing Their Crystal Structure.

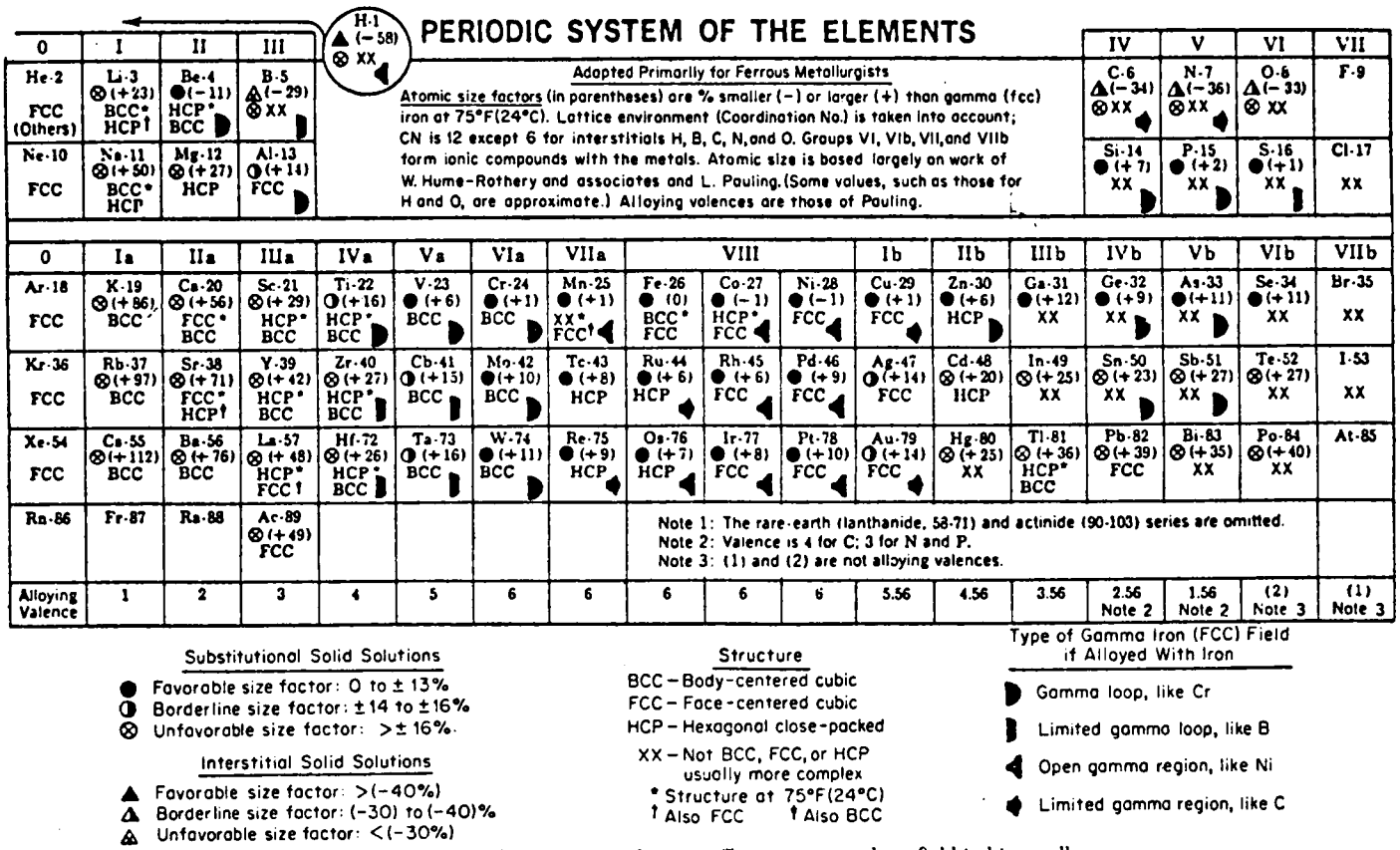
Source: Joint Committee on Powder Diffraction Standards, 1601 Park Lane, Swarthmore, Pennsylvania 19081 (1980).



PERIODIC SYSTEM OF ELEMENTS

Figure A-G-2. Periodic System of Elements Showing Transition Metals.

Source: C. T. Sims and W. C. Hagel (Editors), The Superalloys, John Wiley and Sons (Interscience), New York (1972).



0	I	II	III	IV	V	VI	VII
He·2 FCC (Others)	Li·3 ⊗(+23) BCC* HCP†	Be·4 ●(−11) HCP* BCC	B·5 ◬(−29) ⊗ XX	C·6 ◬(−34) ⊗ XX	N·7 ◬(−36) ⊗ XX	O·8 ◬(−33) ⊗ XX	F·9
Ne·10 FCC	Na·11 ⊗(+50) BCC* HCP	Mg·12 ⊗(+27) HCP	Al·13 ◑(+14) FCC	Si·14 ●(+7) XX	P·15 ●(+2) XX	S·16 ●(+1) XX	Cl·17 XX

0	Ia	IIa	IIIa	IVa	Va	VIa	VIIa	VIII			Ib	IIb	IIIb	IVb	Vb	VIb	VIIb
Ar·18 FCC	K·19 ⊗(+86) BCC	Ca·20 ⊗(+56) FCC* BCC	Sc·21 ⊗(+29) HCP* BCC	Ti·22 ◑(+16) HCP* BCC	V·23 ●(+6) BCC	Cr·24 ●(+1) BCC	Mn·25 ●(+1) XX* FCC†	Fe·26 ●(0) BCC* FCC	Co·27 ●(−1) HCP* FCC	Ni·28 ●(−1) FCC	Cu·29 ●(+1) FCC	Zn·30 ●(+6) HCP	Ga·31 ●(+12) XX	Ge·32 ●(+9) XX	As·33 ●(+11) XX	Se·34 ●(+11) XX	Br·35 XX
Kr·36 FCC	Rb·37 ⊗(+97) BCC	Sr·38 ⊗(+71) FCC* HCP†	Y·39 ⊗(+42) HCP* BCC	Zr·40 ⊗(+27) HCP* BCC	Cb·41 ◑(+15) BCC	Mo·42 ●(+10) BCC	Tc·43 ●(+8) HCP	Ru·44 ●(+6) HCP	Rh·45 ●(+6) FCC	Pd·46 ●(+9) FCC	Ag·47 ◑(+14) FCC	Cd·48 ⊗(+20) HCP	In·49 ⊗(+25) XX	Sn·50 ⊗(+23) XX	Sb·51 ⊗(+27) XX	Te·52 ⊗(+27) XX	I·53 XX
Xe·54 FCC	Cs·55 ⊗(+112) BCC	Ba·56 ⊗(+76) BCC	La·57 ⊗(+48) HCP* FCC†	Hf·72 ⊗(+26) HCP* BCC	Ta·73 ◑(+16) BCC	W·74 ●(+11) BCC	Re·75 ●(+9) HCP	Os·76 ●(+7) HCP	Ir·77 ●(+8) FCC	Pt·78 ●(+10) FCC	Au·79 ◑(+14) FCC	Hg·80 ⊗(+25) XX	Tl·81 ⊗(+36) HCP* BCC	Pb·82 ⊗(+39) FCC	Bi·83 ⊗(+35) XX	Po·84 ⊗(+40) XX	At·85
Rn·86	Fr·87	Ra·88	Ac·89 ⊗(+49) FCC														
Alloying Valence	1	2	3	4	5	6	6	6	6	6	5.56	4.56	3.56	2.56 Note 2	1.56 Note 2	(2) Note 3	(1) Note 3

Periodic chart of the elements showing effect on gamma-phase field in binary alloys.

Figure A-G-3. Periodic System of the Elements for Ferrous Metallurgists.

Source: D. Peckner and I. M. Bernstein, Handbook of Stainless Steels, McGraw-Hill Book Co., New York, p. 4-6 (1977).

APPENDIX H

APPENDIX H

LIST OF SYMBOLS USED IN THE TEXT

δ -- delta iron high-temperature phase

α -- ferrite iron

γ -- austenite iron

σ -- sigma phase (intermetallic compound)

ECC -- equivalent chromium content

CECC -- corrected equivalent chromium content

EVN or $\bar{N}v$ -- average electron vacancy number

$M_{23}C_6$ -- metal carbide

Cr -- chromium

Ni -- nickel

Fe -- iron

C -- carbon

Mo -- molybdenum

Si -- silicon

η -- Laves phase (intermetallic compound)

χ -- Kai phase (intermetallic compound)

c_o, a_o -- lattice parameters of BCT crystal

BCT -- body-centered tetragonal lattice

BCC -- body-centered cubic

FCC -- face-centered lattice

CH_3OH -- methyl alcohol (methanol)

C_2H_5OH -- ethyl alcohol (ethanol)

HCl -- hydrochloric acid

HNO_3 -- nitric acid

H_2O -- water

H_2SO_4 -- sulphuric acid

H_3PO_4 -- phosphoric acid

H_2O_2 -- hydrogen peroxide

KOH -- potassium hydroxide (solid)

$K_3Fe(CN)_6$ -- potassium ferricynide

$NaOH$ -- sodium hydroxide

CH_3COOH -- acetic acid

CrO_3 -- chromic acid

$C_2H_2O_4$ -- oxalic acid (solid)

e/a -- electron:atom ratio

λ -- wavelength of radiation

d -- interplanar distance

2Θ -- Bragg Angle

SEM -- scanning electron microscope

TEM -- transmission electron microscope

RF -- Ratio Factor

EF -- Exchange Factor

wt.% -- weight percent

At.% -- atomic percent

c.w. -- cold work

AGN -- average group number

r -- atomic radius

CC -- camera constant = dR

R -- reciprocal lattice vector

MF -- magnification factor

I -- intensity

eV -- electron volt

E -- energy

m -- mass of an electron

e -- electronic charge of an electron

T -- temperature °C (or °K)

t -- time

N_C -- mole fraction carbon

N_{Ni} -- mole fraction nickel

N_{Fe} -- mole fraction iron

N_{Cr} -- mole fraction chromium

Q -- activation energy

R -- gas constant

k -- rate constant

(hkl) -- indices of a plane

RT -- room temperature (25°C or 77°F)

HCP -- hexagonal close-packed (crystal structure)

CO_2 -- carbon dioxide

CO -- carbon monoxide

Ar -- argon

N_2 -- nitrogen

H_2 -- hydrogen

$\mathring{A}$ -- Angstron unit (10^{-8} cm)

DC -- direct current

AC -- alternating current

EMF -- electromotive force

V -- volt(s)

VITA

Lokanath Patel was born to Mr. Kamal Lochan Patel and Mrs. Khatakuri Patel on June 1, 1943 in Kuntara, India. Kuntara is a small town in the district of Sambalpur, Orissa State, and located about 400 miles southwest of Calcutta. He attended elementary schools in this town and in the nearby town of Kusumi. He graduated from Kuchinda High School in 1961. He received a B.Sc (Honors) degree in Physics from G.M. College of Utkal University in 1965 and a B.Tech (Honors) degree in Metallurgical Engineering from the Indian Institute of Technology--Kharagpur in 1968. The author was a sergeant of the National Cadet Corps and Rifles Association and was the recipient of many scholarships.

After a brief post-graduate study at the Indian Institute of Technology, Bombay, he came to the United States and attended State University of New York at Buffalo beginning in January 1969. He then worked for the Anaconda American Brass Co., Buffalo Plant Division, in the summer of 1969. He attended graduate schools at the University of Pittsburgh and Virginia Polytechnic Institute and State University and received an M.S. degree in Ceramic Engineering from VPI&SU in January 1973.

Following graduation and a brief stay with the Electro-Tec Corporation, Blacksburg, Virginia, he worked for the Babcock & Wilcox Company, Nuclear Power Generation Division, Lynchburg, Virginia for two years. He came to The University of Tennessee, Knoxville in the fall of 1975 to pursue graduate studies in Metallurgical Engineering. In

September 1977, he was employed with the John Deere Co., Plow and Planter Works, Moline, Illinois as a metallurgist and is currently working there.

He is a member of the American Society for Metals and has served the ASM Quad-City Chapter as an executive member. He was president of the Friends of India Association of Quad Cities, Moline, Illinois.

The author is a U.S. citizen and lives with his family--Basanti, Veena, and Suman Kumar--in Coal Valley, Illinois. He is listed in the midwest section of "Who's Who in America" and "Who's Who in Science and Technology."